Durham E-Theses

Electrical properties of zinc selenide

Vincent, B.

ELECTRICAL PROPERTIES OF ZINC SELENIDE

by

B. VINCENT

Presented in Candidature for the Degree of

Doctor of Philosophy

in the

University of Durham
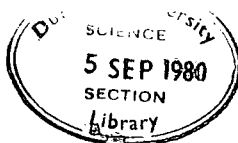
August 1980

To my parents,

to my wife,

to my daughters.

ACKNOWLEDGEMENTS

ABSTRACT

The main purpose of the research reported in this thesis was to investigate the behaviour of zinc selenide crystals doped with group III impurities such as indium and gallium, with the aim of understanding the processess of self-compensation involved which prevent them from being converted to p-type.

The crystals which were grown from the vapour phase, were doped by adding the group III impurity directly to the charge in metallic form or as ZnSe:In or ZnSe:Ga.

Measurements of the photoluminescence and cathodoluminescence revealed that the crystals behaved very similarly to copper doped ZnSe, emitting an orange-red band at 295 K and in the yellow-green and orange-red at 85 K.

Measurements of the electrical conductivity and Hall coefficient were made on as-grown samples and samples heated in zinc vapour, which had been cut from ten crystal boules containing indium or gallium in concentrations between 5 and 1000 ppm. The measurements showed that the crystals obeyed the Meyer-Neldel rule and that their resistivity increased with the dopant concentration. It was also revealed, from the exponential behaviour and low values of the electron Hall mobilities, that the conduction of the lightly doped samples was via impurity centres at 295 K. The heavily doped samples also showed low values of Hall mobility limited by a combination of polar mode and ionized and neutral impurity scattering. The free electron concentration decreased while the activation energies increased with increasing dopant concentration. Activation energies ranged from 0.05 to 0.95 eV . The reduction of the free electron concentration with increasing indium or gallium content in the crystals, is attributed to indium (or gallium) substituting on selenium sites and forming acceptors.

When the heavily doped crystals were heated in zinc the indium or gallium is precipitated. The precipitates have been examined in the optical, scanning electron and transmission electron microscopes, and are found to have particular shapes and to decorate defects such as stacking faults. The mechanism of precipitation is discussed in some detail.

CONTENTS

CHAPTER 1

INTRODUCTION

1.1 II-VI COMPOUNDS

II-VI materials include compounds formed from elements of group II and group VI of the periodic table which, in a broad sense, are the tellu - rides, selenides, sulphides and oxides of zinc, cadmium and mercury. The other elements of these two groups, which strictly should also be included, have received very little attention and are usually omitted.

The early studies in II-VI compounds were conducted almost exclusively on powder samples. Although these investigations did much for the understanding of some of their properties, particularly the phosphors like ZnS, much of the present knowledge on the II-VI's has been obtained through studies on single crystals. It is evident that for a better understanding of the properties of II-VI compounds, it is imperative that good quality pure single crystals should be readily available, therefore, the first step is the setting up and improvement of the techniques of crystal growth. One of the important aspects of the crystal growth of II-VI compounds is the control of the stoichiometry, since a slightly higher proportion of one of the constituents can have a significant effect on the properties of a crystal. Once this is satisfactorily achieved, the next step is the controlled introduction of chemical impurities. In fact, in II-VI compounds, it is the native defects and certain active impurities that give these materials their interesting electrical, magnetic and optical properties. Since most II-VI compounds have a direct energy gap, they have an immediate interest for applications as optical devices in the extended visible spectrum, extending from the ultraviolet to the infra-red.

1.2   PURPOSE OF THE PRESENT WORK

One of the II-VI compounds with a great potential for application as a light emitting device, is zinc selenide. The band gap of ZnSe at room temperature is 2.67 eV, corresponding to light of wavelength 464 nm which is in the blue region. With selected impurities, the radiation can be extended to the red. In order to develop efficient light-emitting devices, p-n diodes would be the optimal choice, so that minority carrier injection in forward bias would lead to efficient electron-hole recombination. So far, semiconducting ZnSe has only been made n-type, therefore no useful p-n junction can be made with ZnSe alone. Some work has been carried out in ion implanted p-n junctions, heterojunctions of ZnSe/ZnTe and MIS structures but, their best efficiencies are still well below that of the commercial III-V LED's. ZnSe is also being developed as an infra-red window.

ZnSe has recently achieved importance however, as far as luminescence studies are concerned, in that, with ZnTe, it forms a prototype for understanding the whole of the II-VI group of compounds. The reason for this is that very pure crystals of both these materials are now being produced, and photoluminescence emission and excitation spectroscopy at helium temperature has become very sophisticated in recent years.

One of the first breakthroughs in device fabrication appeared to have been made by Robinson and Kun (1975). They claimed to have developed a two stage process in which p-type layers, heavily doped with either gallium or indium, were produced on ZnSe or Zn(SSe) single crystals substrates grown by the iodine transport method. Efficient (up to 1 % conversion) light emitting diodes were claimed with orange and yellow light with ZnSe and yellow, green-yellow, green and blue-green light with ZnS_xSe_{1-x}.

In view of this, and the fact that several authors have also reported anomalous behaviour of the electrical properties of ZnSe when doped with gallium or indium, it was decided to study the electrical and optical properties of these crystals. First however it is relevant to summarise

briefly the work carried out to date in this department on ZnSe, ZnS and ZnSSe mixed crystals.

1.3   PROPERTIES OF ZnSe INVESTIGATED IN THIS DEPARTMENT

The study of ZnSe started here after Burr and Woods (1971) obtained single crystals of ZnSe with centimetre dimensions using the vapour phase technique. Subsequently Jones and Woods (1973) were able to use the same growth technique to obtain good quality ZnSe single crystals doped with manganese. They also used the iodine transport method. Jones and Woods reported an extensive investigation of the luminescence excitation and emission spectra of this material (ZnSe:Mn).

Özsan and Woods (1974) prepared electroluminescente devices with crystals of ZnSe:Mn and Zn(S,Se). To achieve low resistivity of the material, the crystals were heated in molten zinc at 850°C. The electroluminescence obtained with the ZnSe:Mn devices was yellow-orange and with Zn(S,Se) was green. Their efficiencies were well under 1%.

Jones and Woods (1974) also studied copper doped ZnSe crystals and measured their luminescence emission and excitation spectra. The emission spectrum at room temperature was in the orange-red. An anomalous photovoltaic effect in ZnSe was observed by Cutter and Woods (1975).

Gezci and Woods (1975) measured the blue edge emission in ZnSe at 10 K. A comprehensive study of the growth and defect stucture of single crystals of ZnSe and ZnSSe was carried out by Cutter et al (1976). The major defects encountered were long thin twin bands in the ZnSe crystals. In the mixed crystals, besides many more twins, intrinsic stacking faults were frequently observed.

At this stage, the growth technique had been well developed and single crystals of ZnSe doped with different impurities were succesfully grown using, mainly, the vapour phase technique. Jones and Woods (1976) measured some of the optical and electrical properties of undoped and doped ZnSe crystals, mostly after heating them in molten zinc in order to reduce their re-

sistivity. The dopants involved were indium, gallium, aluminium and chlorine. Özsan and Woods (1977a) measured the surface states in their electroluminescent diodes, by assuming they were dealing with an MIS device, in which the insulator was a result of the etching process. These same authors, Özsan and Woods (1977b) then made light- emmitting devices prepared on single crystals of solid solutions of ZnSe and ZnS, throughout the entire range of composition. In this way, it was possible to obtain light throughout the visible spectrum, from blue (for ZnS) to yellowish-red (for ZnSe).

More recently, Lawther and Woods (1977) managed to grow chemically an insulating layer of ZnO on ZnSe substrates, and thus achieved MIS diodes which, when forward-biased, emitted light in the yellow-orange for aluminium doped ZnSe or in the red-orange for undoped ZnSe. Here also, the ZnSe crystals had been previously heated in molten zinc. Finally, Lawther and Woods (1978) produced blue light emitting MIS diodes with ZnS. The substrates were semiconducting ZnSe crystals heated in molten zinc plus aluminium. The insulator was evaporated ZnS.

1.4 ARRANGEMENT OF THE PRESENT THESIS

As stated above, the work described in this thesis has been mainly concerned with the electrical properties of indium and gallium doped ZnSe crystals, in an attempt to explain the apparently anomalous behaviour of these two group III impurities.

The theoretical background relevant to this work is presented in the next Chapter. A description of the properties of ZnSe and a review of the recent literature then follow in Chapter three. Chapter 4 is concerned with the technique used in growing the crystals and with the preparation of the samples. A description is also given of the different experimental techniques used throughout this investigation. These involved measurements of the photoluminescence and cathodoluminescence emission spectra; photoconductivity, infra-red quenching, thermally stimulated currents and thermoluminescence. To study the electrical transport properties ; measurements of the electrical

conductivity, Hall coefficient and, whenever possible, **thermoelectric power** were made. Finally, in order to investigate the crystal defects, scanning and transmission electron microscope studies were made.

The results of the optical measurements and a discussion of their significance is given in Chapter 5. Chapter 6 is concerned with the electrical measurements and Chapter seven with the study of the crystalline defects.

Finally, Chapter eight provides a summary of the conclusions from the three previous Chapters, and ends with some suggestions for future work.

CHAPTER 2

TRANSPORT AND OPTICAL PROPERTIES

2.1   INTRODUCTION

This chapter is concerned with the background theory behind the
measurements carried out in this work and the conclusions drawn from it.
The following sections therefore are concerned with electrical transport
properties, luminescence, and photoconductivity.

2.2   TRANSPORT PROPERTIES

2.2.1 Intrinsic and Extrinsic Conduction

In semiconductors, only the upper levels of the valence band,
the lower levels of the conduction band and the intermediate levels are
of importance. At the absolute zero of temperature, the electrons
normally occupy the valence band and the lower energy states of some
impurity levels. Our problem is to find the distribution of these
electrons over the allowed energy states at finite values of temperature
T.

The probability F(E) that a certain level will be occupied is
given by

$$F(E) = \left\{ \exp\left[(E-E_F) \Big/ kT \right] + 1 \right\}^{-1} .\tag{2.1}$$

This function is the so-called Fermi-Dirac distribution valid for particles
obeying the Pauli principle, such as electrons. Here, E_F is the Fermi
energy and k Boltzmann's constant.

Let us take the zero of energy as the energy of the lowest
allowed level in the conduction band. Let N_c (E)dE be the number of
allowed levels per unit volume in the conduction band in the energy range
between E and E + dE, then the number of electrons n(E)dE in the conduction

band with the same range of energies is given by

$$n(E)\,dE = 2\,N_C\,(E)\,F\,(E)\,dE \qquad (2.2)$$

where the fact that two electrons (of opposite spin) may occupy each level has been included. The total number of electrons per unit volume n in the conduction band is then given by

$$n = \int_0^{E_T} N_C\,(E)\,F\,(E)\,dE \qquad (2.3)$$

where E_T is the energy at the top of the conduction band.

The density of levels $N_C(E)\,dE$ may be calculated by assuming first the simplest symmetrical form of a semiconductor, and afterwards the calculation can be extended to other symmetries so that one refers to the effective density of states in the conduction band. However, a few other assumptions have to be made, for example, there is only a small probability of electron occupation of the levels in the conduction band and hence, only the levels closest to the zero energy level will have any electron population. As a result, the upper limit of the integral in equation 2.3 may be extended to infinity, when,

$$n = 4\pi \left\{ \frac{4\,m_e^{*2}}{h} \right\}^3 \int_0^{\infty} \frac{E^{\frac{1}{2}}\,dE}{\exp\left[(E-E_F)\Big/ kT \right] + 1} \qquad (2.4)$$

where m_e^{*} = electron effective mass near the bottom of the conduction band.

h = Planck's constant.

Since we suppose that $E-E_F \gg kT$, then,

$$n = 2 \left(2\pi m_e^* k T/h^2\right)^{3/2} \exp\left[-\left(E_F/kT\right)\right] \tag{2.5}$$

or, $\quad n = N_c \exp\left[-\left(E_F/kT\right)\right]$,

so that the effective density of states is

$$N_c = 2 \left(2\pi m_e^* kT/h^2\right)^{3/2} . \tag{2.6}$$

A similar approach may also be carried out for holes near the top of the valence band. In this way, an equation for the Fermi level for intrinsic semiconductors is obtained as

$$E_F = -\frac{1}{2} E_g + \frac{1}{2} kT \ln \frac{N_v}{N_c} , \tag{2.7}$$

where E_g is the band gap and N_v the effective density of states in the valence band.

For a semiconductor with impurity levels (extrinsic semiconductor), we consider the case of a compensated semiconductor with N_d donors and N_a acceptors per unit volume. If $N_d > N_a$, the acceptor levels will be completely filled with electrons from the donor levels. The actual number of carriers available for extrinsic conduction is given by N_d-N_a for an n-type material. Thus, the density of occupied donor levels, n_d, at temperature T is

$$n_d = \text{density of donors} \times \text{Fermi function}$$

or $\quad n_d = N_d \left[\frac{1}{g} \exp\left\{\frac{\left(E_F-E_d\right)}{kT}\right\} + 1\right]^{-1} \tag{2.8}$

where g is the degeneracy factor of that particular donor and E_d is the position of the donor below the conduction band. At T = 0 K, there will be N_d-N_a electrons in the donor level, then, at some higher T, when there

are n electrons per unit volume in the conduction band, we must have

$$N_d - N_a = n + N_d \left[\frac{1}{g} \exp \left\{ \frac{E_F - E_d}{kT} \right\} + 1 \right]^{-1} \qquad (2.9)$$

which may be transformed to

$$\frac{N_d}{N_d - N_a - n} - 1 = \frac{1}{g} \exp \left\{ \frac{E_F - E_d}{kT} \right\}$$

$$= \frac{1}{g} \left[\exp \left\{ \frac{E_F}{kT} \right\} \exp \left\{ - \frac{E_d}{kT} \right\} \right]$$

or

$$\frac{N_a + n}{N_d - N_a - n} = \frac{1}{g} \left[\exp \left\{ \frac{E_F}{kT} \right\} \bigg/ \exp \left\{ \frac{E_d}{kT} \right\} \right]$$

and substituting this in equation 2.5 and 2.6

$$\frac{N_a + n}{N_d - N_a - n} = \frac{N_c}{g \, n \, \exp \, (E_d/kT)}$$

so that,

$$\frac{n \, (N_d + n)}{N_d - N_a - n} = \frac{1}{g} \, N_c \, \exp \left\{ - \frac{E_d}{kT} \right\} \qquad (2.10)$$

where E_d is also known as the ionization energy of that particular donor impurity.

For heavy compensation, when $n \ll N_a < N_d$, equation 2.10 reduces to

$$n \approx \frac{N_c \, (N_d - N_a)}{N_c + g \, N_a \, \exp \, (E_d/kT)} . \qquad (2.11)$$

The variation of the Fermi level is given by

$$E_F = - kT \quad \ell n \ (N_c/n) \tag{2.12}$$

which approximate to :

$$E_F = - E_d + kT \quad \ell n \left[\left(N_d - N_a \right) / g \ N_a \right) \right] \tag{2.13}$$

when T is small, i.e. $n \ll N_a < N_d$, and

$$E_F = - kT \quad \ell n \left[N_c / \left(N_d - N_a \right) \right] \tag{2.14}$$

when T is large, i.e, $n \sim N_d - N_a$ (the so-called exhaustion range).

Equation 2.11 shows that if we neglect the $T^{3/2}$ dependence of N_c compared with the exponential dependence, then a plot of $\ell n \ n$ versus $1/T$ gives a straight line with slope $-E_d/k$.

2.2.2 Transport Equation

In the so-called Lorentz model in which a perturbation to the Maxwell-Boltzmann distribution for electron velocities produced by the presence of an external disturbance is considered, we are concerned with the transport of the electrical changes associated with an electron gas and also with the transport of the kinetic energy of these same electrons. An electron gas has velocities distributed according to the equilibrium distribution f_o. In the presence of an external field, an electron drift will result and the new velocity distribution will be f and will be different from f_o. Then, anywhere within the crystal, the rate at which f changes in time is given by

$$\frac{df}{dt} = \left| \frac{\partial f}{\partial t} \right|_{Field} + \left| \frac{\partial f}{\partial t} \right|_{Collision} \quad , \tag{2.15}$$

where the first term on the RHS takes account of the influence of the total field applied to the system and the second is concerned with the scattering effects which tend to restore the equilibrium. This equation is known as the Transport Equation. See for example, Nag (1972), Bube (1974), Elliot and Gibson (1974) and Smith (1978).

To obtain solutions to the Transport equation, the system is normally considered to be in the steady state under uniform fields, hence, the first term of equation 2.15 becomes zero. Different approaches are used to solve the equation according to the type of perturbation applied to the system, for example, where it is possible to consider electric fields alone or in conjunction with magnetic fields, or by setting up temperature gradients with or without the presence of electric and/or magnetic fields.

One of the methods employed to solve the equation is the relaxation time approximation. Let us consider $<\tau>$ (τ = relaxation time), the mean time between collisions within the system; let us assume that the original distribution was f_o and in the presence of some perturbation, the system reaches another steady state distribution after a time that is long compared with $<\tau>$. In this approximation it is assumed that the rate at which the perturbed distribution f returns to f_o is proportional to the perturbation $f-f_o$. Hence, the Transport equation may be written as

$$\frac{df}{dt} = - \frac{f-f_o}{<\tau>} \tag{2.16}$$

where $1/<\tau>$ is the constant of proportionality. Following this procedure, equation 2.16 may be solved for each individual case.

Let us suppose that a d.c. field ε is applied in the x-direction ; then equation 2.16 may be re-written as

$$\frac{df}{dt} = \frac{1}{\hbar} \frac{\partial f}{\partial E} \left\{ \vec{F} \cdot \vec{\nabla}_k E \right\} = - \frac{f-f_o}{<\tau>} \tag{2.17}$$

where a transformation from momentum (velocity) space to k-space has been made using $m \vec{v} = \hbar \vec{k}$. Note that this equation in k-space is also known as the Boltzmann equation. After some mathematical manipulation, a solution for the current density in a non-degenerate semiconductor is obtained in the form

$$J_x = \frac{n e^2 \varepsilon_x}{m^*} <\tau> \qquad (2.18)$$

where n represents the number of free electrons per unit volume and m^* is the scalar effective mass. The electron drift mobility, μ_c, which is defined as the ratio of drift speed to applied field, is then

$$\mu_c = \frac{J_x}{n e \varepsilon_x} = \frac{e}{m^*} <\tau> . \qquad (2.19)$$

The conductivity σ is given by

$$\sigma = n e \mu_c = \frac{n e^2}{m^*} <\tau> \qquad (2.20)$$

and the mean relaxation time $<\tau>$ is given by

$$<\tau> = \frac{\int_0^\infty E \, N(e) \, \exp(-E/kT) \, \tau(E) \, dE}{\int_0^\infty E \, N(E) \, \exp(-E/kT) \, dE} \qquad (2.21)$$

where the distribution function f_o has been replaced by the exponential form of the Fermi-Dirac approximation for the classical (non-degenerate) case. $N(E) \, dE$ is the number of allowed levels per unit volume in the energy range from E to E + dE. The term $N(E) \exp(-E/kT)$ is often known as a weighting function.

Over a considerable range of energies, it is found that for many semiconductors we may write

$$\tau = a E^{-s} \qquad (2.22)$$

where s is a constant which is generally derived from the observed variation of mobility with temperature. 'a' may vary with temperature. Substituting equation 2.22 in equation 2.21, the following result is obtained :

$$<\tau> = \frac{a}{(kT)^5} \quad \frac{\Gamma\left\{\frac{5}{2} - s\right\}}{\Gamma\left\{\frac{5}{2}\right\}} \qquad . \qquad (2.23)$$

Some other examples of solutions of the Transport equation now follow :

(a) Hall Effect :

This is the classical case where an electric field ε is applied to a semiconductor simultaneously with a magnetic field of flux density B. The force on an electron travelling with speed v in k-space is

$$\vec{F} = e \left[\vec{\varepsilon} + \frac{1}{\hbar} \vec{\nabla_k} E \times \vec{B} \right] \qquad (2.24)$$

and the Transport equation in steady state becomes

$$\frac{e}{\hbar} \left[\vec{\varepsilon} + \frac{1}{\hbar} \vec{\nabla_k} E \times \vec{B} \right] \cdot \vec{\nabla_k} f = - \frac{f-f_o}{<\tau>} \qquad . \qquad (2.25)$$

Again, after some manipulation, the current density J is given by

$$J_x = \frac{n e^2}{m^*} \left[<\tau> \varepsilon_x - \omega <\tau^2> \varepsilon_y \right] \qquad (2.26a)$$

and

$$J_y = \frac{n e^2}{m^*} \left[<\tau> \varepsilon_y - \omega <\tau^2> \varepsilon_x \right] \qquad (2.26b)$$

where $\omega = e\,B/m^*$, and where we have assumed B to be directed along the z-axis $(B = B_z)$ and to be sufficiently small to allow the effect of the terms in B_z^2 and higher, which should have appeared in the solution of equation 2.25, to be neglected.

For the Hall effect the customary procedure is to have a semi-conducting sample in the form of a bar in the X-direction with a current J_x obtained by the application of an external ε_x field. When the magnetic field B_z is applied, the carriers will suffer a deviation along the y-axis and a restoring field $e\varepsilon_y$ will appear, hence, when equilibrium is reached, J_y in equation 2.26b is zero, and we obtain,

$$\frac{\varepsilon_y}{B_z\,\varepsilon_x} = \mu_H = \frac{e}{m^*}\frac{<\tau^2>}{<\tau>} \cdot \qquad (2.27)$$

The field developed in the y-direction is called the Hall field and μ_H is defined as the Hall mobility. Comparing equation 2.27 with equation 2.19, we see that

$$\mu_H = \frac{<\tau^2>}{<\tau>^2}\,\mu_c = r\,\mu_c \qquad (2.28)$$

where $r = <\tau^2> / <\tau>^2$ is the so-called scattering factor.

The experimental arrangement to measure the Hall effect is shown in figure 2.1. Introducing the Hall coefficient, R_H, defined as the ratio of the electric to the magnetic field per unit current density, i.e.,

$$R_H = \frac{\varepsilon_y}{B_z\,J_x} \qquad (2.29)$$

we have, using equation 2.19 and equation 2.27 :

$$R_H = r/ne \cdot \qquad (2.30)$$
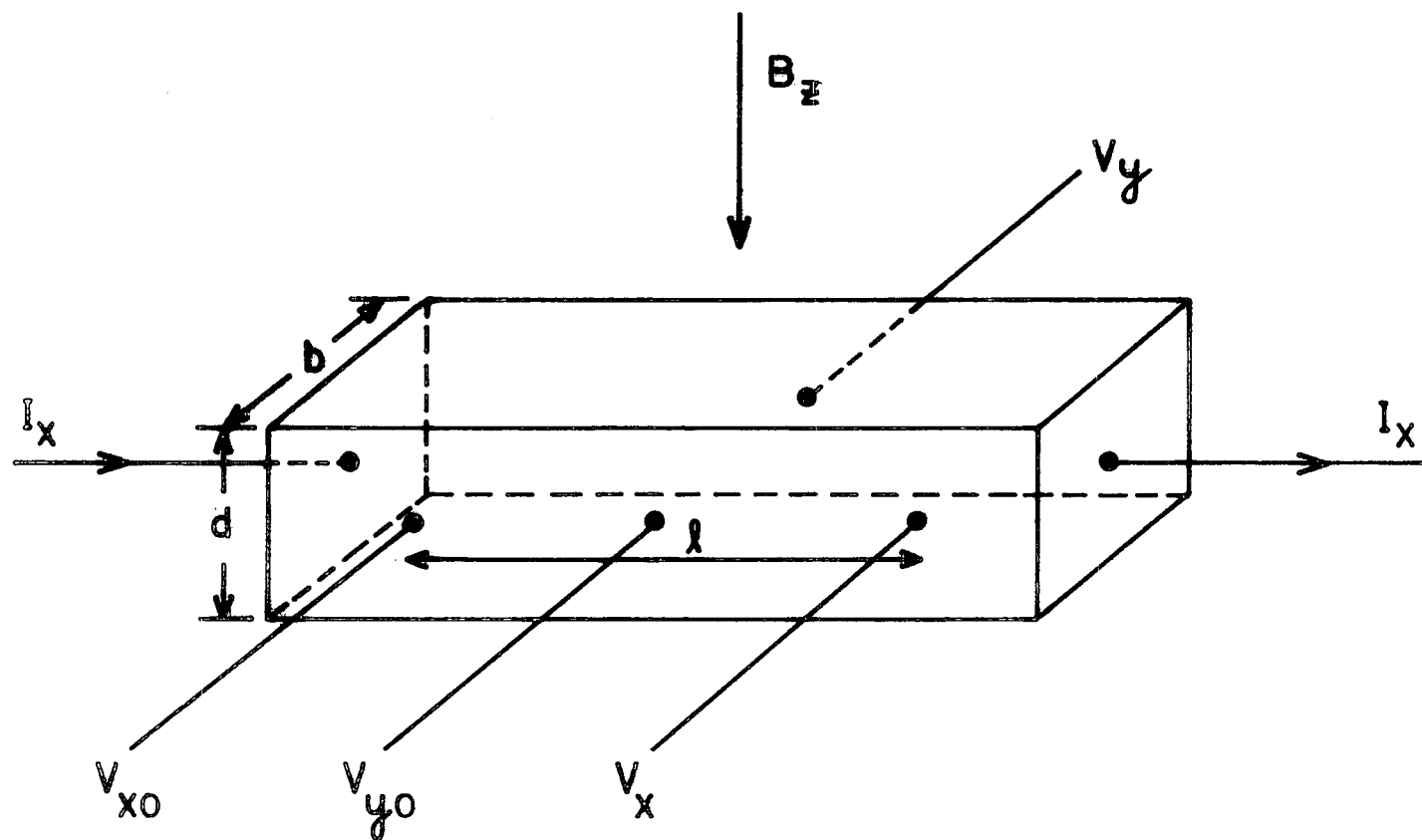
FIG. 2·1   SCHEMATIC   DIAGRAM   OF A TYPICAL HALL EFFECT SAMPLE

Now, from figure 2.1 and equations 2.19 and 2.27,

$$\varepsilon_y = \frac{V_y}{b} = B_z \frac{I_x}{b\ d}\ R_H \qquad (2.31)$$

so that,

$$R_H = \frac{V_y\ d}{B_z\ I_x}\ , \qquad (2.32)$$

where V_y is known as the Hall voltage and I_x is the actual current through the sample. The value of R_H, and hence n, can therefore be obtained by measuring V_y. A measure of the voltage V_x in figure 2.1 gives the value ε_x, namely,

$$\varepsilon_x = V_x/\ell \qquad (2.33)$$

and from equations 2.19 and 2.20, where

$$J_x = \sigma\ \varepsilon_x\ , \qquad (2.34)$$

we obtain $\quad \sigma = \dfrac{\ell\ I_x}{V_x\ b\ d} \qquad (2.35)$

and,

$$\mu_H = \sigma\ R_H\ . \qquad (2.36)$$

(b) Magnetoresistance :

The magnetic field B_z applied to the bar in figure 2.1 may also lead to a change in the resistance of the bar. If, in the development of equation 2.25, we consider the quadratic effects of B on J_x, we then end up with

$$J_x = \frac{n\ e^2}{m^*}\left[<\tau>\varepsilon_x - \omega\ <\tau^2>\varepsilon_y - \omega^2\ <\tau^3>\ \varepsilon_x\right] \qquad (2.37a)$$

$$J_y = \frac{n\ e^2}{m^*}\left[<\tau>\varepsilon_y - \omega\ <\tau^2>\varepsilon_x\right] \qquad (2.37b)$$

and putting $J_y = 0$, we have

$$J_x = \frac{n\,e^2}{m^*}\,\varepsilon_x\left[\,\langle\tau\rangle + \frac{\omega^2\,\langle\tau^2\rangle^2}{\langle\tau\rangle} - \omega^2\,\langle\tau^3\rangle\,\right].\qquad(2.38)$$

If we write $\quad\sigma_o = 1/\rho_o = (n\,e^2/m^*)\,\langle\tau\rangle \qquad\qquad\qquad(2.39a)$

and $\qquad\qquad \sigma = \sigma_o\,(1 + \Delta\sigma/\sigma_o) \qquad\qquad\qquad(2.39b)$

then, for $\quad \Delta\sigma/\sigma_o << 1$

$$-\frac{\Delta\sigma}{\sigma_o} = \frac{\Delta\rho}{\rho_o} = \frac{e^2 B^2}{m^{*2}}\,\frac{\langle\tau^3\rangle\,\langle\tau\rangle - \langle\tau^2\rangle^2}{\langle\tau\rangle^2}\qquad(2.40)$$

which may also be written as

$$\frac{\Delta\rho}{\rho_o} = -\frac{\Delta\sigma}{\sigma_o} = \xi\,R_H^2\,\sigma_o^2\,B^2 \qquad\qquad(2.41)$$

where the quantity ξ is the magnetoresistance coefficient and is given by the equation

$$\xi + 1 = \frac{\langle\tau^3\rangle\,\langle\tau\rangle}{\langle\tau^2\rangle^2} \qquad\qquad\qquad(2.42)$$

(c) Thermoelectric Power :

If we allow the external perturbation of Boltzmann's equation to be a temperature gradient in the x-direction then, after some algebra (see for example the text books of Bube and Smith cited at the beginning of this section) , it can be shown that

$$J_x = \frac{ne}{m^*}\left[\,e\,\varepsilon_x + T\,\frac{\partial}{\partial T}\left(\frac{E_F}{T}\right)\,\frac{d\,T}{d\,X}\,\langle\tau\rangle\right] + \frac{ne}{Tm^*}\,\frac{dT}{dX}\,\langle\tau E\rangle \quad(2.43)$$

where E_F is the Fermi energy. When a temperature gradient is established along a conductor, an e.m.f. is developed. This is known as the Seebeck effect. A quantity useful for semiconductors is the thermoelectric power S or differential Seebeck e.m.f. of a pair of conductors. It is defined as the potential difference ΔV established divided by the temperature difference along the conductor when this ΔT tends to zero, i.e. $S = \Delta V / \Delta T$ for $\Delta T \rightarrow 0$. This is a relative value between the two conductors involved. However, the thermoelectric power of a semiconductor is much greater than a metal, therefore, the absolute S value of a semiconductor can be obtained when suitable metal junctions are placed at its ends.

Hence, putting $J_x = 0$ in equation 2.43, we have

$$\varepsilon_x = - \left[T \frac{d}{dT} \left(\frac{E_F}{T} \right) + \frac{1}{eT} \frac{\langle E\tau \rangle}{\langle \tau \rangle} \right] \frac{dT}{dx} . \tag{2.44}$$

After more mathematical manipulation, the thermoelectric power S is obtained as:

$$S = \frac{E_F \langle \tau \rangle - \langle \tau E \rangle}{e\, T \langle \tau \rangle} . \tag{2.45}$$

For an n-type semiconductor with $\tau = a\, E^{-s}$, this becomes

$$S = - \frac{k}{e} \left[\left(\frac{5}{2} - s \right) - \frac{E_F}{kT} \right] . \tag{2.46}$$

Since generally $s < 5/2$ and E_F/kT is assumed negative, then S is negative for an n-type semiconductor. If a similar calculation is done for a p-type semiconductor, then it is found that S is positive. The sign of the thermoelectric power therefore gives a simple direct test as to whether a semiconductor is n-type or p-type.

When there are two types of carriers, their effects oppose one

another and,

$$S = \frac{-S_e \sigma_e + S_h \sigma_h}{\sigma_e + \sigma_h} \, . \tag{2.47}$$

2.2.3 Carrier Mobility

As equations 2.30 and 2.36 demonstrate, the carrier mobility μ and the carrier concentration n, are relatively easy to determine from Hall effect measurements. The variation of the mobility with temperature usually gives an indication of the operative scattering mechanisms.

There are several mechanisms by which carriers can be scattered, a short description of which now follows. The theoretical details which are described in the books of Smith and Bube are rather complex and only the relevant results will be given here.

In a crystalline solid, the carrier mobilities are mainly limited by lattice or impurity scattering, or a combination of both. Lattice scattering involves the interaction of electrons with phonons and with lattice deformations and hence is important at high temperatures (for most semiconductors, this means T > 150 K). Ionized impurity scattering is the interaction of carriers with charged centres, so it is similar to Rutherford scattering. With semiconductors, this mechanism is usually dominant at low temperatures, i.e. T < 100 K. However, in heavily doped materials, it may become important at room temperature.

We consider first the different types of lattice scattering :

(I)   Lattice Scattering or Electron-Phonon Interactions :

There are three important lattice scattering mechanisms which are referred to as optical, piezoelectric and deformation potential scattering.

(a) Optical Phonon Scattering :

Also known as optical mode scattering in polar (ionic) semiconductors. The vibration of two adjacent atoms in a unit cell in antiphase produces an optical phonon. In compound semiconductors, the

fact that adjacent atoms are oppositely charged allows an electrostatic potential to be associated with an optical phonon. The magnitude of this potential is dependent upon the degree of ionicity of the bonding and is therefore quite important in the II-VI compounds. The effective charges on each ion, and hence the electron-lattice interaction,can be related to the difference between the static and optical dielectric constants. According to Howarth and Sondheimer (1953), the strength of the interaction between an electron and the optical modes is characterized by a coupling constant α defined by the relation

$$\alpha = \frac{e^2}{\hbar} \left\{ \frac{m^*}{2\hbar\omega_\ell} \right\} \left\{ \frac{\epsilon_s - \epsilon_\infty}{\epsilon_s \; \epsilon_\infty} \right\} \qquad (2.48)$$

where ϵ_∞ & ϵ_s are the optical (high frequency) & the static dielectric constants respectively, and $\hbar\omega_\ell$ is the energy of the optical mode (L.O) phonon. In a non-polar crystal, $\epsilon_s - \epsilon_\infty$ is small, so α is small, but for polar crystals it may be just less than unity. The expression for the mobility limited by optical mode scattering proposed by Howarth and Sondheimer is

$$\mu_{OPT} = \frac{1}{2 \alpha\omega_\ell} \frac{e}{m^*} \frac{8}{3\sqrt{\pi}} \psi_Z \, Z^{-\frac{1}{2}} (e^Z - 1) \qquad (2.49)$$

where Z = the ratio of the Debye temperature to the lattice temperature, i.e. Θ_D/T or $\hbar\omega_\ell/kT$, and, ψ_Z is a factor, varying as a function of Z from 0.6 to 1 over the temperature range involved.

(b) Piezoelectric Scattering :

This mechanism is confined to crystals which lack inversion symmetry. These are usually ionic or partly ionic, so that piezoelectric scattering is often overshadowed by optical mode scattering. The interaction arises because acoustic modes generate regions of compression and rarefaction in a crystal, and in piezoelectric crystals, these lead to

electric fields. All the II-VI compounds are piezoelectric although those with the cubic structure are less so than the hexagonal ones. Harrison (1956) gives the mobility limited by piezoelectric scattering as

$$\mu_{p.z.} = \frac{0.044 \; \rho c_L^2 \; \hbar^2 \; \varepsilon_s^2}{e \; C^2 (m^{*3} \; kT)^{\frac{1}{2}}} \tag{2.50}$$

where ρ = density of the semiconductor,

C_L = longitudinal acoustic wave velocity, and

C = piezoelectric electrochemical coupling constant

(c) Acoustic Phonon scattering:

For semiconductors in which the bonding is primarily covalent, electrons are scattered predominantly by longitudinal acoustic (L.A.) phonons. These LA modes produce compressions and dilations which create local deformations in the dielectric constant as well as changes in the width of the energy gap. These LA phonons are the same as those involved in piezoelectric scattering. The deformation produces variations in the kinetic energy of an electron as it passes through the crystal and the resultant interaction is known as acoustic phonon scattering. The main parameter related to this type of scattering is the deformation potential constant ε_1 which gives a measure of the change in position of the conduction band edge due to changes in the volume of the unit cell, and expressed as $-V(\partial \varepsilon_c / \partial V)$. This subject was first introduced by Shockley and Bardeen (1950) who proposed the following equation for the mobility limited by acoustic phonons:

$$\mu_A = \left[\frac{8\pi}{m^{*5} (kT)^3} \right]^{\frac{1}{2}} \frac{e\hbar^4 \; \rho c_L^2}{3\varepsilon_1^2} \tag{2.51}$$

(II)   Impurity Scattering:

Charge carriers are scattered both by ionized and by neutral impurities. However, ionized impurity scattering is usually the more important.

(d)   Ionized Impurity Scattering:

Each ionized impurity in a crystal is a stationary positive or negative charge which can deflect the path of a passing electron. The required mathematical arguments are exactly those used by Rutherford in his model for alpha-particle scattering by atomic nuclei. Following this reasoning, Conwell and Weisskopf (1950) suggested an equation for the mobility limited by this kind of process. However, Brooks and Herring have developed an alternative procedure (see Brooks, 1955) which takes account of the screening of the Coulomb field of ionized impurities by free electrons. The Brooks-Herring formula for a compensated semiconductor is:

$$\mu_I = \left[\frac{2^7 (kT)^3}{\pi^3 m^*}\right]^{\frac{1}{2}} \frac{\varepsilon_s^2}{e^3 N_1} \left\{ \ell n \left[\frac{6m^* \varepsilon_s (kT)^2}{\pi e^2 h^2 n'\,(2 - \frac{n'}{N})}\right] \right\}^{-1} \qquad (2.52)$$

where $N_I = Z_A^2 N_a + Z_D^2 N_d$, N_a and N_d being the number of ionized acceptors and donors per unit volume, and Z_A and Z_B their respective effective charges; n' = number of free carriers per unit volume (i.e. n + p) and $N = |N_d - N_a|$.

(e)   Neutral Impurity scattering:

At very low temperatures, neutral impurities may outnumber ionized impurities since, as the temperature of a semiconductor is lowered, carriers freeze out into the impurity levels. The interaction of the electrons with neutral impurities is analogous to electron scattering by hydrogen atoms. The most common equation for the mobility μ_N limited by neutral impurity

scattering is due to Erginsoy (1950), i.e.

$$\mu_N = \frac{m^*}{20N \, \varepsilon_s} \left\{ \frac{e}{\hbar} \right\}^3 \qquad (2.53)$$

where N is the number of neutral impurity atoms per unit volume. However, Sclar (1956) proposed a rather different approach, but this is only important at very low temperatures and again the behaviour is almost temperature independent.

In addition to all the forms of scattering that occur when objects of atomic size interrupt the periodicity of the lattice, electrons can be scattered by objects which are extensive in one or more dimensions. A dislocation line running through a crystal is not very effective in scattering if it is electrically uncharged, but can be quite effective if it consists of a line of electrically charged acceptors. Grain boundaries within a polycrystalline sample certainly affect the mobility of the carriers and may inhibit electron motion from one grain to another if there is a potential barrier at the interface.

2.2.4 Impurity Conduction

Following the ideas developed so far in this chapter, it is to be expected that the resistivity of a semiconductor would increase towards infinity as the temperature was reduced to absolute zero. This is substantially correct, as long as the spacing between impurities is very large, compared with the radius a_o of the ground state wavefunction of the impurity centre. However, the behaviour would be quite different if the electrons were able to travel from one impurity to another, without entering the conduction band. This process is known as impurity conduction.

If such a process occurs in a semiconductor, the total conduc-
tivity can be written

$$\sigma = \sigma_1 \exp(-E_1/kT) + \sigma_2 \exp(-E_2/kT) + \sigma_3 \exp(-E_3/kT) \circ \qquad (2.54)$$

The first term arises from thermal impurity ionization and is insignific-
ant at very low temperatures. However, the donor ionization energy
$(E_d = E_1)$ decreases as N_d increases and the donors come into closer
proximity. E_1 disappears above a critical concentration N_T which is
given by Mott's criterion (i.e. $a_0 N_T^{1/3} \approx 0.25$; see Mott, 1968). With
an impurity density which does not exceed N_T, if there is about one
electron per donor, the wavefunctions of the electrons overlap and
form an impurity band, which consists of a quasi-continuous narrow band
of levels within the forbidden energy gap. It will be half filled,
hence, conduction will take place as in a metal. When the density of
impurities exceeds N_T, no thermal activation is necessary for the
electrons associated with the impurities. In such a heavily doped
semiconductor, the free carrier density and, probably, the electrical
conductivity are quite insensitive to temperature, except at high
temperatures when intrinsic conduction takes over.

The energy E_2 in equation 2.54 is believed to be associated with
the energy necessary to place a second electron onto a donor which
previously had one. According to recent theories, when impurity band
conduction begins to predominate over transport through the conduction
band, the magnetoresistance becomes negative at temperatures below that
at which the Hall coefficient R_H is a maximum. Thus, in the presence
of a transverse magnetic field , ξ (equation 2.41) is negative and the
resistivity of a crystalline semiconductor decreases. Toyozawa (1962)
explained this in the following way. Even if the transport between
impurities is of band character, partly isolated atoms always exist

owing to the chaotic arrangement of impurity atoms. Such semi-isolated impurity atoms possess a magnetic moment due to the spin moment of electrons partly localized on them. In the absence of an external magnetic field, these magnetic moments are directed randomly and the scattering of electrons moving in the impurity band is large. The magnetic field at low temperatures orients the magnetic moment of localized electrons and the sample resistance decreases. $\Delta\rho/\rho_0$ is proportional to B^2 at low magnetic field strength, but reaches saturation at high fields when all magnetic moments are oriented by the field.

Another interesting aspect of impurity conduction is that an n-type impurity band should give p-type thermopower at very low temperatures (see Mott and Davies, 1979, and references therein, for more information).

Finally, the term $\sigma_3 \exp(-E_3/kT)$ in 2.54 describes the hopping conduction of electrons tunnelling from neutral to ionized donors in a partially compensated semiconductor. This conducting mechanism is important at low temperatures when the number of donors is well below N_T, making the average distance between them as large as 10 a_0 to 20 a_0. The activation energy E_3 is thought to be due to the electric field attracting an electron back towards a centre from which it is hopping. In a.c. conductivity, E_3 is dependent on the frequency, decreasing with increasing frequency and therefore, at high frequency, the conductivity varies very little with temperature. For the situation where tunnelling to more remote but energetically favourable donors becomes dominant, Austin and Mott (1969) have proposed that the hopping conductivity term should be written as $\sigma_3' \exp(-A/T^{1/4})$.

One consequence of the narrowness of the impurity band is that low values of the electron mobility are obtained. Because of this, the Boltzmann equation cannot be used to describe the transport of electrons

in localized states, since the conventional idea of a mean free path and hence, of the relaxation time, is invalid (see Ioffe and Regel, 1960).

In addition to heavily doped semiconductors, there are several classes of solid for which the carrier mobility is small at all temperatures. The preceding remarks concerning hopping are relevant to many of these materials at room temperature. The low mobility found in many ionic solids is partly the consequence of polaron (i.e. optical or L.O. phonons) formation and partly due to the presence of many localized defects which can trap a moving carrier. Apart from ionic crystals, some transition metal oxides and sulphides and organic semiconductors also have very low values of mobility.

Finally, amorphous semiconductors form another important group of materials with low mobilities $(\mu \leqslant 1 \text{ cm}^2 \text{ V}^{-1} \text{ s}^{-1})$. These are characterized by the lack of long range order, even though each atom may have just the conventional number of nearest neighbours at the conventional distance. The difference between crystalline and amorphous semiconductors is illustrated in figure 2.2. Part (a) of this figure shows the conventional density of states for a semiconductor crystal. Valence states are shown below E_V and conduction band states above E_C. A few pockets of localized states within the intrinsic gap correspond with impurities and native defects which perturb the periodicity. When some long range disorder starts to occur, some "tailing" of the bands is expected and increases with the amount of disorder within the lattice, and part (b) of figure 2.2 shows the expected density of states for the same solid forming an ideal glass. Valence and conduction bands are still shown, but now a continuum extends downwards from E_C and upwards from E_V into what was previously the intrinsic gap. Part (c) of the same figure shows the resulting amorphous semiconductor with many broken bonds (known as dangling bonds) resulting from imperfect short range order.
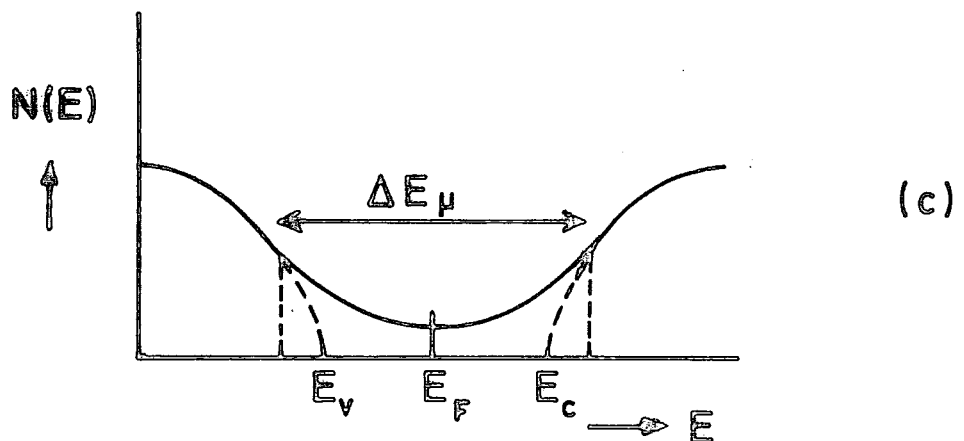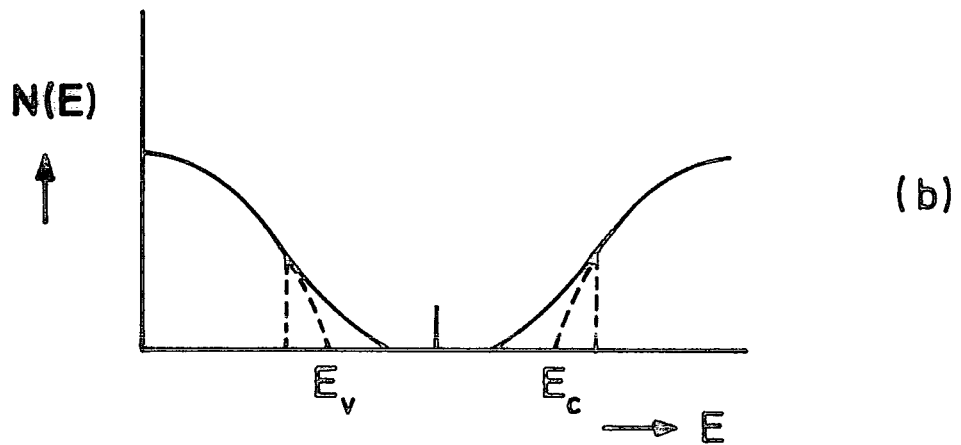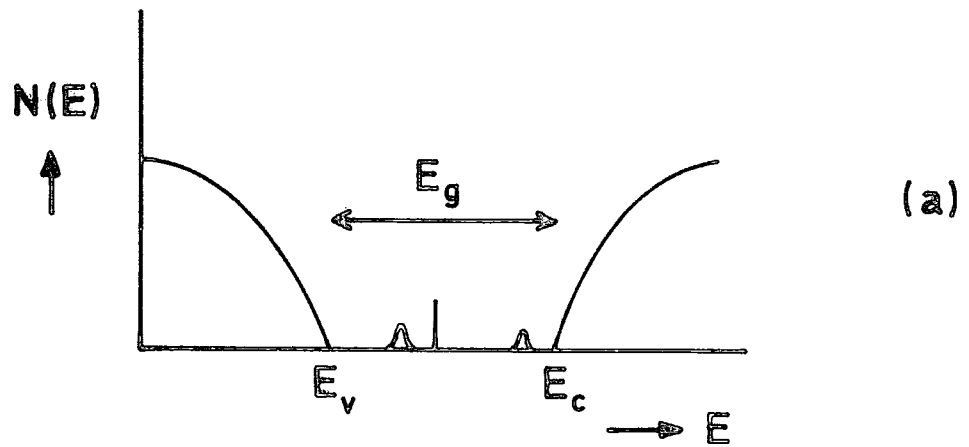
FIG. 2·2   DENSITY OF STATES N(E) versus E FOR
            (a) A CRYSTALLINE SEMICONDUCTOR
            (b) THE SAME SEMICONDUCTOR AS AN
                "IDEAL COVALENT GLASS"
            (c) A LARGELY DISORDERED AMORPHOUS
                SOLID

The localized states within the gap resulting from imperfect short range order will inevitably be divided equally between donor-like and acceptor-like states. Thus, the disorder of an amorphous semiconductor has an automatically self-compensating effect in creating electron and hole traps in equal numbers. As a result, the Fermi energy E_F is "pinned" to the central position of the gap. Conductivity in the localized states is forbidden and the mobility corresponding to them is zero. Thus, instead of an energy gap we have a mobility gap ΔE_μ which is a little bigger in value than E_g, the forbidden energy gap for a crystalline material.

Many theoretical papers have been written on the ideas presented in this sub-section. These have been reviewed and extended in a comprehensive treatment by Mott and Davies (1979).

2.3 OPTICAL PROPERTIES

2.3.1 Luminescence Emission

It is well known that the occurrence of lattice defects or the inclusion of impurities in a solid can give rise to optical absorption. On the other hand, the origin of fundamental optical absorption is either the excitation of vibrational modes or the promotion of electrons from a given set of energy states to others of higher energy. The emission of light is usually dominated by impurities even when their density is as low as 1 in 10^6. Thus a solid can absorb photons of one energy due to electronic transitions characteristic of the host lattice and in consequence, emit photons of a different (usually lower) energy, corresponding to a transition between impurity energy levels.

Figure 2.3 illustrates some of the possible electronic transitions which may take place with the emission of radiation.

Process A: Interband recombination of electrons and holes with photon emission. This event is relatively unlikely and only observed in high purity, high quality, single crystals. The width of the emission bands should be of the order of kT since the electrons and holes involved in
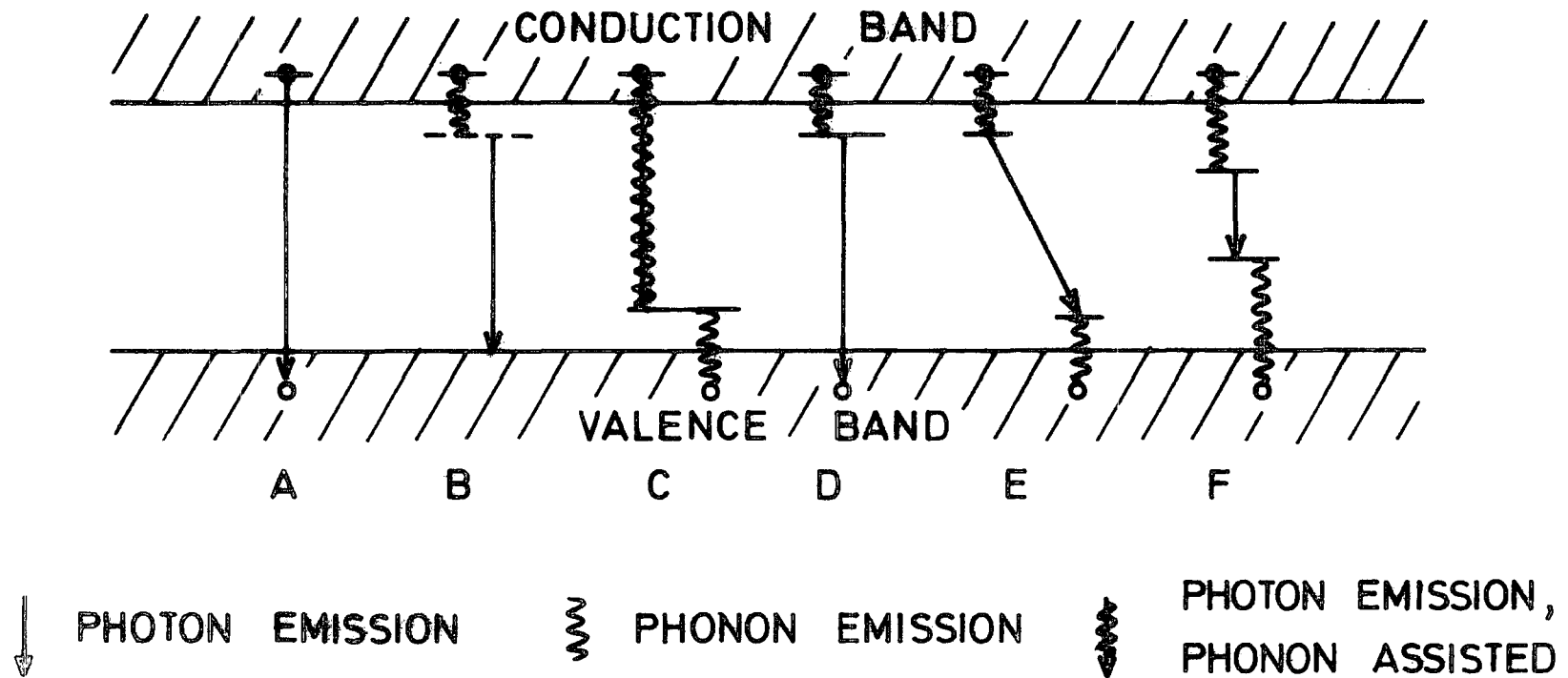
FIG. 2·3   EXAMPLES OF TRANSITIONS LEADING TO PHOTO EMISSION
          FROM SOLIDS

          A : INTER BAND TRANSITION
          B : RECOMBINATION VIA EXCITON STATES
          C,D : CONDUCTION BAND TO NEUTRAL ACCEPTOR , NEUTRAL
                DONOR TO VALENCE BAND TRANSITIONS
          E : DONOR LEVEL TO ACCEPTOR LEVEL TRANSITIONS
          F : RECOMBINATION VIA IMPURITY (EXCITED) STATES

this recombination process lie within this range of their respective band edges.

Process B : The Coulombic attractions of free electrons and holes leads to the formation of excitons. Their subsequent annihilation can be accompanied by the emission of photons. Exciton levels are well defined and sharp emission lines are to be expected. It is believed that there are four different types of bound excitons giving rise to emission lines known as the I_1, I_2, I_3 and I_4 lines. They correspond respectively to excitons bound to neutral acceptors and donors, and ionized donors and acceptors.

Processes C and D : Transitions between band edges and donor and acceptor impurities, which are quite common in solids. Frequently observed transitions are conduction band to neutral acceptor (Process C) and neutral donor to valence band (Process D). They may be phonon assisted.

Process E : Electrons captured at shallow donor impurity levels can recombine with holes captured at shallow acceptor levels. This type of process usually consists of a series of closely spaced lines which are often broadened to form a band.

Process F : Involves optical transitions between levels of a localized impurity which could involve the transition from an excited state to the ground state of a single impurity. This process need not be accompanied by photoconductivity.

Finally, it should be pointed out that recombination of holes and electrons can also take place non-radiatively. In the great majority of solids, non-radiative recombination with the emission of phonons is more likely than photon emission. Non-radiative recombination is often associated with impurities and crystal defects which provide intermediate energy levels between conduction and valence bands. In another non-radiative mechanism which is referred to as the Auger process, an electron

may make an interband transition on giving up energy to another electron in the conduction band, which is promoted to a higher state in the same band. The second electron then drops to the bottom of the band, i.e. thermalises, as it releases its energy by the successive emission of single phonons.

Luminescence emission in solids can be excited in a variety of ways :

(a) Photoluminescence :

Excitation by irradiation with light is known as photoluminescence. Absorption of light across the band gap leads to the generation of electrons and holes and optical emission by any of the processes A to F can then follow.

The II-VI group of phosphors can be made luminescent, that is activated,by the addition of certain impurities. These are of two types called activators (acceptors) and co-activators (donors). The common activator elements are copper, silver and manganese, which occupy group II cation lattice sites and behave as deep acceptor levels. Typical co-activator elements are the halides (Cl, Br, I) occupying anion sites, and aluminium, gallium and indium occupying cation sites. These usually form deep donor levels. In addition to defects created by deliberately added impurities, there are the native defects such as zinc and sulphur vacancies and they provide self-activation and co-activation for the luminescent II-VI compounds.

The location of the activator and co-activator levels in the forbidden gap and the energy transitions which involve luminescent emission can be represented basically in terms of the three general models illustrated in figure 2.4. The Schön-Klasens model (Schön, 1942, and Klasens, 1953) regards luminescence as a result of radiative recombination of an electron from the conduction band with a localized acceptor level above the valence band. Lambe and Klick (1955) proposed a model which
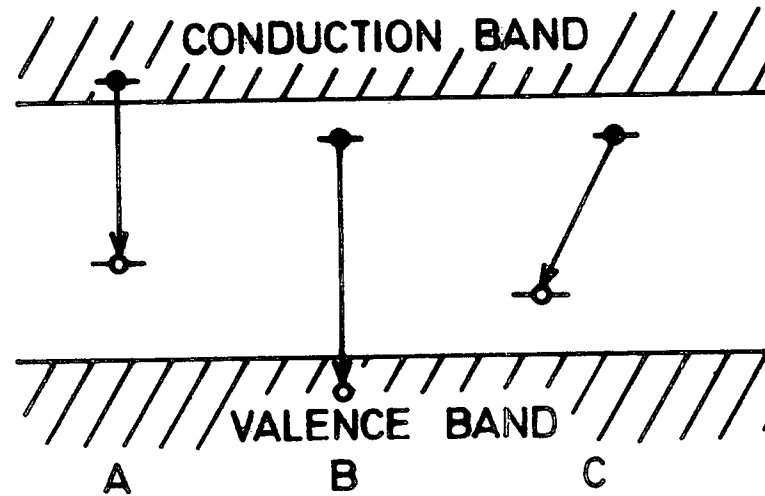
FIG. 2·4   ENERGY MODELS FOR LUMINESCENT EMISSION

IN II-VI COMPOUNDS

A : SCHÖN – KLASENS

B : LAMBE – KLICK

C : PRENER – WILLIAMS

describes the luminescent transition in terms of a free hole combining with a trapped electron at a level below the conduction band. The Prener-Williams model (Prener and Williams, 1956a) considered the emission of luminescence resulting from the recombination of electrons and holes trapped at localized centres in the same region of the lattice.

One major luminescence mechanism in most II-VI compounds is the so-called self-activated emission. Prener and Williams (1956b) suggested that a co-activator-vacancy complex was responsible for the ground state of a Schön-Klasens transition. The vacancy involved was later shown to be a zinc vacancy by Prener and Weil (1959) and Schneider et al (1965). This emission band can be easily distinguished since it is found to shift to shorter wavelengths on heating and it shifts to longer wavelengths with a change in co-activator from the anion, chlorine, to cation, aluminium.

(b) Cathodoluminescence :

Another way to excite the luminescence is by bombarding the solid with an electron beam. This is called cathodoluminescence. This process is usually less efficient than photoluminescence, because many electrons are back-scattered at the entry surface and also because electrons are excited to states high in the conduction band (hot electrons) from which most relax to the bottom of the band with phonon emission (Auger process). The luminescence efficiency may be increased by increasing the primary accelerating energy of the electrons to obtain deeper penetration, however, because of the generation of X-rays, cathode ray tubes are limited to operating voltages of around 15 kV.

(c) Thermoluminescence :

Thermoluminescence is another way in which luminescence can be excited in a solid. This process is explained by assuming the existence of isolated states (due to impurities or other crystal defects) lying below the conduction band which may trap electrons from the conduction band. We suppose that the probability of electronic transitions from these states

to holes in the valence band is negligibly small, but thermal excitation
to the conduction band is possible. Following some primary excitation
the traps store electrons for a period of time determined by their depth
and the temperature. On thermal release from a trap, an electron may
be either re-trapped or captured at a luminescent centre with the emission
of radiation. These processes are illustrated schematically in figure 2.5.
The emission of light on heating, after primary excitation, is known as
thermoluminescence. If the initial excitation is at low temperatures
and the temperature is subsequently raised rapidly and uniformly in the
dark, bright thermoluminescence is obtained whenever a group of traps of
given depth is thermally emptied. Thermally stimulated conductivity due
to the release of electrons from traps into the conduction band also
accompanies thermoluminescence.

2.3.2 Photoconductivity

In discussing photoconductivity it is important to define the
concept of photosensitivity. According to Bube (1978), this term is the
photoconductivity of a solid per unit excitation, i.e. the change in
conductivity caused by excitation, divided by the excitation intensity.
Semiconductors of very high resistivity have, in general, a low sensitivity.
Enhancement of the photosensitivity is achieved by the deliberate intro-
duction of impurity elements. This process is well understood in CdS which
has been successfully made highly photosensitive by introducing halogen or
some group III b impurities. When introducing these donors, an equal
concentration of cadmium vacancies appear for charge compensation. Suitable
doping produces values of about 10^{-2} and 10^{-8} s for the free electron and
free hole lifetimes. In insensitive material, the free electron lifetime
is less than 1 μs. The dramatic increase in the electron lifetime on
sensitization is the key feature. In insensitive photoconductors, the
recombination centres are termed Class I centres while the sensitizing
centres which appear after the introduction of the appropriate impurities
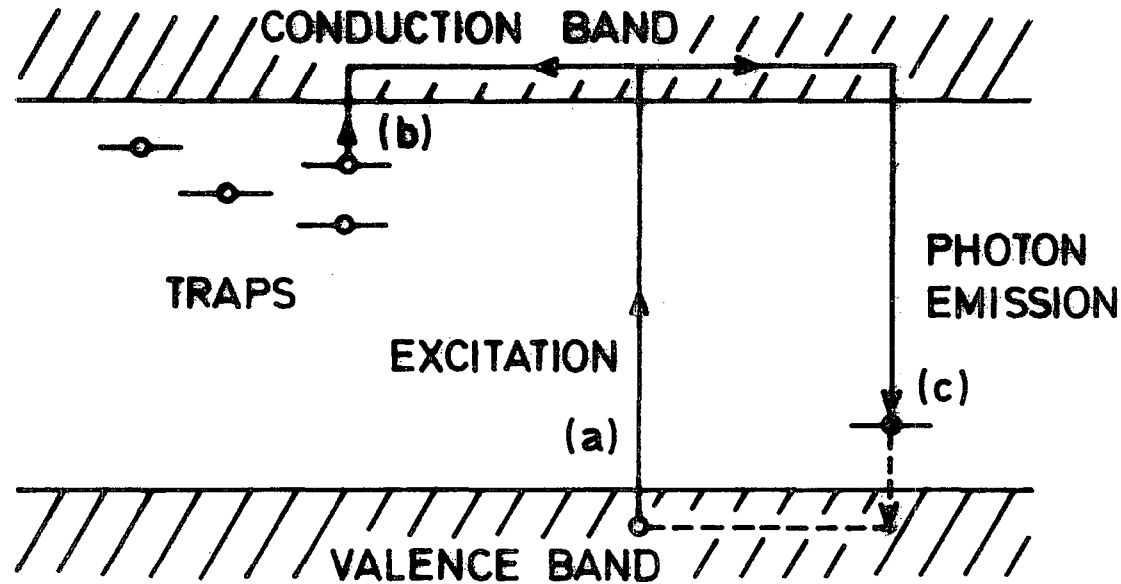
FIG. 2·5 A POSSIBLE ELECTRON TRAP MECHANISM FOR THERMO-LUMINESCENCE

(a) TRAPS ARE INITIALLY FILLED BY SOME EXTERNAL EXCITATION AT LOW TEMPERATURE.

(b) ON HEATING, ELECTRONS ARE LIBERATED FROM THE TRAPS TO THE CONDUCTION BAND.

& (c) THEY ARE EVENTUALLY EITHER RETRAPPED OR RECOMBINE WITH A HOLE GIVING UP THEIR ENERGY AS $h\omega$ EMISSION.

are called class II centres.

The model illustrating this process is shown in figure 2.6 for an n-type photoconductor. Part (a) of this figure shows an unsensitized material with its class I centres. These recombination centres have a large capture cross-section for both electrons and holes, leading to a small free electron lifetime. When class II centres are introduced, they act as recombination centres or as hole traps, depending on their location with respect to the so-called hole demarcation level. If they lie below the demarcation level, figure 2.6(b),they act as hole traps and hence do not change the electron recombination pattern and thus have no effect on the free electron lifetime. However, for high light intensities and/or at low temperatures, the hole demarcation level will move towards the valence band and when it falls below the class II centres, they will behave as recombination centres, figure 2.6(c). Since the capture cross-section of the class I centres for free electrons is much greater than the capture cross-section of the class II centres for electrons, the holes will have a longer lifetime in the class II centres. Class II centres will now be occupied mainly by holes, hence the electrons which were initially in class II centres have been transferred to class I centres, thus filling these so that they no longer act as recombination centres. The lifetime of the free electrons is then increased because they now have to recombine through class II centres.

This model is well accepted and explains satisfactorily the phenomena of superlinearity and thermal and optical (infrared) quenchings.

(a) Superlinearity :

The sensitizing process depends on the light intensity. When a photoconductor is illuminated at a fixed temperature, the positions of the Fermi and demarcation levels depend on the intensity of the light. At low light intensity, the hole demarcation level is above the class II centres which therefore act as hole traps. In this regime, a sub-linear
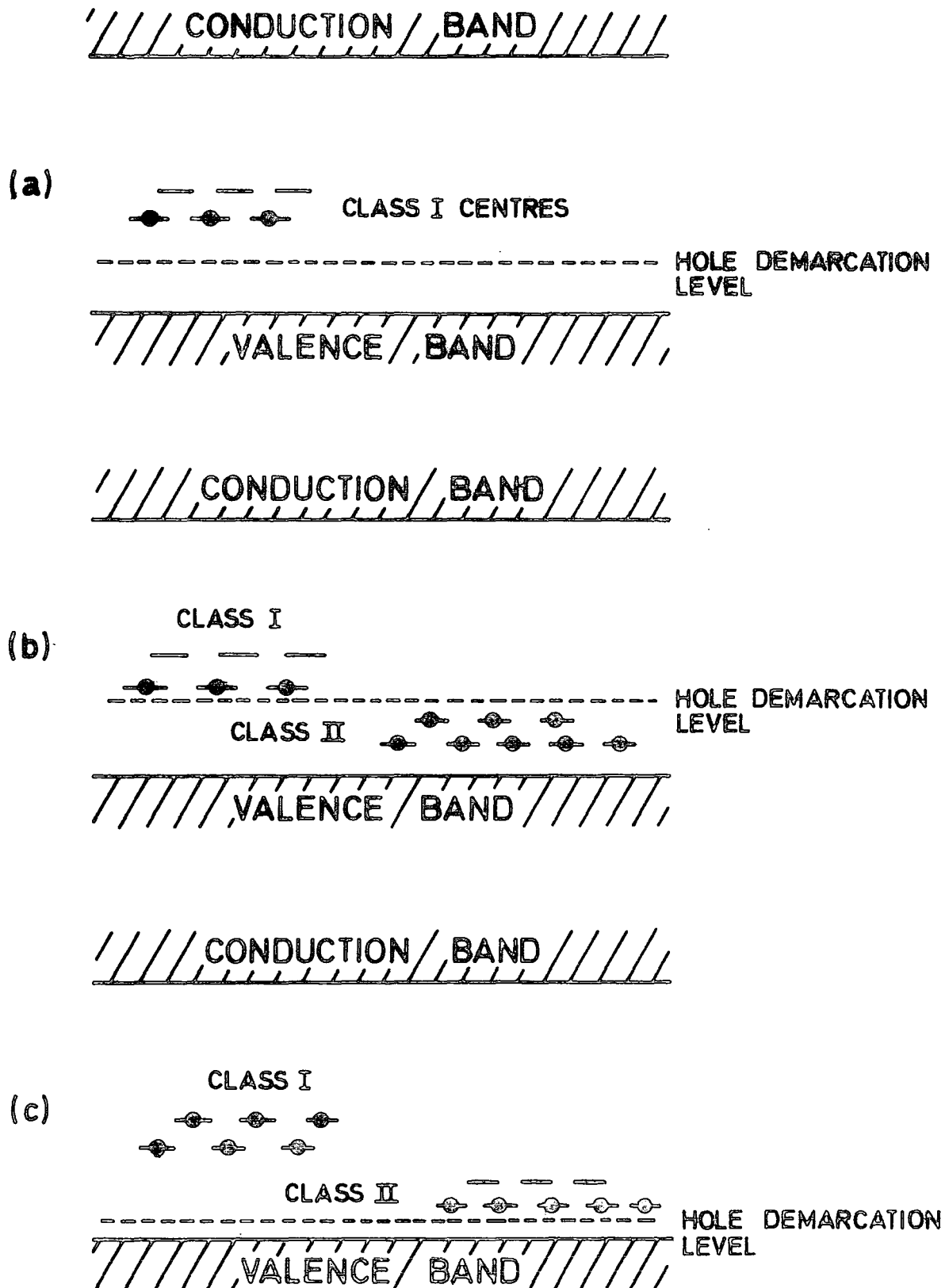
FIG. 2·6 SENSITIZATION OF A PHOTOCONDUCTOR BY THE INCORPORATION OF CLASS II CENTRES TO ENHANCE IT'S PHOTOSENSITIVITY.

(a) & (b), INSENSITIVE STAGE

(c) SENSITIVE

or nearly linear dependence of the photoconductivity on light intensity
is obtained, depending on electron trapping effects. When the illumination
intensity is further increased, the hole demarcation level moves towards
the valence band, and when it passes through the class II centres, they
are converted into recombination centres and, as a result, the photocurrent
increases rapidly and superlinearily with light intensity. Once the hole
demarcation level is below the class II centres, the variation of photo-
conductivity with light intensity will again be affected by the electron
traps and the response becomes sub-linear (the value of the exponent
of the power law dependence on light intensity is determined by the number
and distribution of traps for the sub-linear regime, and lies between 0.5
and almost 1, Rose, 1951). Nevertheless, in this last stage, the free
electron lifetime has been enhanced by the sensitization process. From
the variations of the breakpoints (i.e. where the behaviour changes from
sub-linear to superlinear and back to sub-linear) with light intensity and
temperature, it is possible to estimate the thermal ionisation energy of
the class II centres as well as the ratio of their hole capture cross-section
to their electron capture cross-section (Sp/Sn). The ratio of the density
of class I and class II centres can also be determined.

(b) Thermal Quenching:

The mechanism of thermal quenching is considered as the thermal
desensitization of a sensitized photoconductor containing class I and
class II centres. As the temperature is raised, at constant light intensity,
the hole demarcation level moves towards the conduction band. When it
passes through the class II centres, there will be a decrease in the free
electron lifetime resulting in a net reduction of the photoconductivity, i.e.
the photoconductor is desensitized. At higher light intensities, thermal
quenching occurs at higher temperatures. According to this argument, the
superlinear variation of photocurrent with light intensity occurs in the
region where thermal quenching is taking place.

(c) Infrared Quenching :

This occurs when the photocurrent of a sensitized crystal excited with band or near band gap light, is reduced on irradiation with infrared from a second source. With the first light source alone, electron recombination proceeds via the class II centres and the class I centres are filled with electrons and are thus inoperative. Irradiation from a second source with infrared photons of suitable energy, excites electrons from the valence band to the class II centres. The resulting free holes are captured by the class I centres which become active again for fast recombination, so that decrease in the photoconductivity takes place. By studying the spectral distribution of photocurrent as a function of the wavelength of the light from the second source, it is possible to estimate the separation of class II centres from the valence band.

2.3.3 Thermally Stimulated Current and Luminescence

As explained previously, thermoluminescence, also known as thermally stimulated luminescence (TSL) which is similar to thermally stimulated conductivity (TSC), is a phenomenon in which the crystal is photo-excited at a low temperature in order to fill the traps. On heating, carriers are thermally released from traps and these either recombine at recombination centres giving rise to bursts of light, or in the case of TSC, increase the conductivity. The mechanism is a non-equilibrium process since the temperature is changing with time, hence the kinetics associated with it can be quite complex. Much has been said and written about these two phenomena and so far no unanimous agreement about the solutions to the rate equations exists. Nevertheless, TSL and TSC are widely used with many phosphors and photoconductors, since the experimental technique is relatively easy.

The physical model used to describe TSC and TSL is the one depicted in the diagram of figure 2.5. The appropriate equations are :

$$\frac{d\,n_t}{dt} = n\,(N_t - n_t)\,\beta - \gamma n_t \qquad (2.55)$$

$$\frac{dn}{dt} = -\frac{d\,n_t}{dt} - \alpha\,n\,a_t \qquad (2.56)$$

where the following symbols are used : N_t : trap density ; n_t : concentration of trapped electrons ; n : concentration of free electrons ; a_t : concentration of holes trapped at recombination centres; β: trapping rate constant; α: recombination rate constant; γ: transition probability for electrons from trap to conduction band. Equations 2.55 and 2.56 govern the process of emptying the N_t trap as a function of time. During this process, the condition of charge neutrality, if no free holes are present, is

$$a_t = n + n_t \cdot \qquad (2.57)$$

Here, it must be emphasized that the occupation of any other trap does not change while the processes described by 2.55 and 2.56 are taking place.

If E is the trap depth, then

$$\gamma = s\,\exp\,(-E/kT) \qquad (2.58)$$

where s is the attempt to escape frequency which is given by

$$s = \beta\,N_c/g \quad \cdot \qquad (2.59)$$

N_c is the effective density of states and g is the degeneracy factor of the set of traps (it will be taken as 1). In addition,

$$\alpha = S_r V \quad \text{and} \quad \beta = S_t V \qquad (2.60)$$

V is the mean thermal velocity of the free electrons and S_r and S_t are the cross-sections for capture of electrons at the recombination centres and the traps respectively.

The conductivity σ_n is given by

$$\sigma_n \quad = \quad ne \ \mu_n \qquad\qquad (2.61)$$

and the integrated luminescence intensity is proportional to the change of the occupation of the recombination centre, i.e. da_t/dt.

In making TSC measurements it is assumed that the conductivity may be measured using two contacts only and therefore, they must be ohmic. The carrier mobility is of course a function of temperature, but many workers neglect this since the variation is slow compared with the changes in n when a trap empties.

In most experiments, the heating rate given by

$$w \quad = \quad \frac{dT}{dt} \qquad\qquad (2.62)$$

is kept constant, so that

$$T \quad = \quad T_o \ + \ wt \ \circ \qquad\qquad (2.63)$$

Solutions to equations 2.55 and 2.56 are usually obtained for two limiting and one intermediate case, namely:

(A) Monomolecular recombination (no retrapping), where

St < < Sr   or, α > > β;

(B) Bimolecular recombination, where St = Sr, and,

(C) Fast retrapping, where St > > Sr or α << β.

Further **simplifications are usually considered**:

(a) The free electron lifetime τ_n is small enough so as to have

$$\frac{n}{\tau_n} \ = \ \alpha \ n \ a_t \ >> \ \frac{dn}{dt},$$

where $\tau_n \ = \ (\alpha \ a_t)^{-1}$ \qquad\qquad (2.64)

and

(b) $n \ll n_t$, i.e. there are many more trapped than free electrons in the system.

With these two approximations, equations 2.55 and 2.56 can be re-written as

$$\frac{d\, a_t}{dt} = - \frac{\gamma\, a_t^2}{a_t\,(1-\delta) + \delta\, N_t} \qquad (2.65)$$

where δ , the retrapping ratio, is given by

$$\delta = \frac{\beta}{\alpha} \qquad (2.66)$$

and, (from equations 2.56 and 2.57),

$$n = -\tau_n \frac{d\, a_t}{dt} = \frac{\gamma\, a_t}{\alpha \left[a_t\,(1-\delta) + \delta\, N_t \right]} \qquad . \qquad (2.67)$$

The solutions for $\delta = 1$ (bimolecular recombination) and $\delta \ll 1$ (fast retrapping) will now be considered :

(b) When $\delta = 1$, equations 2.65 and 2.67 reduce to,

$$\frac{d\, a_t}{dt} = -\frac{\gamma\, a_t^2}{N_t} \quad (2.68) \quad \text{and} \quad n = \frac{\gamma\, a_t}{\alpha\, N_t} \qquad (2.69)$$

(c) When $\delta \ll 1$, equations 2.65 and 2.67 become,

$$\frac{d\, a_t}{dt} = - \frac{a_t\, \beta\, N_c\, \exp\,(-E/kT)}{1 + \delta\, N_t/a_t} \qquad (2.70)$$

and

$$n = \frac{\delta\, N_c\, \exp\,(-E/kT)}{1 + \delta\, N_t/a_t} \qquad . \qquad (2.71)$$

Now we proceed to review a few of the methods described in the literature of determining trap depths using equations 2.65 and 2.67.

(i) The method which is perhaps the most utilized is that first suggested by Garlick and Gibson (1948). Taking logarithms of equations 2.65 and 2.67, we obtain,

$$\ell n \left(- \frac{d\, a_t}{dt} \right) = - \frac{E}{kT} + \ell n \left[\frac{s\, a_t^2}{a_t(1-\delta)\, +\, \delta\, N_t} \right] \qquad (2.72)$$

and

$$\ell n\, n = - \frac{E}{kT} + \ell n \left\{ \frac{s\, a_t}{\alpha\, \left[a_t\, (1-\delta)\, +\, \delta\, N_t \right]} \right\} \qquad (2.73)$$

In the initial part of the TSL and TSC trap emptying processes, where a_t and s do not change appreciably compared with the fast exponential increase of γ with T, a further approximation is employed :

$$\ell n \left\{ - \frac{d\, a_t}{dt} \right\} \Bigg|_{init.} \simeq - \frac{E}{kT} \qquad (2.74)$$

and

$$\ell n\, n \Bigg|_{init.} \simeq - \frac{E}{kT} \, . \qquad (2.75)$$

Thus, a plot of the natural logarithm of the initial part of either the TSL or TSC curves, versus reciprocal of temperature, should give a straight line with a slope of $- E/k$.

Some methods rely on making measurements with different values of the heating rate w :

(ii) Here we have to consider the magnitudes of various quantities at the TSC and TSL maxima. For example, $d\, a_{tL}/dt$, T_L and n_c, a_{tc}, T_c, where the subscripts L and c stand for TSL and TSC maxima respectively.

The equations 2.72 and 2.73 can be re-written

$$\ln \left\{ - \frac{d\,a_{tL}}{dt} \right\} = - \frac{E}{k\,T_L} + C_1 \qquad (2.76)$$

and

$$\ln n_c = - \frac{E}{k\,T_C} + C_2 \qquad (2.77)$$

where it has been assumed that a_{tL} and a_{tc} do not depend on w as strongly as $d\,a_{tL}/dt$ and n_c do, and C_1 and C_2 are constants which depend on the values of a_{tL} and a_{tc} respectively. Hence, a plot of $\ln(-d\,a_{tL}/dt)$ or $\ln n_c$ versus $1/T_L$ or $1/T_C$ respectively, for several values of the heating rate, should give straight lines with slopes of $-E/k$. This method was derived by Bube (1955) for TSC only.

(iii) Instead of using the temperature of the maxima in equations 2.76 and 2.77, the temperature T_1, at the lower temperature side of the peak where the intensity equals half its maximum value can be employed. Then, making the same assumptions as above, the following expression is derived :

$$\ln \left\{ - \frac{d\,a_{tL}}{d\,a_t} \right\} = - \frac{E}{k\,T_1} + C_1 - \ln 2 \qquad (2.78)$$

Thus the logarithmic plot of the maximum light intensity is made against $1/T_1$. This is Unger's (1962) method.

At the TSL and TSC maxima, the slopes of each curve are zero, so that when equations 2.65 and 2.67 are differentiated with respect to temperature, the result is identically zero. However, we must allow for the possible variations of s and α with temperature which, according to Chen and Fleming (1973), are as follows :

$$\alpha = \alpha_o \left\{ \frac{T}{T_o} \right\}^b \quad , \text{ with } -3.5 \leqslant b \leqslant 0.5 \qquad (2.79)$$

and, because of the $T^{3/2}$ dependence of N_c,

$$s = s_o \left\{ \frac{T}{T_o} \right\}^c \quad , \text{ with } -2 \leqslant c \leqslant 2 \tag{2.80}$$

where α_o, s_o and T_o are constants.

We will consider first the situation when b = c = 0 :

(iv) Hoogenstraaten's (1958) method :

When $\delta \ll 1$ (fast retrapping), it may be assumed that $a_t \alpha \ll \beta N_t$ on the lower temperature side of the TSL peak, and for almost all its rising limb, thus equation 2.70 is further reduced to

$$\frac{d a_t}{dt} = - a_t \gamma \quad . \tag{2.81}$$

Differentiating both sides with respect to the temperature gives

$$\frac{d}{dT} \left\{ \frac{d a_t}{dt} \right\} = - \gamma \frac{d a_t}{dT} - a_t \frac{d\gamma}{dt} \tag{2.82}$$

from which, using equations 2.58 and 2.62, we get,

$$\frac{d a_t}{dT} = \frac{1}{W} \frac{d a_t}{dt} \quad \text{and,} \tag{2.83}$$

$$\frac{d\gamma}{dT} = \frac{ds}{dT} \exp \left(-E/kT \right) + \frac{s E}{kT^2} \exp \left(-E/kT \right), \tag{2.84}$$

therefore, at $T = T_L$ and $a_t = a_{tL}$,

$$0 = \frac{a_{tL}}{W} s^2 \exp \left\{ - \frac{2 E}{kT_L} \right\} - \frac{a_{tL} s E}{kT_L^2} \exp \left\{ - \frac{E}{kT_L} \right\},$$

i.e.,

$$\frac{E W}{kT_L^2} = s \exp \left(-E/kT_L \right) \tag{2.85}$$

from which a plot of $\ln (W/T_L^2)$ versus $1/T_L$ should yield a straight line with slope $-E/k$. This method is also valid for $\delta = 1$ (i.e. bimolecular recombination) since, by differentiating 2.68 again, with respect to temperature, we obtain,

$$\frac{d}{dT} \left\{ \frac{d\, a_t}{dt} \right\} = - \frac{a_t^2}{N_t} \frac{d\gamma}{dT} - \frac{2\gamma\, a_t}{N_t} \frac{d\, a_t}{dT} , \qquad (2.86)$$

and using equations 2.58, 2.68, 2.83 and 2.84, with $T = T_L$ and $a_t = a_{tL}$,

$$0 = - \frac{s\, E\, a_{tL}^2}{N_t\, kT_L^2} \exp \left(- \frac{E}{kT_L} \right) + \frac{2\, a_{tL}^3\, s^2}{W\, N_t^2} \exp \left\{ - \frac{2\, E}{k\, T_L} \right\}$$

$$(2.87)$$

and, rearranging,

$$\frac{W\, E}{k\, T_L^2} = \frac{2\, a_{tL}\, s}{N_t} \exp \left(- \frac{E}{kT_L} \right) \qquad (2.88)$$

which is equivalent to equation 2.85. Now, for TSC in the case $\delta = 1$, differentiating equation 2.69

$$\frac{dn}{dT} = \frac{n}{\gamma} \frac{d\gamma}{dT} + \frac{n}{a_t} \frac{d\, a_t}{dT} - \frac{n}{\alpha} \frac{d\alpha}{dT} \qquad (2.89)$$

and using equations 2.58, 2.68, 2.83 and 2.84 with $T = T_c$ and $a_t = a_{tc}$,

$$0 = \frac{E}{kT_c^2} - \frac{a_{tc}\, s}{W\, N_t} \exp \left\{ - \frac{E}{kT_c} \right\} \qquad (2.90)$$

we obtain,

$$\frac{E\, W}{kT_c^2} = \frac{a_{tc}\, s}{N_t} \exp \left\{ - \frac{E}{kT_c} \right\} \qquad (2.91)$$

which again is equivalent to equation 2.85. Once again a plot of $\ln(W/T_c^2)$ versus $1/T_c$ should yield a straight line with slope $-E/k$.

(v) Method of Chen and Winer (1970):

For the case of $\delta = 1$, if we use equations 2.76 (Bube's method) and substract from it equation 2.88 (Hoogenstraaten method) previously squared, we find

$$\ln\left\{-\frac{d\,a_{tL}}{dt}\right\} - \ln\frac{W^2 E^2}{k^2 T_L^4} = \frac{E}{kT_L} + C_1 - 2\ln\frac{2\,a_{tL}\,s}{N_t} \qquad (2.92)$$

or,

$$\ln\left[\left\{-\frac{d\,a_{tL}}{dt}\right\}\frac{k^2 T_L^4}{W^2 E^2}\right] = \frac{E}{k\,T_L} + C_3 \qquad (2.93)$$

where C_3 is

$$C_3 = C_1 - 2\,\ln\frac{2\,a_{tL}\,s}{N_t} \qquad (2.94)$$

Then, from equation 2.93, it follows that a plot of the natural logarithm of the value of the intensity at the TSL maximum (i.e. $d\,a_{tL}/dt$) multiplied by T_L^4/W^2 versus $1/T_L$ yields a straight line with E/k as slope. Moreover, because this method is derived from the methods of Bube and Hoogenstraaten, it is also valid for $\delta \ll 1$ and for TSC. In general, the trap depths calculated with these three methods are related according to

$$E(\text{Chen and Winer}) = 2E(\text{Hoogenstraaten}) - E(\text{Bube}). \qquad (2.95)$$

Now let us consider the case in which α and s are temperature dependent, i.e. $b \neq o$ and $c \neq o$. For this, equation 2.67 is transformed, using equations 2.79 and 2.80, to

$$n = \frac{s_o\,a_t\,T_o^{b-c}\,T^{c-b}\,\exp(-E/kT)}{\alpha_o\left[a_t\,(1-\delta) + \delta\,N_t\right]} \qquad (2.96)$$

or,

$$\ln\left\{\frac{n}{T^{c-b}}\right\} = -\frac{E}{kT} + C_4 \tag{2.97}$$

with

$$C_4 = \ln\left\{\frac{s_o \, T_o^{\,b-c} \, a_t}{\alpha_o \left[a_t(1-\delta) + \delta \, N_t\right]}\right\} \tag{2.98}$$

(vi) Boiko et al (1960) assumed c-b = 3/2, hence, they obtained for the TSC maximum :

$$\ln\left\{\frac{n_c}{T_c^{\,3/2}}\right\} = -\frac{E}{kT_c} + C_4 \tag{2.99}$$

from which a plot of $\ln(n_c/T_c^{\,3/2})$ versus $1/T_c$ should give a straight line with slope equal to -E/k. This procedure is known as the method of Boiko, Rashba and Trofimenko 1.

(vii) The same authors have also evolved another method (Boiko, Rashba and Trofimenko 2) which applies when δ= 1 and to the TSC maximum. By differentiating equation 2.69 again and extending equation 2.84 with equation 2.80

$$\frac{ds}{dT} = \frac{s_o \, c}{T_o}\left\{\frac{T}{T_o}\right\}^{c-1} = \frac{s \, c}{T} \tag{2.100}$$

Equation 2.84 is therefore converted to

$$\frac{d\gamma}{dT} = \frac{\gamma c}{T} + \frac{\gamma \, E}{k \, T^2} = \frac{\gamma}{T}\left(c + \frac{E}{kT}\right) \tag{2.101}$$

where equation 2.58 has been used ; also, from equation 2.79 :

$$\frac{d\alpha}{dT} = \frac{\alpha_o \, b}{T_o}\left\{\frac{T}{T_o}\right\}^{b-1} = \frac{\alpha b}{T} \tag{2.102}$$

hence, with equations 2.68, 2.83, 2.100, 2.101 and 2.102, equation 2.89 is transformed to

$$\frac{dn}{dT} = \frac{n}{T} \left(c + \frac{E}{kT} \right) - \frac{n \, a_t \gamma}{W \, N_t} - \frac{nb}{T} \qquad (2.103)$$

which, for $T = T_c$ and $a_t = a_{tc}$ and using equation 2.58, gives,

$$0 = (c-b) \frac{W}{T_c} + \frac{W \, E}{kT_c^2} - \frac{a_{tc}}{N_t} \, s_o \left\{ \frac{T_c}{T_o} \right\}^c \exp - \left\{ \frac{E}{kT_c} \right\} \qquad (2.104)$$

and re-arranging,

$$\frac{W \, E}{k \, T_c^{c+2}} - (b-c) \frac{W}{T_c^{c+1}} = \frac{a_{tc}}{N_t} \frac{s_o}{T_o^c} \exp \left\{ - \frac{E}{kT_c} \right\} . \qquad (2.105)$$

As a first approximation, it is possible to neglect the second term on the LHS, then,

$$\frac{W \, E}{k \, T_c^{c+2}} = \frac{a_{tc} \, s_o}{N_t \, T_o^c} \exp \left\{ - \frac{E}{k \, T_c} \right\} \qquad (2.106)$$

which reduces to equation 2.91 for $c = o$. Taking $c = 3/2$, equation 2.106 reduces to

$$\frac{W \, E}{k \, T_c^{7/2}} = \frac{a_{tc} \, s_o}{N_t \, T_o^{3/2}} \exp \left\{ - \frac{E}{k \, T_c} \right\} \qquad (2.107)$$

thus, a plot of $\ln \, (W/T_c^{7/2})$ versus $1/T_c$ gives a straight line with $- E/k$ as slope.

(viii) Method of Böer, Oberländer and Voigt (1958) :

Starting with equation 2.68 for $\delta = 1$ and differentiating with respect to T gives equation 2.86 ; now, using equations 2.58, 2.68, 2.80 ,

2.83 and 2.100 and the fact that the slope of the TSL curve at $T = T_L$, for which $a_t = a_{tL}$ is zero, we obtain,

$$0 = -\frac{1}{T_L}\left\{c + \frac{E}{kT_L}\right\} + \frac{2\,a_{tL}}{W\,N_t}\,s_o\left\{\frac{T_L}{T_o}\right\}^c \exp\left\{-\frac{E}{kT_L}\right\} \cdot (2.108)$$

Neglecting c with respect to E/kT_L, we obtain :

$$\frac{W\,E}{k\,T_L^{c+2}} = \frac{2\,a_{tL}\,s_o}{N_t\,T_o^c}\,\exp\left\{-\frac{E}{k\,T_L}\right\} \qquad (2.109)$$

which is equivalent to equation 2.106 for the TSC case. This equation is also valid for $\delta \ll 1$, since, starting from equation 2.81 and following the equivalent procedure as for equation 2.108, we obtain,

$$0 = \frac{s_o}{W}\left\{\frac{T_L}{T_o}\right\}^c \exp\left\{-\frac{E}{kT_L}\right\} - \frac{1}{T_L}\left\{c + \frac{E}{k\,T_L}\right\} \qquad (2.110)$$

or, again, neglecting c with respect to $E/k\,T_L$,

$$\frac{W\,E}{k\,T_L^{c+2}} = \frac{s_o}{T_o^c}\,\exp\left\{-\frac{E}{k\,T_L}\right\} \qquad (2.111)$$

which is equivalent to equation 2.109, therefore for $c = -2$, we have,

$$\frac{W\,E}{k} = D\,\exp\left\{-\frac{E}{k\,T_L}\right\} \qquad (2.112)$$

where $D = \dfrac{s_o}{T_o^c}$ for $\delta \ll 1$ and,

$$D = \frac{2\,a_{tL}\,s_o}{N_t\,T_o^c} \quad \text{for } \delta = 1$$

thus a plot of $\ln W$ versus $1/T_C$ or $1/T_L$ for several heating rates, should

yield a straight line with a slope of $-E/k$.

In summary, it can be said that these eight methods are valid

for both TSC and TSL and that they are, to a certain extent, independent

of the retrapping ratio δ.

This is not the complete story of TSC and TSL curve analysis.

Besides these eight methods presented above, there are numerous other

methods available from the literature. Some will be mentioned in chapter

five. New methods are still being developed, and, Maeta and Saguchi

(1980a, 1980b) recently introduced some further ideas in the determination

of trap depths from TSC measurements.

CHAPTER 3

PROPERTIES OF ZINC SELENIDE

3.1   CRYSTAL AND BAND STRUCTURE

As early as 1961 (Aven et al , 1961) it was hinted that there was a direct gap in ZnSe near k = 0. After this, when electrical properties could be measured in n-type ZnSe, a minimum of the conduction band was taken to be at k = 0 and an effective mass for electrons at the bottom of this band of $0.15\ m_e$ was obtained (Aven and Segall , 1963). This value of the effective mass m* was reasonably close to that of $0.17\ m_e$ determined from Faraday rotation studies by Marple (1964). Optical absorption in the near-threshold region (i.e. in the region of the excitation peak) has been studied by transmission on single crystals of ZnSe heat treated in liquid zinc by Hite et al (1967). Comparison was made with similar results on CdTe and no evidence was found for an indirect bandgap. The absorption measurements of Hite et al therefore support the direct gap model. Furthermore, they obtained a hole effective mass $m_h \approx 0.75\ m$.

A direct energy gap seems to be a general characteristic of the band structure of the zinc and cadmium chalcogenides. This indicates that they should be very useful for devices which require high optical absorption or efficient emission of radiation without phonon participation. The crystal structure is determined by the type of bonding which, in the II-VI compounds leads to both cubic (zinc blende) and hexagonal (wurtzite) structures.

This is a result of the covalent contribution to the bonding which produces a tetrahedral coordination in most II-VI compounds. Each of the crystal structures possesses its own Brillouin zone structure ; the shape of the Brillouin zone for the cubic structure is a truncated octahedron. The high symmetry points and lines of the Brillouin zone for this structure are the

zone centre (Γ) and the intersection with the zone faces on the (100),
(110) and (111) symmetry axes. The energy bands for ZnSe along these axes
have been calculated by the pseudo-potential method (Cohen and Bergstresser ,
1966 , and Bergstresser and Cohen , 1967) using data from Aven et al (1961)
and Aven and Segall (1963).

The direct minimum energy gap centred on the Γ point for ZnSe was
found to be 2.8 eV. Another result from the band structure calculations is
the fact that the valence band is six-fold degenerate at k = 0. It may be
split into a four-fold state and a lower two-fold one. The two states are
usually denoted as Γ_8 and Γ_7 respectively. The Γ_8 is itself split into two
parabolic bands termed V_1 and V_2.

The tetrahedral lattice sites which characterize the cubic and
hexagonal structures, suggest that homopolar, i.e. highly directional bonding
is present. The homopolar bond is better understood in terms of a tetrahedral
atom where the electronic wave functions are taken to be sp^3-hybridized and
combined in four independent ways to give this highly directional character
to the bond, which is directed towards the corners of the tetrahedron. How-
ever, there may also be an exchange of electrons among the different atoms,
resulting in an ionic coulombic attraction which is typical of the ionic bond.
The ionic character increases as the atomic weight decreases, i.e. from HgTe
to ZnS ; it also increases with increasing electronegativity difference be-
tween the two constituents. The ionic bond has the effect of strengthening
the lattice, raising the melting point and increasing the energy gap.

As stated above, ZnSe crystals can exist in either the cubic or
hexagonal structure. The existence of each depends on the conditions during
growth but, the cubic is the more stable phase at room temperature. This
structure is similar to that of diamond and consists of two interpenetrating
face centred cubic lattices. The different zinc or selenium ions occupy the
points of the two sub-lattices.

3.2   THE ELECTRICAL PROPERTIES OF ZnSe

One of the first investigations of the transport properties of ZnSe was carried out by Aven and Woodbury (1962) who showed that a marked reduction of the very high resistivity (10^{10} - 10^{12} Ωcm) of as-grown ZnSe crystals could be achieved by heating them in molten zinc. These authors also showed that this process leaches trace impurities of copper out of the crystal because the copper is more soluble in the molten zinc than in the crystal. Since then, several workers have made Hall mobility measurements, in order to esti- mate the purity of their crystals. So far, the highest value of Hall mobility obtained for n-type ZnSe crystals heated in molten zinc is 1.2×10^4 $cm^2 v^{-1} s^{-1}$ measured at 50 K by Aven (1971). At room temperature, the values obtained by most workers lie between 300 $cm^2 v^{-1} s^{-1}$ and just under 600 $cm^2 v^{-1} s^{-1}$.

The interpretation of the Hall mobility measurements seems well es- tablished, as far as highly conductive n-type ZnSe is concerned. The main scattering mechanisms limiting the electron mobility are polar optical scat- tering, at temperatures above 150 K, and ionized impurity scattering at very low temperatures (< 40 K), while a combination of both is effective in the intermediate region (see Fukuda and Fukai, 1967 , and Aven, 1971). Some workers have found Hall mobilities decreasing exponentially with temperature below 50 K, Jones and Woods (1976), Nedeoglo (1977) and Sethi et al (1978a) and they have explained their results in terms of carrier conduction via an impurity band.

However, the difficulty in fitting a complete set of experimental values to a full continuous theoretical curve still remains. Consequently some workers have recently been looking into this in more detail and have in- troduced slight variations in the theoretical assumptions in order to obtain better fits with their experimental results, Sethi et al (1977), Ray and Kröger (1979), Shmelev and Tsurkan (1979) and Emelyanenko et al (1979).

For less conductive n-type ZnSe crystals (i.e. with $\sigma < 10^{-3}$ $\Omega^{-1} cm^{-1}$) the maximum mobility values reported are very small ($\mu_H < 100$ $cm^2 v^{-1} s^{-1}$) .

At room temperature and above, the reported mobility values were found to increase with temperature, Jones and Woods (1976) and Sethi et al (1978a, 1979).

All the Hall measurements in undoped ZnSe crystals heated in molten zinc indicate values of donor ionization energies between 8 and 30 meV which is very close to the hydrogenic value, Aven (1971) and Woodbury and Aven (1974).

Measurements in untreated undoped ZnSe have been reported by Heaton et al (1972) and by Yu and Park (1973). These last two workers made conductivity measurements in the temperature range 320-380 K and obtained resistivities between 10^{10} and 10^{12} Ω cm and an activation energy of 0.92 eV. Yu and Park associated this value with a deep donor level produced by an intrinsic defect such as selenium vacancies.

With as-grown crystals of indium or gallium doped ZnSe, Jones and Woods (1976) found levels below the conduction band at 0.02 and 0.2 eV for ZnSe:In and at 0.07 and 0.13 eV for ZnSe:Ga. They suggested a possible double donor to account for the two different levels introduced by each dopant. They noted, however, that the donor ionization values were bigger for the samples with higher donor content, implying that the donor compensation increased with the dopant concentration.

Several authors have claimed to have produced p-type ZnSe, but with low values of conductivity only. Aven (1962), Haanstra and Dieleman (1965) and Stringfellow and Bube (1968) produced copper doped ZnSe with levels at approximately 0.7 and 0.9 eV above the valence band. Phosphorus doped material was obtained by Reinberg et al (1971) with an acceptor level at 0.685 eV. Park et al (1971) studied p-type lithium doped ZnSe grown from the vapour phase or from the melt. The room temperature resistivity was about 10^{8} Ω cm. The hole concentration p varied between 10^{7} to 10^{10} cm^{-3} yielding an activation energy of 0.66 eV at temperatures between 250 and 350 K. Yu and Park (1973) heated some ZnSe crystals grown from the melt and from the vapour phase in selenium. They reported levels at 0.65 - 0.75 eV above the valence band.

However, Yu and Park also found an additional shallow acceptor level at about 0.1 - 0.15 eV which depended very much on the selenium treatment. The deep acceptor level was associated with intrinsic defects like zinc vacancies or zinc vacancy complexes.

More recently, as mentioned in chapter one, Robinson and Kun (1975) claim to have produced p-type layers of ZnSe doped with some group IIIa elements. The holes had mobilities between 10 and 30 $cm^2V^{-1}s^{-1}$. Robinson and Kun used a two stage heat treatment process to produce the layers on a ZnSe substrate. They have also reported the highest hole density of 10^{19} cm^{-3}. The explanation offered by these authors is that the heat treatments reduced the valence state of the group III element. The reduction suggested was from a trivalent state to a monovalent one, hence they felt that when In^+ substituted for a zinc ion in the lattice, it should act as an acceptor. Surprisingly however, no further work, as far as we are aware, has been carried out on semiconducting p-type ZnSe. Moreover, Ray and Kröger (1978b) have rejected the explanation given by Robinson and Kun.

More recently a second group of workers has been involved in the study of highly resistive p-type ZnSe. Bhargava et al (1979), Neumark (1979), Neumark et al (1980) and Neumark (1980) reported the effect of self-compensation by incorporation of shallow acceptors (Li, Na, Cu, P) in ZnSe grown by liquid phase epitaxy. This was done by combining the identification of the shallow acceptors from photoluminescence studies at 5 K, with several heat treatments between 300° and 900°C . They concluded that the main cause of self-compensation in p-type ZnSe is the presence of accidental amphoteric impurities, such as lithium, which can move out of zinc sites into interstitial positions where it forms shallow donor levels.

Some work has also been done on thin films of ZnSe doped with gallium or indium. The films were prepared by co-evaporation in the presence of zinc and subsequent annealing in zinc vapour. Highly conductive material was then obtained (Aranovich et al , 1978). Lim and Brodie (1977a,b,1978) re-

ported a systematic study of amorphous films of ZnSe and explained their results in terms of carriers hopping in band tail states at high temperatures (room temperature and above) and hopping in localized states at lower temperatures.

3.3   THE OPTICAL PROPERTIES OF ZnSe

Much greater attention has been paid in times past to the luminescence emission of ZnSe because of the interest in the so-called selenium red phosphors. However, more recently, extensive studies have been made of excitation and pair emission in the blue. This is because good quality single crystals of high purity are now being produced. The red emission, which is caused by the presence of copper or chlorine, used to dominate the emission processes,but now that pure and defect free ZnSe crystals are available, highly efficient blue exciton emission can be obtained.

Bube and Lind (1958) used photosensitive crystals of ZnSe doped with bromine and with either group I (copper) or group V acceptors and found that the general photoconductive characteristics of ZnSe were identical with those reported for CdS and CdSe. Thus temperature quenching of photoconductivity, a superlinear variation of photocurrent with light intensity and infrared quenching of photoconductivity were all present. Stringfellow and Bube (1968) made measurements of all of these effects as well as of luminescence emission, in copper doped ZnSe ; from which they concluded that copper forms two acceptor levels at about 0.35 and 0.72 eV above the valence band.

Bouley et al (1975) studied the photoluminescence emission of ZnSe crystals doped with either gallium or aluminium. They compared the lumin - escence before and after their samples were heat treated in zinc vapour. The main feature was the observation of blue emission in highly conductive samples which was either free exciton or band to band recombination. Their conclusions were: (i) There is no effect of zinc annealing on the luminescence emission with aluminium doped samples, (ii) zinc annealing had a strong effect on gallium doped samples by reducing the intensity of the orange or yellow-green

band in favour of blue luminescence, (iii) the luminescence of zinc annealed ZnSe:Ga at 77 K involved the recombination of a free electron with a hole trapped on a shallow sodium substitutional acceptor. They also discussed the deep centre luminescence which, in ZnSe, consists of the red-orange self-activated band and a yellow-green band which appears at low temperatures. They thought that the self-activated luminescence, as suggested earlier by Aven and Halsted (1965), was probably produced by a complex involving a zinc vacancy and the group IIIa element. Moreover, Bouley et al claim that this complex is formed at high temperature and consits of a zinc vacancy, singly or doubly ionized, and a group III impurity located at the vicinity of the vacancy. Two suggestions were offered to describe the different electronic transitions which might be responsible for the self-activation emission. First, a complex is formed by the pairing of a singly ionized zinc vacancy with ionized aluminium or gallium to form a neutral defect. The luminescence may then be associated with an electronic transition described by the configuration-coordinate model within the neutral defect. Secondly, the zinc vacancy could be doubly charged so that when paired with the group III element it becomes a singly charged acceptor. In this case, the luminescence would result from a donor-acceptor (D-A) recombination between the group III donor and the acceptor complex. Finally, Bouley et al explained the yellow-green band in their aluminium doped material by suggesting that the transition involved a defect associated with aluminium and an alkaline impurity.

Yamaguchi et al (1977a) described how hole injection had been obtained in forward biassed ZnSe diodes in two different ways. First, p-n junctions were obtained by nitrogen ion implantation and secondly, MIS structures were formed by oxidizing ZnSe in a hydrogen peroxide solution (H_2O_2) to produce the insulating film. Blue emission in forward-bias at room temperature was obtained for both diodes.

Swaminathan and Greene (1976) reported some photoluminescence measurements at 4.2 K on undoped ZnSe and on ZnSe doped with various alkali

metals, IIIa elements and alkali-halide salts. Melt grown ZnSe was used for their experiment. Post-growth annealing treatments in either zinc or selenium was also carried out as well as electron irradiation at an energy of 1 MeV. The information obtained from studying the effects of these treatments on the edge emission, enabled Swaminathan and Greene to propose models for the chemical identity of the defect centres involved in the D-A pair recombination in ZnSe.

Yamaguchi et al (1977b) studied the photoluminescence of ZnSe single crystals containing diffused-in group IIIa elements. They came to the following conclusions: (1) The blue line, which is probably the I_2 line involving recombination of an exciton bound to a neutral donor, is increased when gallium is diffused in a zinc atmosphere. (2) Heat treatment in zinc causes a reduction of the concentration of zinc vacancies and zinc vacancy - donor complexes, so that the deep centre luminescence involving these complexes also decreases. Furthermore, at the same time, the intensity of the blue emission is increased.

Grimmeis et al (1977) reported photocapacitance, photocurrent and photoluminescence quenching measurements on ZnSe samples which were prepared in different ways, and contained different dopants (i.e. copper or manganese). They concluded that doping with copper creates an impurity level at about 0.68 eV above the valence band. They also observed an additional level at about 0.58 eV above the valence band independent of the dopant.

Papadopoulo et al (1978) described a new vapour phase technique of growing ZnSe crystals doped with indium. They also measured some electrical and photoluminescence properties of as-grown and zinc treated crystals, doped with 50 ppm of indium. The as-grown crystals were highly resistive ($\rho > 10^6$ Ω cm). To reduce the resistivity, they annealed their samples in zinc vapour for 24 h at temperatures between 550° and 750°C. No precipitation or change in the transparency of the samples was observed. However, at 900°C, the samples became dark. Papadopoulo et al concluded, first of all, that the

electrical and photoluminescence properties were greatly influenced by the zinc treatments and, second, that their indium doped ZnSe crystals were highly compensated due to the well known self-compensation phenomenon together with the presence of uncontrolled acceptor impurities such as sodium or lithium.

Fujita et al (1979) grew some epitaxial layers of ZnSe from a Zn-Ga alloy solution, and observed the luminescent spectra under various conditions. They obtained intense blue emission at room temperature. They explained this as the possible reduction of the concentration of V_{Zn}-Ga_{Zn} complex centres which are believed to be the origin of the deep centre luminescence (the green-yellow and red-orange bands).

Tews et al (1979) applied experimental techniques of excitation spectroscopy and selective pair luminescence to ZnSe crystals with different impurity contents. They were able to detect the excited states for the lithium and sodium acceptors at 1.6 K. They also obtained good agreement with theoretical calculations for these excited states.

Shirakawa and Kukimoto (1980) measured the excitation and emission spectra of as-grown and zinc treated crystals of ZnSe grown from an indium solution. They found that the as-grown crystals had relatively high resistivities of about 10^4 Ω cm which were reduced after zinc treatment to about 1 - 10 Ω cm. Shirakawa and Kukimoto then studied the near band-edge photo - luminescence and concluded that the emission resulted from the recombination of free holes and donor electrons.

Dean and Bishop (1980) reported photoluminescence exciton spectra of deep acceptor states in ZnSe. They observed that the copper emission at 1.95 eV can be excited in a prominent band at 3.25 eV. Finally, Shing and Walsh (1980) observed band-edge photoluminescence at 2 K using blue, green and red excitation.

3.4   CONCLUDING REMARKS

Some of the works mentioned in this short review of the electrical and optical properties of ZnSe will be mentioned again in this thesis when our results are discussed. Other relevant papers will also be mentioned then.

There are many more reports, however, available in the literature related to topics of this thesis which have not been mentioned at all. This is not because they are irrelevant to our work, but because most of them are either summarised in some of the papers which are mentioned here and therefore are referenced therein, or because their results are already part of accepted common knowledge and are now implicitly referred to.

CHAPTER 4

EXPERIMENTAL PROCEDURE

4.1   INTRODUCTION

Because the purpose of this work was to obtain information about

the anomalous electrical properties of indium and gallium doped zinc

selenide, a variety of experimental techniques have been used. Measurements

of photoluminescence emission, thermoluminescence, thermally stimulated

current and photoconductivity have been made in addition to straight

forward measurements of the electrical transport properties. This chapter

is concerned with a description of the experimental techniques and apparatus

used. First of all, however, a description of the crystal growth tech-

nique which was used in this department will be given.

4.2   CRYSTAL GROWTH

4.2.1 Preparation of the Compounds

Although ZnSe can be produced by chemical precipitation, prepara-

tion by direct reaction of the ultrapure elements, is the technique which

has normally been used in this laboratory to provide high purity starting

material. The method involves direct synthesis from the elements at

elevated temperatures. 6N purity zinc and selenium obtained from Metals

Research Ltd. were placed in separate silica boats in a furnace with three

temperature zones as illustrated in figure 4.1. The selenium was placed

in the first zone at 300° C with the zinc in the second at 750° C. Streams

of high purity argon were then passed over the zinc and the selenium.

The yellow zinc selenide compound was formed as a powder on a silica liner

in the third zone held at 1050° C.

After this synthesis, the powder was purified in a flow run process

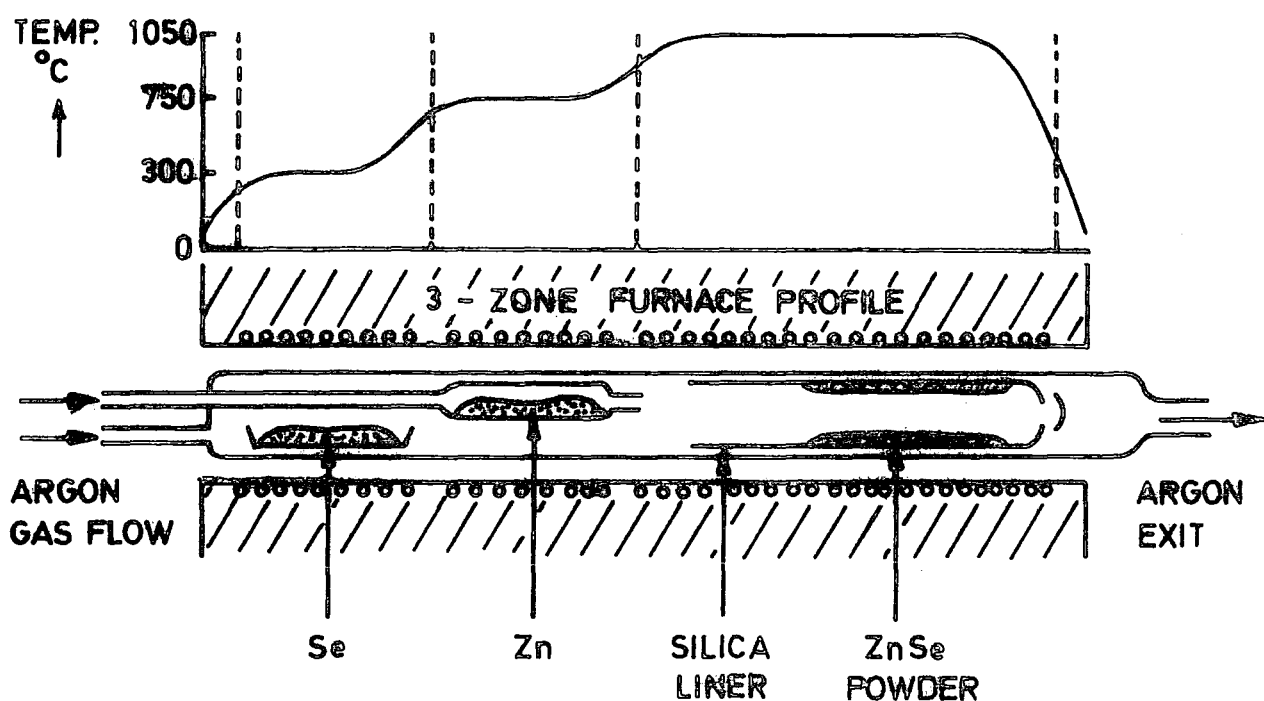involving sublimation in a stream of argon, as shown in figure 4.2. The
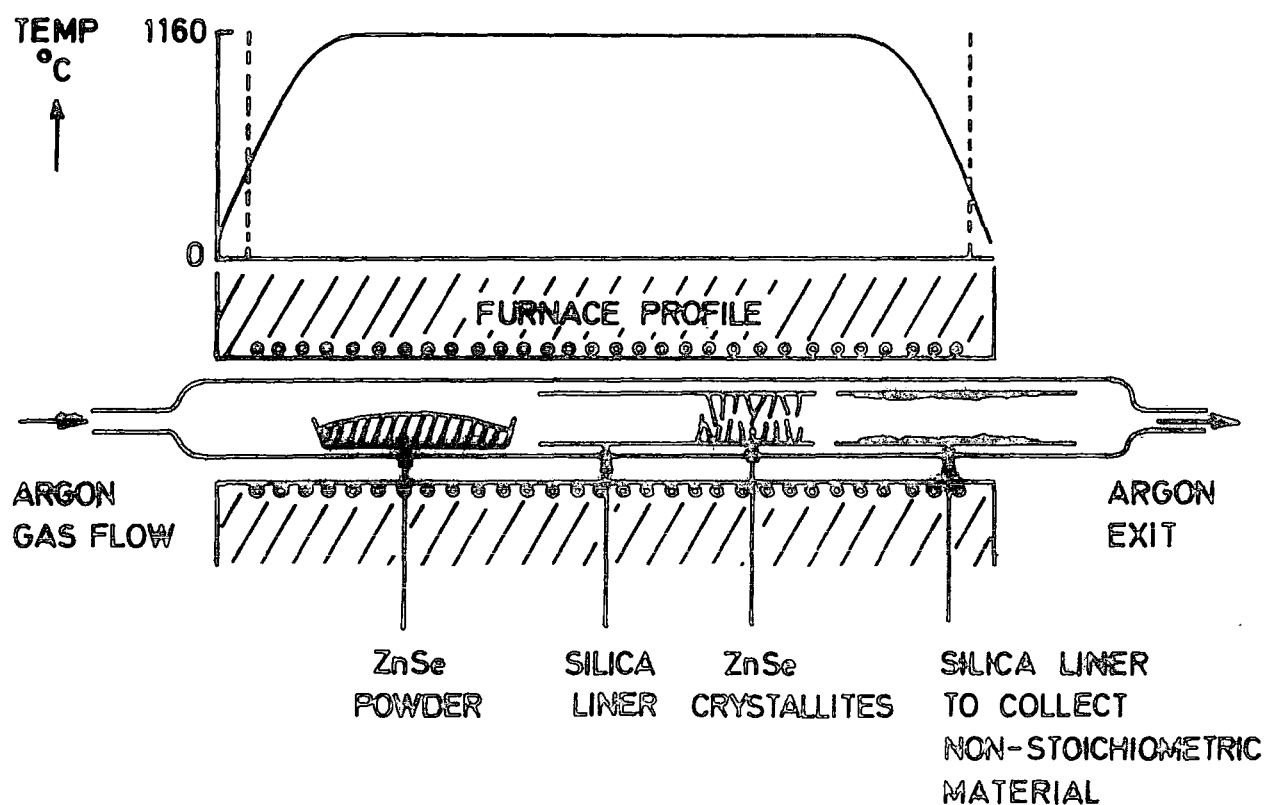
FIG. 4·1   DIRECT COMBINATION OF THE ELEMENTS

FIG. 4·2   ARGON FLOW PURIFICATION

powder was placed in a boat in a silica tube and heated at 600° C for

twelve hours while a stream of high purity argon was passed over it in

order to remove all volatile impurities. The temperature was then raised

to 1160° C for about a week so as to sublime the ZnSe which was transported

by the argon to the cooler region of the tube, leaving non-volatile impurities

behind. In this way, the ZnSe crystallized in the form of small platelets,

which were then collected to provide the starting material for the crystal

growth procedure.

4.2.2 Iodine Transport and Growth from the Melt

In general, three methods can be used for growing large crystals

of the II-VI compounds, (1) growth by chemical transport, (2) growth from

the vapour and (3) growth from the melt. These three techniques are

commonly used by different workers and offer various advantages and dis-

advantages.

Growth by chemical transport, first described by Nitsche et al

(1961), involves the vapour transport of the substance, via an intermediate

compound, mostly using iodine. The advantage of this method is that the

temperature required during growth is low (usually, less than 1000° C).

Robinson and Kun (1975) suggested that ZnSe grown by this technique offers

a more open lattice which increases the solubility of gallium and indium

in the compound hence providing the opportunity for the preparation of

ZnSe p-n junction devices. The obvious disadvantage of this growth method

is the inevitability of the crystal being doped with a large quantity of

iodine.

Growth from the melt involves high temperatures (> 1300° C) and

high pressures, thus making the use of silica tubes as containers difficult.

However, several workers are still developing this technique and prefer

crystals obtained this way, see for example Tsujimoto et al (1966) who

applied an argon pressure of 120 atmospheres to suppress constituent

vapour loss. More recently, Yamaguchi et al (1977a) have also described melt growth, again, under a high argon pressure of 50 atmospheres and a temperature of $1515^{\circ}C$.

4.2.3 Vapour Phase Growth

This method, which is used here, revolves around the technique devised by Reynolds and Czyzack (1950) and modified later by Piper and Polich (1961). This technique has been adapted in this department for CdS crystals by Clark and Woods (1968) and for ZnSe by Burr and Woods (1971). The experimental arrangement is shown in figure 4.3.

The procedure used to grow crystals for the present work was as follows. About 20g of flowrun platelets were used as the charge and 0.2g of zinc (or selenium) was held in the tail of the tube, so as to achieve a near stoichiometric composition of the vapour in the growth region, by providing a vapour pressure of one of the constituents corresponding to P_{min} conditions. The tube was evacuated down to 10^{-6} torr, baked and flushed in argon to remove volatile impurities and re-evacuated. Recently however, this procedure of baking and flushing has been abandoned after analysing the gas content at the end of a growth run and finding that all the tubes contained a high proportion of carbon monoxide (see Russell and Woods, 1979). After loading the charge, the silica tube was sealed and mounted in a vertical furnace. The temperature profile of this furnace was fixed so that the charge was held at $1160^{\circ}C$ and the tail at $570^{\circ}C$ while the growth tip, where condensation of the sublimed ZnSe occurred, was maintained at 1100° C. During growth, the tube was raised by about 3 cm per day by a rack and pinion mechanism for approximately one week, and 1 cm diameter crystals, with a conical tip, and a crylindrical body of 3 to 4 cm overall length were regularly produced.

Metallic indium or gallium dopants were added directly to the charge when concentrations of 50 ppm or more were desired. For smaller concentrations, the indium or gallium was obtained from crystals of ZnSe

PULL ROD

CENTRALISING GUIDE

VERTICAL GROWTH TUBE

CHARGE

UPPER ZONE THERMOCOUPLE (STATIC)

2-ZONE FURNACE PROFILE

TAIL RESERVOIR

LOWER ZONE THERMOCOUPLE (ATTACHED TO GROWTH TUBE)

GROWTH REGION

FOR Zn RESERVOIR

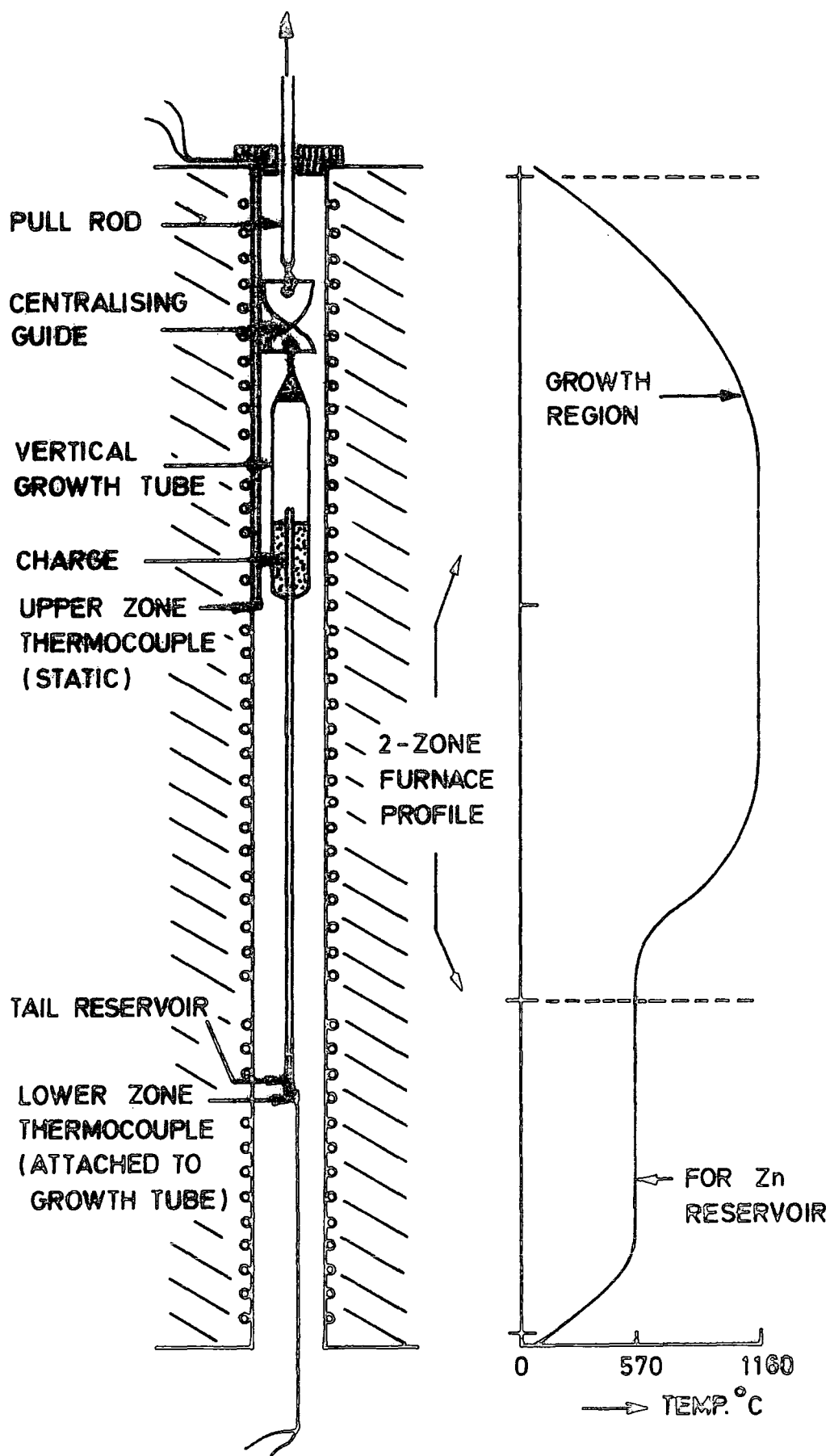0   570   1160

⟶ TEMP.°C

FIG. 4.3   VERTICAL GROWTH OF ZnSe

heavily doped with one of them. A piece of a slice of such a crystal,
which had been partly analysed by atomic absorption spectroscopy to
determine its dopant content, was then crushed to a powder and mixed with
flow run ZnSe material to form the 20 g charge. In this way, a range of
crystals was produced doped with quantities of indium and gallium ranging
from 5 ppm to 1000 ppm.

4.3   HEAT TREATMENT

Some of the as-grown crystals, particularly the heavily doped
ones, had a very high resistivity. In order to reduce this resistivity,
circular slices were first cut from the boules and introduced in a silica
tube with metallic zinc. The tube was evacuated then sealed and placed
vertically in a furnace, as shown in figure 4.4, to permit the sample to
be heated in excess zinc. This technique, already widely used by different
workers, is mainly effective when the crystal is immersed in molten zinc
as described by Aven and Woodbury (1962). However, with ZnSe crystals
doped with indium or gallium, heavy dark precipitates were formed after
heating in liquid zinc as reported by Jones and Woods (1976), and almost
completely degenerate samples were obtained. The material itself also
became very brittle.

In order to minimize this problem, annealing was carried out in
zinc vapour. However, the effect of this treatment was strongly dependent
on the dopant concentration involved. After several trials, the "optimum"
heating conditions were found to be 600° C for 70 hours for indium doped
material and 630° C for the same length of time for gallium doped material.
In this way, crystals with less than about 100 ppm of dopant showed a very
light dark colouration only, after the heat treatment, becoming darker with
increasing concentrations of doping material. A very similar procedure
was used by Bouley et al (1975).

Optical transmission micrographs of the precipitates involved
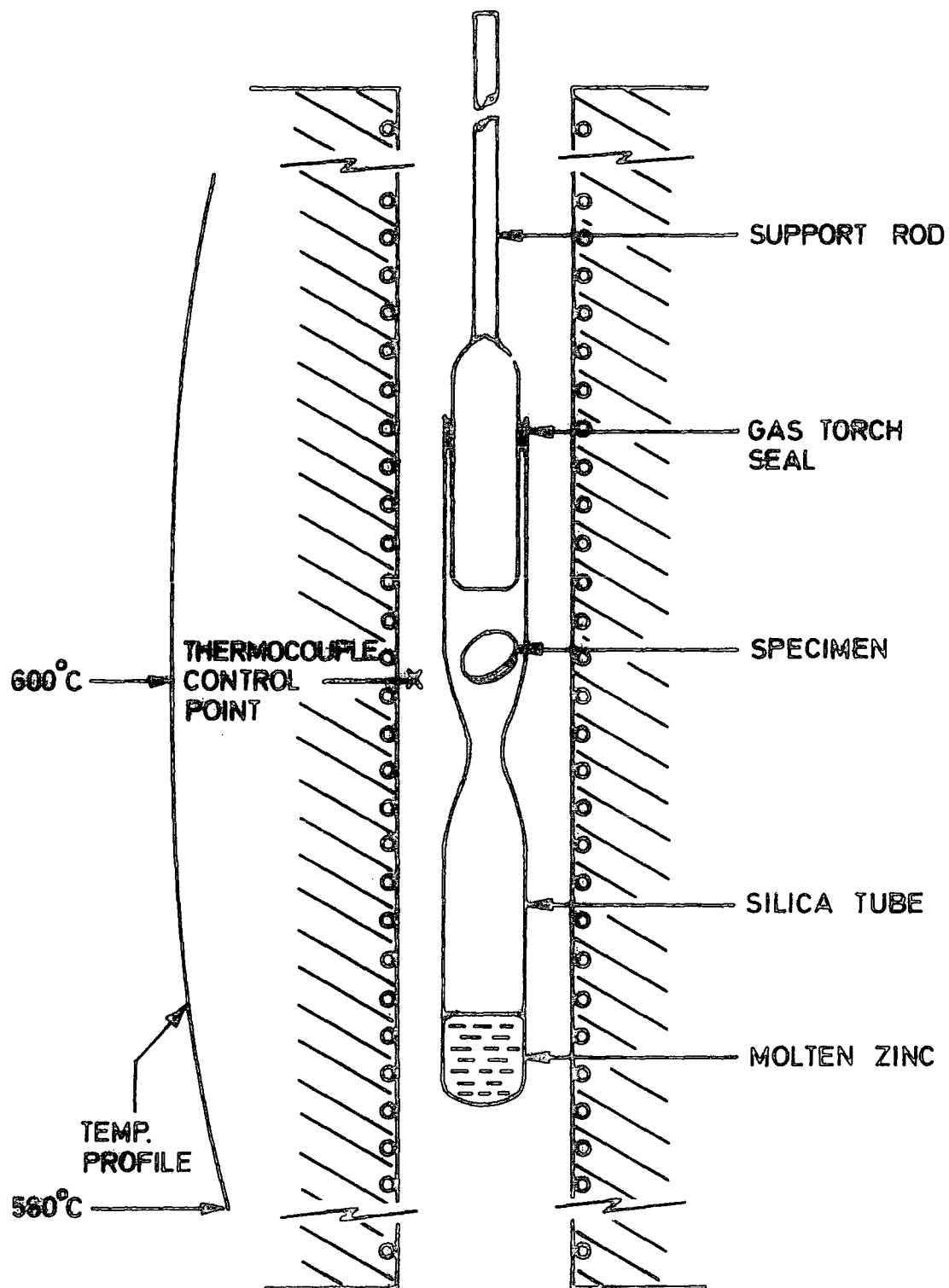have been presented by Jones and Woods (1976) for ZnSe : In and by Ray and

SUPPORT ROD

GAS TORCH SEAL

SPECIMEN

SILICA TUBE

MOLTEN ZINC

600°C

THERMOCOUPLE CONTROL POINT

TEMP. PROFILE

560°C

FIG. 4·4   ARRANGEMENT FOR HEATING INDIUM OR GALLIUM DOPED ZnSe IN ZINC VAPOUR

Kröger (1978b) for ZnSe : Ga. It has been suggested that the precipitates in ZnSe : Ga which seem to be black or red, consist of Ga_2Se or a solid solution of Ga Se or a (Ga, Zn) alloy. A more detailed account of these precipitates is presented in chapter seven.

4.4 ATOMIC ABSORPTION SPECTROPHOTOMETRY

An important part of the work described in this thesis was the study of the behaviour of ZnSe containing different concentrations of indium and gallium. In order to ascertain the exact amount of impurity incorporated into each of the samples, atomic absorption spectroscopy was carried out, using a Perkin Elmer 403 atomic absorption spectrophotometer with Activion reference lamps to discriminate the corresponding lines for indium or gallium.

The analysis is a destructive technique which involves converting the sample into an atomic vapour and measuring its absorbance at a selected wavelength which is characteristic of each individual element. The measured absorbance is proportional to the concentration of the element in question and the analysis is done by comparing this absorbance with that given by reference specimens of known composition under the same experimental conditions.

To determine the indium or gallium content of a crystal, a solution was prepared using about 100 mg of material, usually obtained from the remaining edges of the slice from which the samples studied in this work were cut. The specimen for analysis was etched, then washed and dissolved in 2 ml of $H NO_3$. Finally, distilled water was added to make a total of 6 ml of solution.

Reference sample solutions of 1.25 ppm, 5.00 ppm and 20.0 ppm of indium or gallium were used. The results of the analysis are given in Table 4.1. An estimated error of about 10 to 15% results from this technique.

For completeness, some of the specimens were also analysed for copper. The results are shown in the last column of Table 4.1.

T A B L E   4.1

ATOMIC   ABSORPTION   ANALYSIS   FOR   INDIUM   AND   GALLIUM

Speci-men No.	Boule ≠≠	Dopant and Nominal Content in p.p.m	Amount Disolved in mg	Measured Content in p.p.m	Copper Content in p.p.m
11	342	In : 100	151	82	-
27	342	In : 100	194	85	13
28	342	In : 100	81	114	8.9
7	349	In : 1000	111	800	-
1	375	In : 50	72	101	-
10	375	In : 50	136	91.6	-
2	376	In : 100	60	107	-
8	376	In : 100	131	108	-
3	377	In : 250	55	235	-
5	381	Ga : 50	159	50.6	-
6	382	Ga : 100	101	112	-
36	383	Ga : 250	110	373	5.1
9	386	In : 5	78	34.3	-
4	387	Ga : 5	102	6.3	-
12	405	In : 50	95	55.8	-
19	407	In : 5	98.5	13.9	-
20	407	In : 5	106.5	12.8	-
24	408T	In : 250	109	275	-
15	408T	In : 250	107	261	-
16	408E	In : 250	87	210	-
26	408E	In : 250	180	229	43
17	408T	In : 250 *	102	252	-
30	408T	In : 250 *	117.5	237	4.5
29	408E	In : 250 *	85.5	280	6.6
18	410T	In : 100	104.5	106	-
21	410T	In : 100	108	108	-
31	410T	In : 100	47.5	114	5.3
22	410E	In : 100	108	108	-
23	410E	In : 100	101	105	-
32	410E	In : 100	94	110	5.2
33	410T	In : 100 *	165	107	1.9
34	410E	In : 100 *	115	133	2.0
48	413	In : 20	199	17.0	-

T : Tip of Crystal Boule (first part to grow)

E : End of Crystal Boule (last part to grow)

* : Annealed in zinc vapour.

4.5   SAMPLE PREPARATION

Several samples were cut from different slices from different parts of each crystal boule with a diamond wheel. After this, they were polished on their large faces with 1 μm alumina powder and then etched. The etch used was that recommended by Sagar et al (1968).

The etching procedure consisted of immersing the sample in an 0.4% to 1% solution of bromine in methanol for 30 to 90 sec. The crystal was immediately washed in methanol and then immersed in carbon disulphide for 5 to 10 minutes to remove the red compounds of bromine and selenium which tend to form as deposits on the surface. Finally, the specimen was washed in absolute alcohol.

Ohmic contacts were required on those samples to be used for the measurements of Hall coefficient, thermoelectric power, photoconductivity and thermally stimulated current. These contacts were made by pressing indium pellets on the surface of the sample and then heating to about 250° C for 3 to 5 minutes in an atmosphere of argon. A slow cycling process was used taking about 20 minutes to reach maximum temperature and to cool down.

4.6   MEASUREMENTS OF OPTICAL PROPERTIES

4.6.1 Luminescence

(a) Photoluminescence spectra

The experimental arrangement used for measuring the emission spectra of the crystals is shown in figure 4.5. The photoluminescence of the crystals was excited by ultra-violet radiation from a 250 watt high pressure, compact source mercury lamp. Two Chance glass OX 1 filters were used in order to isolate the 365 nm mercury line. The sample was mounted on the cold finger of a cryostat which was used for measurements down to liquid nitrogen temperatures. This cryostat consisted of a copper enclosure with two silica windows. The sample block was also made of copper and could be rotated about its vertical axis to face any direction. The liquid nitrogen was contained
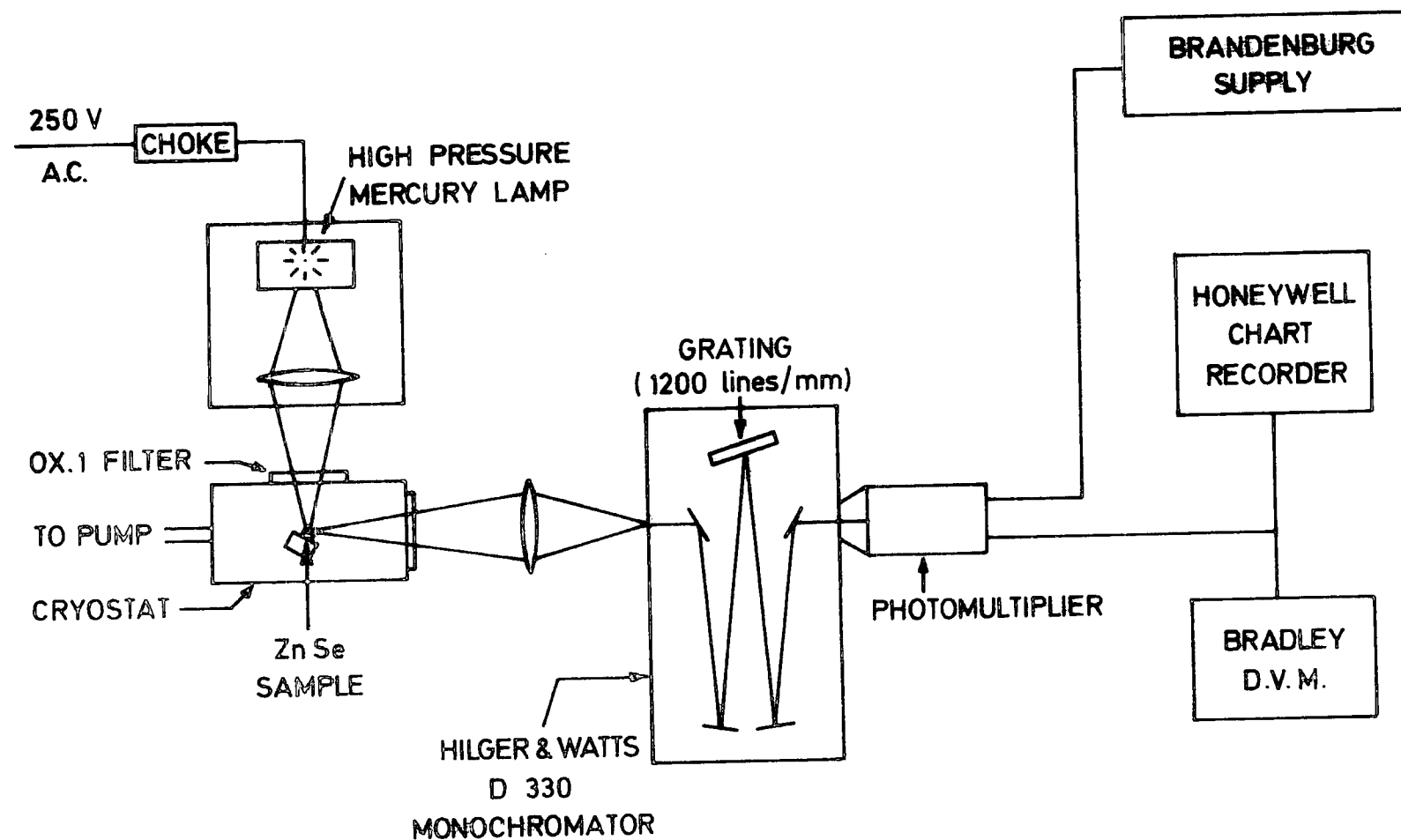
FIG. 4·5 ARRANGEMENT FOR MEASURING THE PHOTOLUMINESCENT EMISSION SPECTRA

in a nickel-silver cylinder above it, which in turn was surrounded by a vacuum jacket. A copper-constantan thermocouple was held in contact with the copper block and the temperature was displayed digitally with a Control & Readout Ltd. temperature indicator. During operation, the pressure inside the cryostat was kept below 0.1 torr by means of a rotary pump.

The emitted luminescence was focussed on to the entrance slit of a Hilger and Watts D330 single monochromator, equipped with a 1200 lines/mm grating from which a resolution better than 20 $\overset{o}{A}$ per mm of aperture slit was obtained in the visible region of the spectrum. An Oriel long pass filter was used at the entrance slit to reject those wavelengths with λ <390 nm.

The radiation was finally detected by an E.M.I. photomultiplier type 9558 with a trialkali S 20 photocathode. This photomultiplier was run at voltages up to 1200 V derived from a Brandenburg stabilised power supply model 472 R. The output from the collector was earthed via a 10 k ohm load resistor and the signal voltage was measured with a Bradley digital voltmeter model 173 B and recorded at the same time on a Honeywell Electronik 196 chart recorder.

(b) Cathodoluminescence

The experimental arrangement for analysing cathodoluminescence spectra is shown in figure 4.6. In this arrangement the excitation source was produced by an electron gun system which was built in this department. The electron gun, manufactured by 20th Century Electronics model ED 221, was a demountable triode type with a tungsten emitter. This electron gun produced a divergent electron beam which could be magnetically focussed to a spot approximately 2 mm in diameter on the sample. Typical operating conditions for the electron gun were : an anode voltage of 20 kV, a filament current of 5 A and a maximum beam current of 1 mA. This system was attached to the demountable bottom-plate of a liquid helium cryostat. This cryostat was also constructed within this department and consisted of a liquid
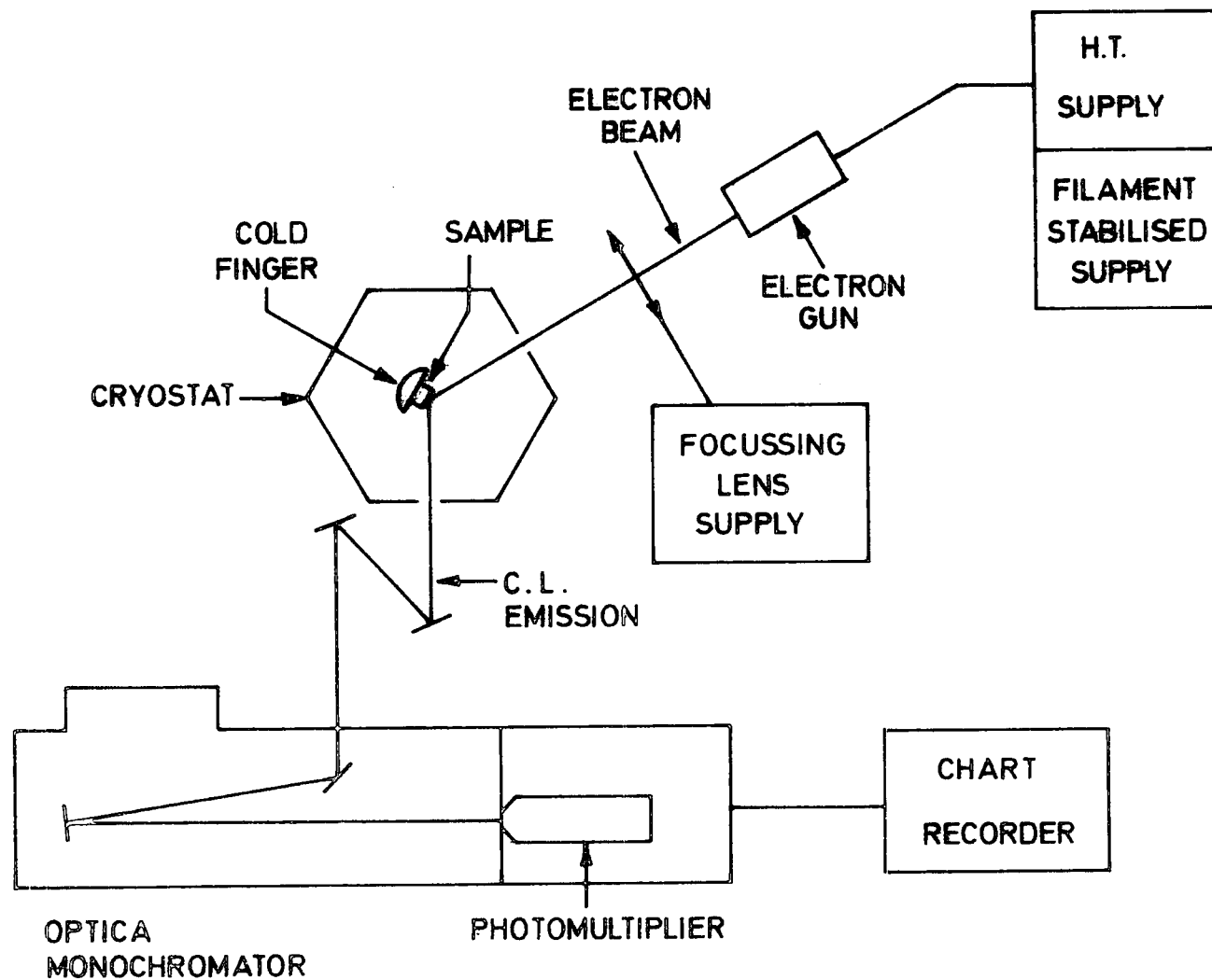
FIG. 4·6   EXPERIMENTAL ARRANGEMENT FOR MEASURING

CATHODELUMINESCENCE   EMISSION   SPECTRA

nitrogen jacket with a two litre capacity, a liquid helium pot with a 1.3

litre capacity and a demountable copper sample holder equipped with a

radiation shield. In the central liquid helium container, two carbon

resistors mounted on a thin stainless steel tube were used to measure

the depth of helium during transfer to give an indication of the temperature

of the sample. The vacuum within the cryostat was maintained at a pressure

of less than 10^{-3} torr by using conventional rotary and oil diffusion

pumps. The central liquid helium container could be pumped on via the

exhaust port in order to lower the pressure above the coolant and thus

further reduce the temperature of the sample.

The sample was placed on the demountable copper cold finger which

was in direct contact with the liquid helium pot. The sample was oriented

at 45° to the electron beam and to the silica window of the bottom-plate

to which a second diffusion pump was coupled in order to ensure a good

vacuum within the system.

The emission from the sample was focussed onto the entrance slit

of a monochromator via a mirror system. An Optica 4 NI grating spectro-

photometer was used to perform the spectroscopic analysis. The standard

monochromator dispersion was approximately 16 $\overset{\circ}{A}$ /mm with a ruled grating

of 600 lines/mm for the visible region. The automatic recording spectro-

meter was equipped with an EMI photomultiplier type 9781 R with an extended

S.5 photocathode.

4.6.2 Photoconductivity

(a) Photoconductive Response

Crystals were prepared for photoconductivity measurements by

cutting them into rectangular bars and alloying indium metal pellets onto

the end faces to form electrical contacts as explained in section 4.5.

The samples were mounted on thin silica glass plates using silicone grease

to ensure good thermal contact. Electrical connections were made by

applying thermosetting silver preparation from Johnson Matthey Metals Ltd.

to the indium probes to which short copper wires were attached. At this
stage, the contacts were examined to establish their ohmicity. The
silica glass plate was mounted on the copper cold-finger using silicone
grease again. A copper-constantan thermocouple was soldered with indium
on the silica cover slip to allow the temperature to be displayed in the
same manner as for the photoluminescence measurements.

To make the electrical measurements, a very low noise battery
operated supply was used, from which a potential of 0-30 V d.c. could be
obtained. A typical value of 25 volts was applied across the sample. The
current passed through the sample was monitored by a Keithley Electrometer
model 602. The output provided by this instrument was fed directly on a
Honeywell chart recorder.

The crystals were excited by a 250 watt quartz-halogen projector
lamp in conjunction with a Barr and Stroud double monochromator type VL-2
fitted with Spectrosil A quality prisms. This arrangement is shown
diagramatically in figure 4.7.

(b) Infrared quenching

The experimental arrangement for the infrared quenching measure-
ments is also shown in figure 4.7. Basically, it was the same as for the
photoconductivity measurements. A second source of light was added which
consisted of a 250 watt tungsten projector lamp. This light was focussed
on an interference filter centred at either 440 or 510 nm. The transmitted
beam provided the primary source. The sample was placed so as to face
this source and the second window of the cryostat at 45°. The second
source, i.e. the quenching radiation, was that used for the straight
forward photoconductivity measurements.

4.6.3 Thermally Stimulated Current and Luminescence

For the thermally stimulated current and luminescence measure-
ments, the same cryostat as for the photoluminescence measurements was used,
while the samples were mounted on a silica cover slip as for the photo-
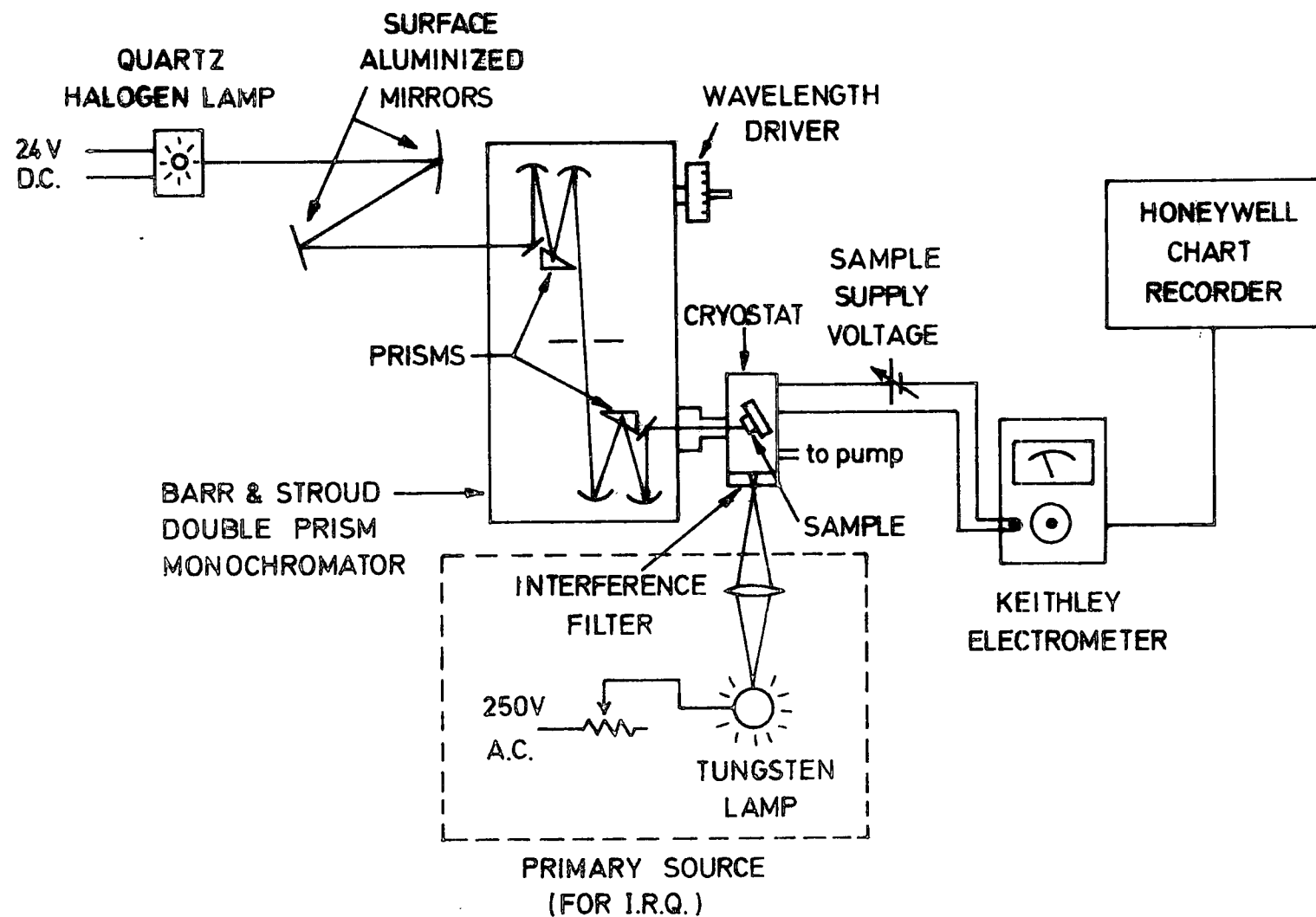
FIG. 4·7   ARRANGEMENT FOR MEASURING THE PHOTOCONDUCTIVITY

AND INFRA-RED QUENCHING SPECTRAL RESPONSE

conductivity measurements. The crystals were initially excited for ten minutes using the ultra-violet radiation from the 250 watt mercury lamp in the same way as for the photoluminescence.

The samples were heated by placing a 10 watt heater inside the nickel-silver liquid nitrogen container and, by varying the d.c. voltage applied to the heater, different heating rates could be obtained. A copper-constantan thermocouple was soldered to an extra indium dot placed on the silica glass and the temperature was displayed in the same way as for the photoluminescence measurements. The experimental arrangement is shown in figure 4.8.

When a thermally stimulated current run was carried out, a potential of 30 V from a highly regulated, low noise, supply was applied to the sample and the current was measured with a Keithley Electrometer model 602. The output of the Keithley was taken to a Honeywell Electronik 196 chart recorder with a small earthing switch placed in between these two in order to produce well defined marks along the trace on the chart at temperature intervals of 5 or 10 K.

When a thermally stimulated luminescence run was made, the sample, after excitation by the UV light, was turned through 90° in order to face the photomultiplier attached to the second window of the cryostat. The bursts of luminescence emitted by the sample when it was heated, were detected by the photomultiplier tube which was used for the photoluminescence measurements, but which was earthed via a 1 M.ohm resistor instead. The voltage drop across this load resistor was then measured with the 602 Keithley Electrometer in the voltage mode, and the output fed to the chart recorder.
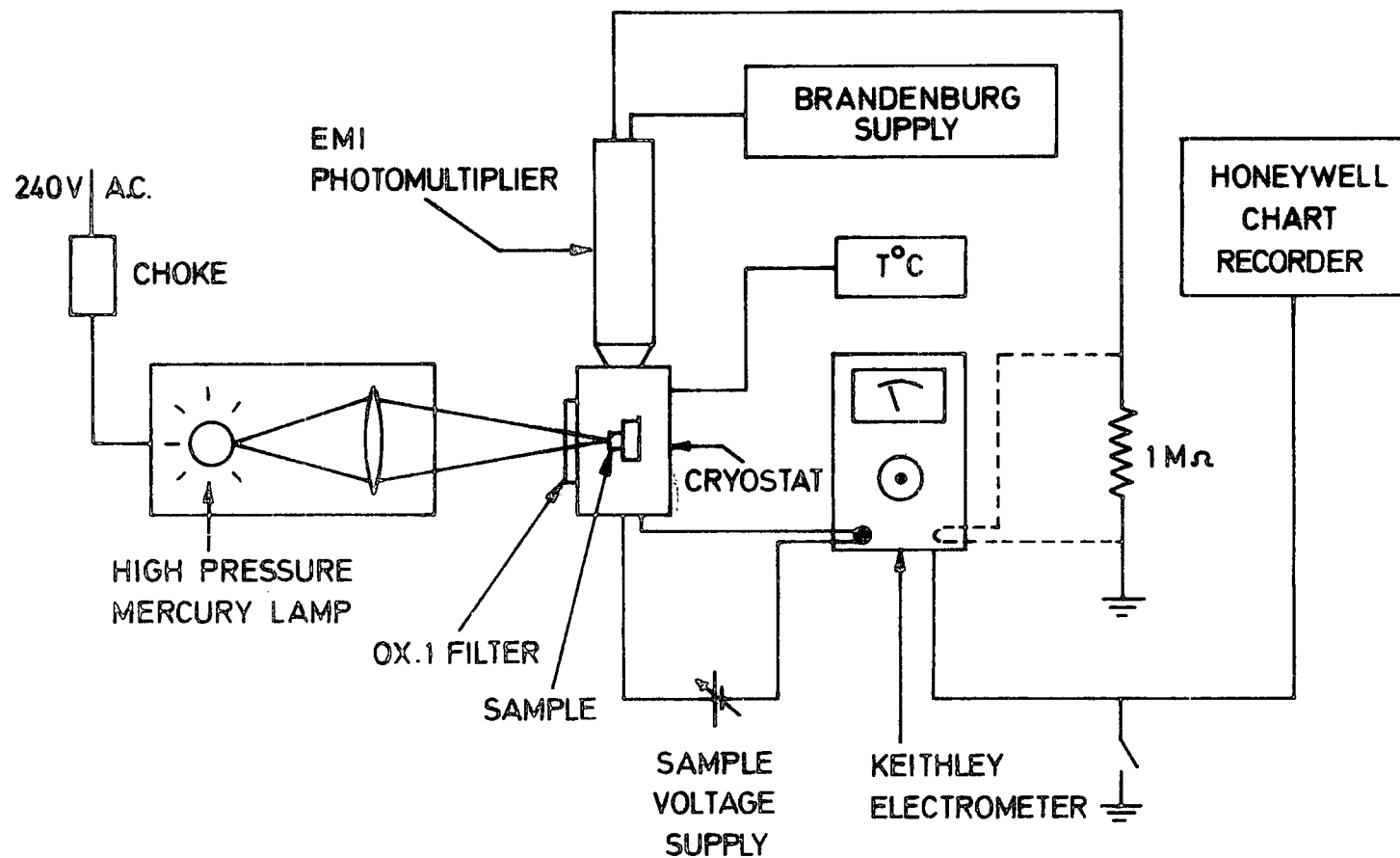
FIG. 4·8   EXPERIMENTAL   ARRANGEMENT   FOR   MEASURING   THERMALLY   STIMULATED   CURRENT   AND   LUMINESCENCE

4.7   ELECTRICAL MEASUREMENTS

4.7.1 Hall Apparatus

A brass cryostat was used for electrical measurements at temperatures down to liquid nitrogen. This cryostat is illustrated in figure 4.9. Liquid nitrogen was held in a container of about 1 litre capacity, connected to the sample block by a 20 cm nickel-silver tube which formed a gas exchange space. This space could be evacuated or filled with liquid nitrogen and then pumped on in order to reduce the temperature to about 68 K when necessary. A silica window was provided opposite the sample and if required, the sample could be illuminated via a mirror mounted at 45° on one of the magnet pole pieces. The illumination consisted of a 48 watt tungsten lamp focussed onto the sample through a copper sulphate filter. The window was kept covered during measurements unless Hall measurements under illumination were required. An 8 watt heater was wound directly onto the copper sample holder block as shown and temperatures of up to 420 K could be attained. Two copper-constantan thermocouples were used to monitor the temperature. One was mounted directly on the block while the other was soldered with indium to the cover slip sample holder. The reference junction for the thermocouples was held in a dewar containing a mixture of ice and water at 0° C. The glass sample holder was held against the block by a mechanical clamp. Six electrically insulated holders were mounted on the sides of the copper block to permit the six copper wires from the sample to be soldered. All electrical connections were made via two 6-way glass to metal seals at the top of the cryostat. The pressure in the cryostat was maintained below 10^{-3} torr by an Edwards 2.5 cm oil diffusion pump.

The magnet used was built in the department and possessed 5 cm diameter tapering pole pieces. It was air cooled and produced a field of 0.225 T across a 5.5 cm gap with a current of 1.75 A derived from a well regulated power supply.
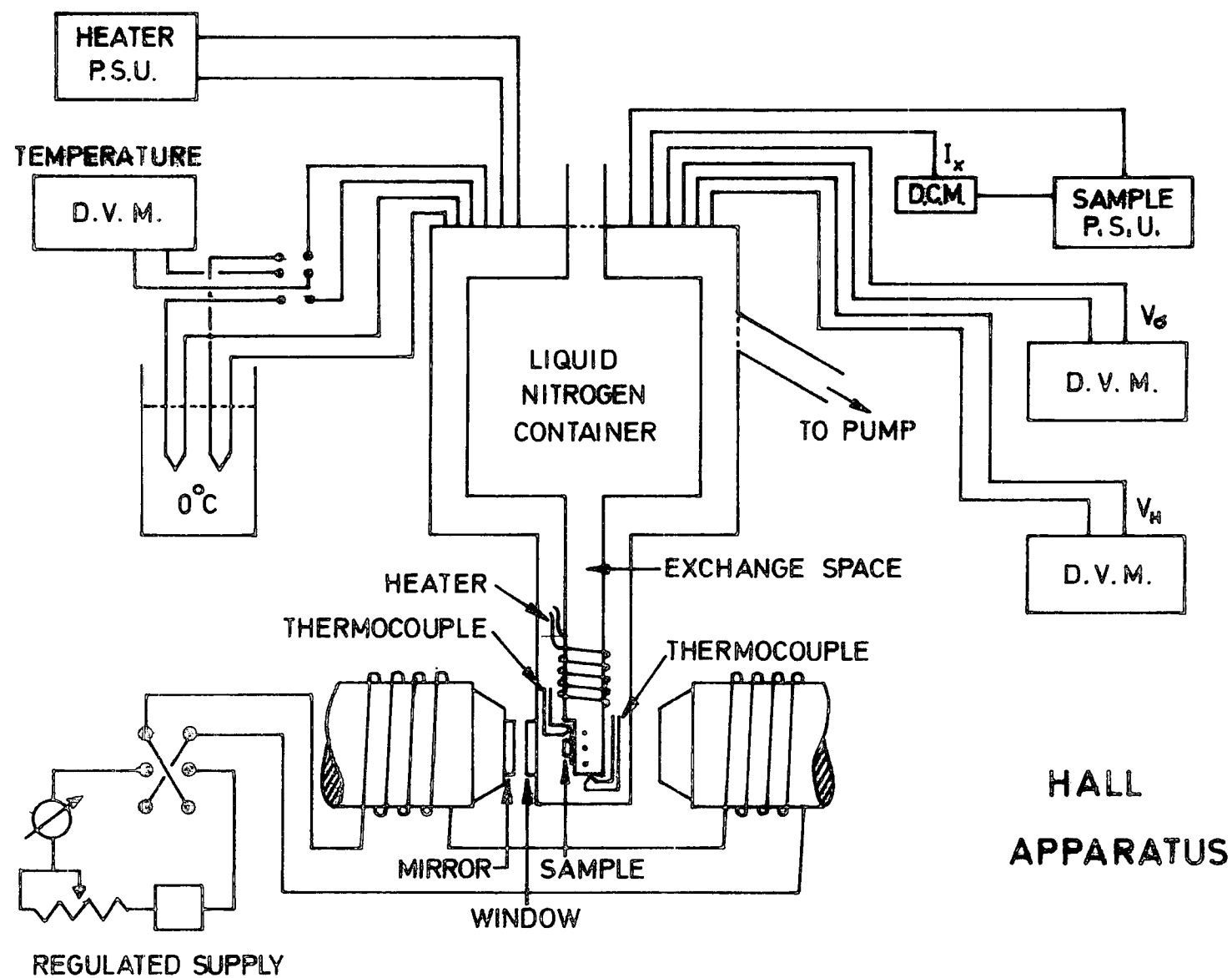
HEATER
P.S.U.

TEMPERATURE

D.V.M.

I_x

D.C.M.

SAMPLE
P.S.U.

V_σ

D.V.M.

LIQUID
NITROGEN
CONTAINER

TO PUMP

V_H

D.V.M.

0°C

EXCHANGE SPACE

HEATER

THERMOCOUPLE

THERMOCOUPLE

HALL

APPARATUS

MIRROR

SAMPLE

WINDOW

REGULATED SUPPLY

FIG. 4·9

The six probe method was used for making measurements (figure 4.10). However, some of the samples were too small for this and then a five probe method was used instead. The electrical supply to the sample was a battery operated 0-30 volts very low noise source, built in this department around a commercially available variable voltage I.C. regulator. Four digital meters were used to monitor the relevant parameters which were : the current through the device, the voltage between the conductivity probes V_σ , the Hall voltage V_H and the e.m.f. of the thermocouples. Because of the high resistivity of many of the samples, very high input impedance (Z_{in}) voltmeters were used. These were a Bradley digital voltmeter model 173 B with $Z_{in} \geqslant 10^9$ ohms for V_σ, a Hewlett Packard digital multimeter model 3465B with $Z_{in} \geqslant 10^{10}$ ohm for V_H. A second Bradley 173 B was used for the temperature measurements. In making the Hall voltage measurements, the $4\frac{1}{2}$ digit capacity of the Hewlett Packard multimeter was fully exploited and hence, no "back-off" voltage was needed to eliminate the offset voltage usually present when making this kind of measurement. In this way, it was possible to read, with very good accuracy, a Hall voltage of just a few tenths of a millivolt in the presence of an offset voltage under two volts. However, for even better accuracy, a special reversing switch was used to invert the current through the electromagnet and therefore, it was possible to produce a variation in the field equal to twice its intensity ; this was done several times and an average value for 2 V_H was obtained.

The values of current, V_σ and V_H were very dependent on the resistivity of the samples. For low resistivity specimens, the current could be as high as 10 mA for values of V_σ of about 1 volt and around 10 to 100 μV for V_H ; on the other hand, for the high resistivity samples, the current was sometimes as low as 1 nA for a V_σ of up to 10 volts while V_H could be as high as 50 mV.
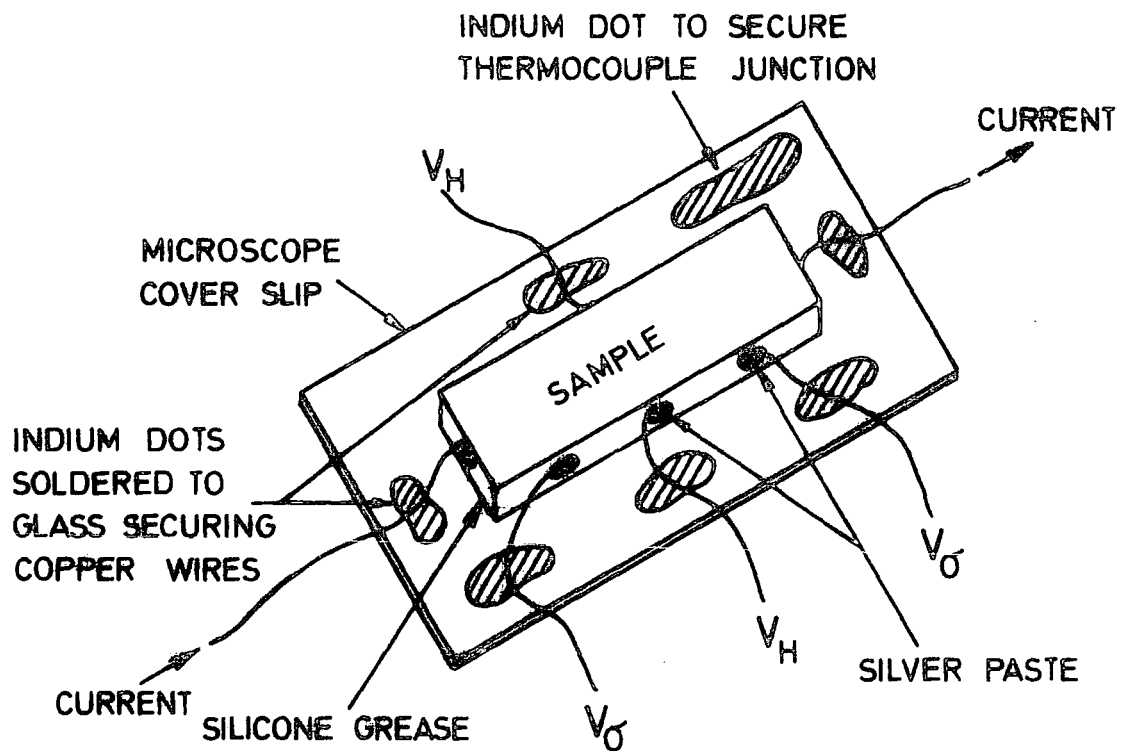
FIG. 4·10   CRYSTAL BAR SHOWING THE SIX PROBES
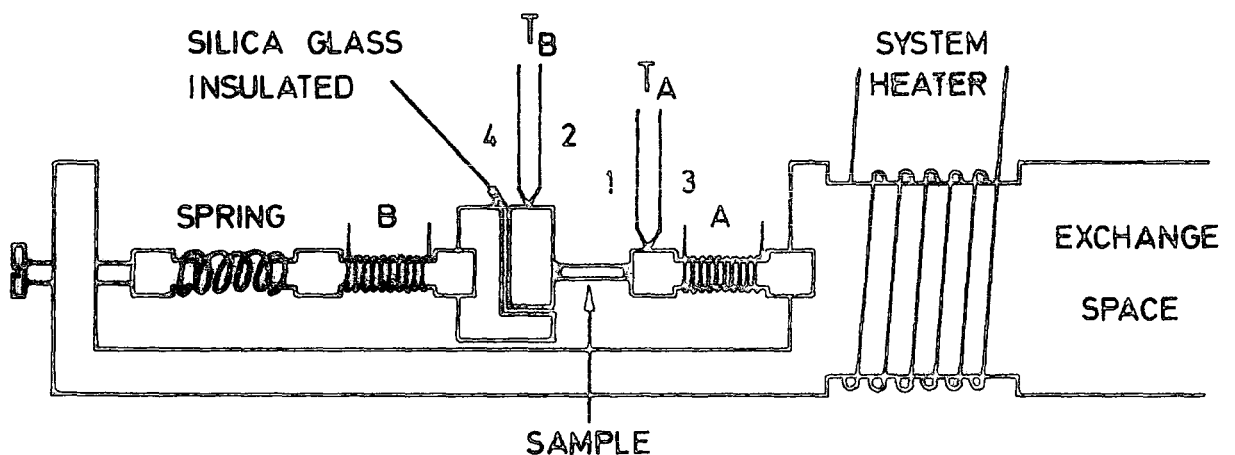
FOR   HALL   MEASUREMENTS

FIG. 4·11   THERMOELECTRIC   POWER   SAMPLE

HOLDER

The sample dimensions were of the order of 8 x 2 x 1 mm^3. The rectangular bar cut from the boule was first ground with 1 μm alumina powder to obtain flat and parallel sides. It was then etched, as previously described, to remove surface damage, and indium contacts were applied. Next, the sample was mounted on a glass microscope cover slip using silicone grease and 40 SWG copper wires were attached to the indium contacts with Johnson Matthey thermo-setting silver preparation type FSP43 or 49 as explained earlier.

4.7.2 Thermoelectric Power Sample Holder

A sample holder as illustrated in figure 4.11 was used for the thermoelectric power measurements. It was mounted at the end of a nickel-silver tube used as an exchange space and connected to a liquid nitrogen container in a similar way as with the Hall apparatus. The same brass cryostat housing was used. The sample was held against two copper end pieces each one with a small indentation to help position the sample. One of the copper pieces was free to move horizontally against a spring. This block shaped piece was electrically insulated from the rest of the system with silica and silicone grease was used to make good thermal contact. Two small heaters, marked A and B in figure 4.11, were used to produce temperature differences of up to 5 K in any direction along the sample and hence, the symmetry of the value of the thermoelectric power of the sample could be checked. A larger 10 watt heater was wound around the holder as for the Hall copper block. Temperatures between 140 K and 420 K could be obtained.

Two copper-constantan thermocouples were held by a copper screw against each one of the small copper pieces pressing onto the sample, and placed close to each end of the bar. The thermocouples wires were continuous all the way, this was achieved by using two 6-way glass-to-metal seals. The reference junctions of the thermocouples were held at 0^oC and

the e.m.f. of each one was measured using the Hewlett Packard digital multimeter 3465B in the microvolt meter mode. The thermoelectric power of the device was measured via the two copper wires ((1)and (2) in figures 4.11 and 4.12) of the thermocouples with the same multimeter or with a Bradley digital voltmeter 173 B. To check on the temperature difference between the ends of the sample with more accuracy, the constantan wires ((3) and (4) in figures 4.11 and 4.12) were connected together and the e.m.f, produced by the temperature difference, was measured via the copper wires using the same multimeter again. The temperature of the sample itself was assumed to be the mean of T_A and T_B. The thermocouple used for T_B measurements (wires (2) and (4) in figure 4.11) was attached to the small insulated copper block and its corresponding copper wire was used as the positive electrode for the thermoelectric power measurements. Hence, for an n-type semiconducting bar, with $T_A > T_B$, the reading on the voltmeter would be negative and thus a negative sign was given to the thermoelectric power. Times of up to 30 minutes were allowed between readings to ensure thermal equilibrium of the system.

4.8   ELECTRON MICROSCOPY

4.8.1 Scanning Electron Microscope

A Scanning Electron Microscope (S.E.M.), the Cambridge Instruments model Stereoscan 600, was used in this part of the present study.

With this instrument, the area to be examined is irradiated with a finely focussed electron beam which is swept in a raster across the surface of the specimen. Numerous effects occur when the focussed electron beam impinges on a specimen surface, for example, true secondary electrons, backscattered electrons, characteristics x-rays, Auger electrons and photons of various energies are emitted, and any of them can be collected to produce the displayed signal. In the S.E.M, the primary signal of interest is the variation in secondary electron emission current that takes place as the
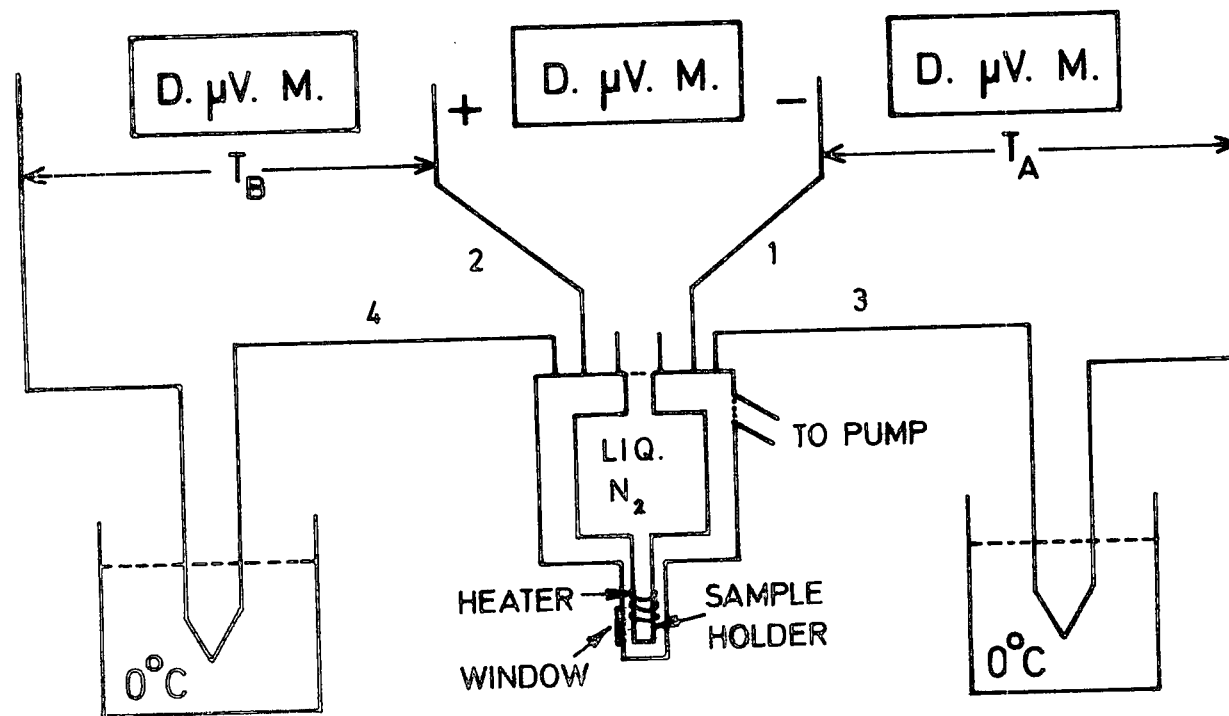
FIG. 4·12   THERMOELECTRIC   POWER   APPARATUS

electron beam is scanned across the specimen. Most variations are due to differences in surface topography. Because of the large depth of focus in the S.E.M, a three dimensional effect is obtained. The basic components of the S.E.M. are the electron gun, the electric lens system, the secondary electron collector, deflecting coils, visual and recording cathode ray tubes (C.R.T's) and the associated electronics. These are shown diagramatically in figure 4.13.

The S.E.M. can be used in a variety of modes of which the Electron-Beam-Induced-Current (E.B.I.C.) mode is particularly interesting in semiconductor applications. Suppose the focussed electron beam bombards a sample in the close proximity of a p-n junction. The incident beam creates free electron-hole pairs. The carriers are separated by the field of the junction so that the minority carriers are collected during their diffusion towards the junction. Thus, if a bias is supplied to the specimen, a beam induced current is produced in the external circuit. It is this current which constitutes the video signal in an S.E.M. used in the E.B.I.C. mode.

To examine our samples in the E.B.I.C. mode, a small biassing circuit was devised to allow electrically active defects in the crystals under study to be detected. The circuit, which is shown in figure 4.14, allowed a voltage variable between -9 to +9 volts to be applied to the sample. The bias current was amplified by a Keithley current amplifier and fed to the display C.R.T. of the S.E.M. The 2.2 M.ohm potentiometer in series with the device was used as a current limiter to protect against accidental destruction and to provide impedance matching. The capacitor served as a low impedance pass for the E.B.I.C. signal and also helped to match time constants.

The S.E.M. can also be used in the cathodoluminescence mode. In this mode, the cathodoluminescence emission produced by the bombarding electrons is collected via a convergent lens and a glass light pipe and
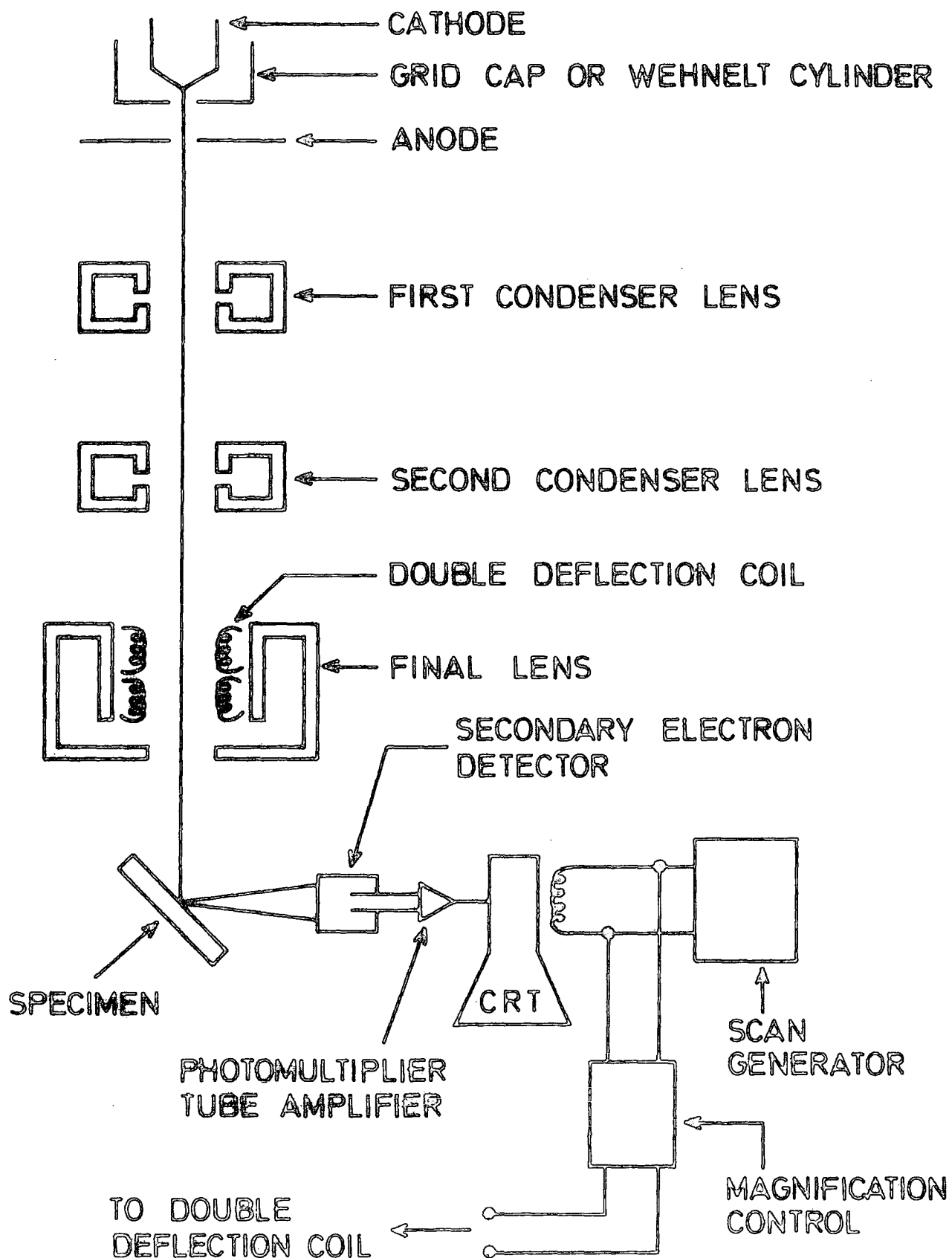
CATHODE

GRID CAP OR WEHNELT CYLINDER

ANODE

FIRST CONDENSER LENS

SECOND CONDENSER LENS

DOUBLE DEFLECTION COIL

FINAL LENS

SECONDARY ELECTRON DETECTOR

SPECIMEN

CRT

SCAN GENERATOR

PHOTOMULTIPLIER TUBE AMPLIFIER

MAGNIFICATION CONTROL

TO DOUBLE DEFLECTION COIL

FIG. 4·13 SCHEMATIC DIAGRAM OF THE SCANNING ELECTRON MICROSCOPE

9 V

9 V

$10\,k\Omega$

V

SAMPLE

$10\,\mu F$

$2.2\,M\Omega$

TO C.R.T.

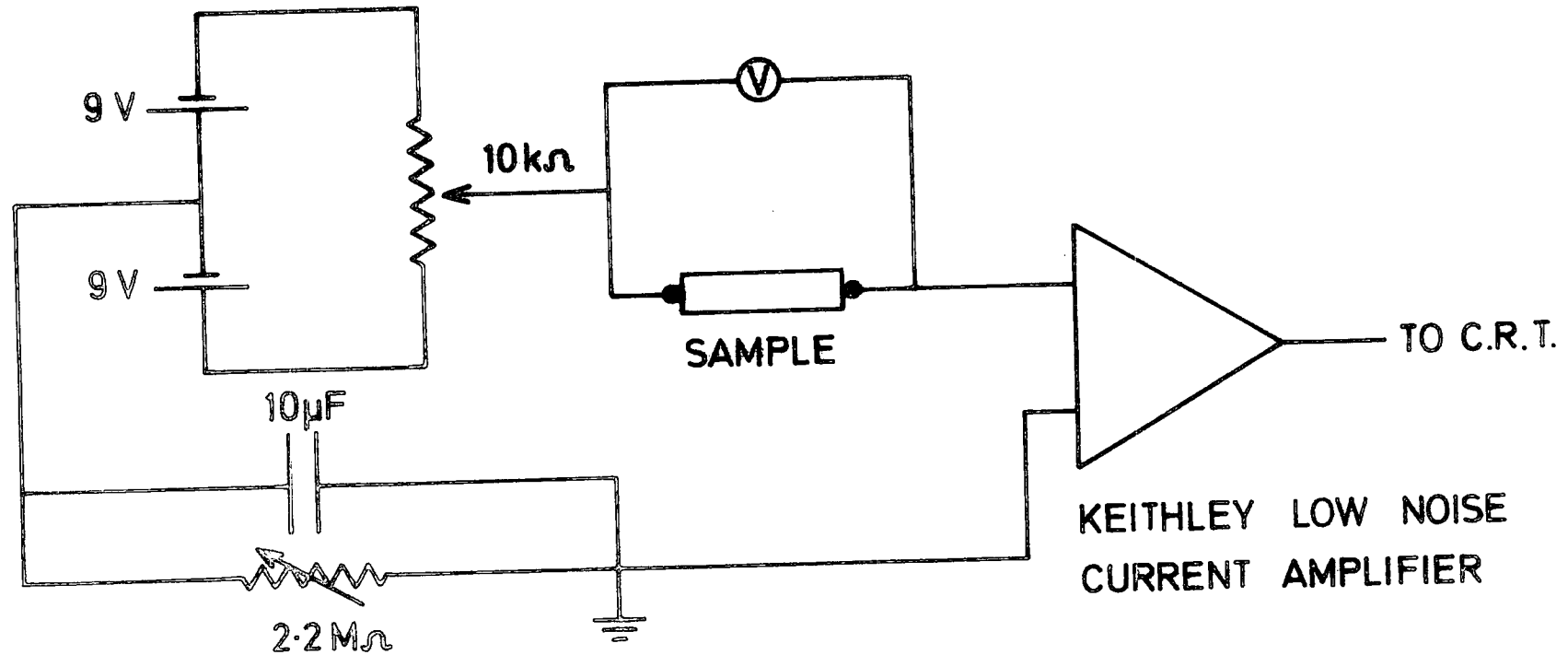KEITHLEY LOW NOISE
CURRENT AMPLIFIER

FIG. 4·16   BIASSING AND EBIC SIGNAL DETECTION CIRCUIT FOR
HIGH IMPEDANCE SAMPLES

fed to the S.E.M. photomultiplier. Then, the topography of the material

can be examined as a function of the emitted cathodoluminescence intensity,

indicating the distribution of recombination centres which either emit

light or are radiationless. The information is obtained only from the

immediate surface and for a region a few hundred angstroms below it

depending on the accelerating voltage of the electron beam.

In our investigation, the cathodoluminescence mode was achieved

by removing the scintillator from the photomultiplier tube and replacing

it with a light pipe made from perspex.

4.8.2. Transmission Electron Microscope

A transmission electron microscope consists basically of an

illuminating system and an imaging system. The former includes the

electron gun and a condenser lens arrangement, while the latter includes

an objective and projector lens with usually an intermediate lens situated

between the other two lenses of the imaging system. These three successive

stages of enlargement project the image onto the fluorescent screen of the

microscope. Typical enlargements obtained by each one of the lenses

forming the imaging system are 25 x 10 x 100 respectively, giving a total

enlargement of 25,000 X. In contrast with optical microscopes, the depth

of field of the electron microscope is very large and hence, it is possible

to position the camera for photographic recording of the image below the

fluorescent screen without necessitating any adjustment of the objective

lens focussing. Because the photographic emulsions usually used are

relatively slow and have a small grain size, a much better contrast and

resolution is obtained on the photographic plate than appears on the

fluorescent screen. Because of the high accelerating voltage used for the

electron beam (typically 80 kV to 200 kV) and its very small spot size,

highly regulated voltage supplies are used with each one of the lenses.

The specimens must be very thin (a maximum of just a few micrometers in

thickness) in order to allow the electron beam to pass through and produce

a clear diffraction pattern.   The instrument in use in this department

is a Jem 120 electron microscope.

CHAPTER 5

OPTICAL PROPERTIES

5.1   INTRODUCTION

This chapter introduces the results obtained from the optical measurements carried out on the ZnSe:In and ZnSe:Ga crystals grown in this department.   The experimental technique has been described in the previous chapter.

The measured photoluminescence and cathodoluminescence spectra will be described in the first part ; photoconductivity and infrared quenching measurements are presented in the following section, and finally, the results from the thermally stimulated current and luminescence are introduced.   At the end of each section, the results are discussed and in the final section a summary of the various conclusions is given.

5.2   EMISSION SPECTRA

5.2.1 Photoluminescence

The peak wavelengths, photon energies and widths of the photo-luminescence (P.L.) emission bands of several of the indium and gallium doped ZnSe crystals are summarised in tables 5.1 and 5.2.   Some representative emission spectra are shown in figures 5.1 to 5.4.   The curves are uncorrected for system response, however, in this range, the S-20 photomultiplier (P.M.) tube spectral sensitivity does not vary too much.

A common feature in all the crystals is the broad band emitted at room temperature and centred at about 625 nm with its maximum varying between 600 nm to 635 nm from sample to sample.   At 85 K, all the samples showed two bands, overlapping to a certain extent, one in the green at about 555 nm and the other in the orange at 625 nm approximately, again,

T A B L E   5.1

PHOTOLUMINESCENCE BANDS OF AS-GROWN ZnSe:In CRYSTALS

Crystal Boule #	Nominal Doping p.p.m	Actual In content p.p.m.	BLUE BAND @ 85 K			GREEN BAND @ 85 K			RED BAND @ 85 K			I_G/I_R	RED BAND @ 295 K		
			λ(nm)	E(eV)	$E_{\frac{1}{2}}$(eV)	λ(nm)	E(eV)	$E_{\frac{1}{2}}$(eV)	λ(nm)	E(eV)	$E_{\frac{1}{2}}$(eV)		λ(nm)	E(eV)	$E_{\frac{1}{2}}$(eV)
342	100	85	442	2.81	0.30	562	2.21	0.24	629	1.97	0.19	0.51	630	1.97	0.25
349	1000	800	-	-	-	567	2.19	0.29	625	1.98	0.17	2.13	620	2.00	0.22
375	50	95	-	-	-	553	2.24	0.24	626	1.98	0.20	1.66	630	1.97	0.26
376	100	108	-	-	-	555	2.23	0.26	625	1.98	0.21	1.62	625	1.98	0.30
377	250	235	-	-	-	560	2.21	0.24	626	1.98	0.21	1.50	628	1.97	0.27
386	5	34	-	-	-	566	2.19	0.24	613	2.02	0.26	0.74	630	1.97	0.26
405	50	56	-	-	-	553	2.24	0.25	627	1.98	0.24	1.07	632	1.96	0.26
4C5	50	56	-	-	-	546	2.27	0.23	622	1.99	0.28	1.16	620	2.00	0.37
405	50	56	-	-	-	551	2.25	0.24	620	2.00	0.22	1.47	613	2.02	0.38
407	5	13	460	2.70	0.09	555	2.23	0.20	622	1.99	0.26	1.19	632	1.96	0.29
407	5	13	460	2.70	0.09	555	2.23	0.25	626	1.98	0.23	1.55	636	1.95	0.33
408	250	250	-	-	-	551	2.25	0.29	619	2.00	0.23	1.64	603	2.06	0.28
410	100	107	-	-	-	547	2.27	0.28	625	1.98	0.24	0.94	630	1.97	0.29
410	100	107	-	-	-	553	2.24	0.22	623	1.99	0.22	1.24	632	1.96	0.28

T A B L E   5.2

PHOTOLUMINESCENCE BANDS OF SOME DOPED ZnSe CRYSTALS

Crystal Boule #	Nominal Doping p.p.m	Actual Dopant content p.p.m	BLUE BAND @ 85 K			GREEN BAND @ 85 K			RED BAND @ 85 K			I_G/I_R	RED BAND @ 295 K		
			λ(nm)	E(eV)	$E_{\frac{1}{2}}$(eV)	λ(nm)	E(eV)	$E_{\frac{1}{2}}$(eV)	λ(nm)	E(eV)	$E_{\frac{1}{2}}$(eV)		λ(nm)	E(eV)	$E_{\frac{1}{2}}$(eV)
Indium Doped - Annealed in Zn Vapour															
405	50	56	458	2.71	0.08	548	2.26	0.22	629	1.97	0.27	0.51	604	2.05	0.36
408	250	250	458	2.71	0.06	545	2.27	0.27	630	1.97	0.22	0.81	630	1.97	0.31
410	100	107	-	-	-	547	2.27	0.25	626	1.98	0.22	0.90	622	1.99	0.33
410	100	107	-	-	-	548	2.26	0.24	627	1.98	0.24	0.70	615	2.02	0.35
Gallium Doped - As - grown															
381	50	51	-	-	-	567	2.19	0.20	630	1.97	0.19	0.09	631	1.96	0.24
382	100	112	-	-	-	555	2.23	0.20	625	1.98	0.29	0.43	625	1.98	0.25
Gallium Doped - Annealed in Zn Vapour															
381	50	51	438	2.83	0.42	564	2.20	0.14	633	1.96	0.19	0.10	632	1.96	0.25
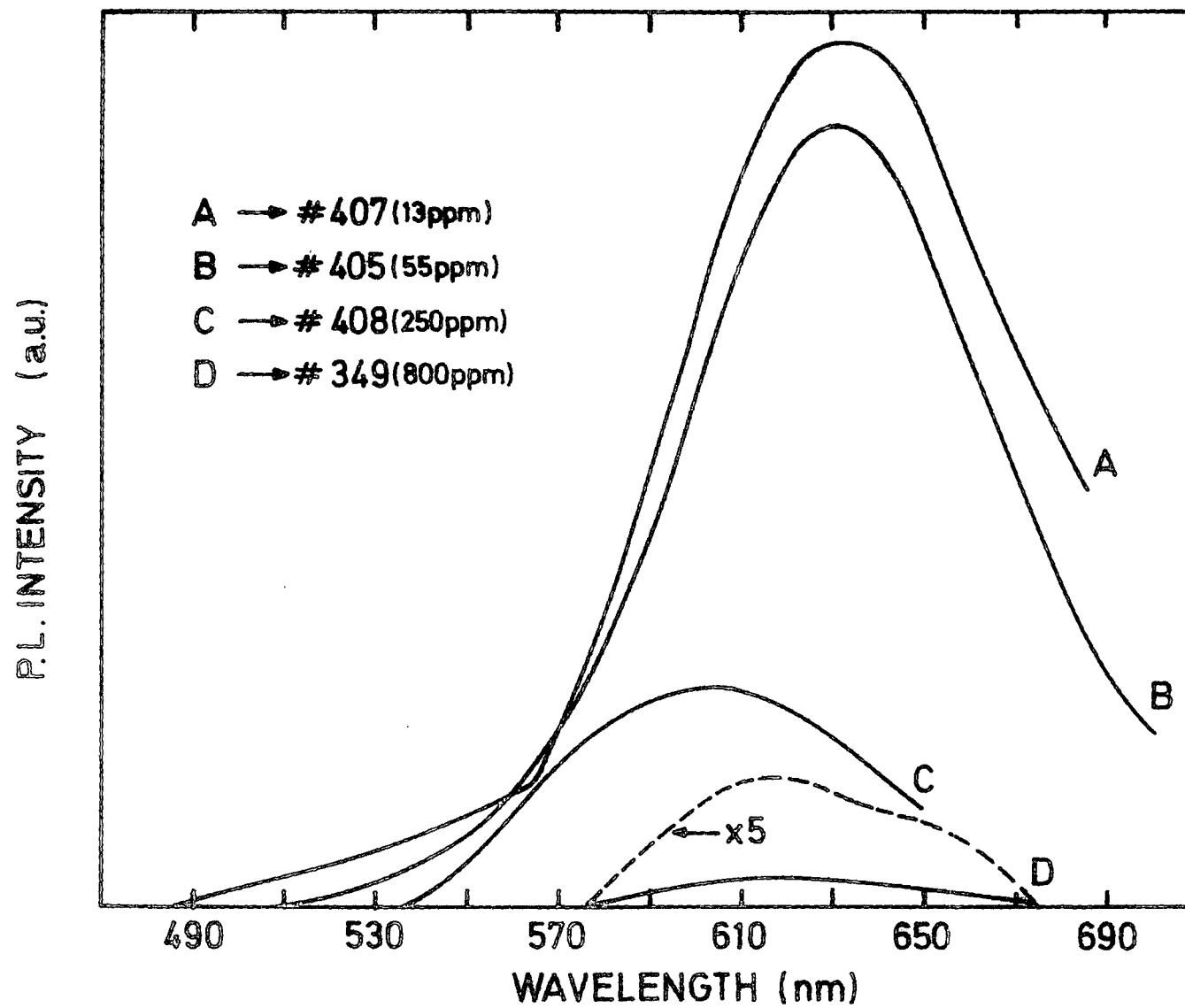
FIG. 5·1   P. L. EMISSION AT 295 K OF ZnSe CRYSTALS WITH DIFFERENT
In CONCENTRATIONS
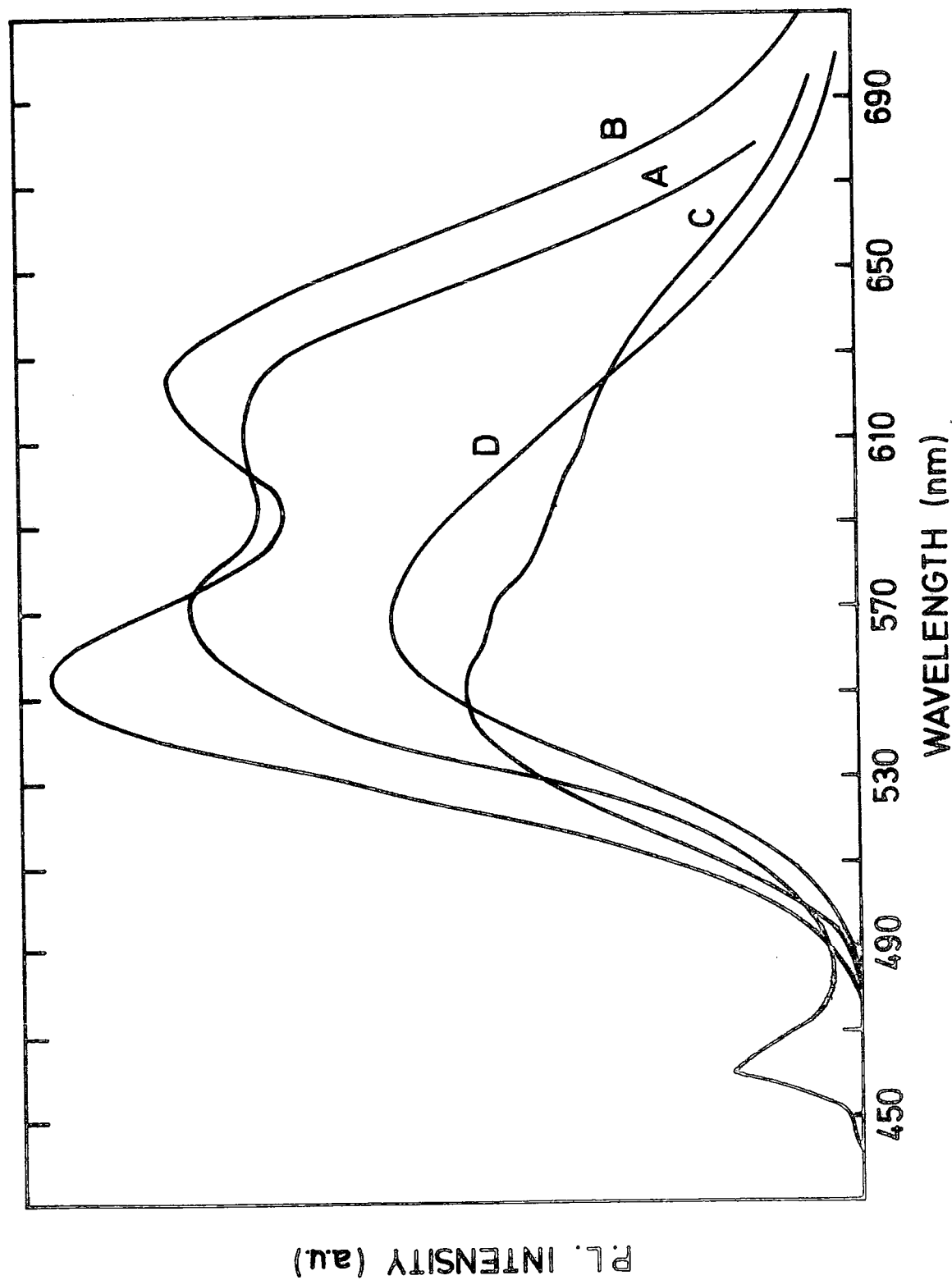
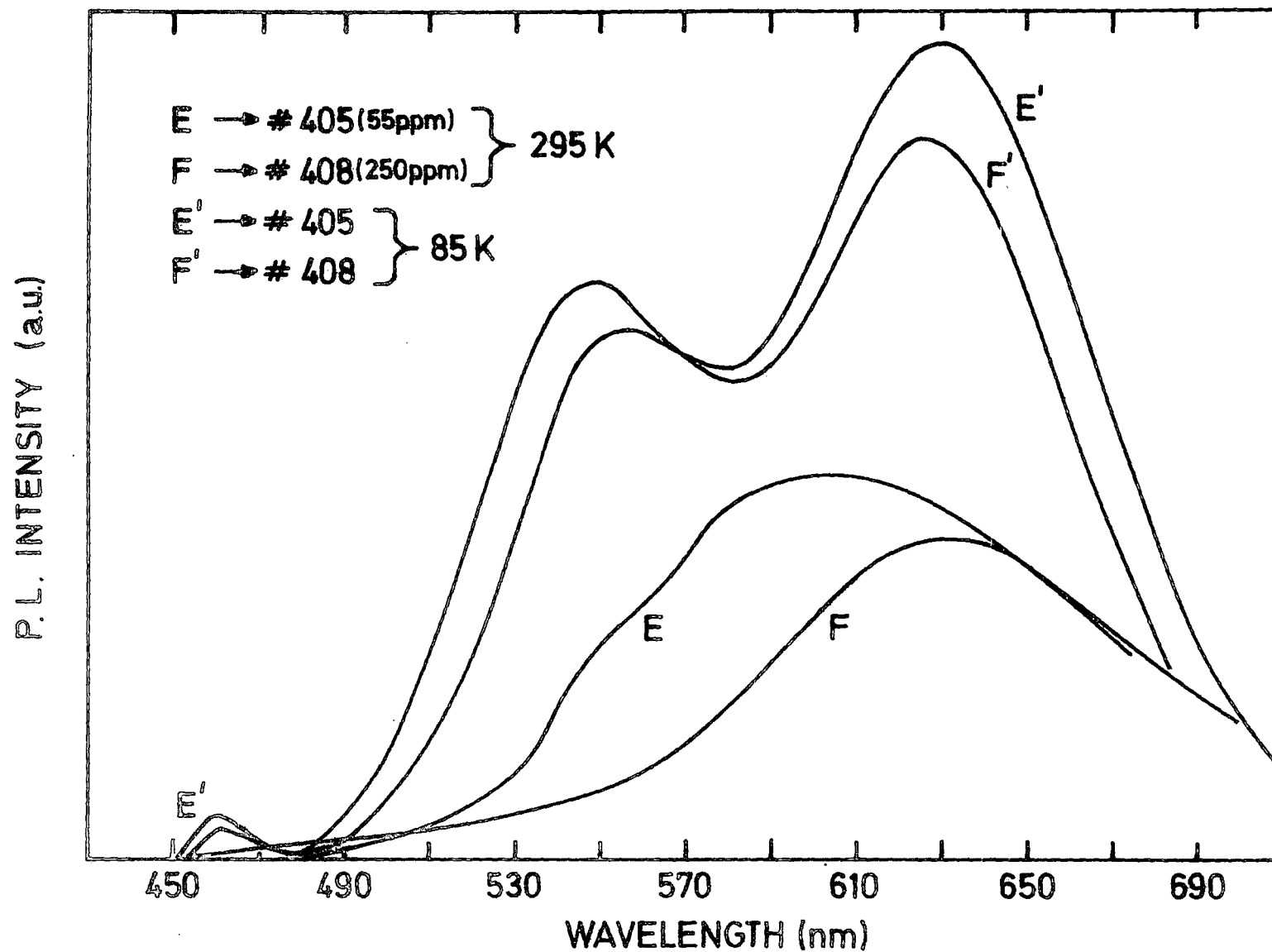FIG. 5.2   P.L. EMISSION AT 85 K OF THE ZnSe CRYSTALS
AS IN FIG. 5·1.

FIG. 5·3   P.L. EMISSION AT DIFFERENT TEMPERATURES OF TWO ZnSe:In
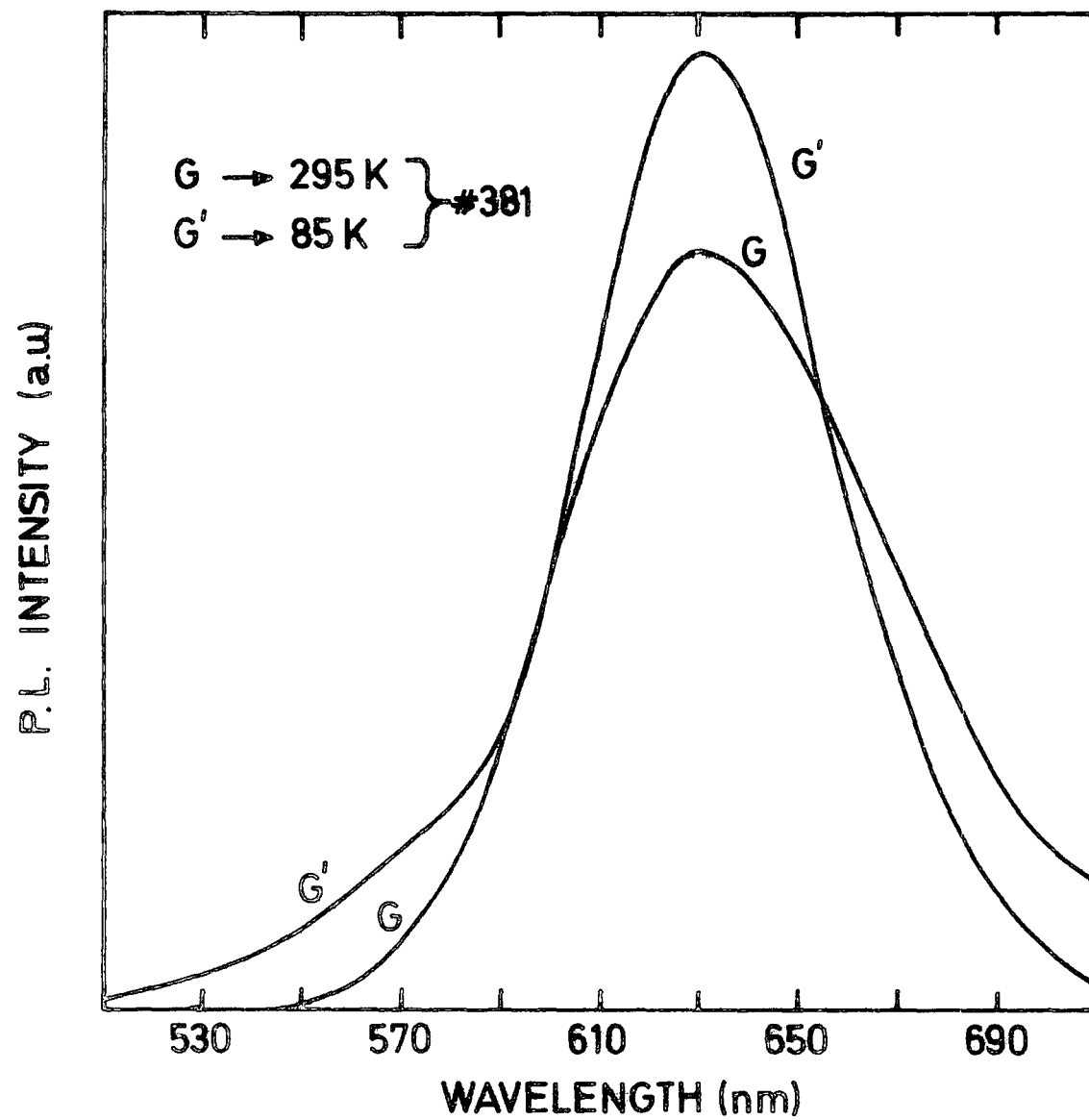CRYSTALS ANNEALED IN Zn VAPOUR

FIG. 5·4   P.L. EMISSION OF A 50ppm Ga DOPED ZnSe CRYSTAL
AT DIFFERENT TEMPERATURES

varying slightly from sample to sample. Unresolved edge emission near 460 nm was also exhibited by some crystals at 85 K. Even though the 625 nm band was centred in the orange part of the spectrum, it will in what follows be referred to as the red band.

In an attempt to see if there were a correlation between the quantity of indium in the different samples and the ratio, I_G/I_R, of the intensities of the green and red bands at 85 K, the results have been plotted graphically in figure 5.5 ; where although the spread is quite large, it is apparent that the ratio tended to increase with indium content. The actual concentrations of indium and gallium were determined by atomic absorption spectroscopy. With the gallium doped material, the red band was more intense than the green, compared with the emission in material doped with similar concentrations of indium.

After heating in zinc vapour for a period of three days at 600° C, the intensity of the luminescence emission was reduced, this effect has been reported by several authors. The decrease was more pronounced with the green band so that the ratio I_G/I_R was smaller than unity for all zinc treated material.

The half-width of the red band at room temperature was always greater than that at 85 K ; with values near 0.3 eV and 0.25 eV respectively. This difference has been mentioned by Yamaguchi et al(1977b) for similar material.

5.2.2 Cathodoluminescence

The cathodoluminescence (C.L.) emission spectra of one of the crystals, namely ⧺ 405, before and after heat treatment in zinc, are shown in figures 5.6 and 5.7. A major difference compared with the P.L. emission is the total disappearance of the red band as well as a large enhancement of the edge emission (blue) bands, both at room temperature and at 85 K. A further enhancement of the blue emission was also seen on cooling the crystal even more.
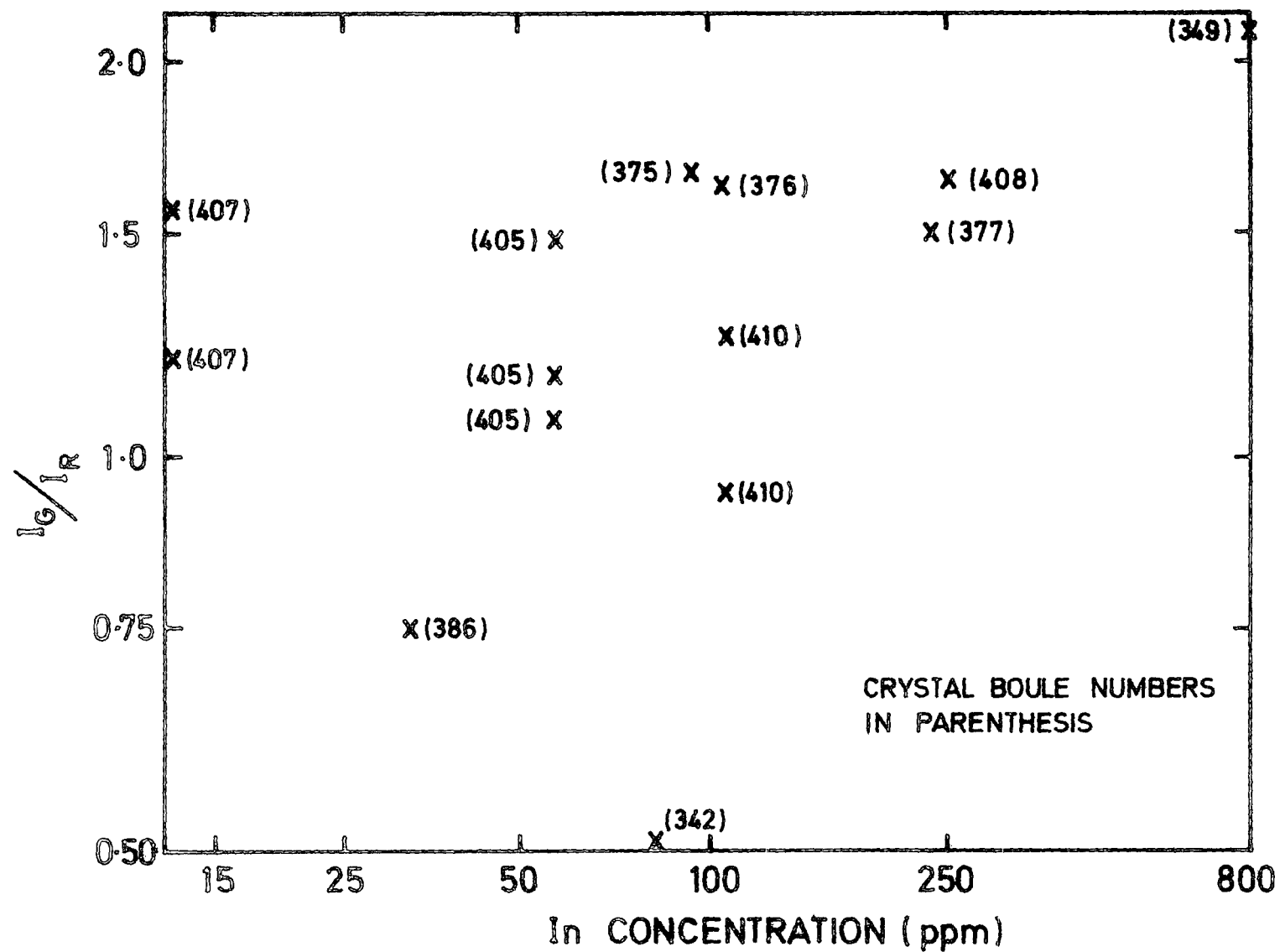
FIG. 5.5   RATIO OF P.L. EMISSION, AT 85 K, OF GREEN TO RED BANDS
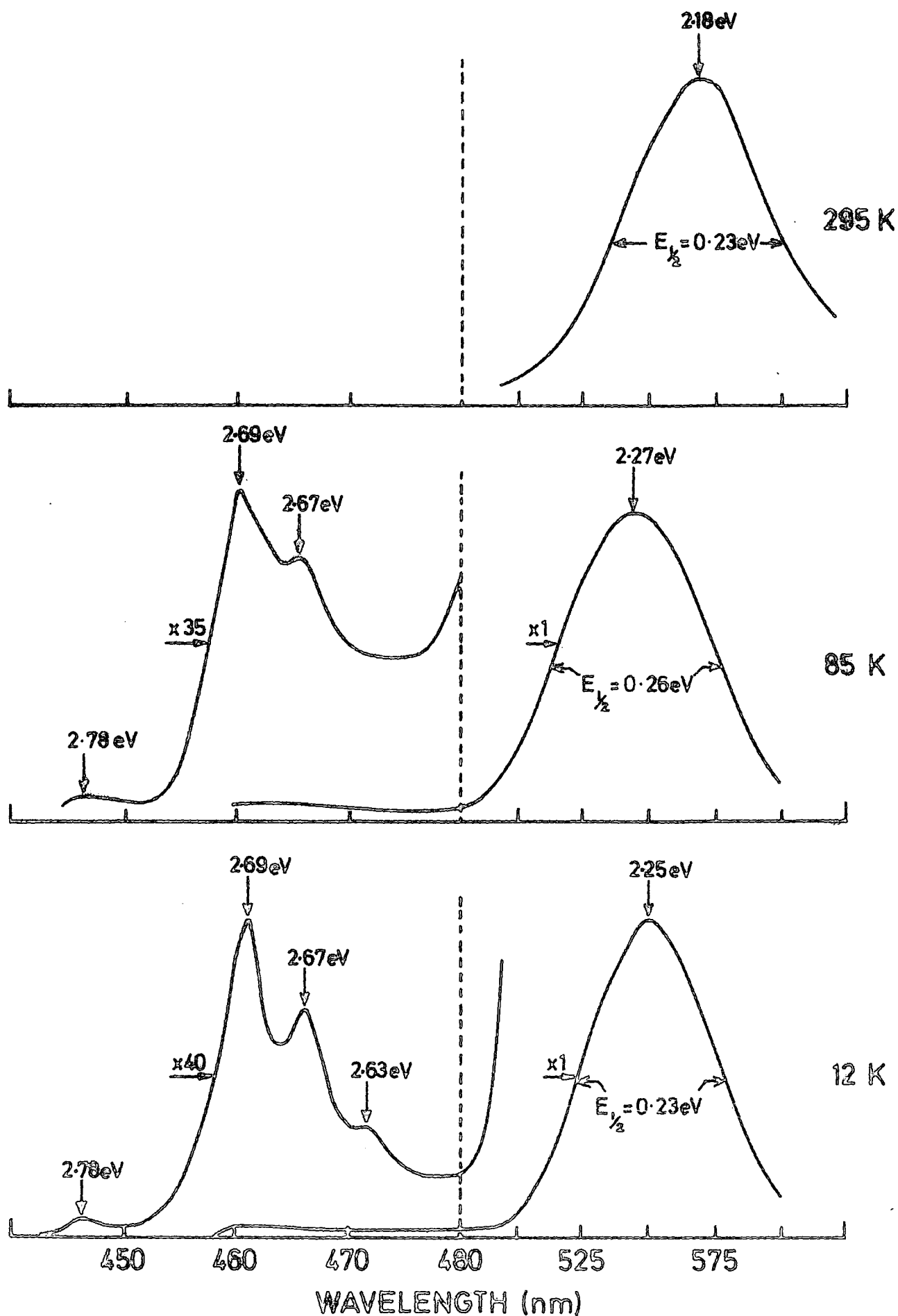VERSUS In CONCENTRATION, FOR SEVERAL ZnSe:In CRYSTALS.

FIG. 5·6   C.L. EMISSION OF, AS GROWN, 55ppm In DOPED
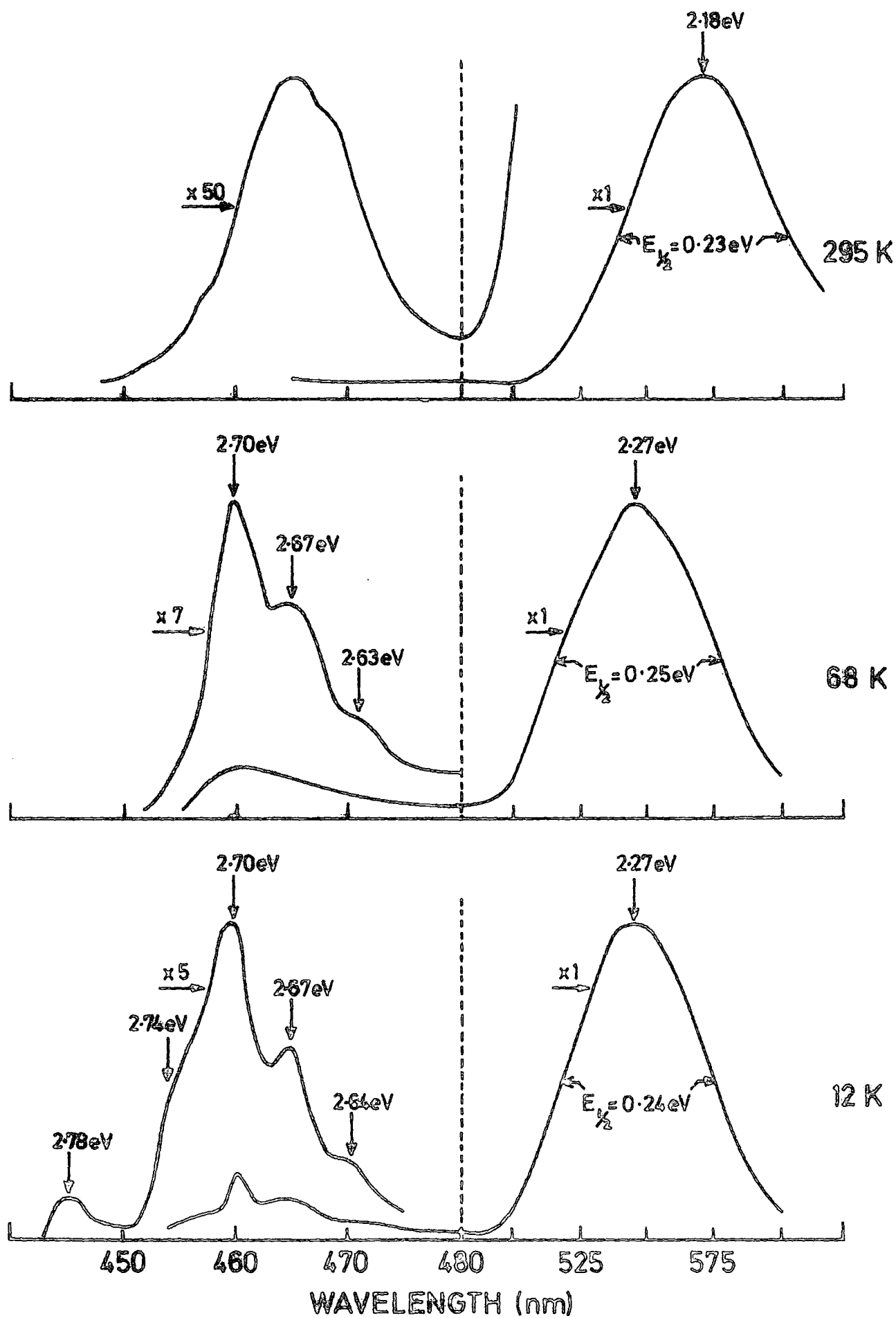ZnSe(#405) AT DIFFERENT TEMPERATURES.

FIG. 5·7 C.L. EMISSION, AT DIFFERENT TEMPERATURES, OF ZnSe(#405) IN FIG. 5·6, AFTER ANNEALING IN Zn VAPOUR.

The wavelengths of these blue and green C.L. peaks are in good agreement with those of similar emission bands obtained at 4 K using U.V. excitation either from a laser or from a mercury lamp as reported by previous workers on similar ZnSe doped crystals ; see for example Bouley et al (1975), Etienne and Bougnot (1975), Swaminathan and Greene (1976), Yamaguchi et al (1977b) and Papadopoulo et al (1978).

Although the P.L. emission appeared orange-pink to the eye at room temperature, and strong yellow at 85 K, the C.L. emission on the other hand, with a current density of the electron beam of $\sim$ 13 A/m^2, appeared yellow at room temperature and green at 85 K and below. When electron microprobe analysis in a similar sample was attempted at room temperature, the light emission (C.L.) from the region where the electron beam, of 15 to 20 kV and 40 nA, was striking the surface with a 5 μm diameter spot (i.e., with a current density of the electron beam of some 2×10^3 A/m^2) was blue-green. This indicates that the larger the current density of the source of excitation, the stronger the edge emission bands and the weaker the deep level emission. This fact has already been mentioned by Bouley et al (1975) and by Fitzpatrick et al (1979) for ZnSe:Ga.

5.2.3 Discussion of the Results

If the results on PL and CL are considered, then three groups of emission lines and bands are expected. First, there are lines resulting from the radiative recombination of bound excitons which, for ZnSe, occur in the range from 2.80 eV to 2.72 eV, which includes the so-called I_2 lines (recombination of excitons bound to neutral donors) and the I_1 lines (recombination of excitons bound to neutral acceptors). Second, there are bands between 2.72 eV and 2.50 eV which are called the edge emission and are attributed to distant donor acceptor (D-A) pair recombination with LO phonon cooperation ; and, third, the low energy bands which are the green and red or self-activated (S.A.) bands.

Of the first group, only a broad structureless peak centred at 2.78 eV was observed, see figure 5.7 (c), which probably includes the I_2 lines reported by Merz et al (1972) and attributed to excitons bound to the donors Al, Ga, In, Cl and F ; it probably also includes the I_1 lines reported by Dean and Merz (1969) and Merz et al (1973).

In figures 5.6(c) and 5.7(b) and (c) three peaks from the second group, i.e. the edge emission, can be seen. The prominent one, situated between 2.69 and 2.70 eV, is present in as-grown undoped ZnSe or in ZnSe doped with a group IIIa element after annealing in zinc. According to several authors (see for example Gezci and Woods, 1975 ,Bouley et al, 1975 , Etienne and Bougnot, 1975 , Swaminathan and Greene, 1976 , and Shirakava and Kukimoto, 1980), it is attributed to the recombination of an electron from a shallow hydrogenic donor such as aluminium, gallium or indium (see Merz et al 1972) to a hole in a shallow acceptor like sodium or lithium, or even some native defect such as a singly charged zinc vacancy (V_{zn}') (see Merz et al,1972 and 1973) . The other two smaller peaks, decreasing in intensity with increasing wavelength and separated by equal intervals of 30 meV, are phonon replicas of the first one.

Finally, the two bands centred at about 555 nm and 625 nm at 85 K (see figures 5.2 and 5.3) have been reported by most of the above mentioned workers and also by Iida (1968,1969) and Fujita et al (1979). The origin of these bands is still uncertain, however, it seems well accepted that transitions from either shallow or deep donors to deep acceptors are involved. In particular, Stringfellow and Bube (1968) suggested that the emission at 1.95 eV is produced by a pair transition between a shallow donor level and a deep acceptor 0.72 eV above the valence band which is associated with a copper impurity. It was suggested that another red emission at 1.97 eV was produced by a transition from the conduction band to the same acceptor level ; while the green emission at 2.34 eV is produced by a transition between the conduction band and another

acceptor level 0.35 eV above the valence band also associated with copper but with a different charge state. Furthermore, the acceptor level at 0.72 eV, according to these authors, was identified as a singly negatively charged copper ion on a zinc site $(Cu_{Zn}^{|})$ while the other copper level at 0.35 eV is supposed to be neutral (Cu_{Zn}^{x}). Jones and Woods (1974) and Gezci and Woods (1975) also attributed the red and green bands to copper centres, but they placed these two levels at 0.46 and 0.86 eV above the valence band because they took the value of the band gap to be 2.82 eV instead of 2.7 eV as assumed by Stringfellow and Bube.

Another suggestion given for the green emission is that it might be a Lambe-Klick type transition from a donor level produced by interstitial copper, in a similar manner as described by Shionoya et al (1966).

Jones and Woods (1974) suggested three models to explain the red band :

(a) it could be the S.A. band which involves a transition from a coactivator (i.e. a donor level) to a zinc vacancy and hence, it is of the Prener-Williams type,

(b) it could be the copper red band which is a transition from the conduction band to an isolated copper acceptor level 0.86 eV above the valence band and therefore, it is a transition of the Schön-Klasens type, and,

(c) again, it could be a copper band but involving a transition from a deep donor, probably the same as for the S.A. band, to the second copper acceptor level 0.46 eV above the valence band.

It has also been suggested that S.A. emission is produced by donor acceptor pair recombination that in our samples the group III element act as a donor, while the acceptor is a complex centre consisting of a zinc vacancy and a neighbouring group III ion (see, for example, Fujita et al, 1979) .

The fact that these two bands, the red and green, are present in the crystals studied in this investigation, is not surprising since, as can be seen in table 4.1, all the as-grown crystals contained relatively large amounts of copper, i.e. 4 to 10 ppm (and about 40 ppm in the worst case) and in the region of 2 to 5 ppm for those annealed in zinc vapour, as calculated from the atomic absorption analysis. However, even though this analysis may be relatively unreliable for copper content measurements, because this element is usually present almost everywhere, we must conclude that some copper is certainly present in all our specimens.

From figure 5.5 and table 5.2, the following three conclusions can be drawn :

(i) the ratio of the intensities of the green luminescence to the red luminescence I_G/I_R was increased by increasing the indium concentration ;

(ii) for similar concentrations of indium or gallium, I_G/I_R was smaller in the gallium doped material ; and,

(iii) after the heat treatment in zinc, the ratio I_G/I_R was very much reduced.

Stringfellow and Bube (1968) noticed that after annealing their ZnSe:Cu crystals in selenium, the ratio I_G/I_R was increased. Furthermore, they also pointed out that this ratio could also be increased by adding more copper to ZnSe:Cu, whereas after adding donors, the ratio was drastically reduced. When ZnSe is annealed in selenium, the number of selenium vacancies acting as donors is decreased while the number of zinc vacancies, acting as acceptors, is increased ; the effective native compensation is then increased and the crystal becomes more resistive. Now, by adding more copper in ZnSe, the number of acceptors is also increased. On the other hand, when annealing in zinc, the opposite of what happens with a heat treatment in selenium occurs, i.e. the number of acceptors is decreased and the crystal becomes more conductive. All this indicates that the ratio

I_G/I_R increases when the ratio of acceptor to donor concentration is increased and vice-versa.

It follows therefore, according to the first conclusion that, when more indium is added, the ratio of acceptor to donor concentration is increased and hence, the crystal becomes more compensated and less conductive. The second conclusion suggests that gallium does not compensate as much as indium but does follow the same trend, i.e. I_G/I_R increases with increasing gallium concentration as can be seen in table 5.2. The third conclusion indicates that heat treatment in zinc removes some of the compensation since after this treatment, the I_G/I_R ratio is reduced.

A final point to be mentioned in this section is the fact that the spectral response apparently depends on the type of excitation. When these crystals were photo-excited with U.V. light from a lamp or from a laser (P.L.), the red band only was obtained at room temperature; whereas when excited with an electron beam (C.L.) at relatively high current densities, the red band completely disappeared at 295 K and at 85 K, while the green band was very much enhanced at 295 K. Furthermore, the edge emission increased drastically with the current density of the electron beam. Even though Bouley et al (1975) and Fitzpatrick et al (1979) also mentioned these phenomena, no explanation was given.

Several tentative explanations may be suggested, but obviously the recombination traffic through the different centres involved changes as the intensity of the bombardment increases. The presence of a large number of electrons in the conduction band with large kinetic energies may, perhaps via the agency of Auger processes, increase the hole capture rate through the Cu_{Zn}^{x} centres relative to that through the Cu_{Zn}' centres, thus allowing more electrons to recombine at the neutral acceptor level thus increasing the intensity of the green band.

We are, however, aware that this explanation is far from

satisfactory and more work should be done. For example, the different

emission spectra could be measured at different beam current densities

from very low values upwards to see if there is some gradual change in

the ratio I_G/I_R as well as in the ratio of intensity of band edge and

deep centre luminescence intensities at room temperature.

5.3   PHOTOCONDUCTIVITY

   5.3.1 Photoconductive Spectral Response

      The normalized photoconductive spectral responses of some of the bar

shaped indium doped samples, measured at 295 K and 85 K, are shown in figures

5.8 to 5.13. The peaks are summarised in table 5.3. Because of the very slow

photoconductive response of this material, it was necessary to scan the wave-

lengths at very slow speeds; the time taken to reach equilibrium was longer at

85 K, and became even longer for those crystals with higher indium concentra-

tions, and for these, where the time to reach a steady state was up to 10

minutes, the spectral response was measured point by point.

      The photoconductive sensitivity was about one order of magnitude

greater at room temperature than at 85 K, although crystal ⧣ 405 was

not photoconductive at all at 295 K, because of its relatively high dark

d.c. conductivity. The main feature of these response curves is the

presence of a peak near 510 nm shifting to higher energies on cooling,which

has been reported by Bube and Lind (1958) in ZnSe:Br:Cu. At room temperature,

a substructure seems to give rise to a shoulder on the low energy side of

this peak. Also, a small broad infrared band at 85 K, centred at about

2.25 μm (0.55 eV), with a much faster response, was present in these

samples ; it was about five orders of magnitude smaller than the near band

gap response. The complicated shape of this infrared response was caused

by the fact that the lamp (quartz halogen) along with the double prism

monochromator used for this experiment, produced a weak structured incident

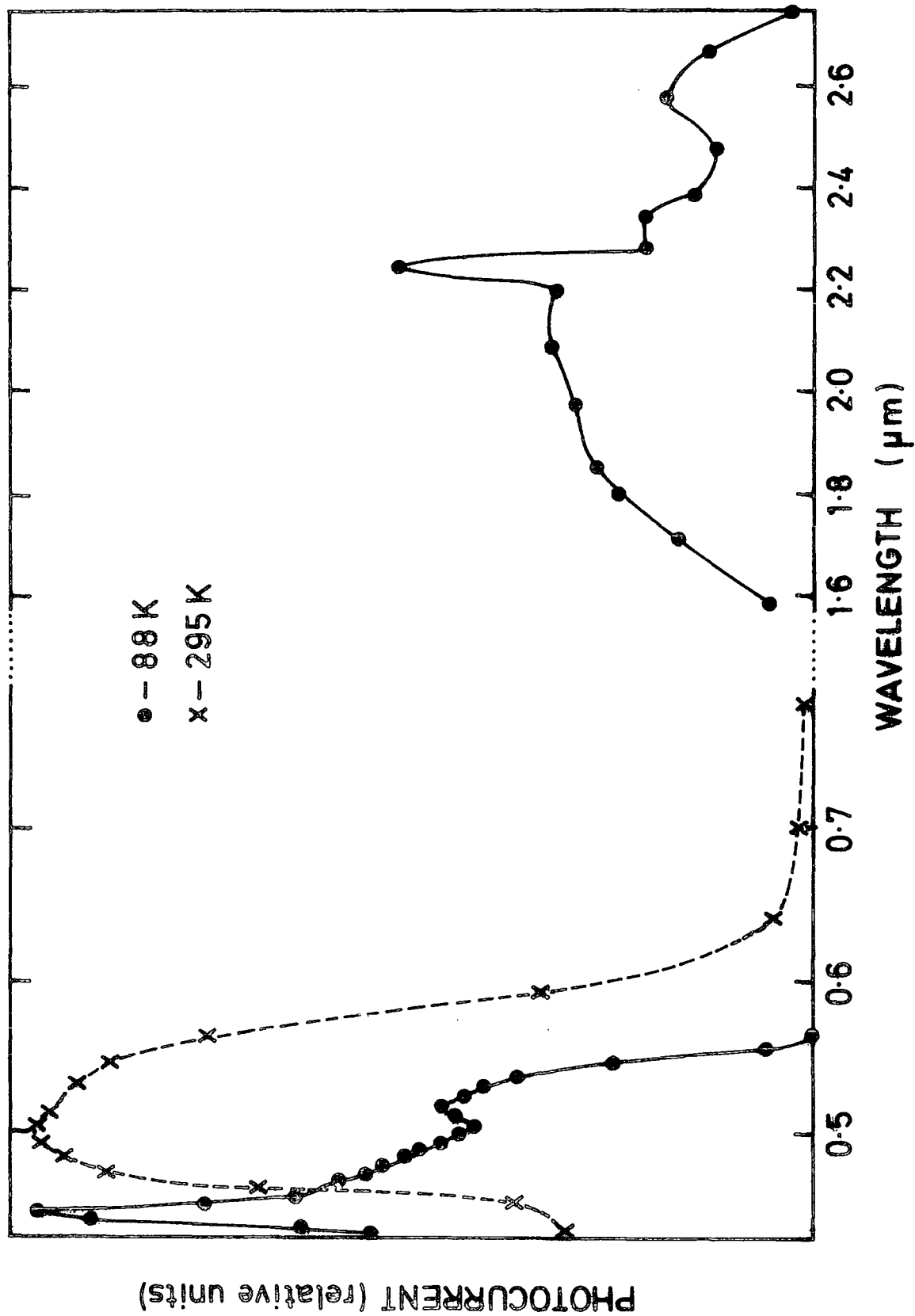illumination at those wavelengths, and it was very difficult to obtain a

FIG. 5·8   PHOTOCONDUCTIVE RESPONSE FOR ZnSe : In #342 E (85ppm) AT
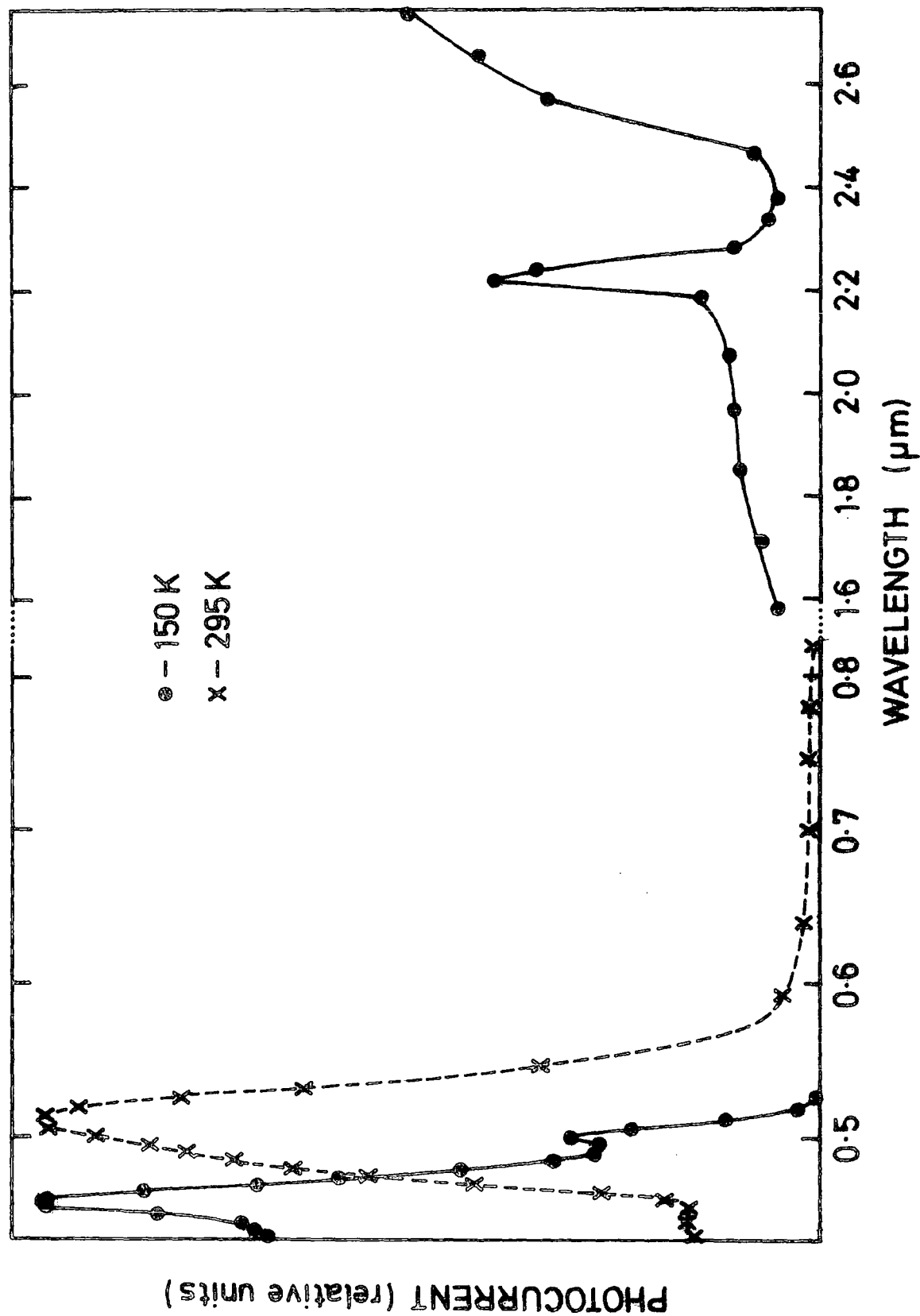DIFFERENT TEMPERATURES.

FIG. 5.9   PHOTOCONDUCTIVE   RESPONSE   FOR   ZnSe : In#349 (800ppm)   AT
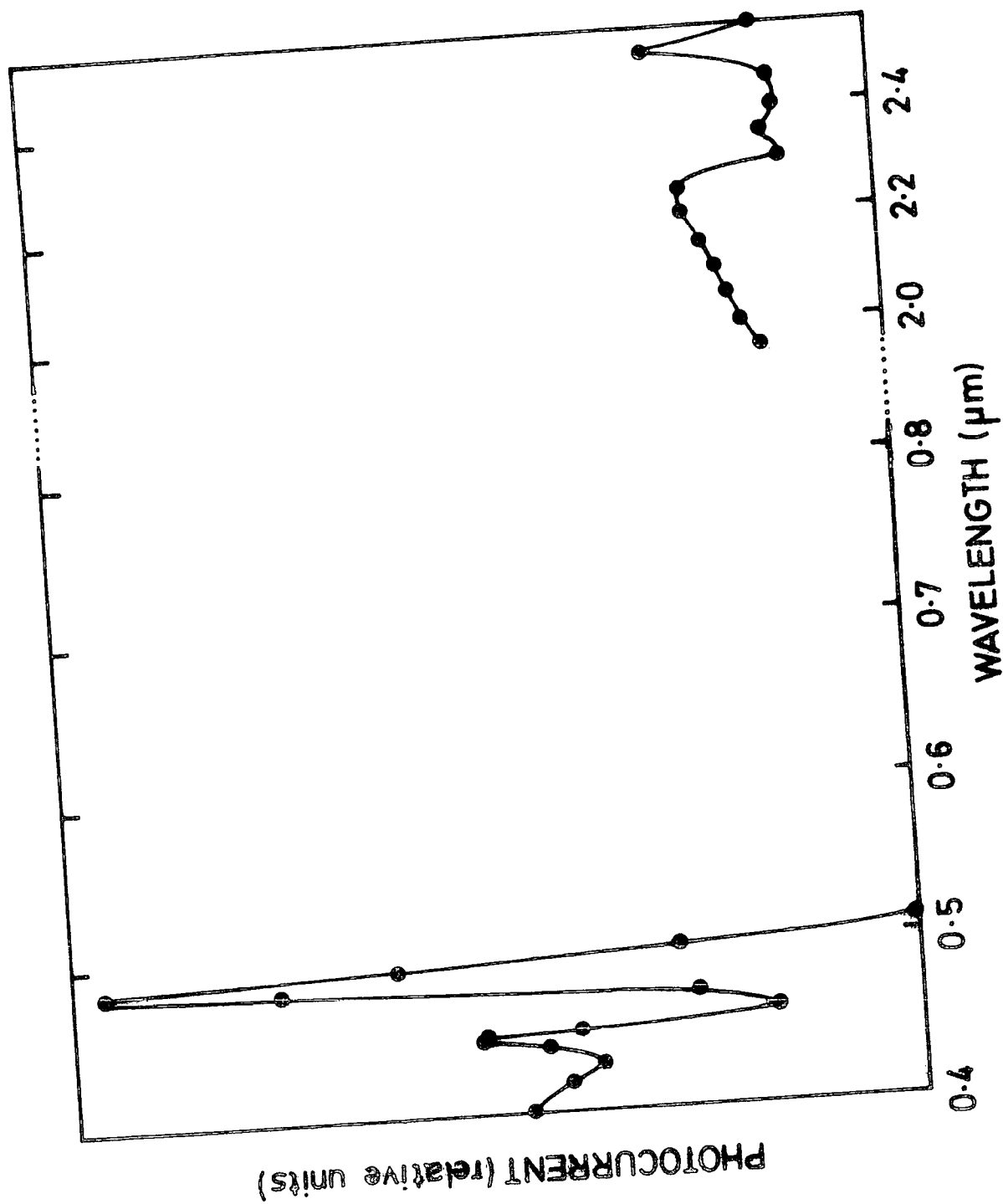DIFFERENT TEMPERATURES.

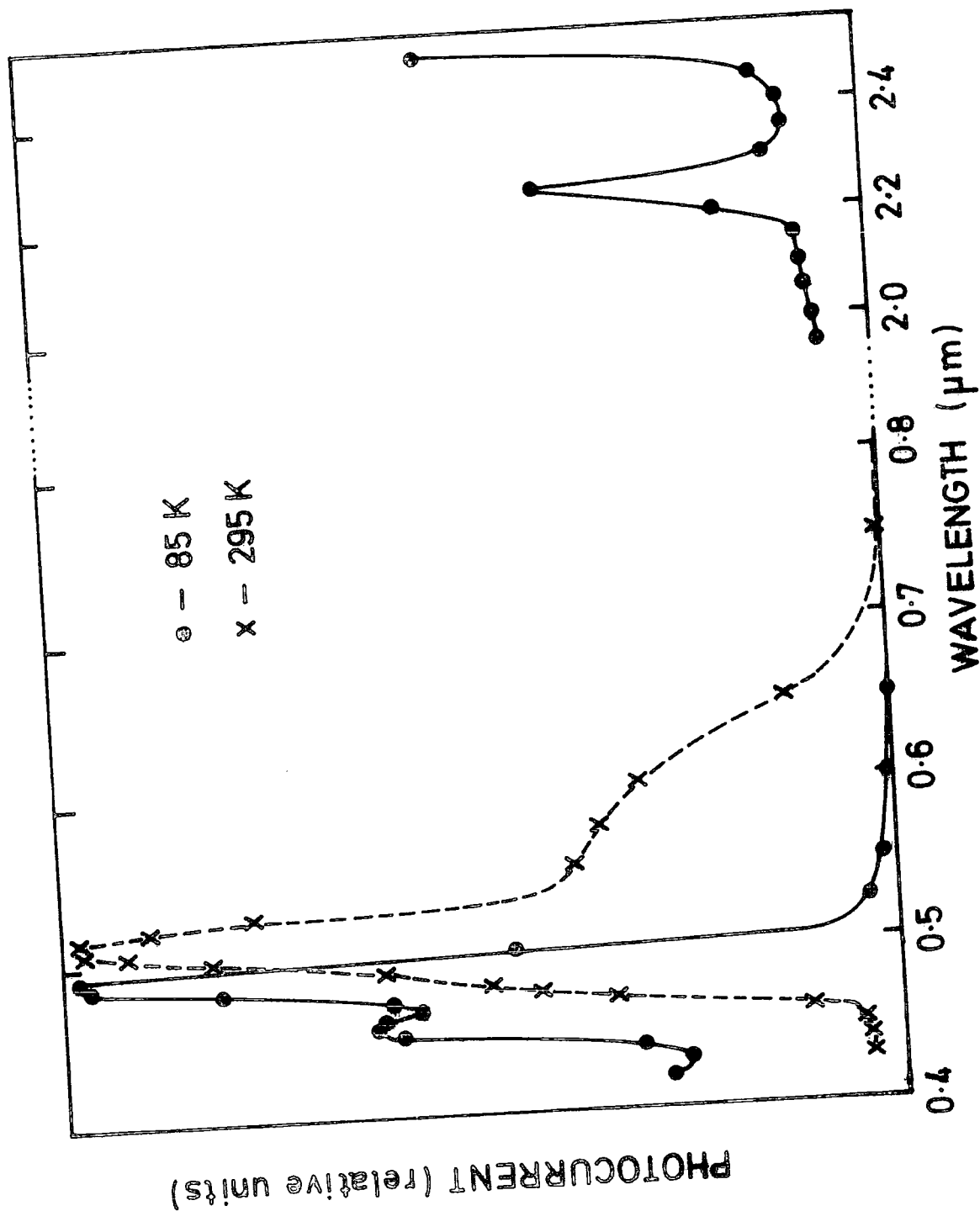FIG. 5.10 PHOTOCONDUCTIVE RESPONSE FOR ZnSe : In # 405 (55ppm) AT 85 K.

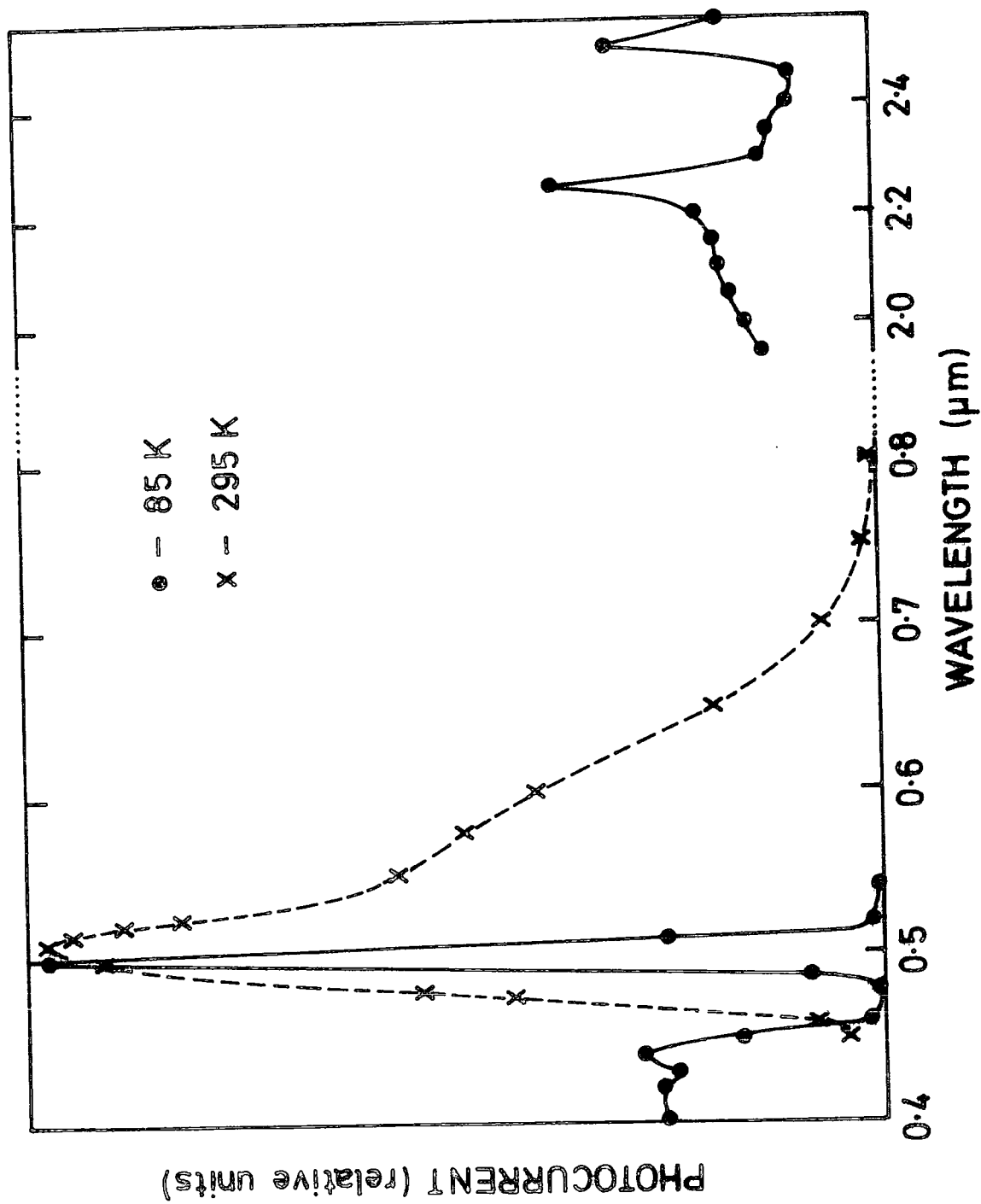FIG. 5·11 PHOTOCONDUCTIVE RESPONSE FOR ZnSe:In#408T (250ppm) AT DIFFERENT TEMPERATURES.

FIG. 5.12   PHOTOCONDUCTIVE   RESPONSE   FOR   ZnSe : In #410 T (105ppm)
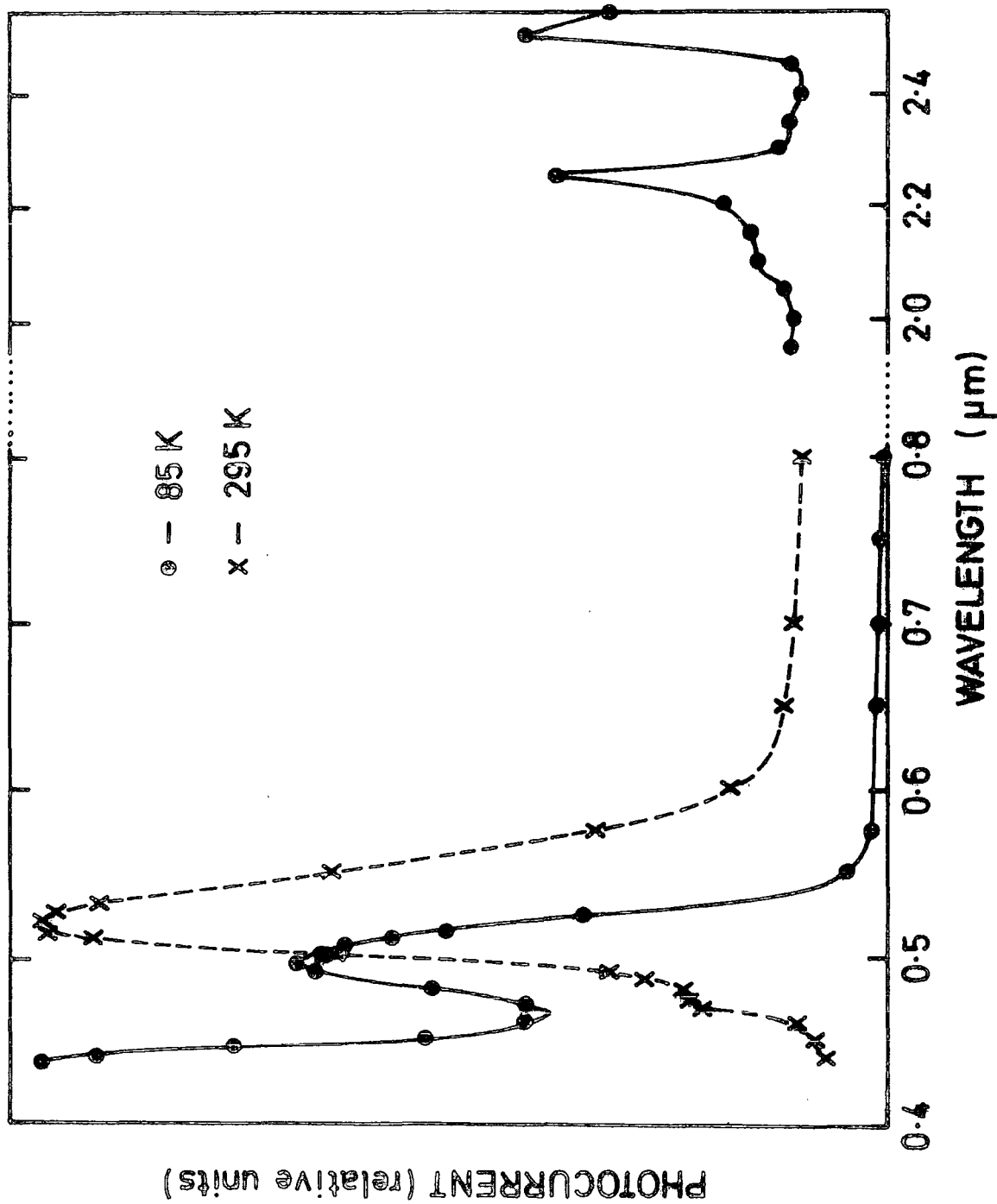
AT   DIFFERENT   TEMPERATURES.

FIG. 5·13 PHOTOCONDUCTIVE RESPONSE FOR ZnSe : In #410 E (105ppm) AT DIFFERENT TEMPERATURES.

T A B L E 5.3

SUMMARY OF PHOTOCONDUCTIVITY PEAKS OF SOME AS-GROWN ZnSe:In CRYSTALS

Crystal Boule ≠≠	In- dium Con- tent p.p.m	T = 85 K						T = 295 K	
		λ (nm)	E(eV)	λ (nm)	E(eV)	λ (μm)	E(eV) ☆	λ (nm)	E(eV)
405	55	448	2.76	484	2.56	2.22	0.56	-	-
342E	85	450	2.75	520	2.38	2.12	0.58	503	2.46
410T	105	440	2.82	500	2.48	2.25	0.55	510	2.43
410E	105	-	-	496	2.50	2.30	0.54	520	2.38
408T	250	457	2.71	490	2.53	2.25	0.55	530	2.34
		T = 150 K							
349	800	457	2.71	501	2.48	2.20	0.56	512	2.42

☆ Very Broad Peak ; Estimated Position

smooth uniform source response. The infrared band has also been reported
by Burr and Woods (1971) in ZnSe. In an attempt to determine the type
of carriers involved in this transition, photo-Hall effect and photo-
thermoelectric power measurements were carried out, using an OX-2 infra-
red filter which excludes visible light. However, because the photo-
conductive band appeared at low temperatures and the photocurrent was so
small, the resistivity of the material was too high for any appreciable
photo-Hall effect to be obtained while the thermoelectric power measure-
ments suggested an inconclusive p-type character.

Measurements of photocurrent as a function of light intensity,
at a wavelength of 500 nm, were carried out, by using neutral filters, for
each of the samples. The response for all cases, at room temperature and
at 85 K, was sub-linear, with exponents lying between 1/2 and almost unity,
which is the accepted behaviour of photoconductors with trapping centres
when the hole demarcation level is either well above or well below the
class II centres.

The response curves in figures 5.12 and 5.13 were taken from
different samples cut from the same crystal ; one from the tip of the
boule, which was the first part to grow, and the other from the last part
of the boule to grow. This was done because the last 3 mm or so of this
crystal (and some other heavily indium doped crystal boules) had a marked
gradation of colour, so that this last part was reddish, while the rest
was yellowish. The main difference between the two response curves is
the absence of the room temperature shoulder on the long wavelength side
of the 510 nm peak in the sample cut from the tip of the boule.

5.3.2 Infra-red Quenching

Infra-red quenching measurements were performed at 85 K only,
since no quenching of the photocurrent was obtained at room temperature.
The wavelength of the primary light was centred at either 440 nm or 510 nm
and a similar response was obtained in each case. The quenching curves

can be seen in figure 5.14. The response was very slow, so the measure-ments were done point by point. The lamp source used as the secondary (quenching) radiation was calibrated with the aid of a thermopile which was used to detect the intensity of the light passing through the double prism monochromator. The light was chopped at 5 Hz and the output of the thermopile was fed into a lock-in amplifier. Because this lamp had a non-uniform spectral distribution of light intensity with a very strong and broad response at about 1 μm, neutral filters were used in order to minimize the differences in transmitted light energy at the different wavelengths. In this way, only small corrections were needed to normalize the curves in figure 5.14.

The quenching bands were all very similar. Each one consisted of a broad undefined band, as reported by Burr and Woods (1971), for undoped ZnSe crystals previously grown in this department, with apparently a few substructures. Similar effects have been mentioned by Bube and Lind (1958) in ZnSe:Br:Cu and by Stringfellow and Bube (1968) in ZnSe:Cu. The low energy threshold of the quenching below 0.8 eV could not be determined because of lack of high intensity monochromatic excitation in this spectral region. However, by extrapolating the last two or three points from the curves towards the low energy side, intercepts with zero quenching were obtained at energies of 0.6 to 0.7 eV ($\sim$ 1.8 μm) as shown in figure 5.14 ; these values are very close to the one obtained by Bube and Lind (1958) of about 0.63 eV for ZnSe:Br:Cu who also extrapolated the last few points.

5.3.3 Discussion of Results

Although a substantial amount of work has been done recently on the luminescence of ZnSe, much less attention has been paid to the photo-conductive properties of this material. As already mentioned, Bube and Lind (1958) investigated ZnSe:Br:Cu and obtained a photoconductive peak near
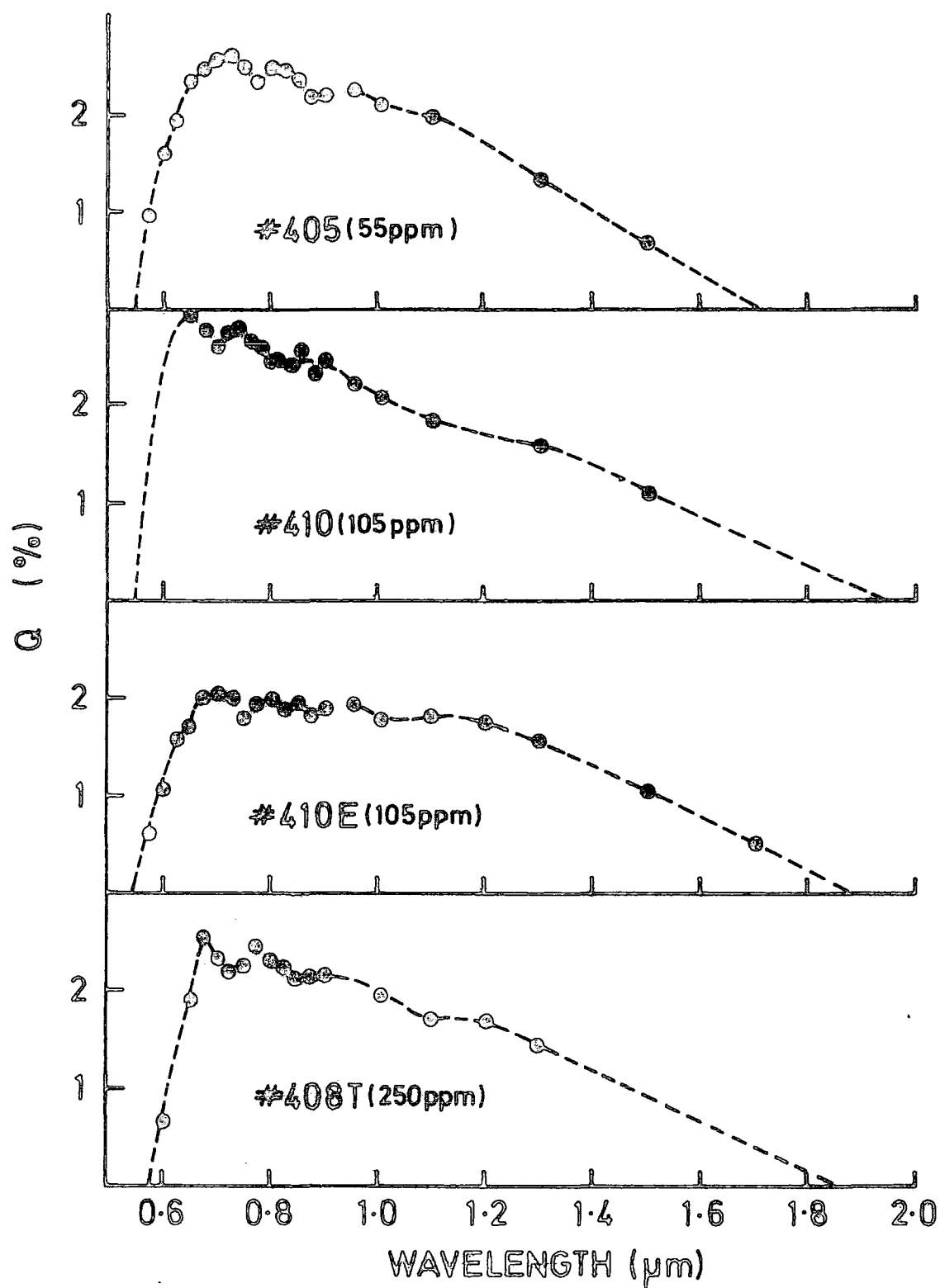
FIG. 5·14   INFRA − RED   QUENCHING   ON   ZnSe : In
CRYSTALS   AT   85 K .   PRIMARY   LIGHT
CENTRED   AT   440 nm.

510 nm at room temperature and a threshold of infrared quenching at about 0.63 eV at low temperatures. Stringfellow and Bube (1968) compared infrared quenching data from undoped and copper doped ZnSe, and concluded that the centres involved in the optical quenching for undoped ZnSe at about 0.5 eV were closer to the valence band than those in ZnSe:Cu. They also found, from photo-Hall measurements, that the infrared photoconductivity excited at 0.93 eV gave rise to p-type conduction. From the thermal quenching of the photoconductivity at 250 K, they obtained an activation energy of about 0.8 eV indicative of the presence of some sensitizing class II centre at about that level above the valence band. The existence of this class II centre was later confirmed by Grimmeis et al (1979), as the "Cu-Red" centre at 0.83 eV above the valence band, by using a modified photocapacitance technique.

Reinberg et al (1971) found a threshold at 0.6 eV for the optical quenching of the photoconductivity at 77 K in p-type ZnSe:P. They interpret this quenching in terms of an acceptor centre associated with the presence of phosphorus, i.e., an acceptor level due to $P_{Se}^{'}$ at approximately 0.6 eV above the valence band. They also stated that the photoconductivity which results from band-gap radiation is n-type as shown by their photo-Hall effect measurements at 77 K. However, 1 μm radiation, which is near the peak of the infrared quenching band, liberated holes as was verified by the reversal of the sign of the Hall voltage when band-gap radiation was replaced by the infrared.

Later, Adachi and Machi (1975a) reported that the photoconductivity peak in undoped ZnSe at about 0.51 μm corresponds to the transition from the copper native impurity centre located at about 0.37 eV above the valence band. Gavrikova et al (1975) also found some infrared photoconductive bands at room temperature in ZnSe single crystals at wavelengths of 1.25 μm and 1.45 μm after a thermal treatment at 400 K. They suggested that the

centres involved were the same as those responsible for the quenching of the photoconductivity and that they also produced p-type photoconductivity. More recently, Birchak et al (1976) found photoconductivity peaks at 475 nm and at 525 nm at room temperature, while Terada (1976) found peaks at 450 nm and 510 nm at 100 K. Mitchell (1977) reported peaks at 466 nm and 516 nm at 300 K and at 450 nm and 500 nm at 85 K in ZnSe crystals grown by the iodine transport technique in this department.

Summarizing all this work, it seems clear that there are two near band-gap photoconductive peaks in ZnSe, which shift to higher energies on cooling. These give n-type photoconductivity. There are, however, some bands in the infrared which apparently depend on the type of impurity present, and give p-type photoconductivity.

The conclusions that can be drawn so far about the ZnSe:In and ZnSe:Ga crystals studied here, are that their emission and absorption spectra are characteristic of copper doped ZnSe, which is usually dominated by a double acceptor defect localized anywhere between 0.3 and 0.8 eV above the valence band and associated with Cu_{Zn}^{x} and Cu_{Zn}' centres. The so-called self-activated transition is also observed in luminescence. Probably produced by a transition to the $(V_{Zn}-group\ III_{Zn})$ associated complex (see Dunstan et al, 1977) . Some of these levels could be sensitizing class II centres for photoconductivity and hence, account for the values of 0.4 to 0.6 eV obtained from the optical quenching measurements, and values of about 0.3 and 0.8 eV from the thermal quenching (see Stringfellow and Bube, 1968) ; or, it could be that the Cu-Red centre at about 0.8 eV above the valence band as confirmed from photocapacitance measurements (see Grimmeis et al, 1979) acts as the sensitizing centre.

On the other hand, the p-type photoconductivity excited by infrared radiation at about 0.56 eV in our crystals, is probably caused by some hole trap, which may well be the same infrared quenching centre at about 0.6 eV.

The final conclusion, therefore, is that there seem to be a series of hole traps, recombination centres and class II sensitizing centres lying between 0.3 and 0.8 eV above the valence band, in the indium and gallium doped ZnSe crystals.

5.4 THERMALLY STIMULATED CURRENT AND THERMALLY STIMULATED LUMINESCENCE

5.4.1 Introduction

Measurements of thermally stimulated current (TSC) and thermally stimulated luminescence (TSL) were carried out on several of the crystals using the apparatus described in chapter four. These results are illustrated graphically in figures 5.15 to 5.18. A common feature in all the samples studied here is the presence of three main peaks between 85 and 245 K in both, the TSC and TSL curves. The peaks were located at approximately 110, 160 and 220 K, depending on the heating rate. In the TSC curves, one or two additional smaller and unresolved peaks were located between 270 and 320 K. For these TSC curves, the dark current took over at the high temperature end of the plots and it sometimes became dominant as for example with crystal ‡‡ 405 in figure 5.16. In most of these curves, a sudden thermal quenching of luminescence and photoconductivity set in between about 240 to 280 K ; this effect was reported by Stringfellow and Bube (1968) and by Jones and Woods (1974), and it can be seen in almost all the TSC curves and in all the TSL curves from figures 5.15 to 5.18.

It is clear from the complexity of these graphs that the evaluation of the results to find the corresponding trap depths is not simple, since the peaks overlap to varying extents. In an attempt to overcome this problem, several techniques were used :

(a) various runs were made at different heating rates from about 0.1 K s^{-1} to about 1 K s^{-1},

(b) the shallower traps were thermally cleaned, i.e. after filling the traps, the crystal was heated up to just below the temperature
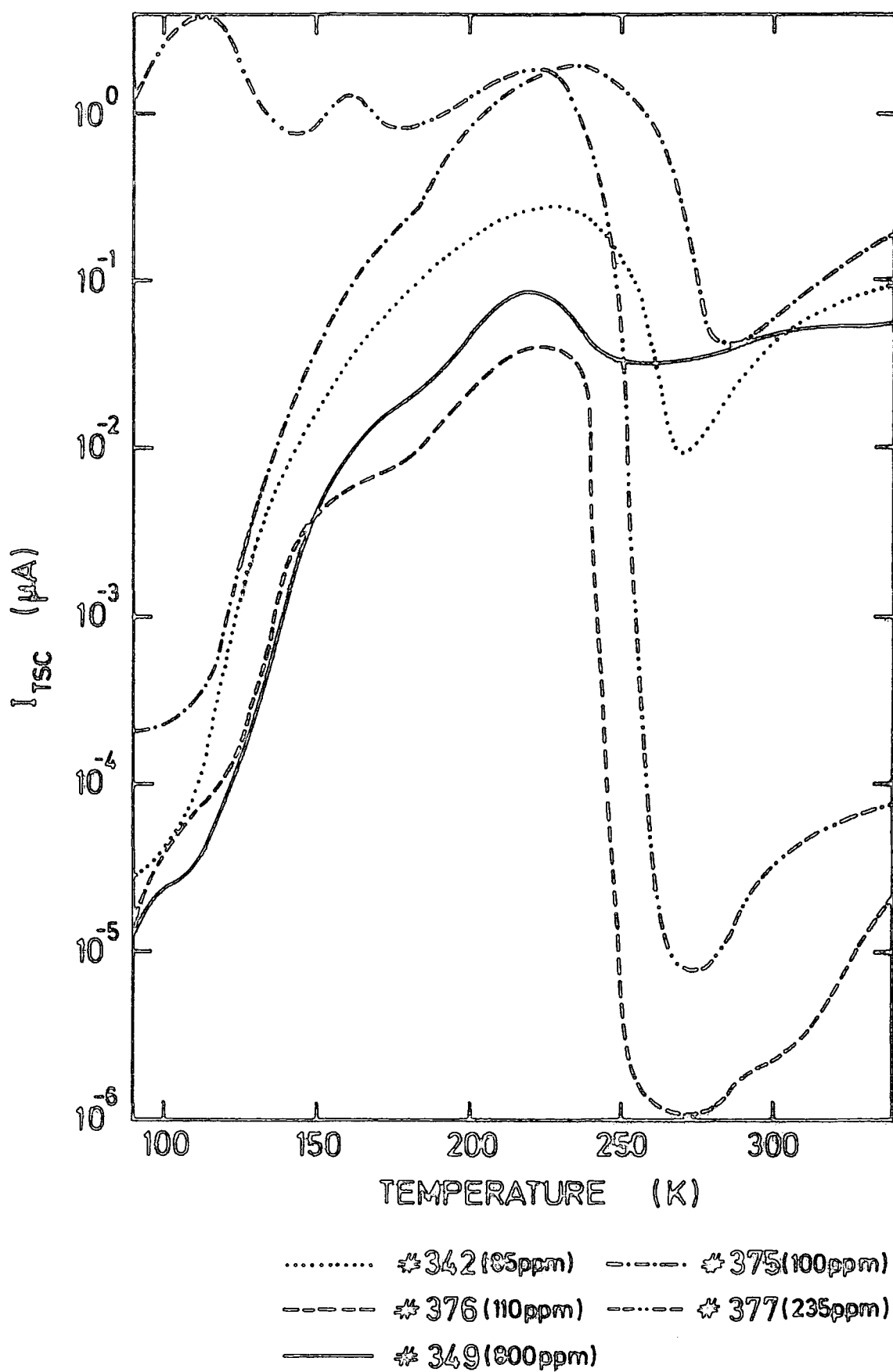
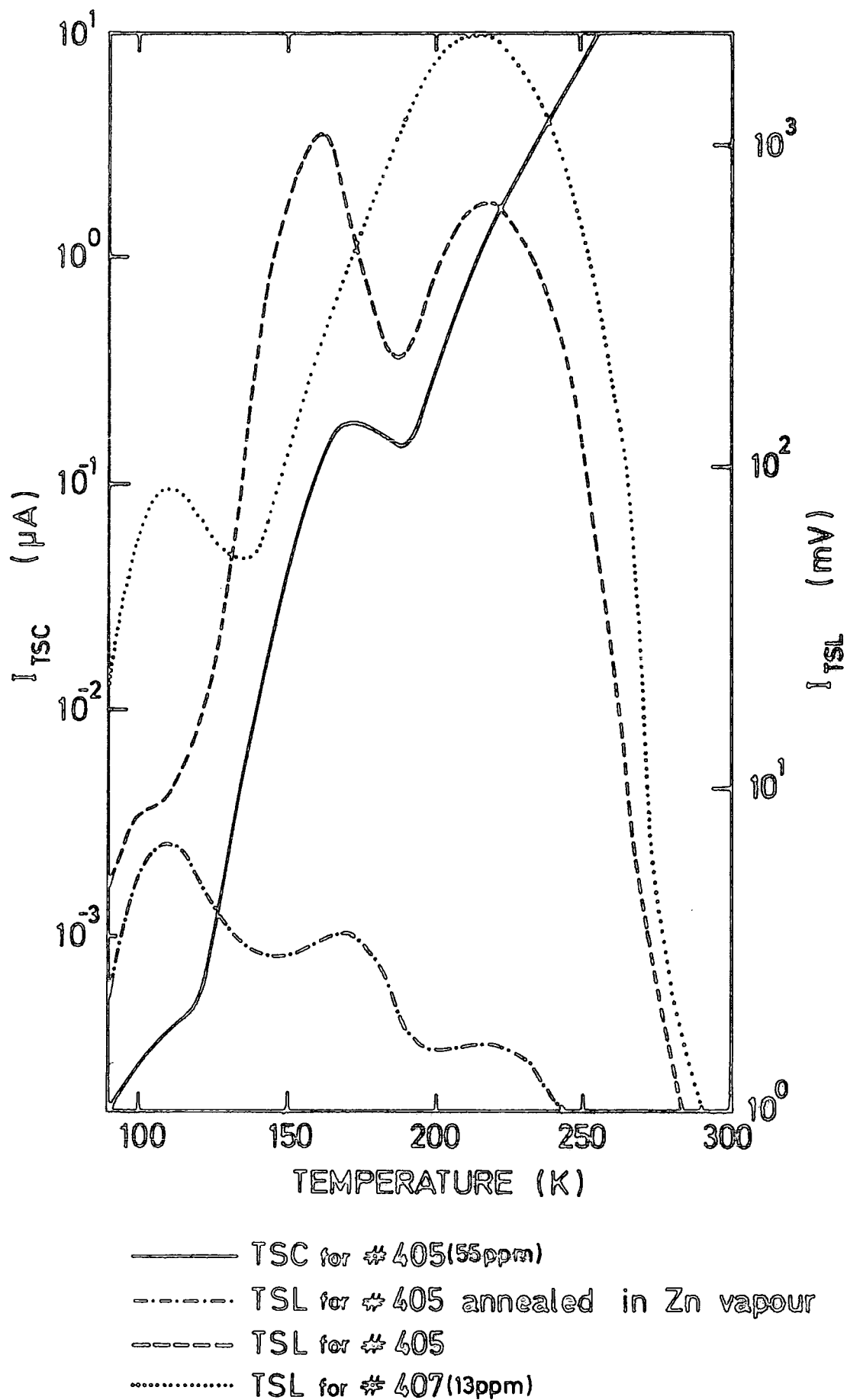FIG. 5·15   T.S.C. FOR ZnSe CRYSTALS WITH DIFFERENT In CONCENTRATIONS

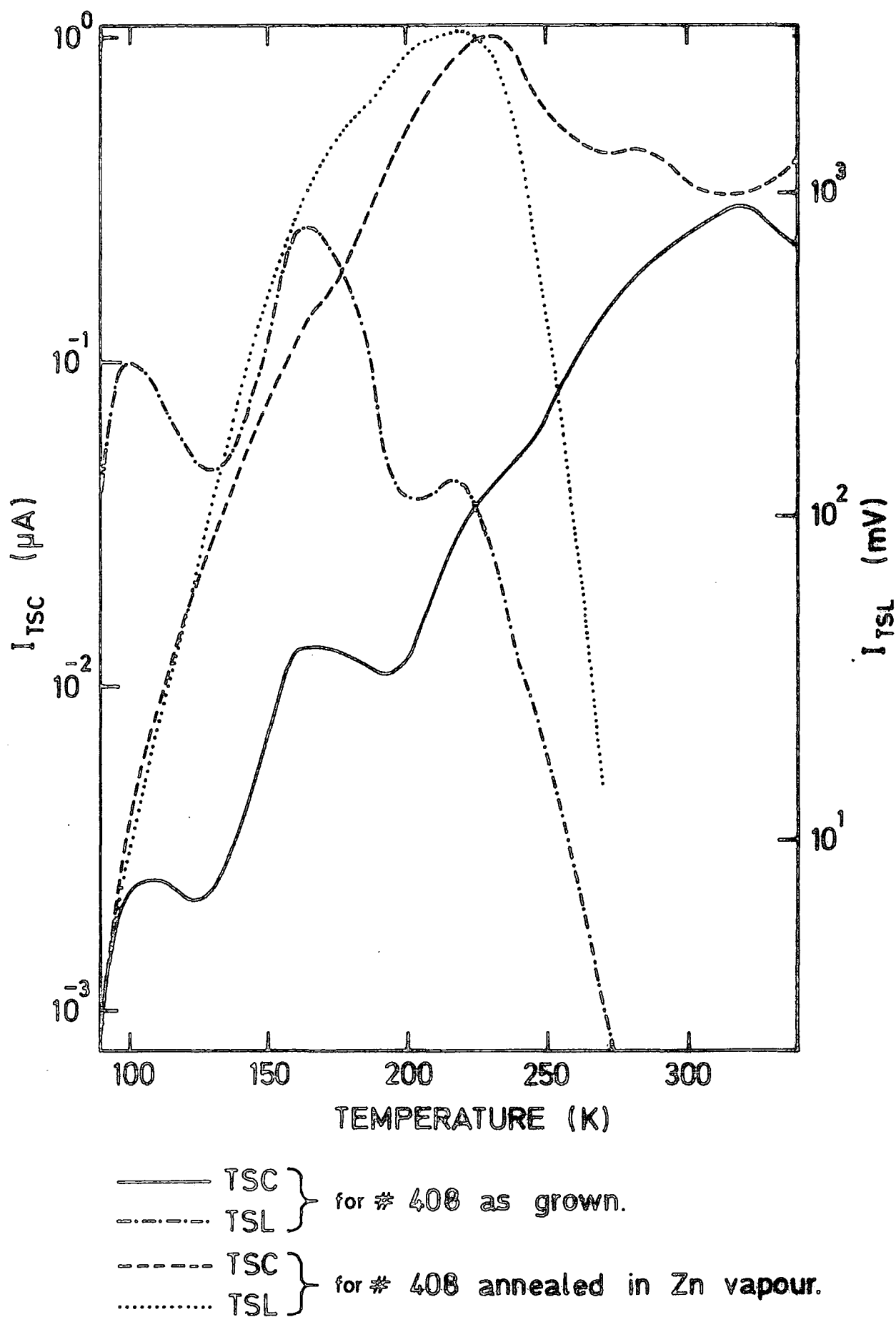FIG. 5·16   T.S.C. AND T.S.L. FOR ZnSe:In CRYSTALS

FIG. 5·17   T.S.C. AND T.S.L. FOR A 250ppm In DOPED
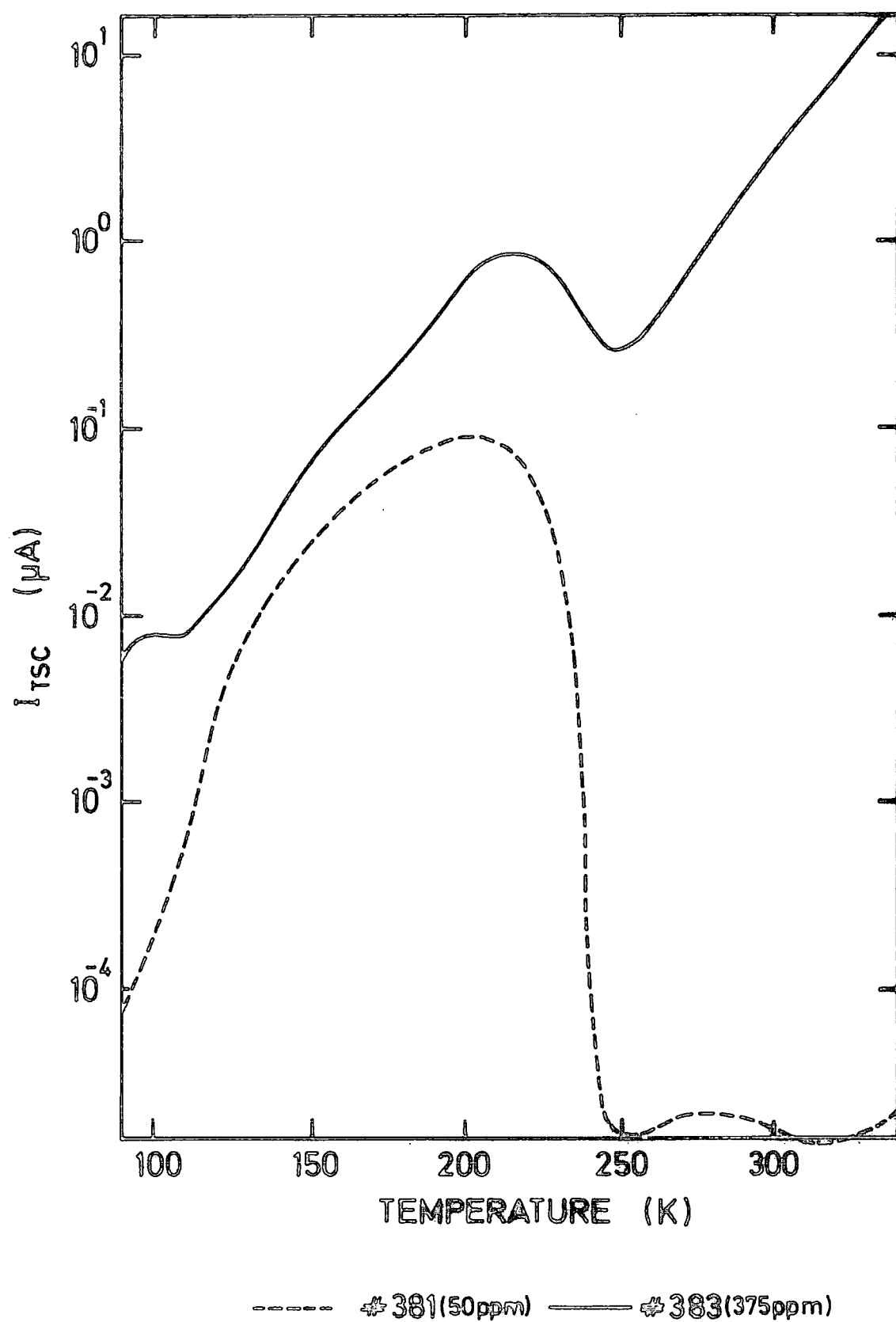ZnSe CRYSTAL

FIG. 5·18   T.S.C. FOR Ga DOPED ZnSe CRYSTALS

of the peak under study, whereupon the sample was cooled to the starting temperature and reheated at the same constant rate. It is expected that the rising part of the peak would then be measured without any influence from the shallower traps. This technique is the "thermal cleaning" process described by Nicholas and Woods (1964) ;

(c) a progressive thermal cleaning was employed, that is, the previous technique was used repeatedly up to consecutively increasing intervals of 5 or 10 K. The Garlick and Gibson (1948) method was applied to all the rising curves to evaluate the corresponding trap depth, after subtracting the next curve in the sequence, which includes the dark current in the case of TSC. In this way, a series of activation energies was obtained. An example of one of these runs is shown in figures 5.19 and 5.20 before and after subtracting the consecutive curve in the sequence, respectively. This technique is similar to the method of decayed TSC described by Bube (1964), and to the fractional glow technique described by Gobrecht and Hofmann (1966) ;

(d) the traps were filled at a temperature just below that at which a prominent peak is expected for each heating rate and then, the sample is cooled down in the dark to start the process as in a normal run. However, this technique has the disadvantage that the height of the peak is dependent on the temperature at which the traps were filled and hence, the analysis can only be made by using those methods which are independent of the height of the maximum of the peak ; these methods of analysis, along with a few others, will be described in the next sub-section.

5.4.2 Methods of Analysis

The technique which has been used in this work is the one described by Kivits and Hagebeuk (1977). In their review paper, the authors made an extensive summary of most of the existing methods of calculating trap depths from TSC and TSL curves assuming a simple model with one set of connected traps and one set of disconnected traps.
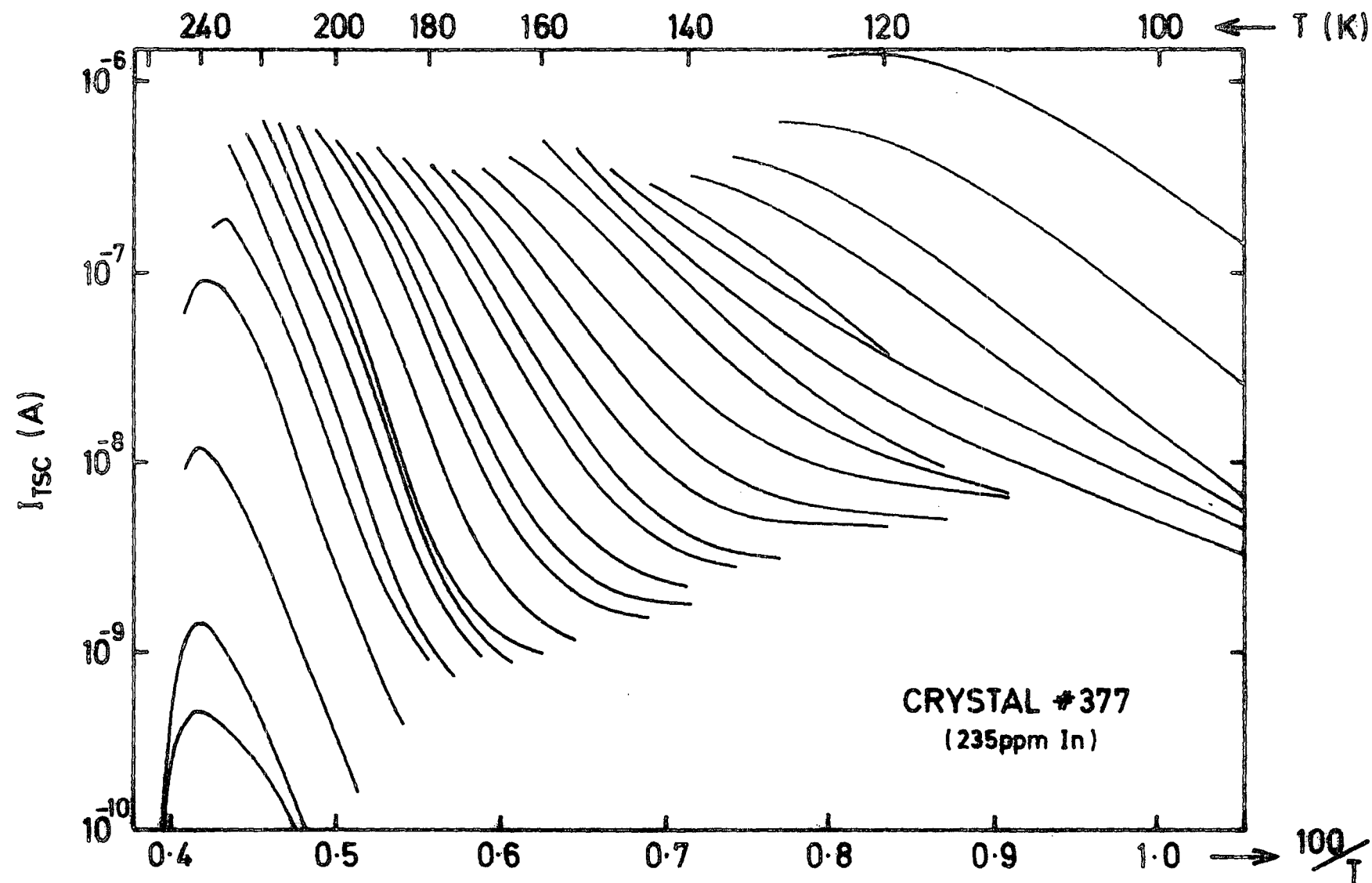
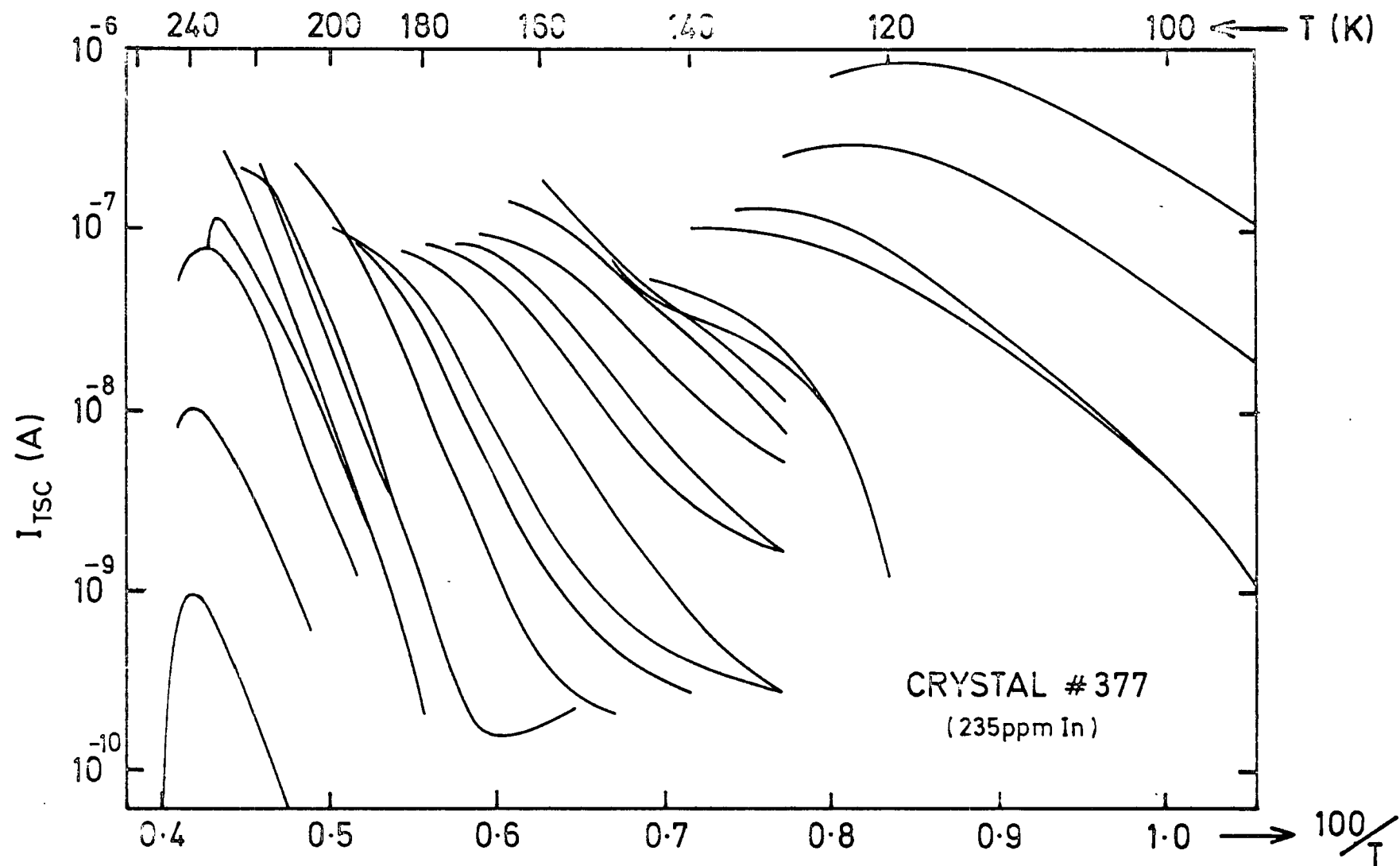FIG. 5·19   EXAMPLE OF A T.S.C. PROGRESSIVE THERMAL CLEANING RUN

FIG. 5·20   EXAMPLE OF A T.S.C. PROGRESSIVE THERMAL CLEANING PROCESS
AFTER SUBTRACTING   THE   SUBSEQUENT   RE-RUN   OBTAINED
FROM   THE   RUN   IN   FIG. 5·19.

Connected traps communicate with the conduction band but disconnected

traps do not. Kivits and Hagebeuk also compared the results obtained

from the different methods, by using them to evaluate a theoretically

generated curve obtained after fixing reasonable values for the different

parameters involved, and pointed out the assumptions that have to be made

with each of the methods. In this way, they discussed 31 methods, divided

in three groups, namely,

(A) methods making use of a variation in the heating rate, labelled methods

1 to 9,

(B) methods employing geometrical approximations, i.e. using the shape of

the curve about a peak ; these are methods 10 to 24; and,

(C) other methods, i.e. the rest of the methods which are not included

in the first two groups and are numbered 25 to 31.

The methods were also classified according to the value of the retrapping

ratio δ, i.e. First class for fast retrapping or $\alpha << \beta$, Second-class

methods for slow retrapping including the bimolecular recombination

obtained when $\alpha = \beta$ and General class methods where the shape of the curve

is assumed to be independent of δ.

Only those methods actually applied in this work will be mentioned.

Some of these methods have been discussed in chapter two, so they will only

be mentioned briefly here:

Group A methods (i.e., variation of heating rate) :

Method 2 : Böer, Oberländer and Voigt (1958) ; a plot of $\ln w_i$ versus $1/T_{mi}$,

where the subscript indicates one of the runs, w is the heating rate in

$K s^{-1}$ and T_m is the absolute temperature at the maximum of the peak, should

give a straight line with $-\rho E/k$ as slope, where $0.7 < \rho < 0.9$, E is the

value of the trap depth and k is Boltzmann's constant. However, following

Kivits and Hagebeuk's work, a value of 1 will be given to ρ.

Method 3 : Chen and Winer (1970) ; a plot of $\ln(I_{mi} T_{mi}^4 / w_i^2)$ versus $1/T_{mi}$,

where I_m is the intensity at the maximum of the peak, should give a

straight line with E/k as slope.

Method 4 : Hoogenstraaten (1958) ; a plot of $\ln(T_{mi}^2/w_i)$ versus $1/T_{mi}$ should

give a straight line with a slope E/k.

Method 5 : Bube (1955) and Haering and Adams (1960) ; a plot of $\ln I_{mi}$

versus $1/T_{mi}$ yields a straight line with a slope -E/k.

Method 6 : Unger (1962) ; a plot of $\ln I_{mi}$ versus $1/T_{1i}$, where T_1 is the

temperature on the rising side of the peak where the intensity equals half

its maximum value, should give a straight line with slope -E/k.

Method 8 : Boiko, Rashba and Trofimenko (1960) 1 ; a plot of $\ln(I_{mi}/T_{mi}^{3/2})$

versus $1/T_{mi}$ yields a straight line with slope -E/k.

Method 9 : Boiko, Rashba and Trofimenko (1960) 2; a plot of $\ln(w_i/T_{mi}^{7/2})$

versus $1/T_{mi}$ should give a straight line with -E/k as slope.

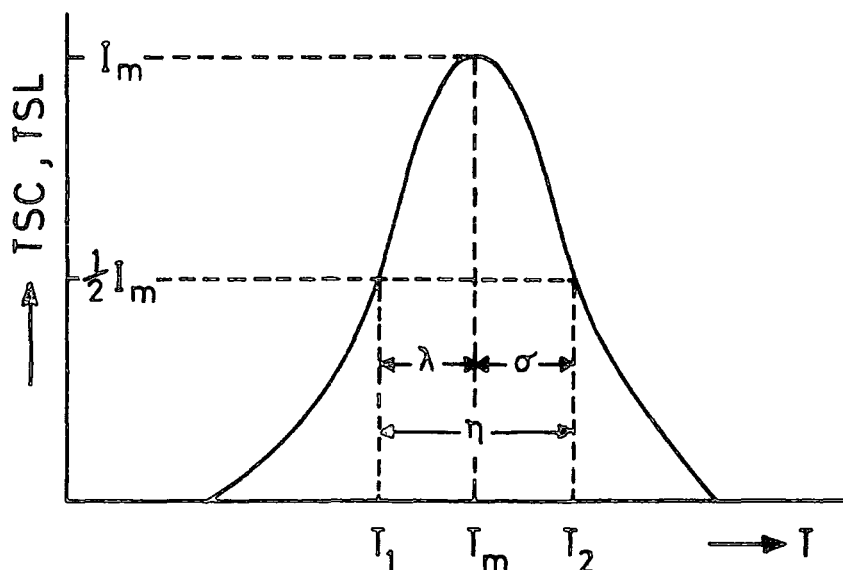Group B methods (which depend on the shape of the curve) :

The following diagram, representing a hypothetical TSC or TSL peak, will

help to illustrate the relevant parameters which will be used while discuss-

ing this group of methods :

$$\eta = T_2 - T_1$$

$$\lambda = T_m - T_1$$

$$\sigma = T_2 - T_1$$

$$\chi = \sigma/\lambda$$

Method 10 : Luschik (1955) ; $E = k\ T_m^2/\sigma$

Method 13 : Chen (1969) 1 ; $E = 2\ k\ T_m\ (1.25\ T_m/\eta - 1)$

Method 14 : Chen (1969) 2 ; $E = 2.29\ k\ T_m^2/\eta$

Method 16 : Chen (1969) 4 ; $E = 1.52\ k\ T_m^2/\lambda\ -3.16\ k\ T_m$

Method 17 : Chen (1969) 5 ; $E = 0.976\ k\ T_m^2/\sigma$

Method 18 : Chen (1971) 6a ; $E = 3\sigma\ k\ T_m^2/\eta\lambda$

         Chen (1970) 6b ; $E = 2.8\sigma\ k\ T_m^2/\eta\lambda$

Method 20 : Halperin and Braner
         (1960) 4 ; $E = 2\ k\ T_m^2/\sigma$

Method 21 : Halperin and Braner
         (1960) 5 ; $E = (1 +\eta/\lambda)k\ T_m^2/\sigma$

Method 22 : Chen (1969) 7 ; $E = 2\ k\ T_m(1.77\ T_m/\eta - 1)$

Method 23 : Chen (1969) 8 ; $E = 1.813\ k\ T_m^2/\lambda - 4\ k\ T_m$

Method 24 : Chen (1969) 9 ; $E = 1.706\ k\ T_m^2/\sigma$

Group C methods :

Method 26 : Grossweiner (1953) ; $E = 1.51\ k\ T_m\ T_1/\lambda$

Method 27 : Franks and Keating $E = k\ T_m/\left[(\eta/T_m)\,(1.2\chi - 0.54) - 0.25(\chi - 0.75)^2 + 0.0055\right]$
         (1961) ;

Method 28 : Dussel and Bube (1967) ; $E = G\ k\ T_m T_1/\lambda$ where G is taken as 1.41

Method 29 : Garlick and Gibson (1948) ; a plot of ℓn I versus 1/T on the
initial rising limb of the curve should yield a straight line with slope
$-E/k$.

Method 30 : Sandomirskii and Zhdan (1970) ; $E = 1.455\ k\ T_m\ T_1/\lambda - 0.79\ k\ T_1$

    Some of the methods from the last two groups differ only by a
correction factor. Thus Method 14 is a simplification of method 13 ;
Method 17 is a correction to method 10 ; Methods 20, 22 and 23 are
equivalent to methods 10, 13 and 16 respectively but have been derived

for the slow retrapping case and give values which are about twice as large ;

Method 24 is a correction to method 20 ;

Method 28 is a correction to method 26 ;

Method 30 is another correction to method 26.

5.4.3 Expression of Results

With those methods involving several heating rates, i.e. Group A methods, as well as the Garlick and Gibson method, a least square fit was employed to calculate the slope and its error ; the latter was usually less than 1%. With the other methods, the values obtained from each run were averaged and the standard deviation was usually within 10%.

Following Kivits and Hagebeuk's technique, the value of the trap depth calculated using each method has been compared to that most likely to be correct, and its relative difference from that, expressed in %, will be shown in parenthesis alongside the corresponding trap depth from the respective method in table 5.4.

5.4.4 Results

A detailed account of the way in which the TSC and TSL curves of the samples from the crystal boules ‡‡ 377 and ‡‡ 405 were analysed will now be given. A very similar analysis was carried out with the main peaks of the rest of the samples studied here. All the results are collected together in table 5.4, where each column shows the results of the different ways of analysing a particular peak. In what follows, detailed reference will be made to only a few of these calculations.

Crystal ‡‡ 377 : In the appropriate curve in figure 5.15 for this crystal with about 235 ppm of indium, a well defined TSC peak is apparent at 110 K. There are also two other peaks, at 160 and 220 K, but with this last one, the low temperature limb rose very slowly indicating the possibility of another peak at about 200 K, as happened with crystal

T A B L E   5.4

TRAP DEPTHS IN ZnSe:In AND IN ZnSe:Ga CALCULATED FROM VARIOUS TSL AND TSC PEAKS WITH DIFFERENT METHODS FROM THE LITERATURE

	AUTHOR	Crystal Boule and Peak		
		[a] #342 TSC 235 K	[b] #349 TSC 220 K	[c] #375 TSC 230 k
GENERAL CLASS METHODS				
4	Hoogenstraaten	0.37 (0)	0.49 (0)	0.44 (0)
5	Bube , Haering and Adams	0.31 (-16)	0.38 (-22)	0.39 (-11)
6	Unger	0.31 (-16)	0.26 (-47)	0.38 (-14)
8	Boyko, Rashba & Trofimenko 1	0.28 (-24)	0.35 (-29)	0.33 (-25)
9	Boyko, Rashba & Trofimenko 2	0.34 (-8.1)	0.46 (-6.1)	0.40 (-9.1)
29	Garlick and Gibson L	-	0.37 (-24)	0.37 (-16)
29	Garlick and Gibson U	-	0.40 (-18)	0.39 (-11)
FIRST CLASS METHODS				
2	Boer, Oberlander and Voigt	0.41 (11)	0.53 (8.2)	0.48 (9.1)
10	Luschik	0.19 (-49)	-	0.22 (-50)
13	Chen 1	0.15 (-59)	-	0.20 (-55)
14	Chen 2	0.18 (-51)	-	0.23 (-48)
16	Chen 4	0.13 (-65)	-	0.20 (-55)
17	Chen 5	0.19 (-49)	-	0.21 (-52)
18a	Chen 6a	0.16 (-57)	-	0.23 (-48)
18b	Chen 6b	0.14 (-62)	-	0.22 (-50)
26	Grossweiner	0.16 (-57)	-	0.24 (-45)
27	Franks and Keating	0.29 (-22)	-	0.18 (-59)
28	Dussel and Bube	0.15 (-59)	-	0.21 (-52)
30	Sandomirskii and Zhdan	0.14 (-62)	-	0.20 (-55)
SECOND CLASS METHODS				
3	Chen and Winer	0.42 (14)	0.61 (24)	0.53 (20)
20	Halperin and Braner 4	0.39 (5.4)	-	0.42 (-4.6)
21	Halperin and Braner 5	0.52 (41)	-	0.58 (32)
22	Chen 7	0.23 (-38)	-	0.29 (-34)
23	Chen 8	0.15 (-59)	-	0.23 (-48)
24	Chen 9	0.33 (-11)	-	0.36 (-18)

The trap depths are expressed in eV.
The value in parenthesis is the relative difference of the trap depth obtained using the method in question from the trap depth calculated using Method 4, and expressed in %.
L and U for the Garlick & Gibson method stand for lower and upper limits respectively.

	Crystal Boule and Peak					
	(d) ## 375 TSC 250 K	(e) ## 377 TSC 110 K	(f) ## 377 TSC 160 K	(g) ## 377 TSC 220 K	(h) ## 377 TSC 320 K	(i) ## 405 TSC 175 K
GENERAL CLASS METHODS						
4	0.43 (0)	0.13 (0)	0.32 (0)	0.49 (0)	0.86 (0)	0.36 (0)
5	- -	0.11 (-15)	0.28 (-13)	0.42 (-14)	- -	0.32 (-11)
6	- -	0.13 (0)	0.25 (-22)	0.23 (-53)	- -	0.30 (-17)
8	- -	0.10 (-23)	0.26 (-19)	0.39 (-20)	- -	0.30 (-17)
9	0.40 (-7.0)	0.12 (-7.7)	0.30 (-6.3)	0.48 (-2.0)	- -	0.34 (-5.6)
29	0.47 (9.3)	0.10 (-23)	0.16 (-50)	0.41 (-16)	0.35 (-59)	0.29 (-19)
29	0.49 (14)	0.12 (-7.7)	0.32 (0)	0.45 (-8.2)	0.39 (-55)	0.37 (2.8)
FIRST CLASS METHODS						
2	0.47 (9.3)	0.15 (15)	0.33 (3.1)	0.53 (8.2)	- -	0.40 (11)
10	0.45 (4.7)	0.10 (-23)	- -	- -	0.59 (-32)	- -
13	0.43 (0)	0.10 (-23)	- -	- -	0.58 (-33)	- -
14	0.43 (0)	0.11 (-15)	- -	- -	0.58 (-33)	- -
16	0.44 (2.3)	0.11 (-15)	- -	- -	0.59 (-32)	- -
17	0.44 (2.3)	0.10 (-23)	- -	- -	0.57 (-34)	- -
18a	0.43 (0)	0.13 (0)	- -	- -	0.58 (-33)	- -
18b	0.40 (-7.0)	0.12 (-7.7)	- -	- -	0.54 (-37)	- -
26	0.47 (9.3)	0.12 (-7.7)	- -	- -	0.63 (-27)	- -
27	0.51 (19)	0.08 (-38)	- -	- -	0.61 (-30)	- -
28	0.44 (2.3)	0.11 (-15)	- -	- -	0.59 (-32)	- -
30	0.44 (2.3)	0.11 (-15)	- -	- -	0.59 (-32)	- -
SECOND CLASS METHODS						
3	- -	0.16 (23)	0.35 (9.4)	0.59 (20)	- -	0.40 (11)
20	0.89 (107)	0.20 (54)	- -	- -	1.17 (36)	- -
21	1.22 (184)	0.29 (123)	- -	- -	1.62 (88)	- -
22	0.63 (47)	0.15 (15)	- -	- -	0.84 (-2.4)	- -
23	0.52 (21)	0.12 (-7.7)	- -	- -	0.70 (-19)	- -
24	0.76 (77)	0.17 (31)	- -	- -	1.00 (16)	- -

	Crystal Boule and Peak				
	(j) ≠≠ 405 TSL 170 K	(k) ≠≠ 405 TSL 245 K	(l) ≠≠ 405 * TSL 110 K	(m) ≠≠ 405 * TSL 170 K	(n) ≠≠ 407 TSL 220 K
GENERAL CLASS METHODS					
4	0.38 (0)	0.66 (0)	0.13 (0)	0.23 (0)	0.42 (0)
5	0.38 (0)	0.70 (6.1)	- -	- -	0.39 (-7.1)
6	0.37 (-2.6)	1.01 (53)	- -	- -	- -
8	0.35 (-7.9)	0.67 (1.5)	- -	- -	0.36 (-14)
9	0.36 (-5.3)	0.62 (-6.1)	- -	0.20 (-13)	0.39 (-7.1)
29	0.29 (-24)	0.43 (-35)	0.09 (-31)	0.22 (-4.4)	0.35 (-17)
29	0.32 (-16)	0.47 (-29)	0.12 (-7.7)	0.23 (0)	0.39 (-7.1)
FIRST CLASS METHODS					
2	0.41 (7.9)	0.70 (6.1)	- -	0.25 (8.7)	0.46 (9.5)
10	0.21 (-45)	0.36 (-46)	- -	0.17 (-26)	0.24 (-43)
13	0.23 (-39)	0.35 (-47)	- -	0.18 (-22)	0.27 (-36)
14	0.24 (-37)	0.36 (-46)	- -	0.19 (-17)	0.28 (-33)
16	0.27 (-29)	0.35 (-47)	0.10 (-23)	0.20 (-13)	0.31 (-26)
17	0.20 (-47)	0.35 (-47)	- -	0.16 (-30)	0.24 (-43)
18a	0.31 (-18)	0.36 (-46)	- -	0.25 (8.7)	0.38 (-9.5)
18b	0.28 (-26)	0.34 (-49)	- -	0.23 (0)	0.35 (-17)
26	0.29 (-24)	0.39 (-41)	0.11 (-15)	0.22 (-4.4)	0.34 (-19)
27	0.18 (-53)	0.37 (-44)	- -	0.14 (-39)	0.21 (-50)
28	0.27 (-29)	0.36 (-46)	0.10 (-23)	0.21 (-8.7)	0.32 (-24)
30	0.27 (-29)	0.36 (-46)	0.10 (-23)	0.21 (-8.7)	0.32 (-24)
SECOND CLASS METHODS					
3	0.39 (2.6)	0.39 (-41)	- -	0.28 (22)	0.45 (7.1)
20	0.41 (7.9)	0.72 (9.1)	- -	0.33 (44)	0.49 (17)
21	0.62 (63)	1.00 (52)	- -	0.50 (117)	0.73 (74)
22	0.33 (-13)	0.51 (-23)	- -	0.26 (13)	0.39 (-7.1)
23	0.31 (-18)	0.42 (-36)	0.11 (-15)	0.24 (4.4)	0.37 (-12)
24	0.35 (-7.9)	0.61 (-7.6)	- -	0.29 (26)	0.42 (0)

* Annealed in zinc vapour.

	Crystal Boule and Peak				
	(o) ≠≠ 408 TSL 180 K	(p) ≠≠ 408 TSL 215 K	(q) ≠≠ 408 * TSL 245 K	(r) ≠≠ 381 TSC 215 K	(s) ≠≠ 383 TSC 220
GENERAL CLASS METHODS					
4	0.40 (0)	0.66 (0)	0.47 (0)	0.32 (0)	0.47 (0)
5	0.37 (-7.5)	0.66 (0)	0.36 (-23)	-	-	0.39 (-17)
6	0.37 (-7.5)	-	-	0.46 (-2.1)	-	-	0.34 (-28)
8	0.29 (-28)	0.61 (-7.6)	0.33 (-30)	-	-	0.36 (-23)
9	0.39 (-2.5)	0.61 (-7.6)	0.44 (-6.4)	0.29 (-9.4)	0.45 (-4.3)
29	0.19 (-53)	0.32 (-52)	0.45 (-4.3)	0.35 (9.4)	0.33 (-30)
29	0.23 (-43)	0.36 (-45)	0.53 (13)	0.39 (22)	0.37 (-21)
FIRST CLASS METHODS					
2	0.43 (7.5)	0.64 (-3.0)	0.51 (8.5)	0.36 (13)	0.51 (8.5)
10	0.23 (-43)	0.29 (-56)	0.37 (-21)	0.31 (-3.1)	0.32 (-32)
13	0.26 (-35)	0.31 (-53)	0.40 (-15)	0.31 (-3.1)	0.33 (-30)
14	0.27 (-33)	0.32 (-52)	0.41 (-13)	0.32 (0)	0.34 (-28)
16	0.32 (-20)	0.33 (-50)	0.44 (-6.4)	0.32 (0)	0.37 (-21)
17	0.22 (-45)	0.29 (-56)	0.37 (-21)	0.30 (-6.3)	0.31 (-34)
18a	0.37 (-7.5)	0.35 (-47)	0.48 (2.1)	0.33 (3.1)	0.41 (-13)
18b	0.35 (-13)	0.33 (-50)	0.44 (-6.4)	0.31 (-3.1)	0.38 (-19)
26	0.34 (-15)	0.35 (-47)	0.48 (2.1)	0.35 (9.4)	0.40 (-15)
27	0.20 (-50)	0.26 (-61)	0.33 (-30)	0.32 (0)	0.29 (-38)
28	0.32 (-20)	0.33 (-50)	0.44 (-6.4)	0.32 (0)	0.37 (-21)
30	0.32 (-20)	0.33 (-50)	0.44 (-6.4)	0.32 (0)	0.37 (-21)
SECOND CLASS METHODS					
3	0.45 (13)	0.69 (4.6)	0.68 (45)	-	-	0.50 (6.4)
20	0.46 (23)	0.55 (-17)	0.75 (60)	0.62 (94)	0.63 (34)
21	0.70 (83)	0.78 (18)	1.08 (130)	0.87 (172)	0.91 (94)
22	0.39 (-2.5)	0.41 (-38)	0.58 (23)	0.45 (41)	0.49 (4.3)
23	0.38 (-5.0)	0.34 (-48)	0.53 (13)	0.38 (19)	0.44 (-6.4)
24	0.39 (-2.5)	0.47 (-29)	0.64 (36)	0.53 (66)	0.54 (15)

* Annealed in zinc vapour.

‡‡ 349. Finally, a small group of TSC peaks between 290 and 330 K can be seen.

By using the progressive thermal cleaning technique, the results of which are given by way of example in figures 5.19 and 5.20, before and after subtracting the next run in the sequence, the maxima of the various peaks were found to occur at 110, 160, 220, 240 and 320 K. With the aid of the Garlick and Gibson method, the trap depths were evaluated as follows :

Peak @ 110 K : values between 0.10 and 0.12 eV

Peak @ 160 K : values between 0.16 and 0.32 eV

Peak @ 220 K : values between 0.41 and 0.45 eV

Peak @ 240 K : values between 0.48 and 0.55 eV

Fifteen runs were made to investigate the peak at 110 K. Six of the peaks measured with different heating rates are illustrated in figure 5.21 and the appropriate plots for some of the group A methods of analysis are shown in figures 5.22 to 5.24. The results from the different methods are summarised in table 5.4 (e).

The peaks at 160 and at 220 K were analysed in the same manner. The suspected presence of a small peak between these two, even though not confirmed by the thermal cleaning process, prevented any meaningful calculations using the geometrical methods. The results for the 160 K peak are recorded in table 5.4 (f), while the results of the analysis of the 220 K peak may be found in table 5.4 (g).

An attempt was also made to analyse one of the high temperature peaks, which, in this sample ‡‡ 377, was easy to separate from the other at the lower temperature. Two runs were carried out after illuminating the sample at 275 K. After substracting the apparent effect of the dark current, the trap depths were obtained using methods from groups B and C. (see table 5.4 (h)).
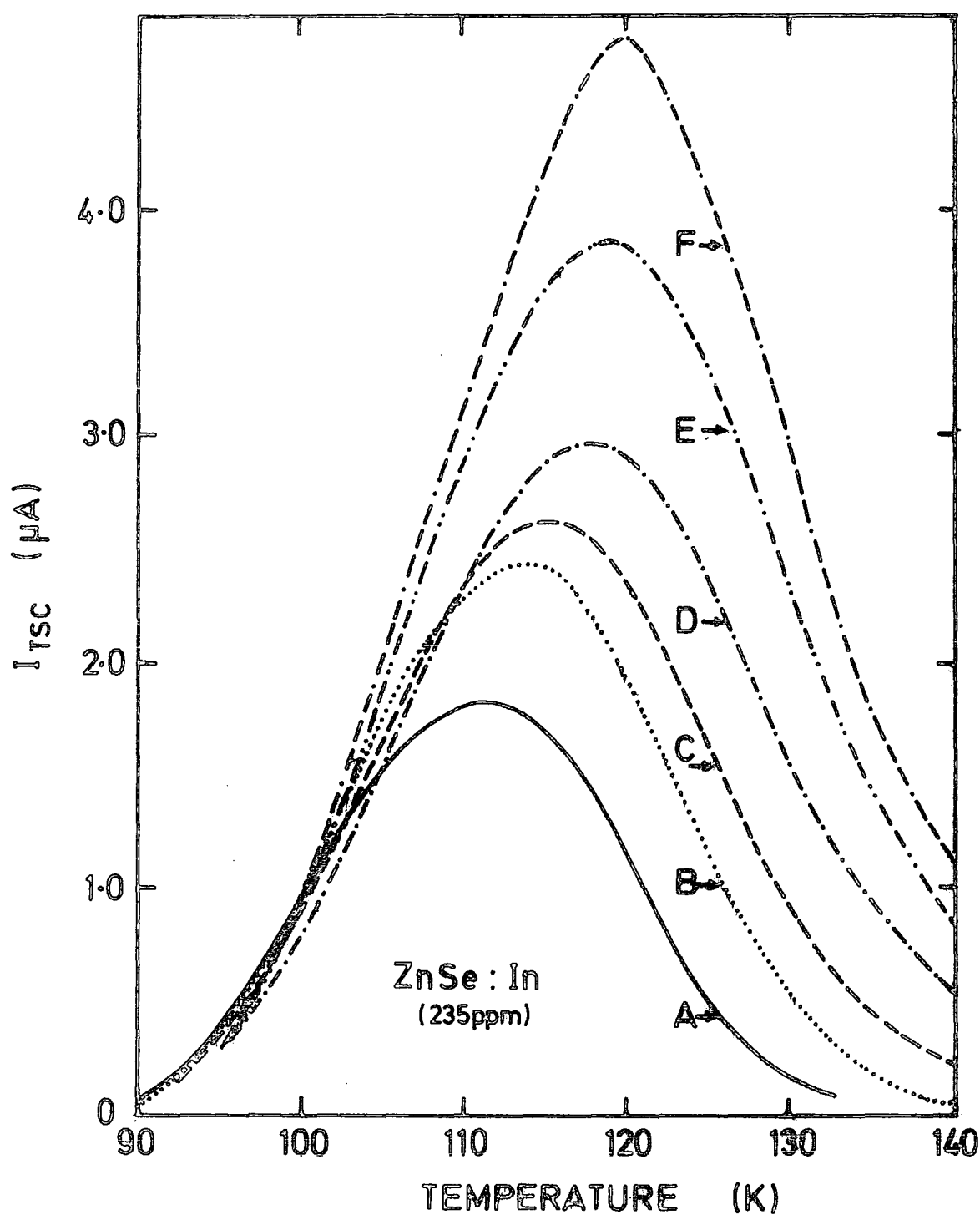
A - 0·14 K/s	D - 0·31 K/s
B - 0·20 K/s	E - 0·39 K/s
C - 0·24 K/s	F - 0·52 K/s

FIG. 5·21   T.S.C. PEAK AT 115 K OF CRYSTAL #377 AT DIFFERENT HEATING RATES.
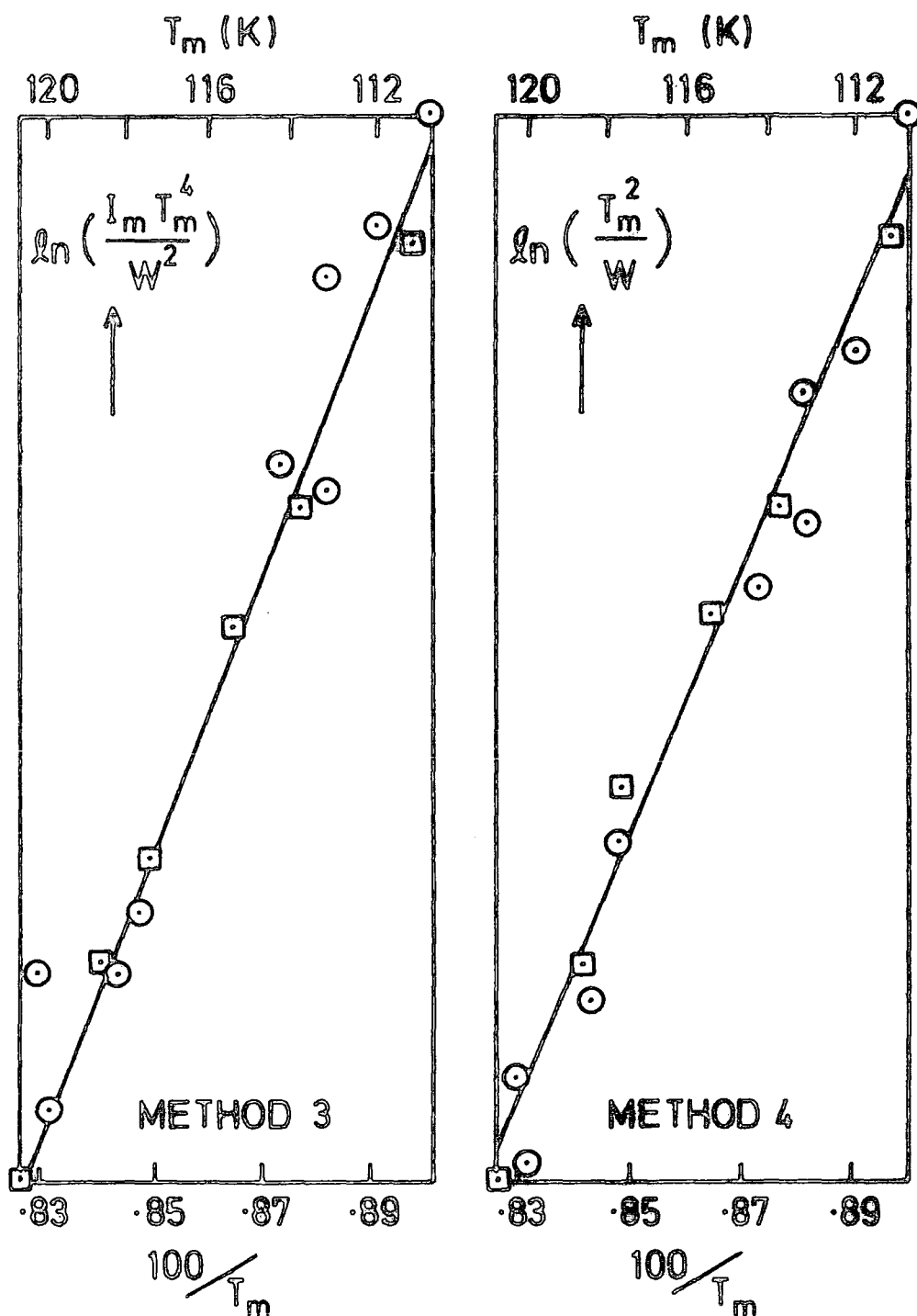
□ — OBTAINED FROM THE PEAKS SHOWN
IN FIG. 5·21.

FIG. 5·22 ANALYSIS USING METHOD 3 (CHEN &
WINER) AND METHOD 4 (HOOGENSTRAATEN)
FOR THE T.S.C. PEAK AT 115 K OF
CRYSTAL #377.
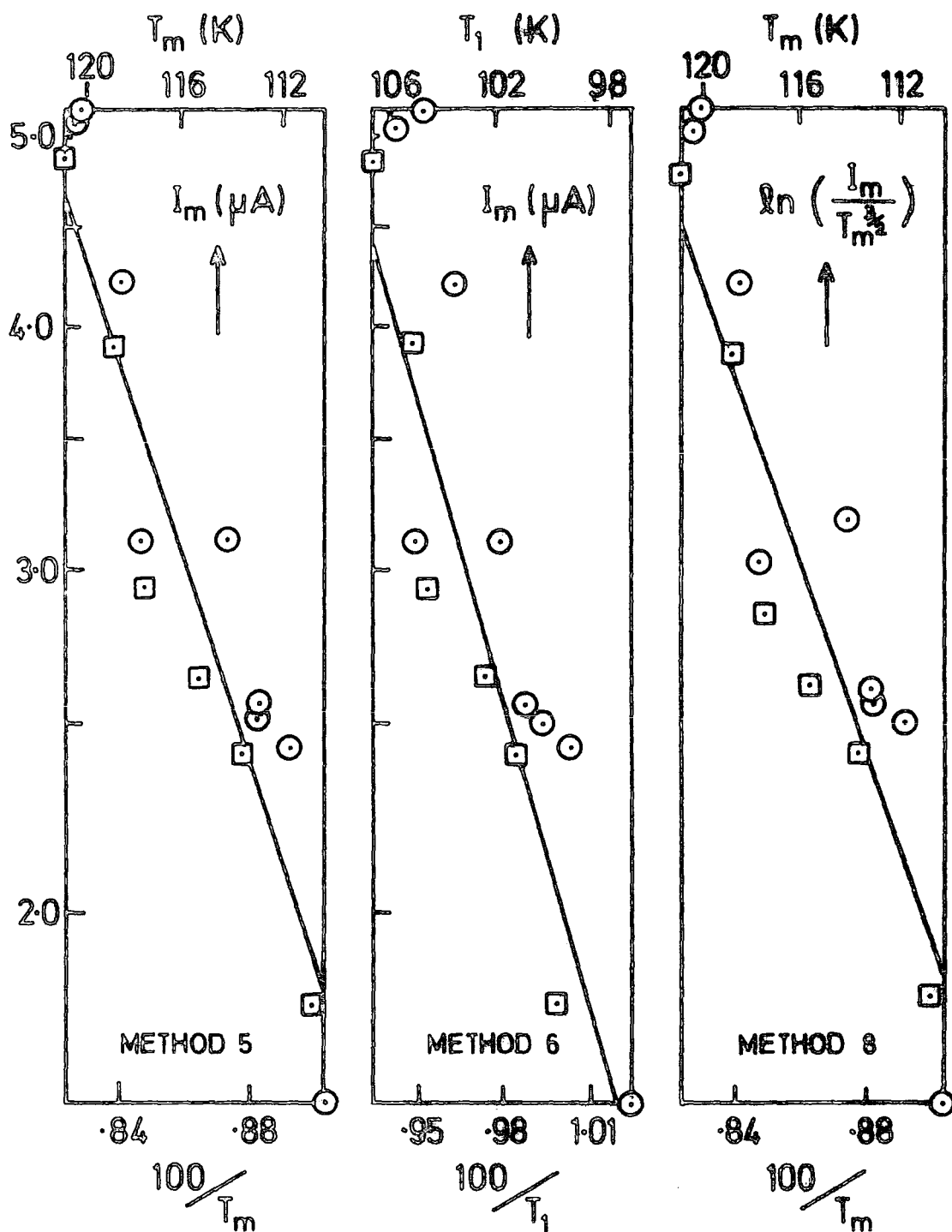
□ — OBTAINED FROM PEAKS SHOWN
IN FIG. 5·21.

FIG. 5·23 ANALYSIS USING METHOD 5 (BUBE,
HAERING & ADAMS), METHOD 6 (UNGER)
AND METHOD 8 (BOIKO, RASHBA &
TROFIMENKO 1) FOR THE T.S.C. PEAK
AT 115 K OF CRYSTAL # 377.
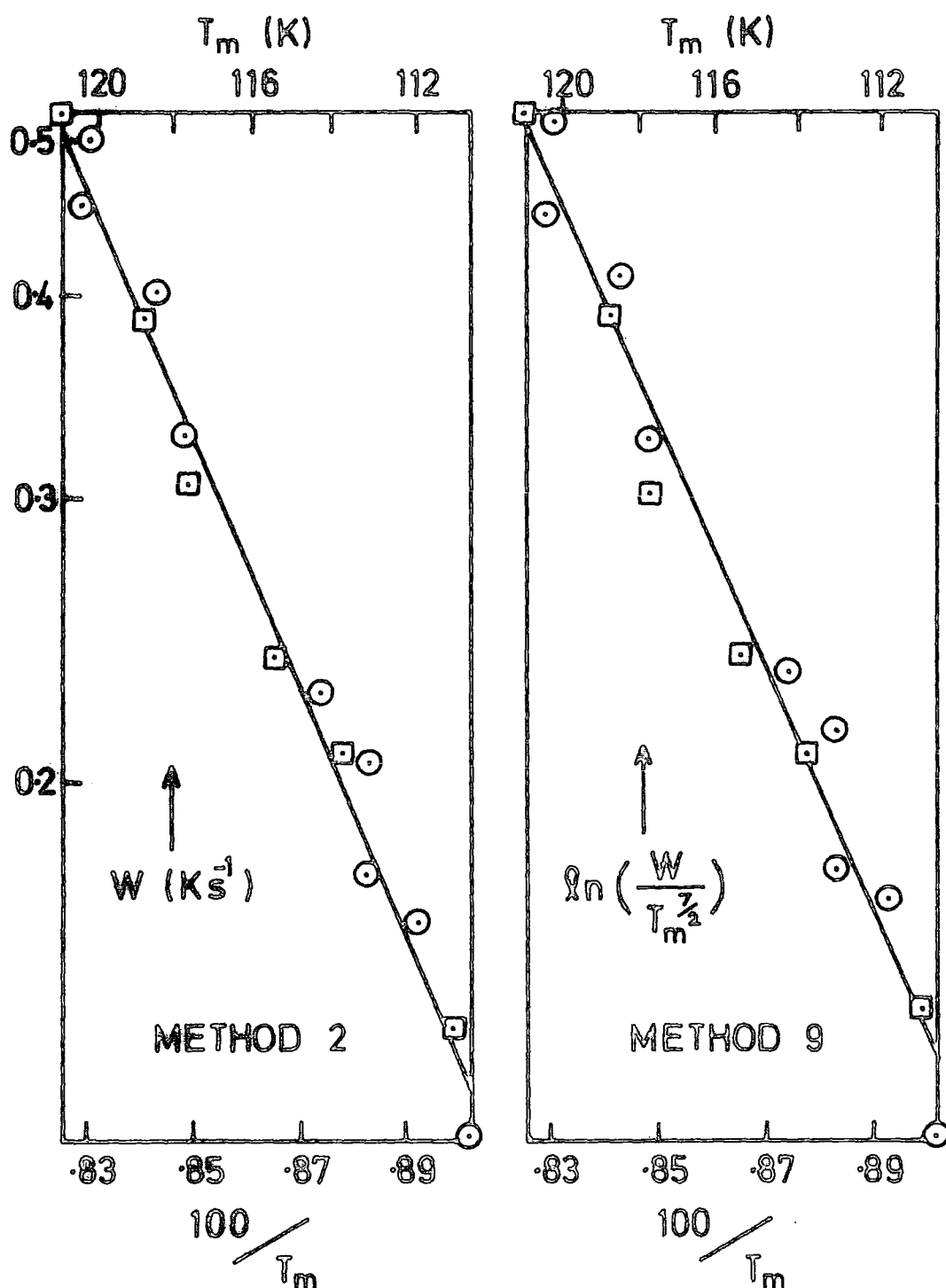
□ — OBTAINED FROM THE PEAKS SHOWN
IN FIG. 5·21

FIG. 5·24   ANALYSIS USING METHOD 2 (BOËR,
OBERLÄNDER & VOIGT) AND METHOD 9
(BOIKO, RASHBA & TROFIMENKO 2) FOR
THE T.S.C. PEAK AT 115 K OF
CRYSTAL #377.

Crystal ‡‡ 405 : TSL as well as TSC measurements were carried out on this sample doped with about 55 ppm of indium. The results are shown graphically in figure 5.16. The TSC curve has only two peaks which can be distinguished from the dark current, one at about 110 K and the other at about 175 K. The TSL curve, on the other hand, shows two well defined peaks at about 165 K and 220 K with a small unresolved shoulder at about 105 K. However, by a careful process of thermal cleaning, it was possible to resolve the major peak at 220 K into two peaks at about 215 K and 245 K. Because of this large overlapping, the analysis for the 215 K peak could not be made.

Using the TSC data from a progressive thermal cleaning programme, the Garlick and Gibson method gave the following activation energies :

Peak @ 110 K : values between 0.08 and 0.10 eV

Peak @ 175 K : values between 0.29 and 0.37 eV

At higher temperatures, where the dark current was relatively important, another set of values of trap depth was obtained using the Garlick and Gibson method, even though no isolated peak was involved.
These were :

(a) between about 180 to 220 K, values ranging from about 0.41 to 0.45 eV and,

(b) between about 220 to 250 K, values ranging from about 0.47 to 0.54 eV.

Eleven runs on the peak at 175 K were made and the trap depths calculated using several of the analytical methods are expressed in table 5.4 (i).

When the TSL curve was subjected to a progressive thermal cleaning sequence, the Garlick and Gibson method produced the following results :

Peak @ 170 K : values between 0.29 to 0.32 eV

Peak @ 215 K : values between 0.33 to 0.39 eV

Peak @ 245 K : values between 0.43 to 0.47 eV.

Eight runs were made to provide the data for the analysis of each of the peaks at 170 and at 245 K. The results of the calculations on the first peak can be found in table 5.4 (j). The results of the trap depth analysis using the different methods for the second peak are given in table 5.4 (k).

5.4.5 Discussion of Results

No measurements of the temperature dependence of the steady state photoconductivity was made on these crystals. However, for most of them, photo-Hall measurements were carried out (these are illustrated in figure 6.22 of chapter six) ; and these measurements indicated that the steady state photoconductive response was almost constant in the temperature range over which the TSC measurements were made.

With TSL, the curves were not corrected for the PM spectral response ;but, as stated previously, the spectral sensitivity of the PM does not change appreciably between the green and orange where the major emission in these ZnSe crystals lies. Furthermore, as mentioned by Stringfellow and Bube (1968) and by Jones and Woods (1974), the green luminescence quenches rapidly at 130 K and hence, above this temperature the orange luminescence will be much stronger, which in its turn, quenches at about 240 K ; and this corresponds with the rapid decrease in all the TSL curves at 250 K.

In the analysis of the different peaks we will follow Kivits and Hagebeuk's technique which they illustrated with an application to a particular ternary compound in a later paper (see Kivits et al, 1978). As expected, not all methods produced the same values for the trap depth. Therefore, a comparison of the relative deviations of all methods from the true trap depth has been made with the same relative differences which Kivits and Hagebeuk (1977) calculated and tabulated as the average relative error $\bar{\epsilon}_\delta$(%), and presented as tables 2,3 and 4 in their article. These three tables will be referred to as tables A, B and C respectively. The

first two are reproduced here in table 5.5 for guidance. In this way, if

the set of experimental relative differences fits with one of these three

tables, some qualitative knowledge is obtained about the retrapping ratio

(i.e. either slow or fast retrapping is indicated) and some information

about the type of trap (i.e, thermally disconnected or not) is also

obtained. Unfortunately, the real value of the trap depth is not known.

However, Kivits and Hagebeuk argue that method 4 (Hoogenstraaten's method)

is the least influenced by variations in parameters such as the retrapping

ratio. For this reason, and following Kivits et al's example mentioned

above, the trap depth calculated using this method has been chosen as the

correct one, as long as it was possible to apply the method successfully

to the particular peak. The relative deviations of the calculated trap

depths, obtained by comparing the answers from other methods with the

trap depths calculated using method 4, were then compared with the correspond-

ing relative deviations in tables A, B and C.

With this procedure, fourteen trap systems were obtained which

gave good agreement with one of the three Kivits and Hagebeuk's tables.

Description of traps :

Here again, an extended analysis for the crystals from boules

‡‡ 377 and ‡‡ 405 will be given. A similar process was followed for all

the other trap depths from the different crystals.

For crystal ‡‡ 377, a very well defined trap at 0.13 eV gives

rise to the peak at 110 K. Very good agreement is obtained with

table B with $\delta \sim$ 1. With this same crystal, the peak at 160 K was

analysed using group A methods and the Garlick and Gibson technique only ;

the calculations, even though not conclusive, produced a value of 0.32 eV

from the Hoogenstraaten method ; a partial agreement between relative

differences was then obtained with table B assuming $\delta \sim$ 0.01. With the

peak at 320 K, the similarity among the results from the different applied

AVERAGE RELATIVE ERRORS (in %) REPRESENTING A RELATIVE SEPARATION OF THE VALUE FROM EACH PARTICULAR METHOD FROM THE REAL TRAP DEPTH, AFTER KIVITS AND HAGEBEUK (1977).

METHOD No.	TABLE A One Trap Centre Retrapping Ratio δ			TABLE B Two Trap Centres Retrapping Ratio δ		
	0.01	1	3	0.01	1	3
GENERAL CLASS METHODS						
4	0.1	+0.25	+0.7	0.1	+0.25	+0.7
5	+0.25	+0.5	+1.0	+0.25	+0.5	+1.0
6	+0.1	+0.2	+0.3	+0.1	+0.2	+0.3
8	-6.0	-5.7	-5.5	-6.0	-5.7	-5.5
9	-6.0	-5.9	-5.5	-6.0	-5.9	-5.5
29	-2.7	-4.5	-8.5	-2.7	-4.5	-8.5
29	-10.0	-13.7	-20.8	-10.0	-13.7	-20.8
FIRST CLASS METHODS						
2	+7.9	+8.5	+9.0	+7.9	+8.5	+9.0
10	+2	-42	-56	+1.7	-20	-31
13	0.5	-32	-48	+0.7	-20	-34
14	2	-30	-45	1.8	-19	-32
16	1	-15	-33	1	-15	-33
17	0.5	-43	-57	-0.8	-22	-33
18a	-5	3	-15	-7	-17	-31
18b	-12	-6.0	-21	-13	-23	-36
26	+6	-10	-27	+6	-10	-27
27	-41	-72	-80	-41	-57	-61
28	1	-15	-32	1	-15	-32
30	-0.5	-16	-33	-0.5	-16	-33
SECOND CLASS METHODS						
3	-0.3	0.05	+0.7	-0.3	0.05	+0.7
20	+103	+17	-12	+103	+60	+37
21	+180	+80	+40	+177	+123	+90
22	+44	0.1	-24	+43	+16	-2.9
23	+20	0.5	-22	+20	0.5	-22
24	+73	0.5	-25	+73	+37	+17

methods indicates, using table B with $\delta \sim 3$, that if a value of 0.86 eV

is assumed for method 4, then the relative differences obtained this way,

and shown in table 5.4 (h), fit remarkably well with table B, the only

exception being method 27, of Kivits and Hagebeuk's technique. It is not

unreasonable therefore to take this value as the correct one.

With the TSC peak at 175 K in crystal ‡‡ 405, only group A

methods and the Garlick and Gibson technique could be applied. If the

value of 0.36 eV derived from method 4 is assumed correct, then good

partial agreement is obtained,with table B,with $\delta \sim 3$. With the correspond-

ing TSL peak at 170 K, the same value of trap depth is obtained from

methods 4 and 5, indicating a correct value of 0.38 eV. Then, the relative

differences of the other methods agree very well with the relative differences

of table A for the case $\delta \sim 3$. Method 4 applied to the TSL peak at 245 K

gives a value of 0.66 eV. Taking this to be the correct trap depth, then

good agreement with table A is also obtained for $\delta \sim 3$.

The fourteen trapping peaks actually analysed in this way are

summarised in table 5.6.

The first conclusion to be drawn from these results, is that

there is no observable relation at all between the peaks and the presence

of indium or gallium in the samples. This conclusion arises, because the

relative maximum intensities of the peaks have a completely random distri-

bution, and do not follow any definite trend as the dopant is increased

or decreased or even changed. Furthermore, some TSC and TSL measurements

carried out on two undoped ZnSe crystals grown in this department, also

showed the three peaks, at about 110, 160 and 220 K, but with the 110

and 220 K peaks very much reduced compared with the middle one, for which

a trap depth of about 0.23 eV for one of the crystals and 0.29 eV for the

second crystal was obtained, using methods mainly from group A, Waite

(1979). The presence of these three peaks in undoped ZnSe crystals in

T A B L E   5.6

TRAP DEPTHS OBTAINED USING THE KIVITS AND HAGEBEUK's TECHNIQUE
OF SOME ZnSe:In AND ZnSe:Ga CRYSTALS

Crystal Boule ##	Location of Peak	Trap Depth (eV)	Retrap-ping Ratio + δ
377	C : 110 K	0.13	1
405 *	L : 110 K	0.13	1
377	C : 160 K	0.32	0.01
405	L : 170 K	0.38	3
405 *	L : 170 K	0.23	1
405	C : 175 K	0.36	3
408	L : 180 K	0.40	1
381	C : 215 K	0.32	0.01
407	L : 220 K	0.42	1
383	C : 220 K	0.47	3
375	C : 230 K	0.44	3
405	L : 245 K	0.66	3
408 *	L : 245 K	0.47	1
377	C : 320 K	0.86	3

* Annealed in zinc vapour
C and L stand for TSC and TSL peak respectively
+ These values represent a rough estimate only.

the same places confirms that they are not associated with indium or
gallium.

The second conclusion is that, apart from the well defined trap
with a depth of 0.13 eV, which is present in all the samples, there seems
to be a distribution of trap depths corresponding to TSC and TSL maxima
between 150 and 250 K. The fact that the activation energies, obtained
from the several progressive thermal cleaning runs, form a quasi-continuous
set of values between these temperatures, supports this conclusion. In
the higher temperature range from 270 K to 320 K, it is the trap system,
with a depth of about 0.8 to 0.9 eV, which is responsible for the observed
TSC.

A final point is that, if the values of the retrapping ratio are
taken into account (i.e. $\delta \sim 3$), then in most crystals, a strong recombina-
tion of carriers occurs (i.e.,bimolecular recombination). It also indicates
that the capture cross-section of the traps is very similar to that of the
recombination centres.

Very little information about trapping phenomena in ZnSe can be
obtained from the literature. Stringfellow and Bube (1968) made TSC and
TSL measurements on self-activated ZnSe and on ZnSe:Cu:Al and obtained three
similar peaks to the ones obtained in the undoped ZnSe crystals mentioned
above (Waite, 1979) and from which, Stringfellow and Bube were only able
to analyse the peaks for the two deeper traps. By using the decayed TSC
method, they obtained values of 0.28 eV and 0.38 eV for these traps.
Wakim (1970) observed two peaks from TSC and TSL at 118 K and 158 K in
nominally undoped ZnSe, which was known to contain traces of copper and
other unintentionally added impurities. Using the method of Garlick and
Gibson on the rising limb of the prominant peak at 158 K, Wakim obtained
a value of 0.38 eV. He mentions in his paper that this result agrees with
those reported by Stringfellow and Bube. This is not completely true
since the latter two authors reported that their values of 0.28 eV and

0.38 eV corresponded to the deeper traps, which, it is logical to assume, correspond to the peaks, shown in figure 14 of their paper, located at about 170 K and 210 K respectively ;in other words, Wakim associates a value of 0.38 eV with the 160 K peak, but Stringfellow and Bube calculated a value of 0.28 eV. This discrepancy is probably due to the fact that these investigators used different methods of analysis. More recently, Satoh and Igaki (1980) also found three TSC peaks in undoped ZnSe crystals heat treated in zinc. The peaks were located near 120 K, 150 K and 180 K. From the analysis using the heating rate method, they found that the two TSC peaks observed at 150 K and 180 K originated from two electron trapping levels at 0.19 and 0.31 eV respectively. It was suggested that these trap levels were caused by trace impurity defects, for example Cl_{Se} or In_{Zn} or an associated defect consisting of a native defect (V_{Se} or Zn_i) and some impurity.

The presence of the three peaks in the ZnSe:Cu samples studied by Stringfellow and Bube again supports the view that the addition of indium or gallium to the samples does not influence the relative heights of the observed TSC and TSL peaks, since their three peaks coincide quite well with the main peaks observed in the present study. It should be stated, however, that the peaks near 220 K, all have a relatively greater intensity than those reported by Stringfellow and Bube, and by Wakim and by Waite and by Satoh and Igaki, at the same temperature. This, once more, seems to indicate that the optical properties of these crystals are swamped by the presence of (1) copper impurity and hence, the similarity with the TSC peaks of Stringfellow and Bube's ZnSe copper doped crystals and/or (2) some native defect such as the zinc vacancy shown by the similarity of our TSC peaks with those reported in undoped ZnSe crystals.

It is perhaps worth pointing out that the high temperature TSC peaks, more or less well defined in all our crystals, were not reported by these earlier authors. The fact that this last group of small peaks do

not appear in our TSL curves is probably due to the strong thermal
quenching of the luminescence at about 240 K as reported by Stringfellow
and Bube (1968).

5.5   CONCLUSIONS

Summarizing the discussion sections of this chapter, leads to
the conclusion that either unintentional copper impurity or donor defects
associated with zinc vacancies (see for example Watkins, 1974 , and
Dunstan et al, 1977)   screen any effect of indium or gallium on the
optical properties of ZnSe.   Secondly, the presence of a well defined
trap at 0.13 eV,as determined from the TSC and TSL measurements, has been
confirmed. Unfortunately, the presence of this level has not been con-
firmed by other means, in particular, by the measurements of the electrical
properties described in the next chapter. No mention of it has been found
in the available literature. It should be possible with some of our
samples to make Hall measurements while emptying the trap, to verify the
sign of the carriers liberated. Finally, with the other trap depths, our
results are mainly inconclusive but suggest a continuous distribution of
trapping levels between 0.2 to 0.9 eV with increased concentrations at
particular discrete values.

CHAPTER 6

ELECTRICAL PROPERTIES

6.1   INTRODUCTION

A short survey describing how the measurements were carried out
will be presented in the next sub-section. In the second section, a
summary of all the relevant results obtained from the conductivity and Hall
effect measurements is given. An extended discussion of these results
follows in section three with special stress on the strong compensating
effects observed in the crystals studied. This is summarised in the final
section.

6.1.1 Measurements

Hall effect and conductivity measurements were made on twenty
six samples cut from eleven different crystal boules of ZnSe doped either
with indium or gallium, in as-grown form or heat treated in zinc (i.e.,
annealed in zinc vapour), in the dark or under illumination.

All the samples were prepared as explained in chapter four.
Whenever the specimen bar was large enough, six indium contacts were made
on the sample. When the bar was too short, five contacts only were used,
with a common one for conductivity and Hall voltage measurements.

However, the main practical difficulty was in obtaining long
(>6 mm) uniform bars, because the low resistivity samples had grain
boundaries producing high resistance barriers which, if present in a
specimen, prevented any meaningful electrical measurements from being made
(see Russell et al, 1980) . This topic will be discussed in detail in the
next chapter. To overcome this problem, circular slices of the crystal were
equipped with suitable indium contacts and subjected to a preliminary study

in the scanning electron microscope, in the electron beam induced current mode. This revealed the grain boundaries introducing the barriers. Specimen bars were then cut from any uniform parts of the slice. The bars obtained in this way were usually rather short.

The sample, with its contacts, was then mounted on a cover slip, and placed on the cold-finger of the cryostat as explained in chapter four. The system was heated to about 145° C for a few minutes to empty any traps and the contacts were then tested.

The end contacts of each bar were tested for their ohmicity by measuring the V-I characteristic ; the resistance between pairs of the other four contacts was measured two at a time in order to check the uniformity of the specimen. After this test, conductivity and Hall measurements were made, starting at around 420 K and then, as the temperature was reduced in stages, towards 85 K.

6.2   EXPERIMENTAL RESULTS

In order that the experimental results may be more clearly understood, the measurements made on as-grown doped samples will be described first, and this will be followed by an account of the results obtained with samples annealed in zinc. The electrical conductivity of as-grown samples containing low concentrations of indium (10-20 ppm) was quite high ($\sim 10^{-2} \Omega^{-1} cm^{-1}$ at room temperature), but decreased with increasing concentrations of indium. It is convenient, in describing the experimental results, to divide the as-grown samples into five groups of increasing resistivity, and to describe measured properties of each group in turn. In the same way, the annealed crystals can be divided into two groups with somewhat different electrical properties ; the distinction here is between crystals which were heavily or lightly annealed.

The results are presented in graphical form for each group of crystals. Four sets of curves are plotted for each group illustrating

(a) the variation of $\ln \sigma$ with $1/T$, (b) $\ln \mu_H$ as a function of $\ln T$,

(c) the same results as in (b) but plotted as $\ln \mu_H$ against $1/T$, to reveal

the presence of any possible impurity banding effects and (d) the variation

of $\ln n$ versus $1/T$ in order to calculate donor ionisation energies where

appropriate. From the straight line portions of each of these curves,

linear regressions were carried out and the standard deviations from the

slopes and the intercepts usually lay within 1 and 5% respectively.

6.2.1 As-grown Crystals

The samples comprising the five groups mentioned above, are

listed in table 6.1 along with some of the experimental data.

Group I : The first group includes those samples exhibiting the highest

conductivity and containing the lowest indium concentration ; these are

samples 132 ; 138 and 139. Curves illustrating the variation of the

conductivity σ, Hall mobility μ_H and carrier concentration n with tempera-

ture are shown in figures 6.1 to 6.4. Figure 6.1 represents the plots of

$\ln \sigma$ versus $1/T$ for the three samples. With samples 132 and 139, a strong

exponential behaviour can be seen, giving an activation energy of about

0.27 eV from both slopes, which differs very much from the behaviour of

the third sample 138, which displays three different slopes. The highest

value of conductivity was just under 0.09 $(\Omega \text{ cm})^{-1}$ near 420 K for sample

138. At room temperature the conductivity was about 0.03 $(\Omega \text{ cm})^{-1}$ for

sample 138 and about 2×10^{-3} $(\Omega \text{ cm})^{-1}$ for the other two. Figure 6.2 shows

the plots of $\ln \mu_H$ versus $\ln T$ for the same group. What is apparent from

these curves is that the Hall mobility of sample 138 was almost constant

with a value of about 60 $\text{cm}^2 \text{ V}^{-1} \text{ s}^{-1}$ between 150 K to 280 K, increasing

slightly to 120 $\text{cm}^2 \text{ V}^{-1} \text{ s}^{-1}$ at 415 K. The mobilities of the other

two samples had a marked exponential behaviour as the curves in figure 6.3

also show. The mobility activation energies were 0.33 eV and 0.36 eV,

between 270 and 320 K. The highest value of μ_H was 120 $\text{cm}^2 \text{ V}^{-1} \text{ s}^{-1}$ for

sample 138 at 415 K, while for sample 139, the mobility was as low as

T A B L E   6.1

ELECTRICAL PROPERTIES AT 410 K OF SOME
AS-GROWN ZnSe:In AND ZnSe:Ga CRYSTALS.

| Group	Crystal Boule $\neq\neq$	Dopant Content p.p.m.	Sample No.	σ $(\Omega \, cm)^{-1}$	μ_H $cm^2 V^{-1} s^{-1}$	n cm^{-3}
I	407	12	132	6.4×10^{-2}	63	7.4×10^{15}
	413	17	138	8.4×10^{-2}	120	4.3×10^{15}
			139	5.3×10^{-2}	24	1.4×10^{16}
II	405	55	121	4.1×10^{-3}	97	2.8×10^{14}
			123	3.1×10^{-3}	196	1.0×10^{14}
			128	1.6×10^{-3}	225	4.5×10^{13}
III	375	95	101	2.0×10^{-4}	160	7.4×10^{12}
	342	95	102	7.1×10^{-6}	195	2.3×10^{11}
	408	250	126	1.2×10^{-5}	220	3.2×10^{11}
	410	110	134	3.5×10^{-5}	180	1.1×10^{12}
IV	408E	250	127	2.4×10^{-6}	177	8.5×10^{10}
	410E	105	135	1.5×10^{-7}	85	1.1×10^{10}
	342E	95	141	9.2×10^{-7}	162	3.6×10^{10}
	349	800	142	4.6×10^{-7}	111	2.6×10^{10}
V (Ga)	383	370	112	1.6×10^{-4}	63	1.7×10^{13}
	382	110	140	1.1×10^{-2}	43	1.4×10^{15}
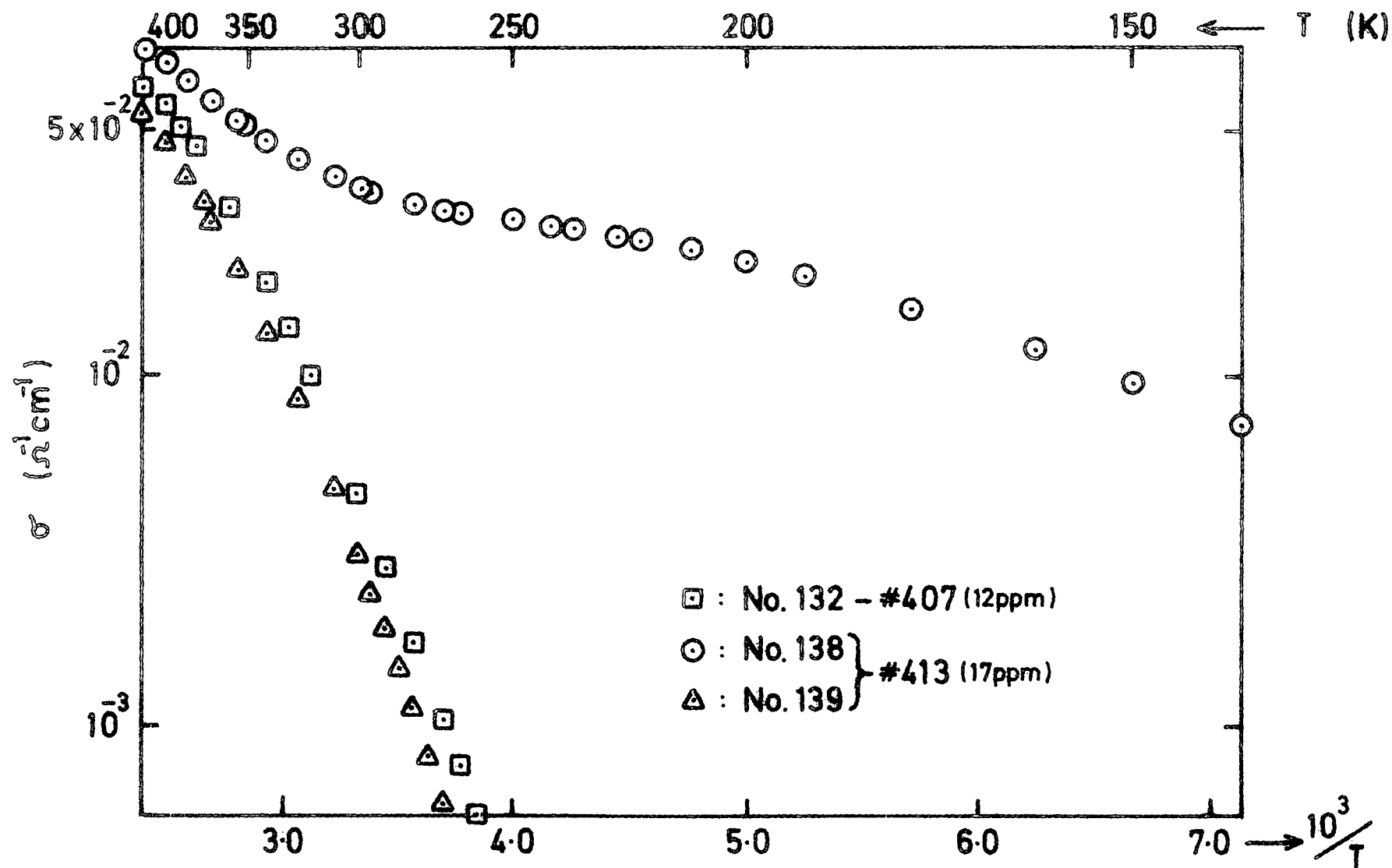
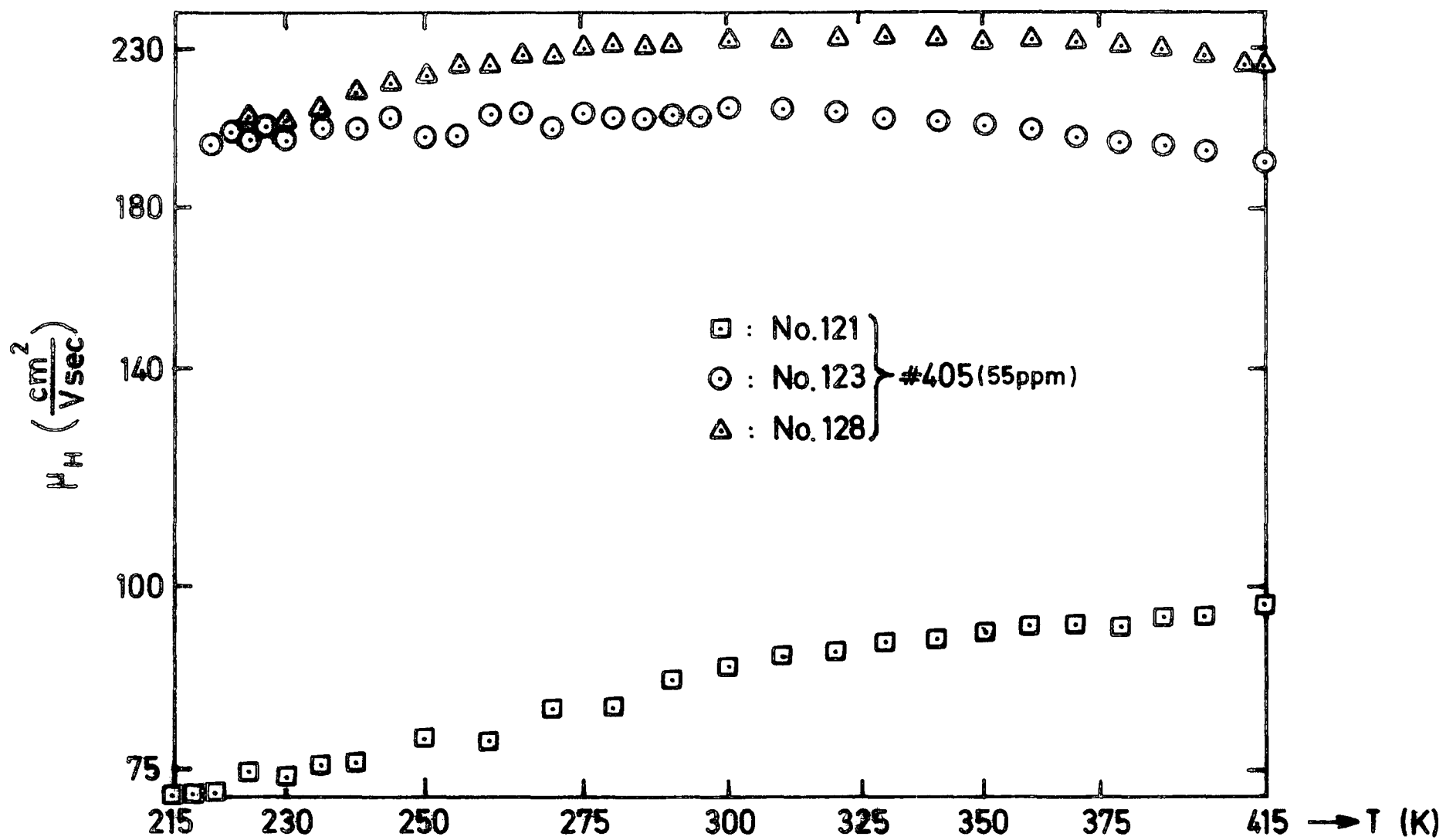FIG. 6·1 ELECTRICAL CONDUCTIVITY AS A FUNCTION OF RECIPROCAL TEMPERATURE FOR SOME ZnSe:In SAMPLES.
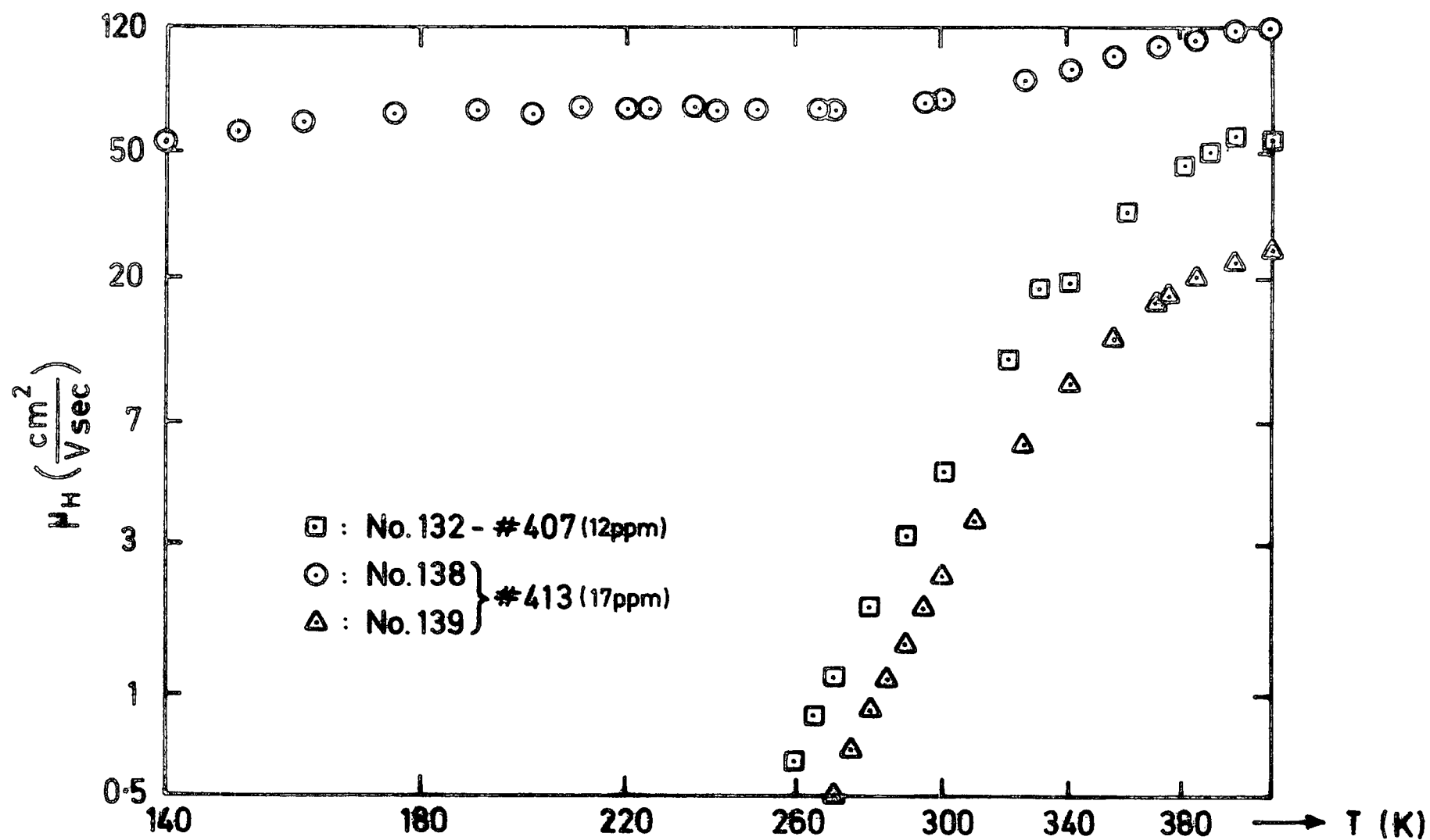
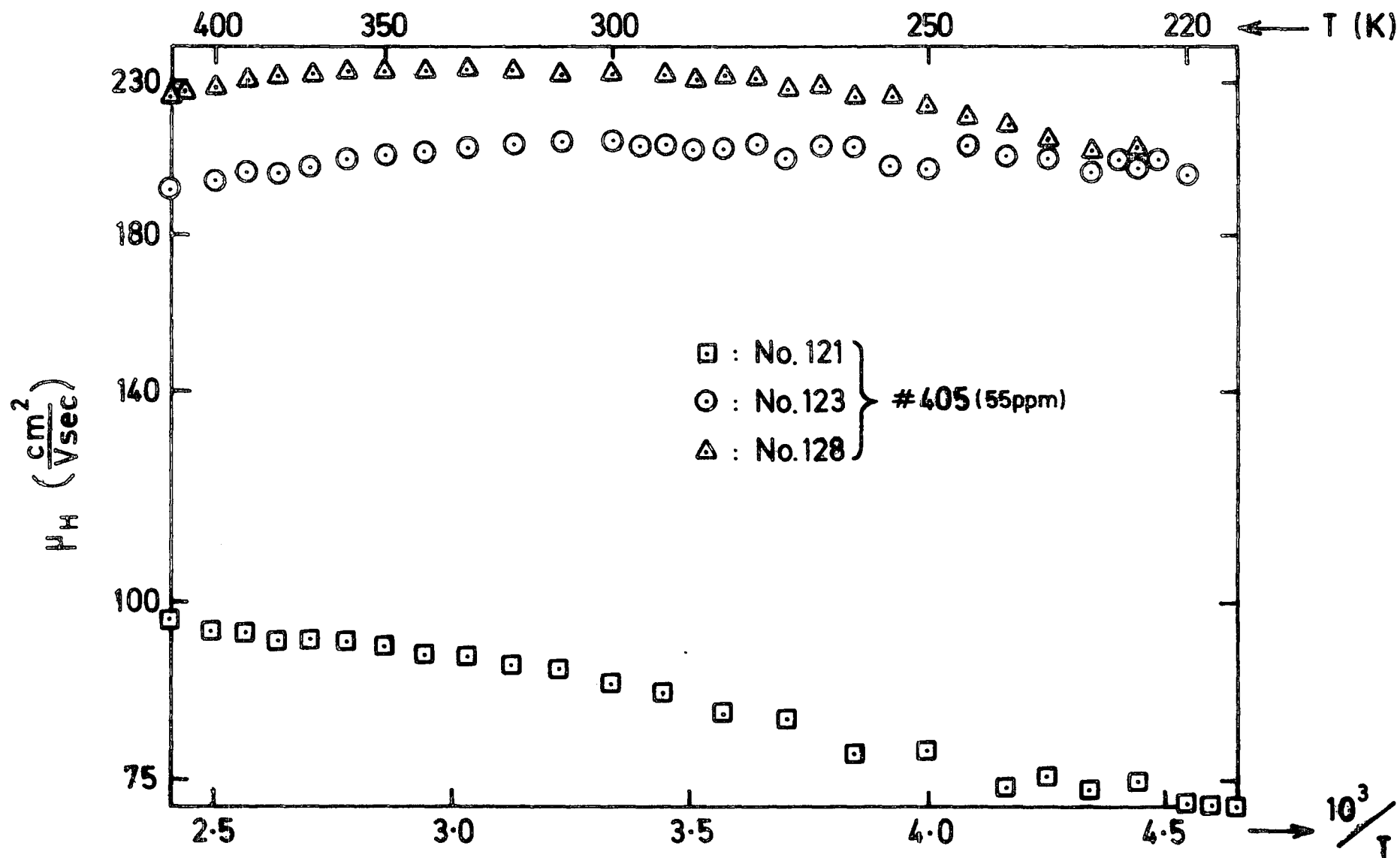FIG. 6·2   HALL MOBILITY AS A FUNCTION OF TEMPERATURE FOR
SOME ZnSe:In SAMPLES.
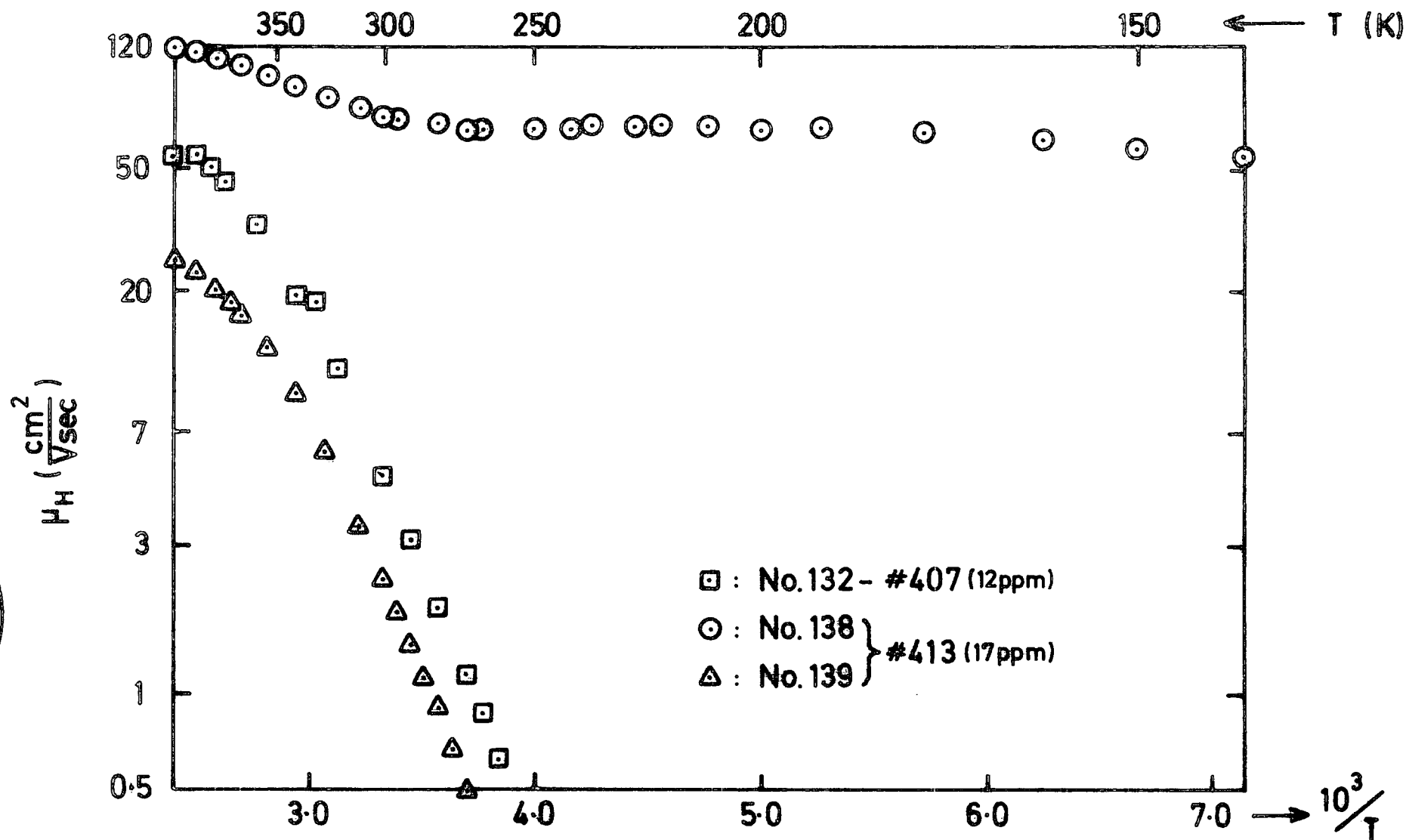
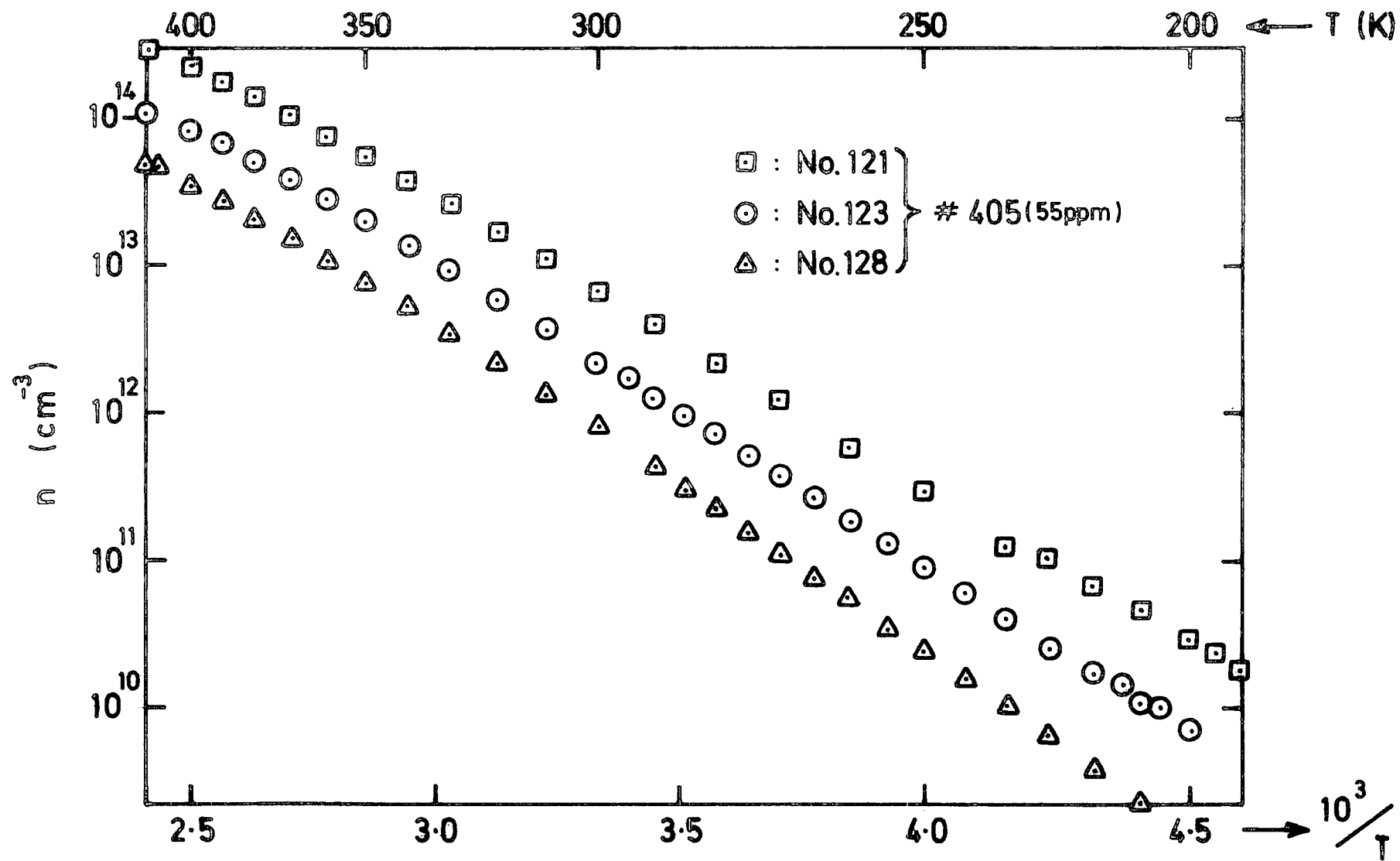FIG. 6·3   HALL MOBILITY AS A FUNCTION OF RECIPROCAL TEMPERATURE
FOR SOME ZnSe:In SAMPLES.
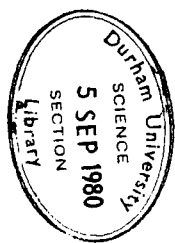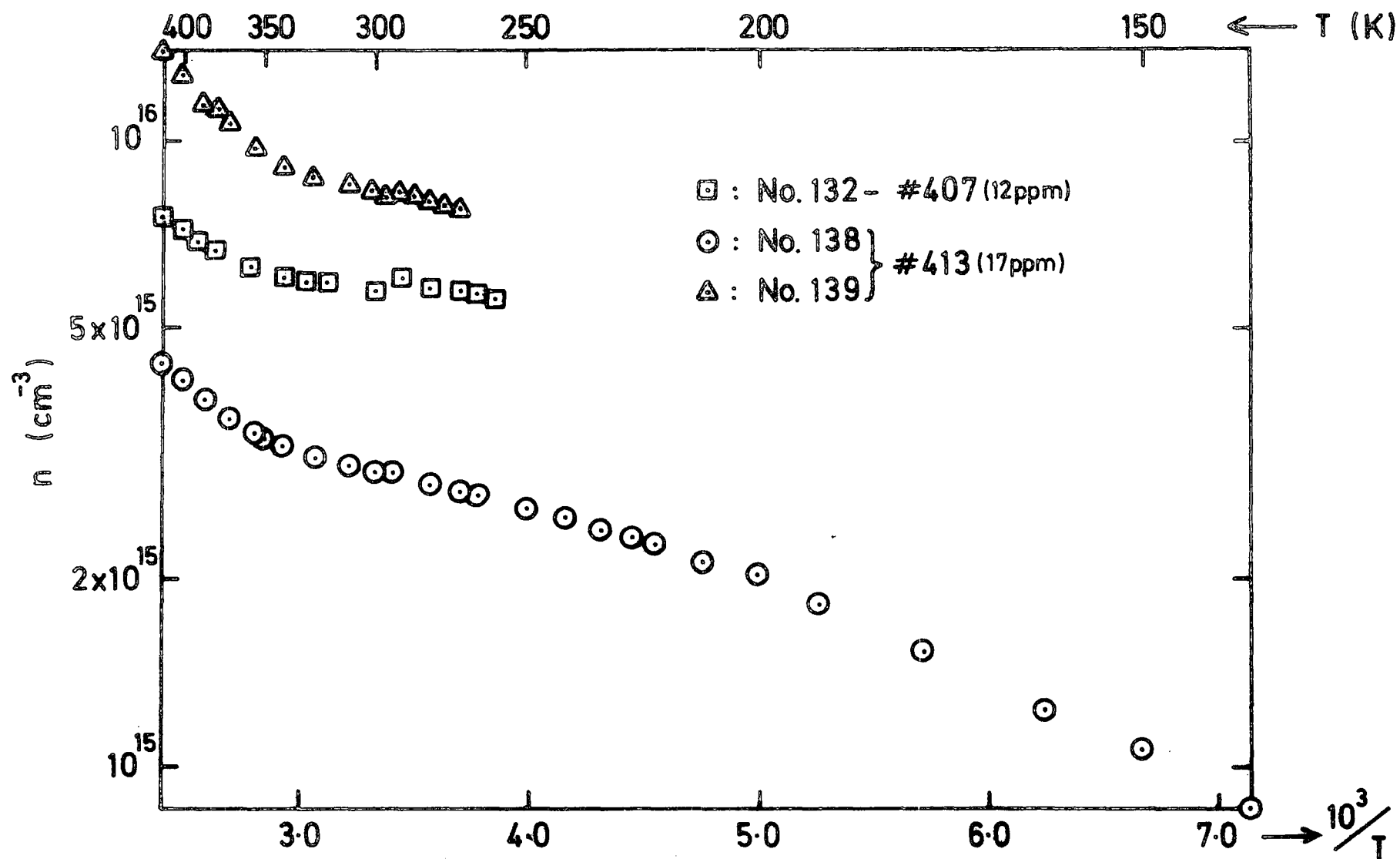
FIG. 6·4   CARRIER   CONCENTRATION   AS   A   FUNCTION   OF   RECIPROCAL
TEMPERATURE   FOR   SEVERAL   ZnSe : In   SAMPLES.

0.5 cm^2 V^{-1} s^{-1} at 270 K.   Finally, figure 6.4 illustrates the correspond-

ing plots of ℓn n versus 1/T.   Near room temperature, the values of n were

only weakly dependent on temperature while at higher temperatures, the slopes

began to increase ; no explanation was found to account for this.   The maxi-

mum value of n was obtained with sample 139 with a value of 1.4 x 10^{16} cm^{-3}

at 415 K; at room temperature, the free electron concentrations were between

3 x 10^{15} and 8 x 10^{15} for samples 138 and 139 respectively.

Group II : Includes samples 121 ; 123 and 128, all three cut from different

regions of boule ## 405 (containing some 55 ppm of indium). Their electrical

properties are shown graphically in figures 6.5 to 6.8. Plots of ℓn σ

against 1/T in figure 6.5 give very similar activation energies of about

0.4 eV for all three samples. The lowest value of σ for this group was

7 x 10^{-8} $(\Omega\ cm)^{-1}$ at 225 K for sample 128 while the highest obtained was

just under 5 x 10^{-3} $(\Omega\ cm)^{-1}$ at 415 K for sample 121. Room temperature

conductivities were about 7 x 10^{-5} $(\Omega\ cm)^{-1}$. Hall mobilities (figure 6.6)

were almost independent of temperature, although samples 123 and 128 had

poorly defined maxima just above room temperature in the range from 200

to 230 cm^2 V^{-1} s^{-1}.   On the other hand, sample No.121 had much smaller

values of about 70 cm^2 V^{-1} s^{-1} at 215 K rising slowly to just under

100 cm^2 V^{-1} s^{-1} at 415 K.   The curves in figure 6.7, where the Hall

mobilities are plotted logarithmically against 1/T, reveal only a very

weak exponential behaviour. The mobility activation energies calculated

from the linear portions of the curves, together with those from other

relevant samples are listed in table 6.2.

    Plots of carrier concentration versus 1/T (figure 6.8) are very

similar to those of figure 6.5 (ℓn σ vs 1/T), which is not surprising

since the mobilities of these samples were very weakly temperature depend-

ent and,hence, the slopes of the carrier concentration and conductivity

curves are almost identical and equal to about 0.4 eV. Towards higher
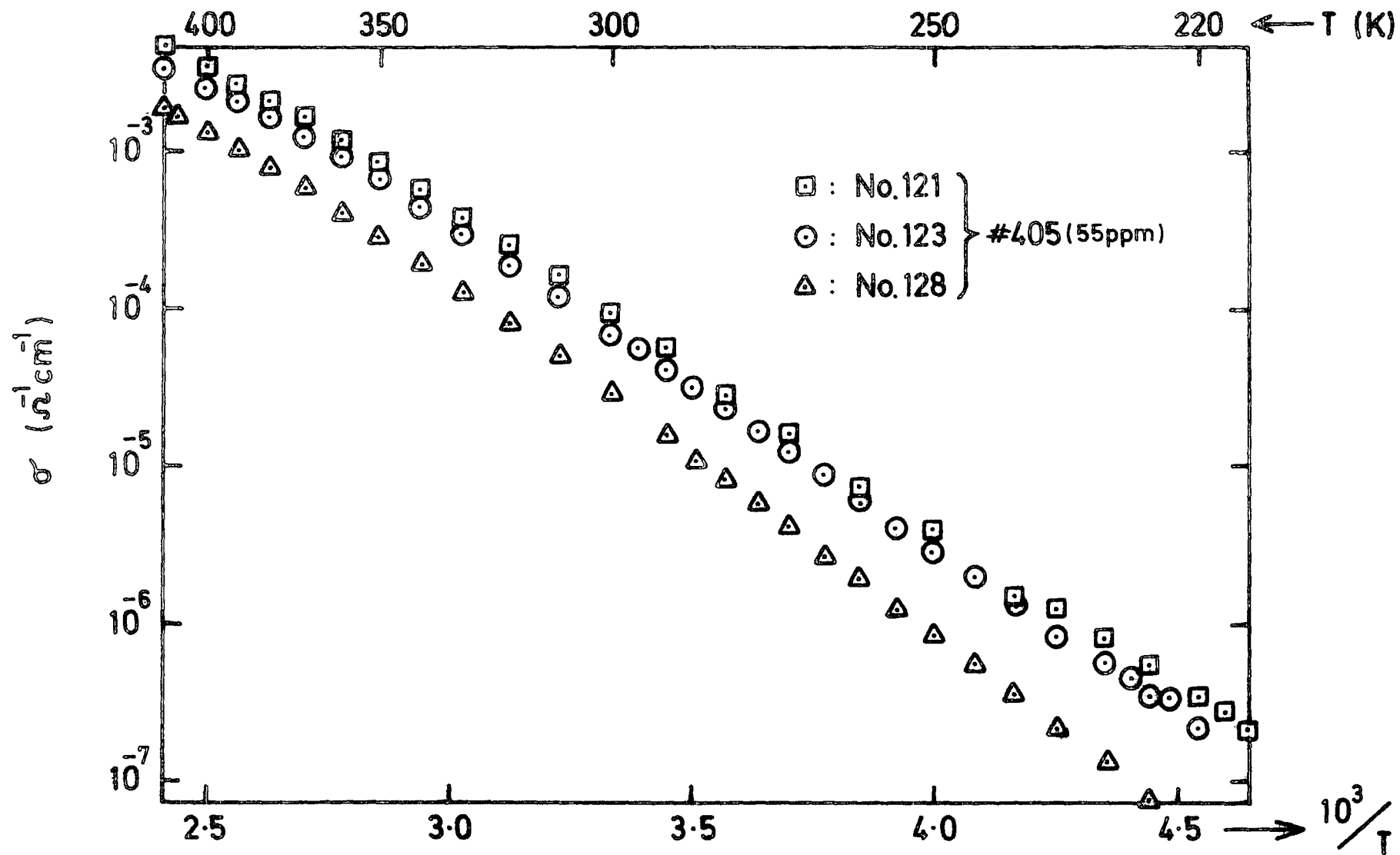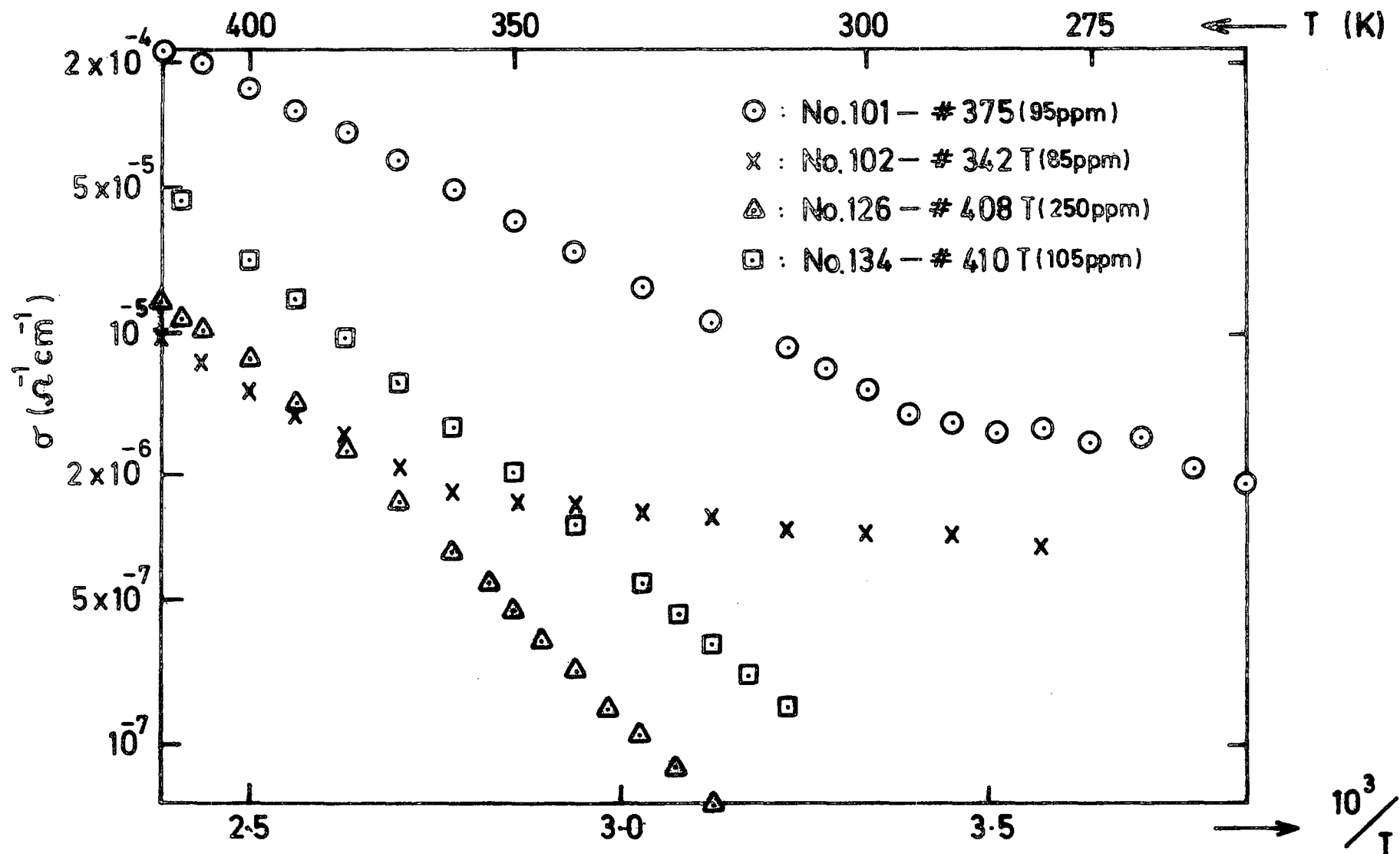
FIG. 6.5   ELECTRICAL   CONDUCTIVITY   AS   A   FUNCTION   OF   RECIPROCAL
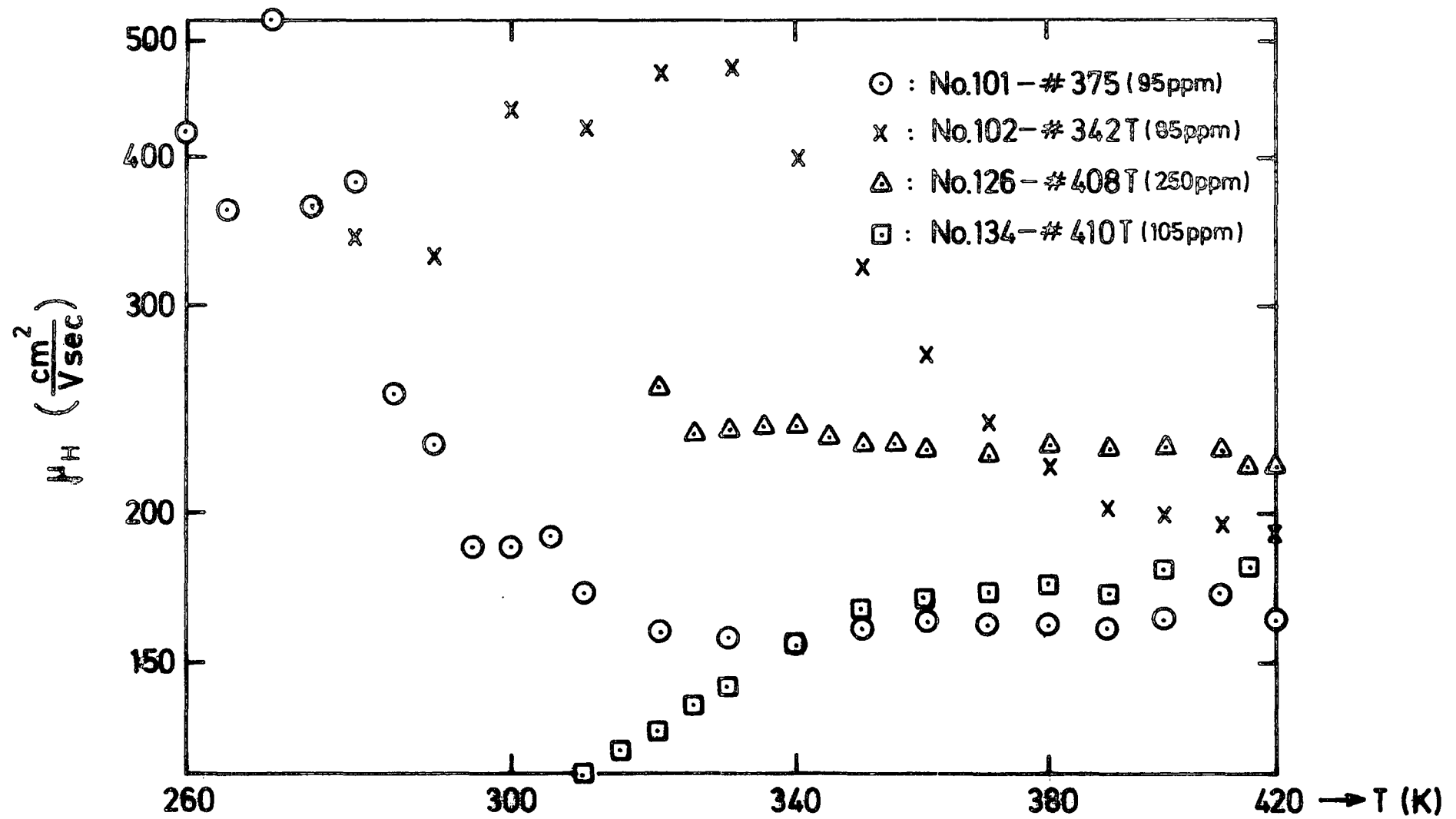TEMPERATURE   FOR   SOME   ZnSe : In   SAMPLES.

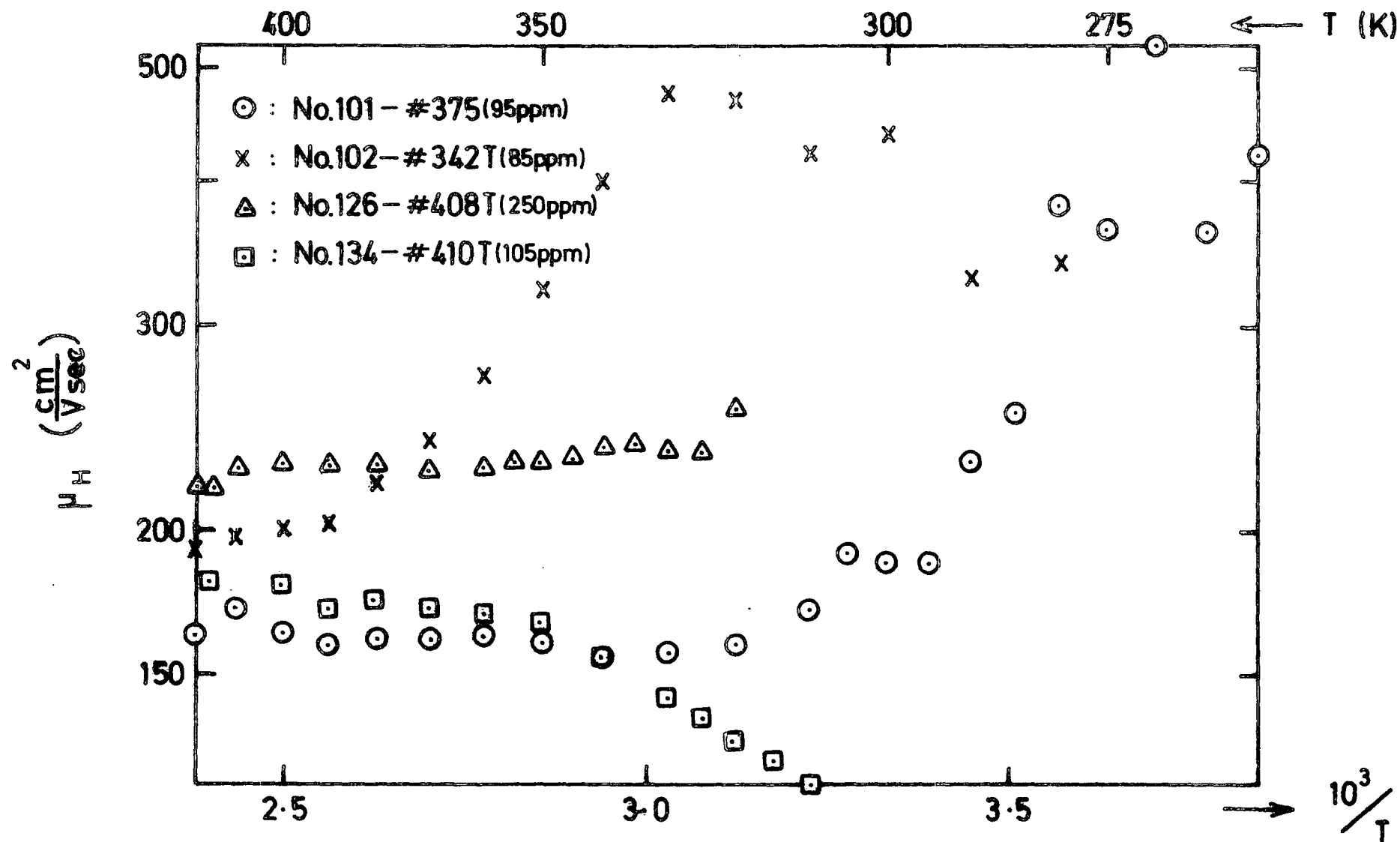FIG. 6·6   HALL MOBILITY AS A FUNCTION OF TEMPERATURE FOR SOME
ZnSe : In SAMPLES.

FIG. 6·7   HALL MOBILITY AS A FUNCTION OF RECIPROCAL TEMPERATURE
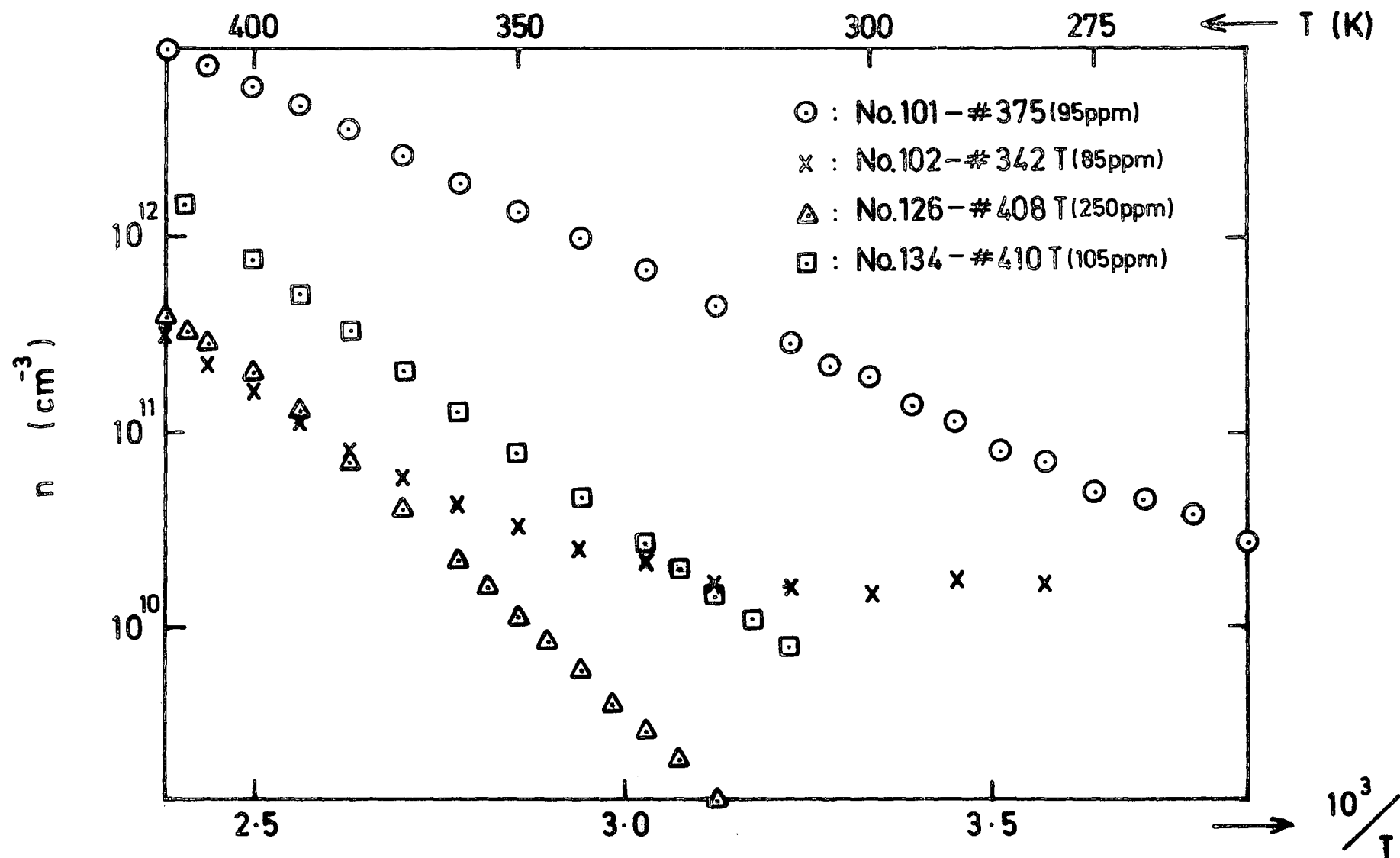FOR SOME   ZnSe : In SAMPLES.

FIG. 6·8 CARRIER CONCENTRATION AS A FUNCTION OF RECIPROCAL
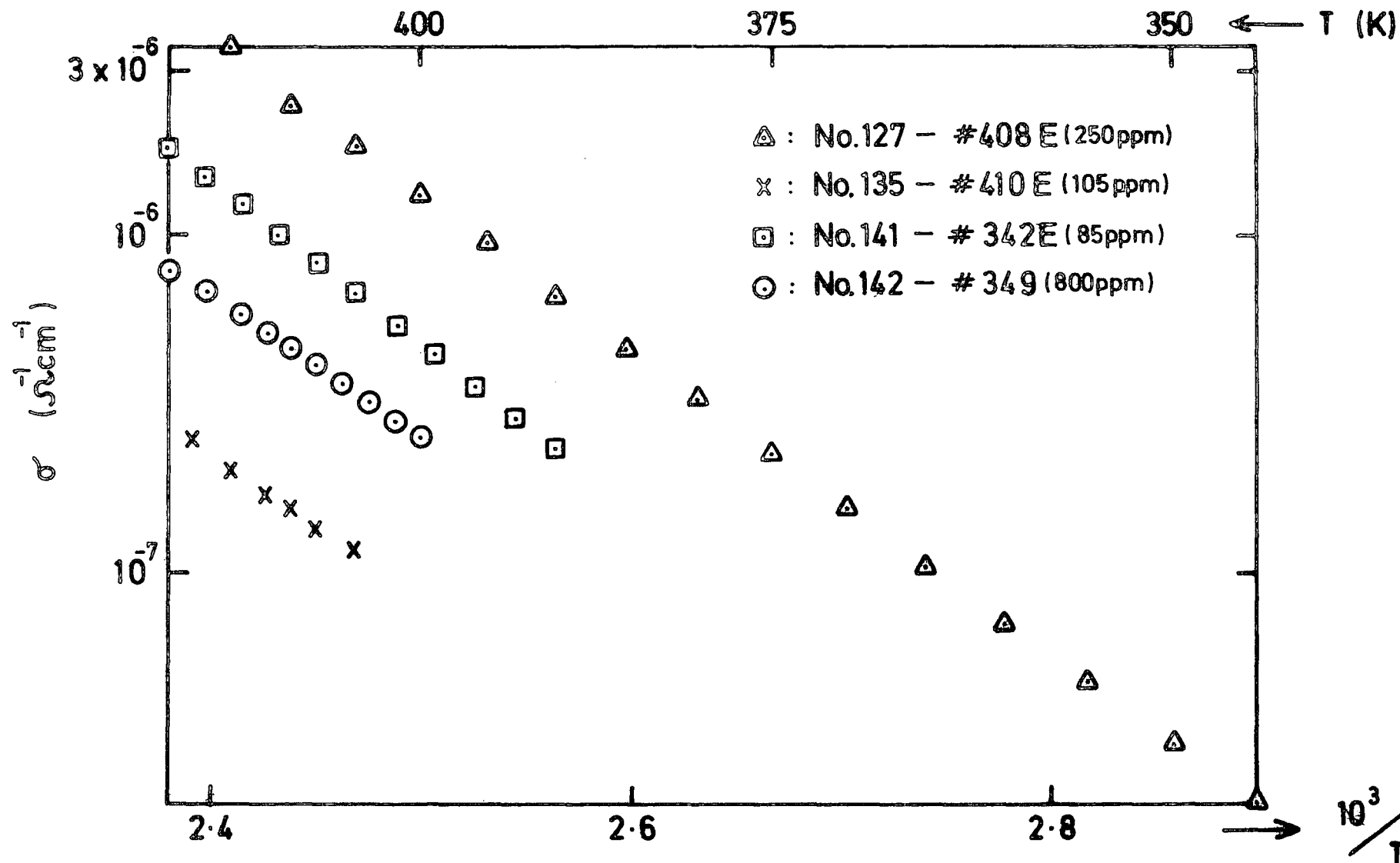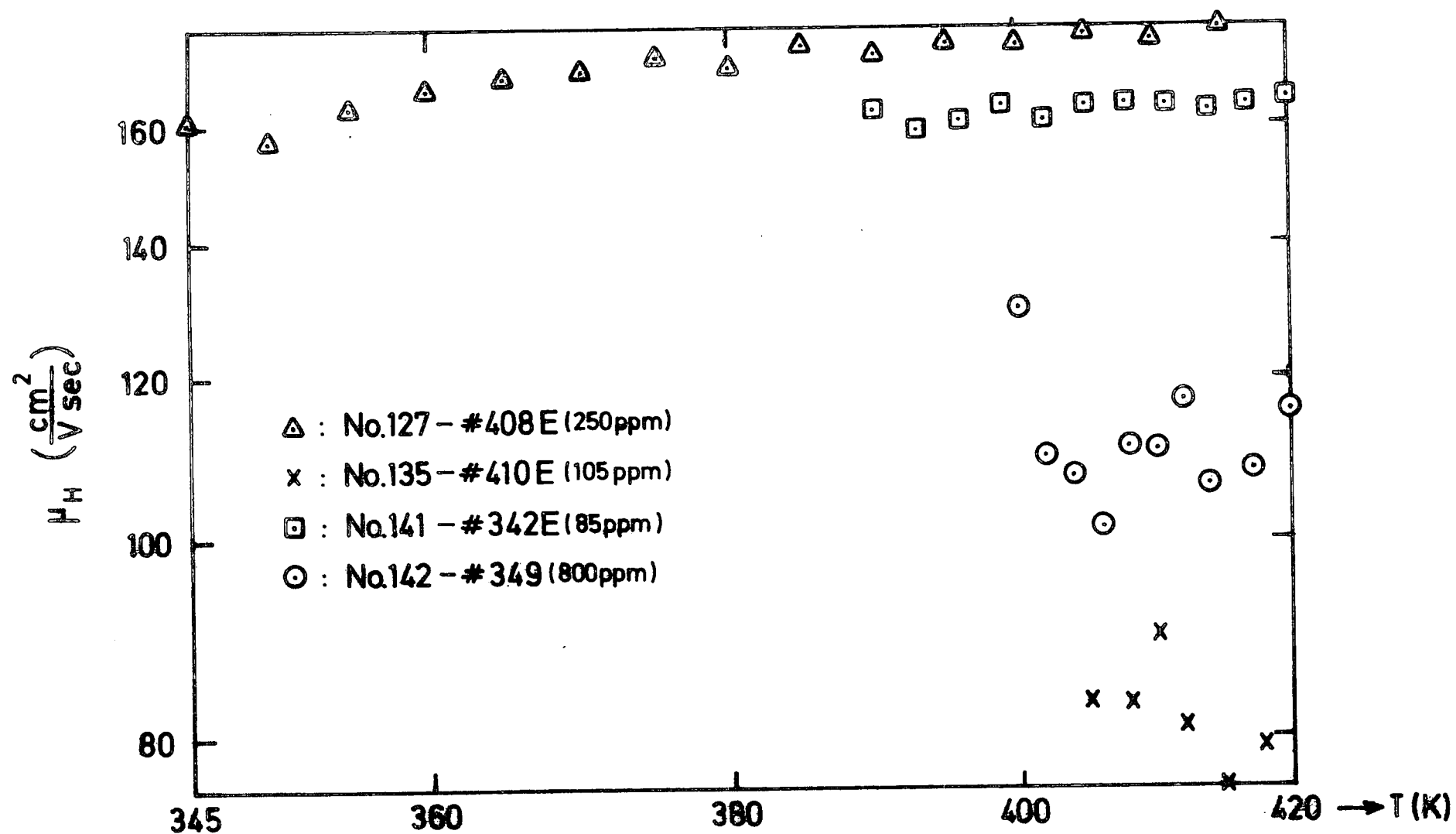TEMPERATURE FOR SEVERAL ZnSe : In SAMPLES.

ACTIVATION ENERGIES OBTAINED FROM SEVERAL OF THE $\ell n \; \mu_H$
v.s. 1/T CURVES OF FIGURES 6.3 ; 6.7 ; 6.11 AND 6.19

Sample No.	Mobility Activation Energy E_μ (meV)	Temperature Range for which it was Obtained (K)
121	13	220 - 310
128	14	230 - 270
132	334	260 - 330
134	75	310 - 350
138	50	280 - 400
139	356	260 - 310
140	33	230 - 270
140	42	260 - 400

temperatures, the plots begin to deviate from the exponential behaviour, indicative of the near presence of the exhaustion range.

Group III : Samples 101 ; 102 ; 126 and 134 are included in this group and the corresponding measurements on these samples are illustrated in figures 6.9 to 6.12. With the exception of sample No.102, the plots of $\ln \sigma$ against $1/T$ (figure 6.9) were exponential. Because of the relatively high resistivities of this group, measurements were limited to the range above room temperature. Conductivity activation energies ranged between 0.34 eV for sample 101 to 0.68 eV for sample 126. Figure 6.10 shows the corresponding mobility values which once again were almost independent of temperature above 340 K. In figure 6.11 where $\ln \mu_H$ is plotted against $1/T$, only sample 134 has any exponential region of mobility in the range from 310 to 350 K. Plots of $\ln n$ against $1/T$ are shown in figure 6.12 and, again, the behaviour reflects that of conductivity, indicative of the weak dependence on temperature of the mobility. The slopes calculated from these plots vary between 0.37 eV for No.101 to 0.68 eV for sample 126, which has the lowest carrier concentration of just over 10^9 cm^{-3} at 320 K. Sample 101 has the highest n of this group with a value of just under 10^{13} cm^{-3} at 420 K.

Group IV : Includes sample 142 from boule $\#$ 349 which had the highest indium content and one of the lowest conductivity values. The group also includes three anomalous samples, namely 127, 135 and 141 , which were cut from the last end to grow of their respective crystal boules. Each had much higher resistivities than the equivalent samples cut from the bulk of the boule. Their electrical properties, measured on the restricted range from 345 to 420 K are illustrated graphically in figures 6.13 to 6.16. The curves of $\ln \sigma$ vs $1/T$ in figure 6.13 show almost perfect exponential behaviour with slopes ranging from 0.84 eV for sample 135 to 0.96 eV for sample 141. The plots in figure 6.14 show that the Hall

FIG. 6·9 ELECTRICAL CONDUCTIVITY AS A FUNCTION OF RECIPROCAL
TEMPERATURE FOR SOME ZnSe : In SAMPLES.

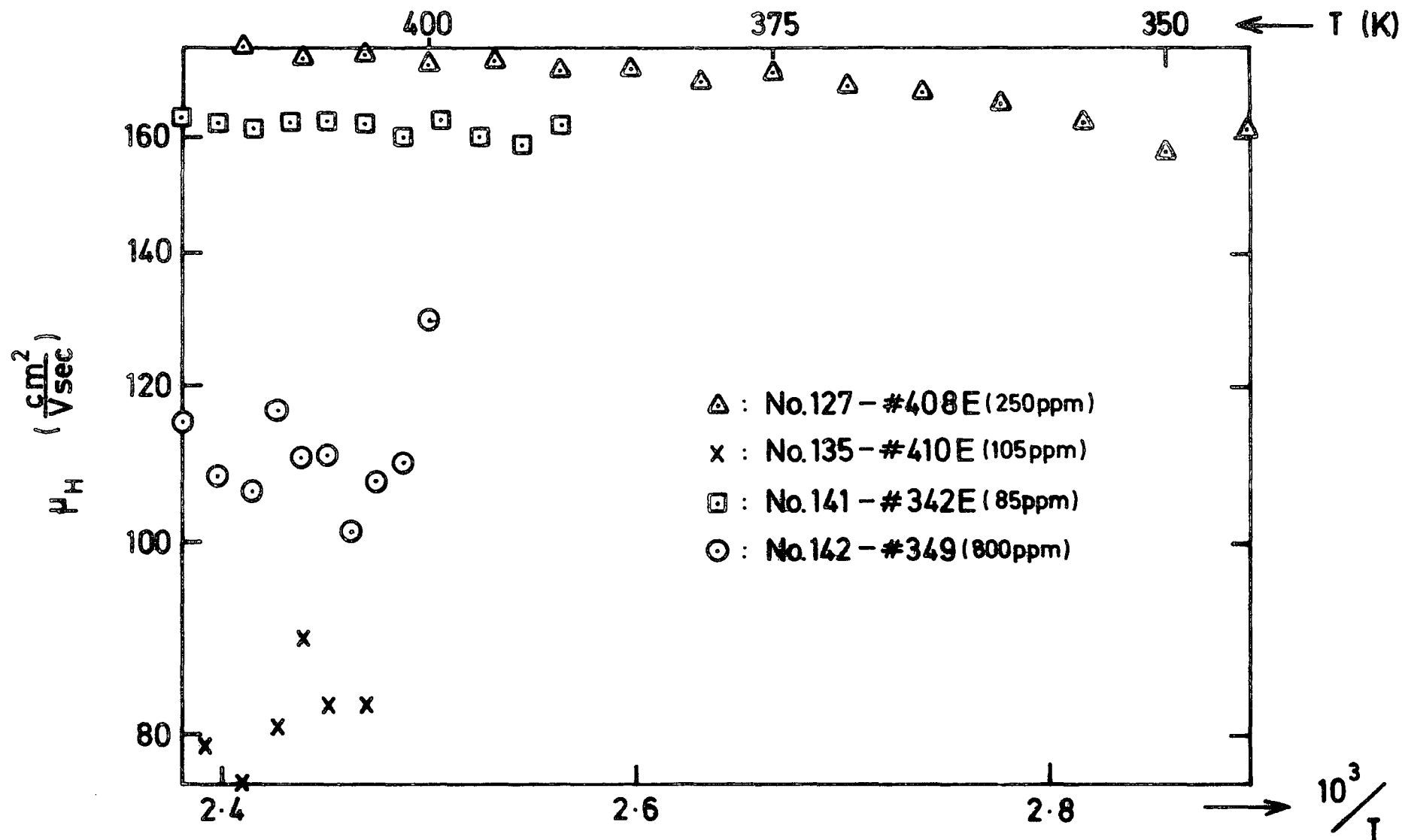FIG. 6·10 HALL MOBILITY AS A FUNCTION OF TEMPERATURE FOR SOME ZnSe : In SAMPLES.

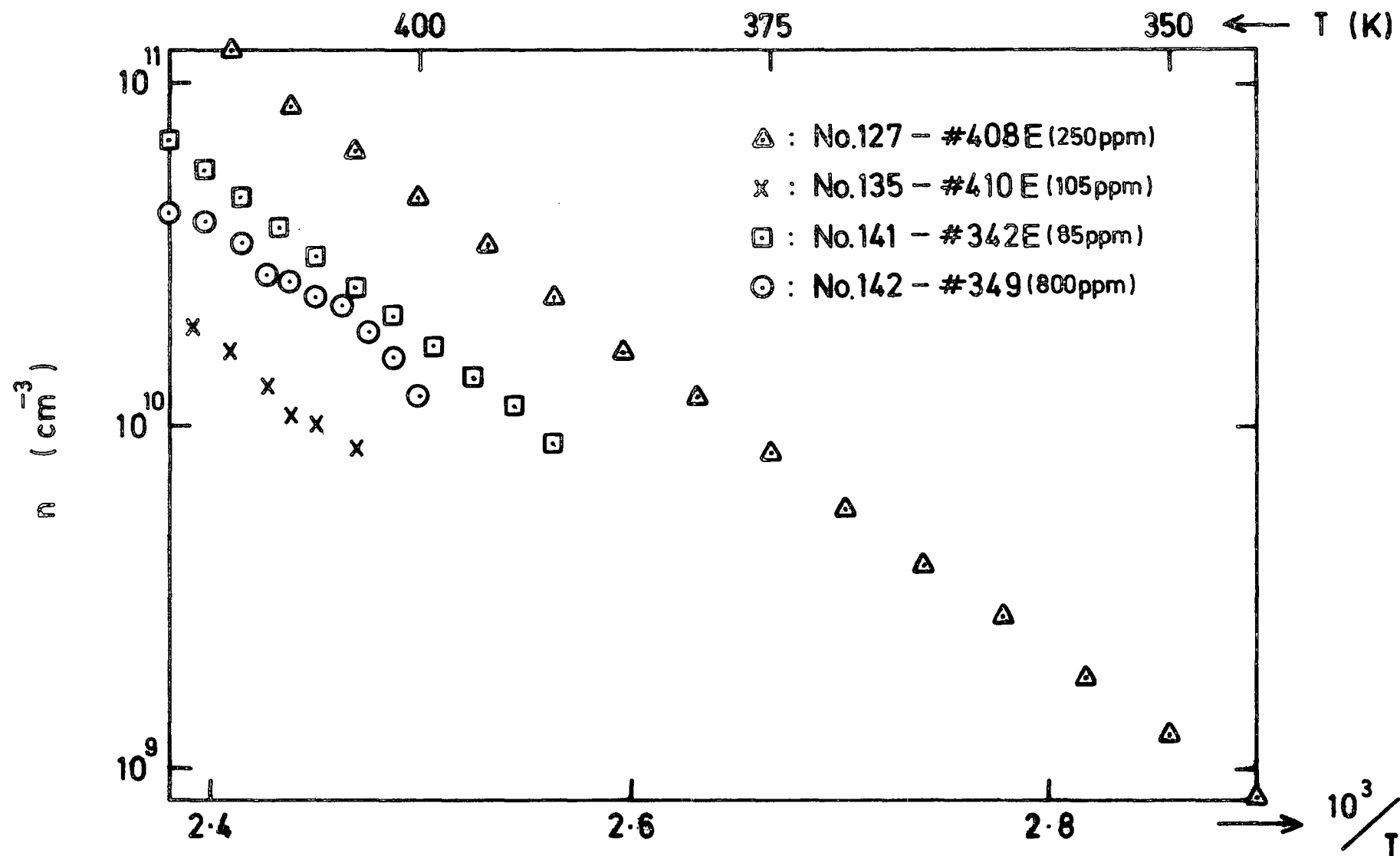FIG. 6·11   HALL MOBILITY AS A FUNCTION OF RECIPROCAL TEMPERATURE FOR SOME ZnSe : In SAMPLES.

FIG. 6·12 CARRIER CONCENTRATION AS A FUNCTION OF RECIPROCAL TEMPERATURE FOR SEVERAL ZnSe : In SAMPLES.
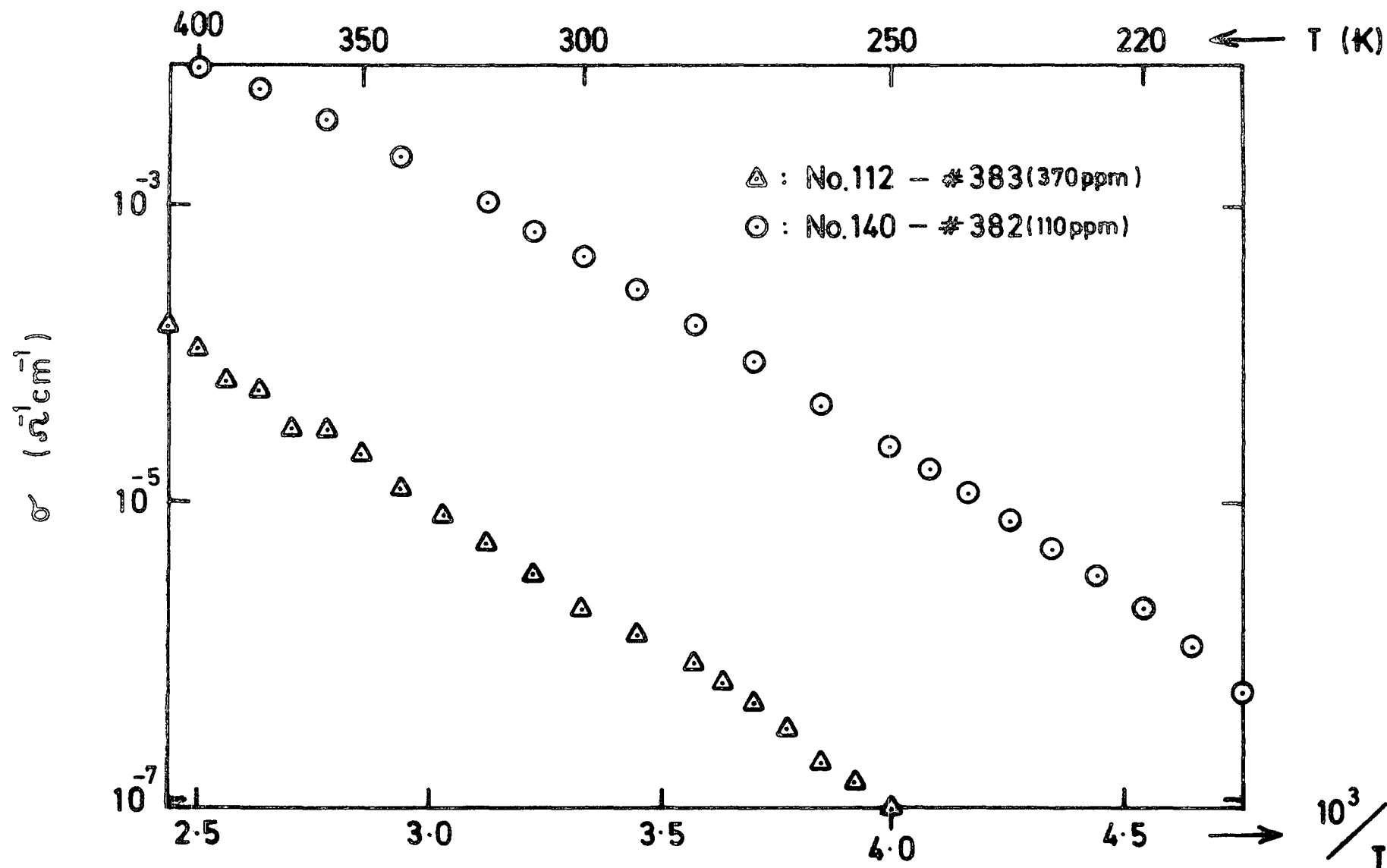
FIG. 6·13   ELECTRICAL CONDUCTIVITY AS A FUNCTION OF RECIPROCAL
TEMPERATURE   FOR   SOME   ZnSe : In SAMPLES.

FIG. 6·14   HALL   MOBILITY   AS   A   FUNCTION   OF   TEMPERATURE   FOR
SOME   ZnSe : In   SAMPLES.

FIG. 6·15   HALL   MOBILITY   AS   A   FUNCTION   OF   RECIPROCAL   TEMPERATURE
FOR SOME   ZnSe : In SAMPLES.

FIG. 6·16 CARRIER CONCENTRATION AS A FUNCTION OF RECIPROCAL TEMPERATURE FOR SEVERAL ZnSe : In SAMPLES.

mobilities of these four samples were almost independent of temperature in the limited range investigated. As a result,therefore, the carrier concentration increased exponentially as did the conductivity, with activation energies varying between 0.87 eV for sample 142 and 0.95 eV for sample No.141.

Group V : This group includes two gallium doped samples and the appropriate curves can be seen in figures 6.17 to 6.20. The curves of $\ln \sigma$ vs $1/T$ in figure 6.17 are not quite exponential. Nevertheless, at room temperature an activation energy of 0.37 eV was obtained for sample 140, while for sample No.112, with a better exponential behaviour, an activation energy of 0.42 eV was calculated. The mobility curves in figure 6.18 show that these two samples possess very small Hall mobilities, varying from just under 16 cm^2 V^{-1} s^{-1} for sample 140 to almost 65 cm^2 V^{-1} s^{-1} for sample No.112. The mobility of sample 112 varied in a curious way with temperature oscillating between maximum and minimum values of 59 and 24 cm^2 V^{-1} s^{-1}. On the other hand, the mobility of sample 140 increased steadily with temperature leading to a $\ln \mu_H$ vs $1/T$ plot with two different, almost exponential regions, with slopes of 33 meV in the low temperature range and 42 meV at higher temperatures. Finally, the free carrier concentrations are shown in figure 6.20. Here again, the plot for sample 140 shows some departure from a truly exponential behaviour but still giving an activation energy of 0.37 eV between 215 and 305 K, while a value of 0.41 eV was obtained for sample 112.

6.2.2 Measurements Under Bandgap Illumination

The electrical properties of all the samples in groups II to V were also measured with the specimen under illumination with bandgap radiation. The curves in figures 6.21 and 6.22 illustrate the observed variations of the Hall mobility and the carrier concentration under steady state conditions. The magnitudes of the mobilities and the temperature variations were relatively little affected by the illumination, with

FIG. 6·17   ELECTRICAL   CONDUCTIVITY   AS   A   FUNCTION   OF   RECIPROCAL
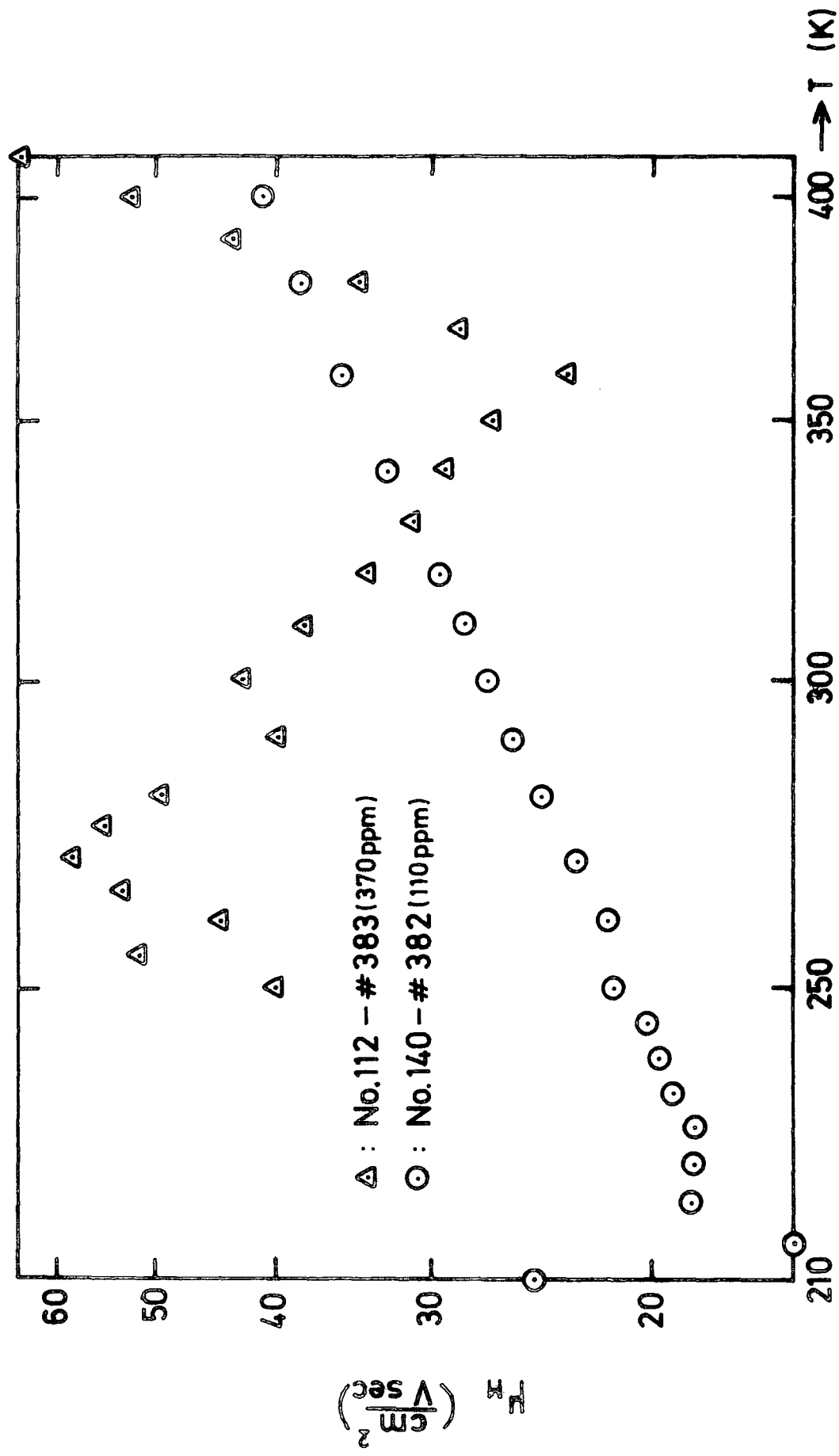TEMPERATURE   FOR   SOME   ZnSe : Ga   SAMPLES.

FIG. 6.18   HALL   MOBILITY   AS   A   FUNCTION   OF   TEMPERATURE   FOR
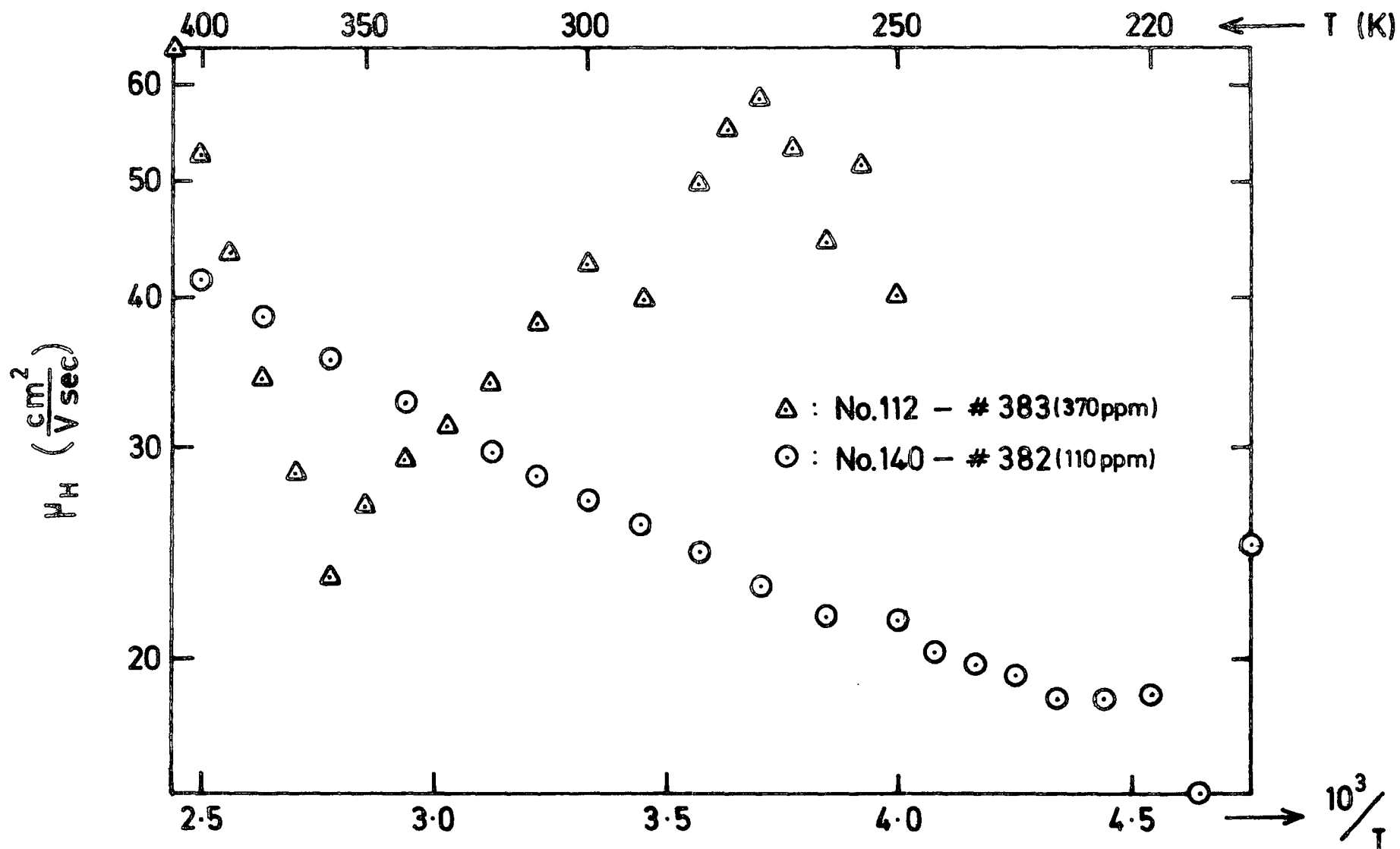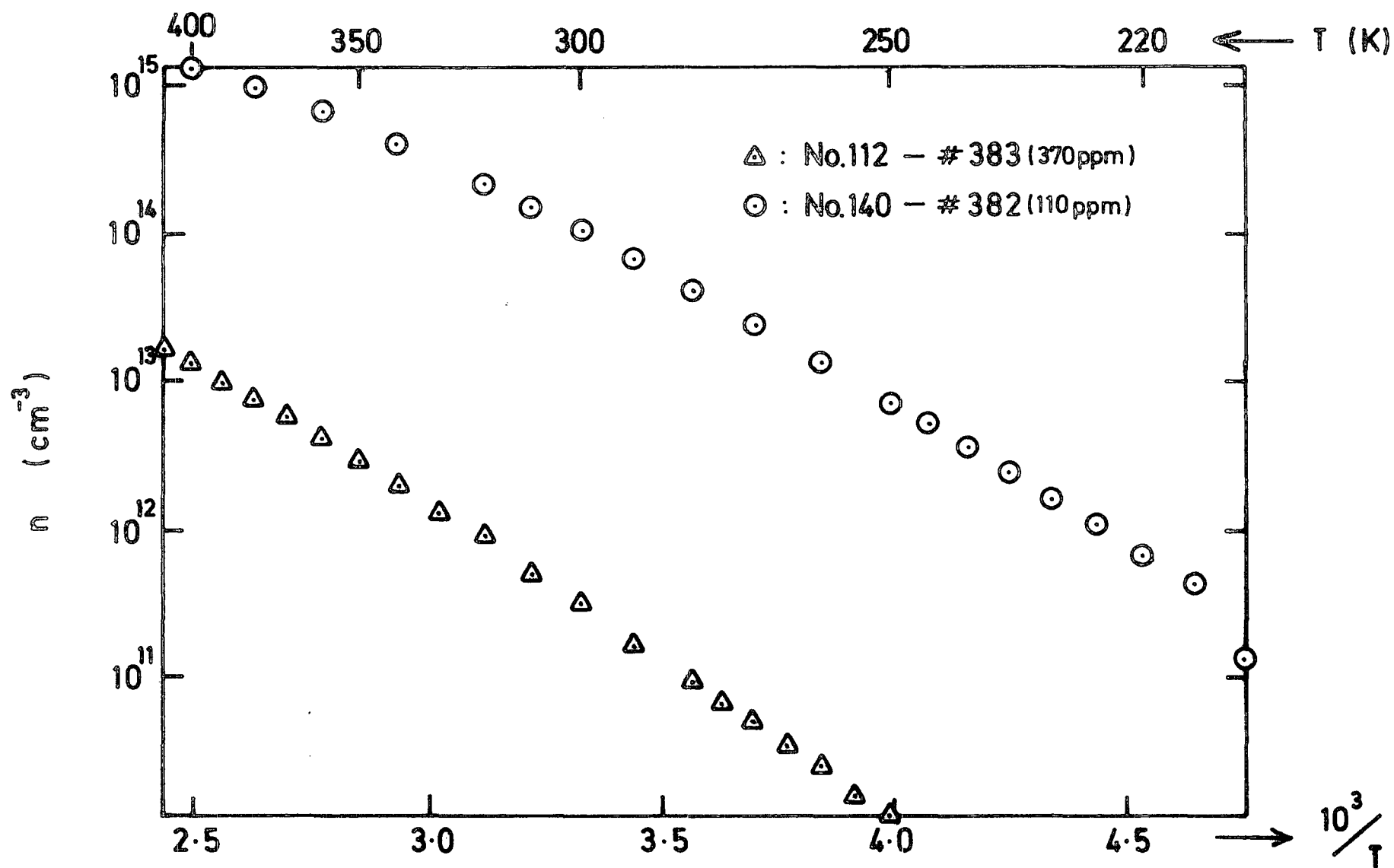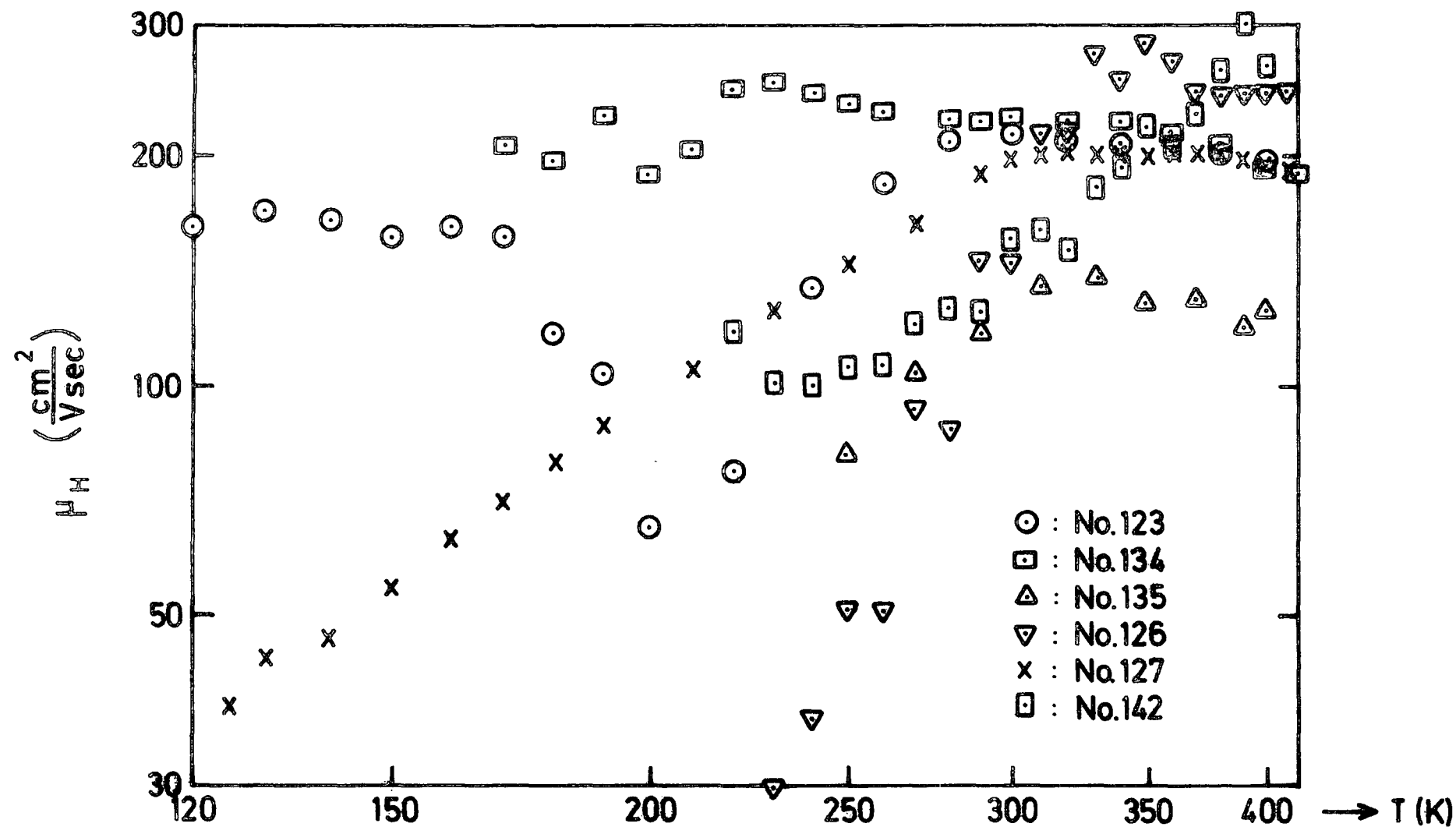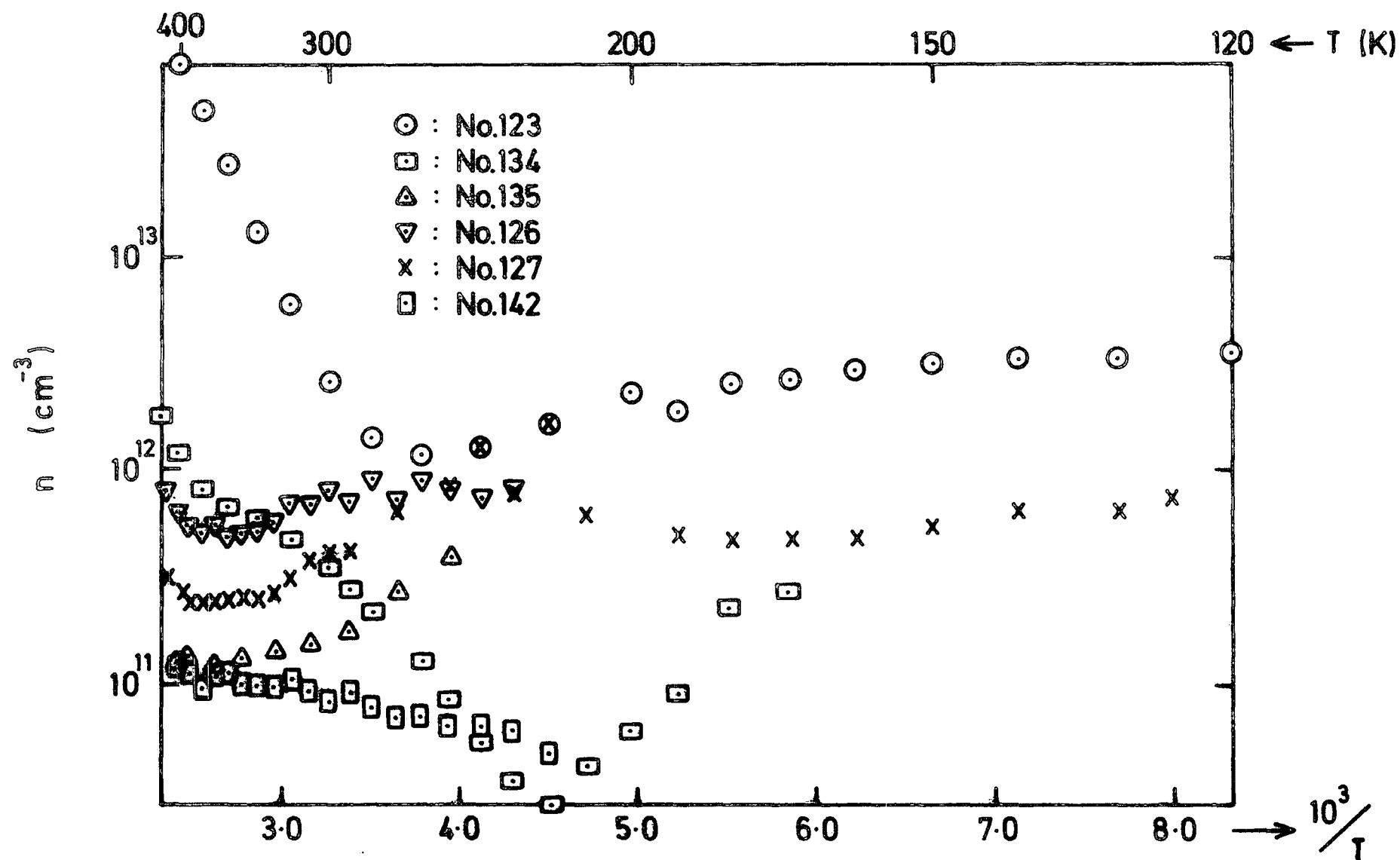SOME   ZnSe : Ga   SAMPLES.

FIG. 6·19   HALL   MOBILITY   AS   A   FUNCTION   OF   RECIPROCAL   TEMPERATURE
FOR   SOME   ZnSe : Ga   SAMPLES.

FIG. 6·20   CARRIER   CONCENTRATION   AS   A   FUNCTION   OF   RECIPROCAL   TEMPERATURE   FOR   SEVERAL   ZnSe : Ga   SAMPLES.

FIG. 6·21   HALL   MOBILITY   AS   A   FUNCTION   OF   TEMPERATURE   FOR
SOME   ZnSe : In   SAMPLES   UNDER   ILLUMINATION.

FIG. 6·22   CARRIER   CONCENTRATION   AS A FUNCTION OF RECIPROCAL
TEMPERATURE   FOR SOME   ZnSe : In SAMPLES   UNDER   ILLUMINATION.

values ranging from just under 30 $cm^2 V^{-1} s^{-1}$ for sample 126 to just under 300 $cm^2 V^{-1} s^{-1}$ for sample 142. On the other hand, the carrier concentrations, which were extremely dependent on light intensity, are presented merely to give some idea of the change which occurred under illumination. The values of n were almost constant with T but started to increase exponentially at high temperatures for some samples ; this was simply due to the dark conductivity taking over, indicating that such samples were poor photoconductors at these temperatures, especially sample No. 123 from boule ǂ 405, and,at higher temperatures, sample No.134 from boule ǂ 410.

6.2.3 Zinc Treated Crystals

The measurements on zinc treated crystals will be described in terms of two groups of heavily and lightly annealed samples. All specimens were zinc treated in vapour for three days.

The heavily annealed group included samples No.124 from boule ǂ 405, annealed at $700^{\circ}C$, sample 137 from boule ǂ 410, annealed at $850^{\circ}C$, and sample No.145 from boule ǂ 382 annealed at $700^{\circ}C$. The electrical properties of these samples are illustrated in figures 6.23 and 6.24. Sample No.137, which was annealed at the highest temperature, had a Hall mobility steadily decreasing from a maximum value of 520 $cm^2 V^{-1} s^{-1}$ at 120 K to about 250 $cm^2 V^{-1} s^{-1}$ at 400 K with a $T^{-0.9}$ variation over the higher temperature range. Sample 124 had an almost constant mobility of about 300 $cm^2 V^{-1} s^{-1}$ with a maximum of 310 $cm^2 V^{-1} s^{-1}$ near 190 K. The mobility of sample 145 was almost independent of temperature above 200 K with a value near 250 $cm^2 V^{-1} s^{-1}$, but decreased rapidly below this temperature, falling to just over 80 $cm^2 V^{-1} s^{-1}$ at 130 K. The carrier concentration curves in figure 6.24 show a weak temperature dependence from which activation energies between 13 meV and 25 meV were calculated.

The lightly annealed group of samples include No.116 from boule ǂ 349, No.133 from boule ǂ 408 and No.146 from boule ǂ 342 ; all
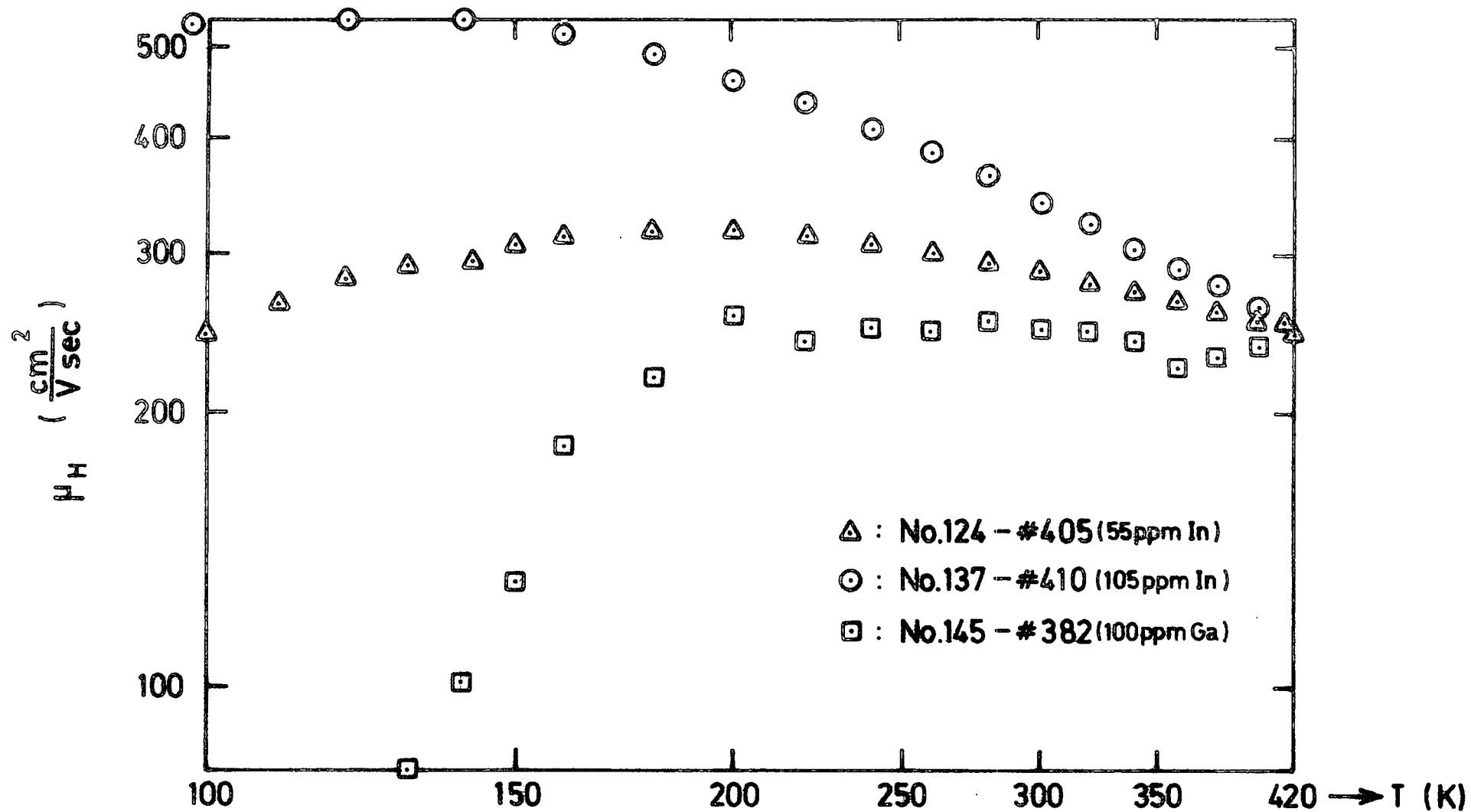
FIG. 6·23   HALL MOBILITY AS A FUNCTION OF TEMPERATURE FOR
SAMPLES FROM THE HEAVILY ANNEALED GROUP.
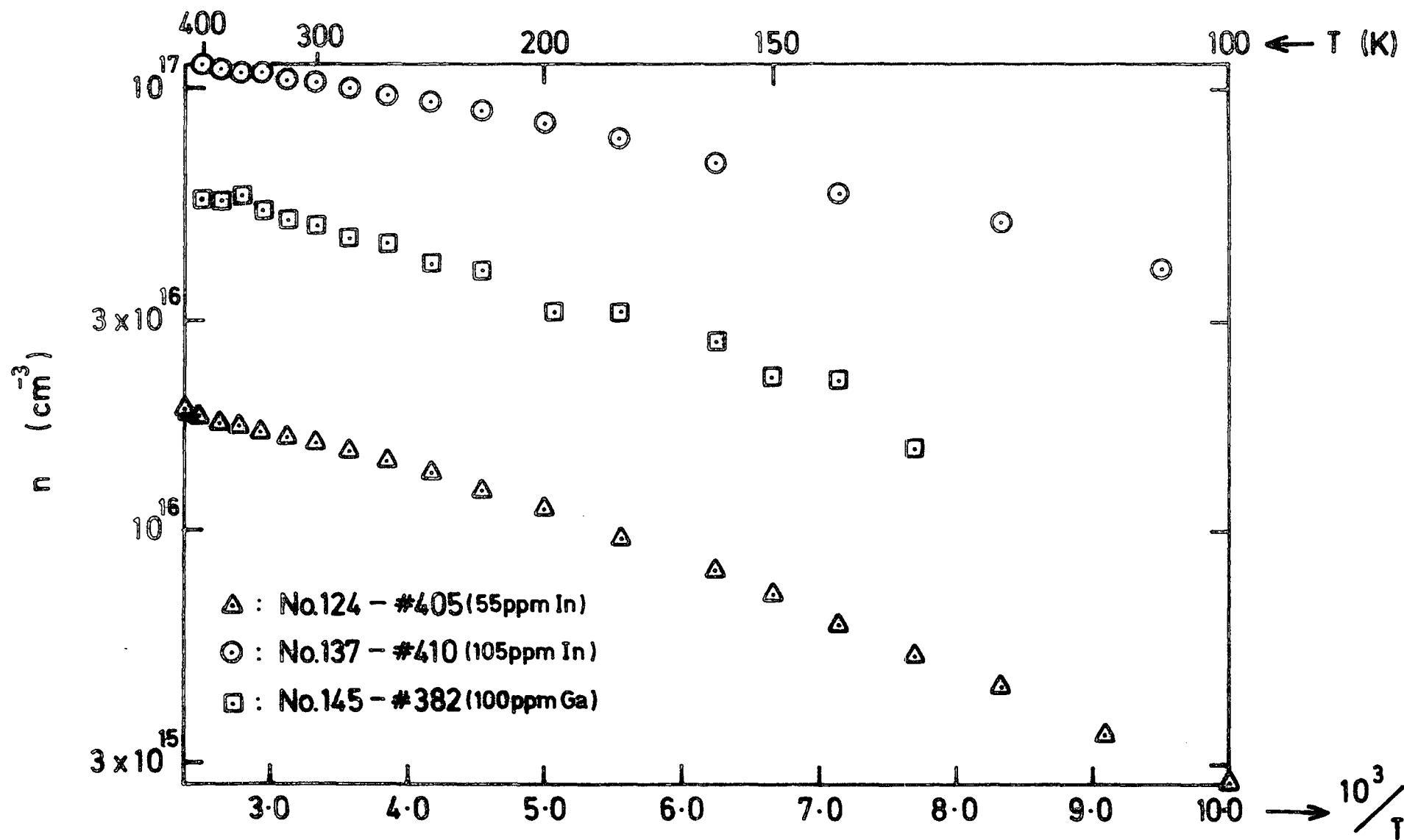
FIG. 6·24   CARRIER   CONCENTRATION   AS   A   FUNCTION   OF   RECIPROCAL
TEMPERATURE   FOR   SAMPLES   FROM   THE   HEAVILY
ANNEALED   GROUP

of which were heated in zinc vapour at 600° C. Their mobilities and carrier concentrations are shown in figures 6.25 and 6.26 respectively. The mobility of sample 146 was only weakly dependent on temperature above 300 K with a low value of about 30 cm^2 V^{-1} s^{-1} which decreased steadily to just under 10 cm^2 V^{-1} s^{-1} at 180 K. The mobility of the other two samples varied exponentially at lower temperatures, with mobility activation energies of 0.12 eV for each of them. In figure 6.26, where the plots of $\ln n$ versus $1/T$ are drawn, the curve for sample 146 seems to have two different slopes, i.e., 75 meV at the low temperature end, 0.14 eV at high temperatures. The carrier concentrations of the other two samples increased exponentially with $1/T$ with slopes of 0.41 eV for sample No.116 and 0.52 eV for sample No.133.

6.3 DISCUSSION OF RESULTS

In discussing the electrical measurements in the indium and gallium doped crystals we shall consider first of all the way in which the results fall into the general framework of the Meyer-Neldel rule. After this, the possible scattering mechanisms which might limit the electron mobility will be investigated. Finally, the free carrier concentration will be considered paying particular attention to the role of autocompensation.

6.3.1 The Meyer-Neldel Rule

One of the most interesting relationships in the field of electrical conduction is that known as the so-called Meyer-Neldel rule or compensation law. This rule is valid for both organic and inorganic substances and relates the magnitude of the conductivities and activation energies of particular groups of materials, as for example, in a group of samples containing different concentrations of impurity. The electrical conductivity of a semiconductor can be written $\sigma = \sigma_o \exp(-E_A/kT)$.

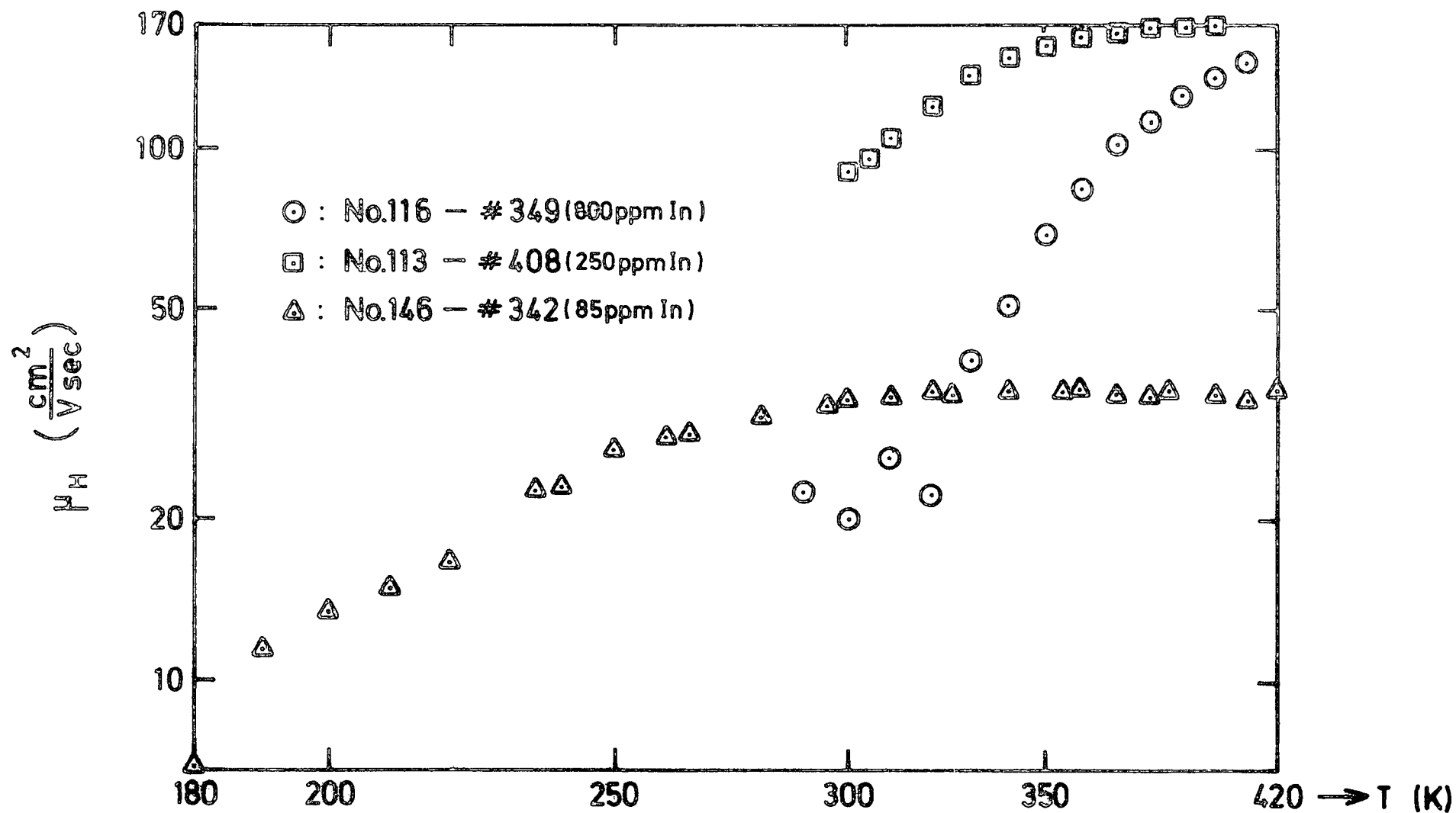The Meyer-Neldel rule, Meyer and Neldel (1937), Busch (1950), Mooser and

FIG. 6·25   HALL   MOBILITY   AS   A   FUNCTION   OF   TEMPERATURE   FOR
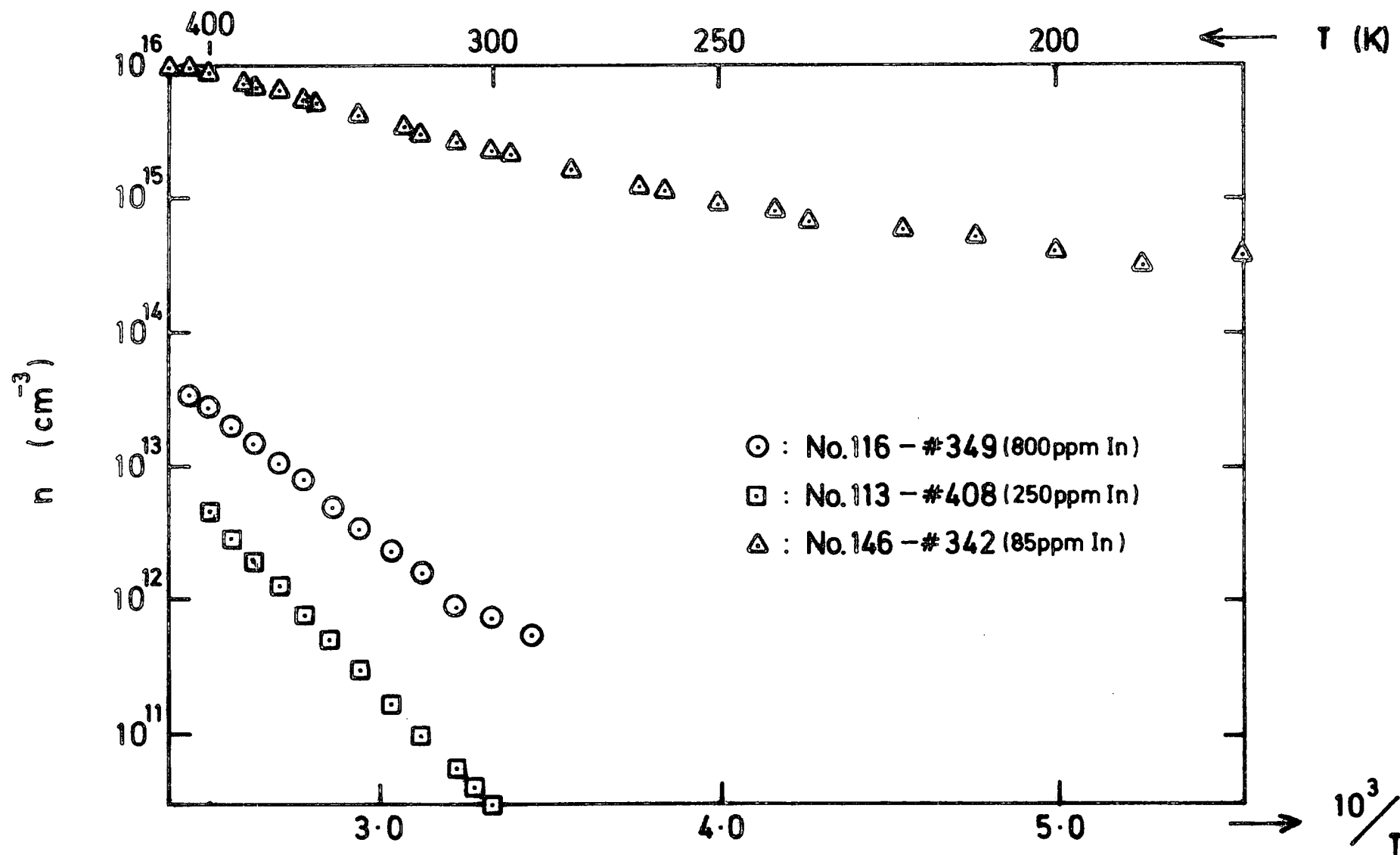SAMPLES   FROM   THE   LIGHTLY   ANNEALED   GROUP.

FIG. 6·26   CARRIER CONCENTRATION AS A FUNCTION OF RECIPROCAL
TEMPERATURE   FOR SAMPLES   FROM   THE   LIGHTLY
ANNEALED   GROUP.

Pearson (1960) and Weichman and Kužel (1970), also known as the compensation law, Gutmann and Lyons (1967), suggests that a correlation of the form

$$\ln \quad \sigma_O \quad = \quad \alpha \ E_A \ + \ \beta \tag{6.1}$$

exists between the activation energies E_A of the samples within the group and the pre-exponential factors σ_O. α and β are constants. If a set of semi-logarithmic plots of conductivity versus reciprocal temperature are drawn for the group of materials in question, then, according to the Meyer-Neldel rule, the straight lines, when extrapolated to higher temperatures, should all meet at $1/T = 0$ and $\sigma = \sigma_O$. As a refinement, Rosenberg et al (1968) proposed a three constant equation for the conductivity because their experimental plots, when extrapolated, intersected at a focal point at finite temperature $T = T_O$. They discussed their data in terms of an equation of the form,

$$\sigma(T) \ = \ \sigma_O{}' \ \exp \ (E_A/kT_O) \ \exp \ (-E_A/kT) \tag{6.2}$$

T_O is called the characteristic temperature. Equation 6.2 is equivalent to equation 6.1 if

$$\sigma_O{}' \ = \ \sigma_O \ \exp \ (-E_A/kT_O) \quad . \tag{6.3}$$

In figure 6.27 the plots of conductivity versus reciprocal temperature for several of the crystals studied in this work are shown in one diagram. If the resultant straight lines are divided in three groups, each group of lines, after extrapolating to higher temperatures, can be seen to intersect, within experimental error, at focal points all of which occur at the same temperature $T_O = 600$ K. The samples which were used to provide
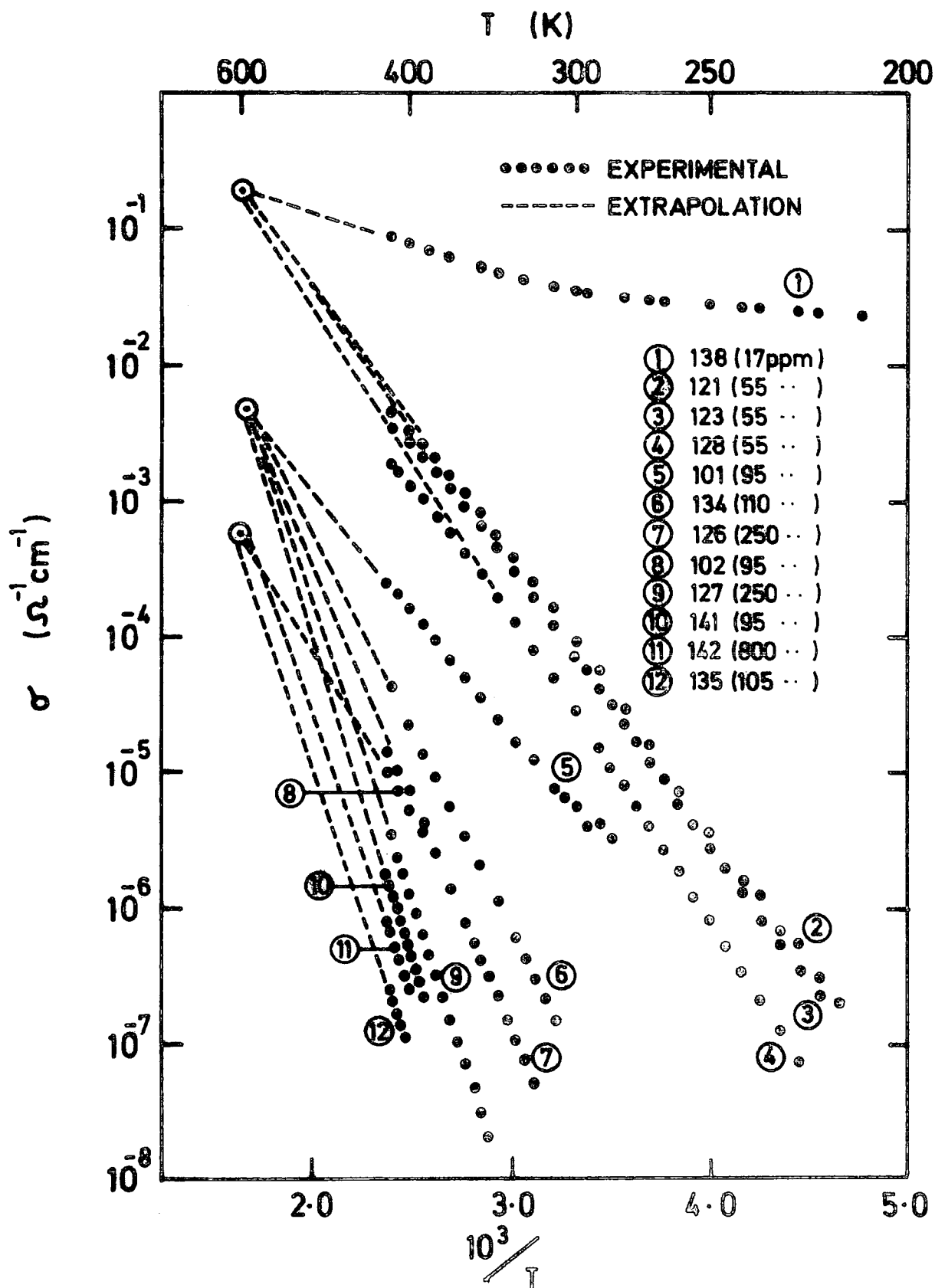
FIG. 6·27   A SET OF ℓn σ VERSUS ¹/ₜ CURVES
FOR ZnSe CRYSTALS WITH DIFFERENT
INDIUM CONCENTRATIONS.

the information given in this graph are those for which the Hall mobility did not vary appreciably over the temperature range considered here (see figures 6.2 ; 6.6 ; 6.10 and 6.14). It can be concluded therefore that the curves of figure 6.27 also represent the behaviour of the carrier concentration of these samples.

In figure 6.28, points are plotted showing how the pre-exponential factors of the various samples vary with E_A. Both the pre-exponential factor and E_A were calculated using linear regression technique on the data contained in figures 6.1, 6.5, 6.9, 6.13 and 6.17. It is apparent that the data for each group of samples defines a straight line, the slope and intercept of which is equal to $1/kT_o$ and σ_o' respectively. Since there are three lines, three values of T_o were determined and were found to lie within 1.5% of the average value of T_o = 600 K. We conclude, therefore, that our samples obey the Meyer-Neldel rule.

Various mechanisms have been proposed to account for the Meyer-Neldel rule. The first two were put forward by Roberts (1971). One mechanism is based on the so-called non-extrinsic (or pseudo-intrinsic) conduction process, introduced by Roberts and Schmidlin (1969), where the conduction current is considered to be controlled by a dominant level (donor for n-type semiconductor) supplying the majority carriers. Following the model depicted in the schematic band diagram of figure 6.29 where the subscripts m and q correspond to dominant electron and hole states, and assuming that Maxwell-Boltzmanns' statistics are a good approximation, the Fermi level is given by,

$$E_f = \frac{1}{2}(E_m + E_q) + \frac{1}{2}kT \ln(N_q/N_m), \qquad (6.4)$$

so that the electron concentration in the conduction band becomes,

$$n = N_c \left\{ \frac{N_q}{N_m} \right\}^{\frac{1}{2}} \exp\left[(E_c - E_m)/2\,kT + (E_c - E_q)/2\,kT \right]. \qquad (6.5)$$
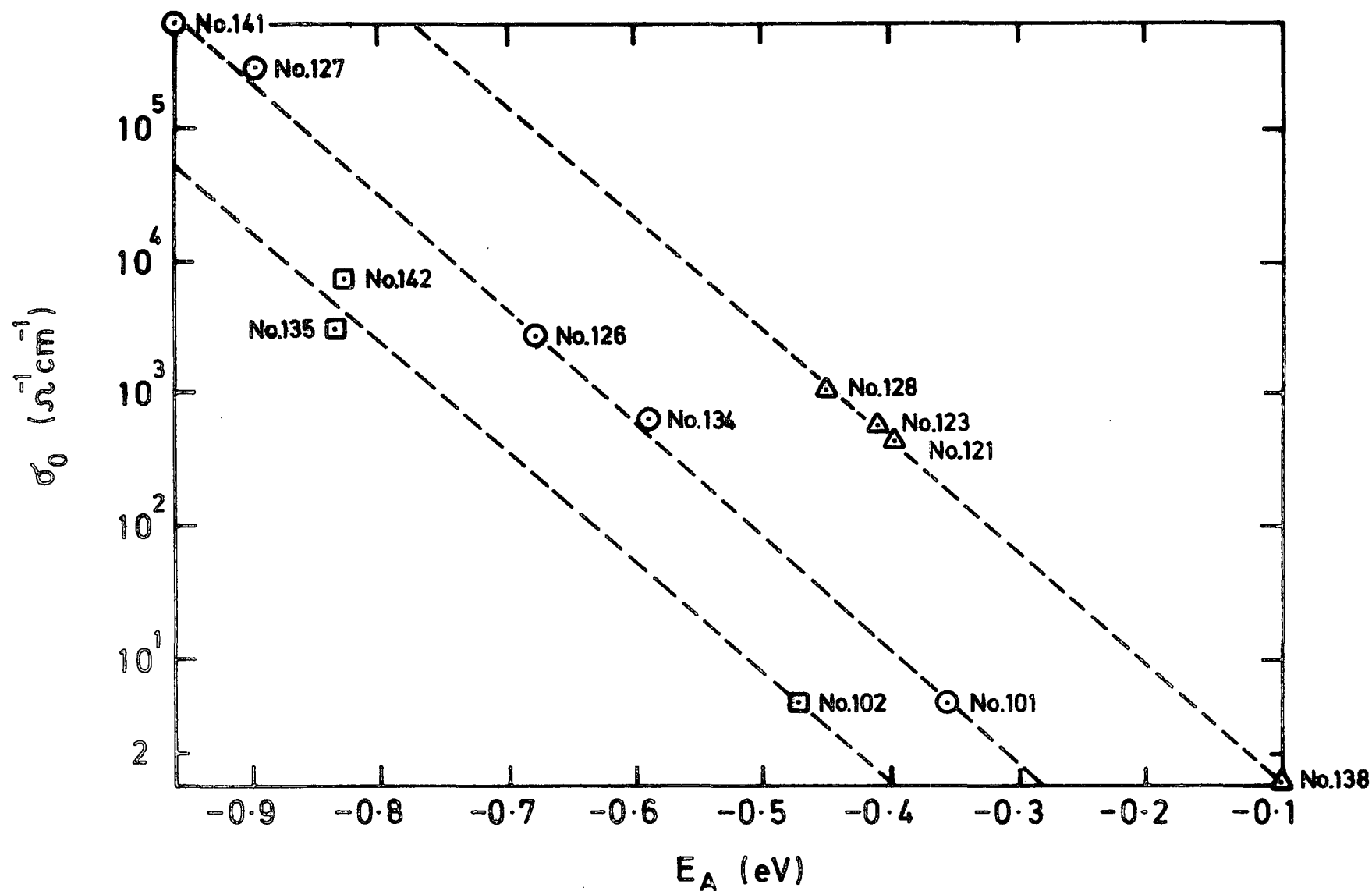
FIG. 6·28 PRE-EXPONENTIAL FACTORS AS A FUNCTION OF THE ACTIVATION ENERGY OBTAINED FROM THE CURVES SHOWN IN FIG. 6·27.

E_c

E_d

E_m

E_f

E_q
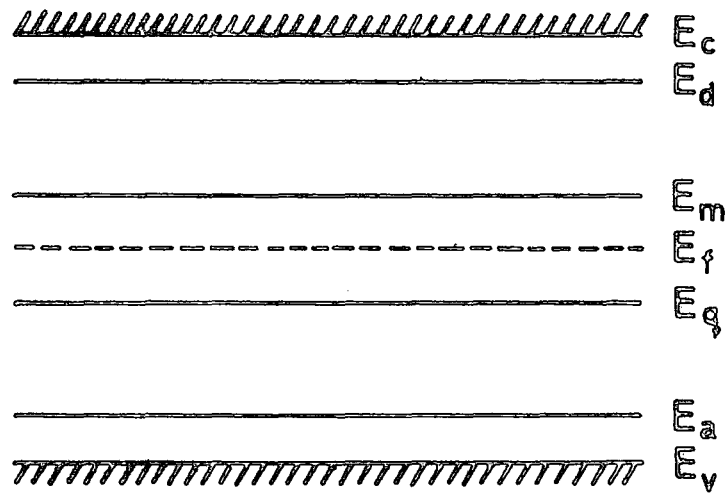
E_a

E_v

FIG. 6·29 SCHEMATIC ENERGY LEVEL DIAGRAM
FOR A SOLID IN WHICH THE DOMINANT
ELECTRON AND HOLE STATES ARE
LABELLED m AND q RESPECTIVELY.

Let us assume that we have an n-type semiconducting crystal with a dominant compensating level at a depth $E_c - E_{q_1}$ with a density N_{q_1} and let us also consider that by some process, another compensating level at $E_c - E_{q_2}$ with a density N_{q_2} takes over the dominant role. Furthermore, if we assume that the dominant donor level at $E_c - E_m$ with a density N_m does not change appreciably, then, by using equation 6.5 to find values of n with each of the two compensating levels, the two plots of $\ln n$ versus $1/T$ will intersect at $T = T_o$ where

$$N_{q_2}/N_{q_1} = \exp\left[(E_{q_2} - E_{q_1}) / k\, T_o \right] \qquad (6.6)$$

and, from this, $1/T_o$ will only be zero if $N_{q_2} = N_{q_1}$.

This idea of changing the compensating levels may also be used when there is a distribution of energy states within the bandgap. A substantial amount of experimental evidence suggests that distributed levels are to be expected in crystalline as well as in amorphous materials. In these latter, distributed trap levels and band tailing can arise associated with intrinsic disorder of the lattice, such as variations in the nearest neighbour distances. If, in the non-extrinsic conduction case, we consider the conduction band as the dominant electron level with its density of states falling off exponentially and tailing a finite distance towards the valence band, then let the Fermi level be controlled by some fixed dominant hole level. This can be expressed in the following way : For a continuous band varying exponentially with energy and extending between two energies E_c and E_m (here, E_m could represent the energy at which the conduction band states become localized), the number of free carriers is given by,

$$n = \int_{E_m}^{E_c} (N/k\, T_c)\, \exp\, (\varepsilon/k\, T_c)\, \exp\left[(E_f - \varepsilon)/kT \right] d\varepsilon \,. \qquad (6.7)$$

By extending the upper limit to infinity, this equation becomes,

$$n = \left[N'T/(T_c - T) \right] \exp \left[(E_f - E_m)/kT \right] \exp \left[(E_m - E_f)/k\ T_c \right]. \quad (6.8)$$

This is similar to equation 6.2 with $T_c \Rightarrow T_o$, which is the Meyer-Neldel rule. In equation 6.8, T_c describes the manner in which the concentration of states falls off with energy. Many amorphous chalcogenide semiconductors have a common σ_o and a focal point which occurs when T_o is infinite (see Davis and Mott, 1970), indicating that in materials of this kind the band states tail off uniformly in energy.

A second mechanism proposed by Roberts is that of thermally assisted tunnelling (T.A.T.). However, because it is important only to conduction processes in thin films, it will not be discussed here.

Finally, in a letter by Adler and Yoffa (1976) the differences between the properties of two classes of amorphous semiconductors (i.e amorphous solids and chalcogenide glasses) were considered. The amorphous solids have a positive effective electronic correlation energy (Hubbard, 1963) , U, while the glasses have a negative one. Amorphous materials with positive U have an n-type thermopower, variable range hopping at low temperatures, show an EPR signal and have a Fermi energy which can be moved by varying the electron density. In contrast to this, chalcogenide glasses generally have p-type thermopower, do not exhibit variable-range hopping, do not show an EPR signal and have a Fermi energy which does not vary much with electronic density. From a series of calculations using the Maxwell-Boltzmann approximation, Adler and Yoffa obtained an equation for the Fermi energy as a function of electronic concentration and temperature

$$E_f = E_s - kT\ \ell n \left\{ \left| \frac{1}{n_v} - 1 \right| + \left[\left| \frac{1}{n_v} - 1 \right|^2 + \left| \frac{2}{n_v} - 1 \right| e^{U/kT} \right]^{\frac{1}{2}} \right\} \quad (6.9)$$

where n_v represents the average number of electrons per defect site, E_s is

the energy location of the defect, and U, the correlation energy, represents

the effective electrostatic attraction that exists when two electrons (one

of each spin) are simultaneously present in the vicinity of the same defect

(i.e, the Hubbard U). This equation has also been obtained recently by

Roberts et al (1980) from a theoretical analysis of multivalent centres.

Using equation 6.9, two different variations of E_f versus n_v are obtained,

depending on the sign of the effective correlation energy U ; see figure

6.30. In figure 6.30(a), for U >O, there is a rapid variation of the Fermi

energy in the vicinity of n_v = 1, while no such behaviour occurs for U <O,

see figure 6.30 (b). Banda and Roberts (1980) showed that if computed curves

of $\ln \sigma$ versus 1/T are plotted using the values of E_f from figure 6.30 (a),

a series of straight lines converging to a focal point are obtained. This

model may be considered then as a third mechanism to explain the Meyer-Neldel

rule.

It is expected that in most semiconductors, U will always be

positive, however, a negative effective correlation energy was postulated

to exist in chalcogenide glasses because these might contain a type of

defect for which it is energetically favourable to put two electrons, due

to the existence of localized states in the gap, appearing as dangling

bonds (see Street and Mott, 1975,and Mott et al, 1975) . The idea that

these localized states may possess a negative U was first suggested by

Anderson (1975) to account for the diamagnetic properties of these glasses.

Thus we conclude that either of the two mechanisms, i.e. the

pseudo-intrinsic conduction model with its extension to semiconductors

exhibiting some band tailing, and the last model which considers the

concept of the correlation energy U, may be used to explain the d.c.

conductivity of our crystals. The possibility exists therefore that heavily

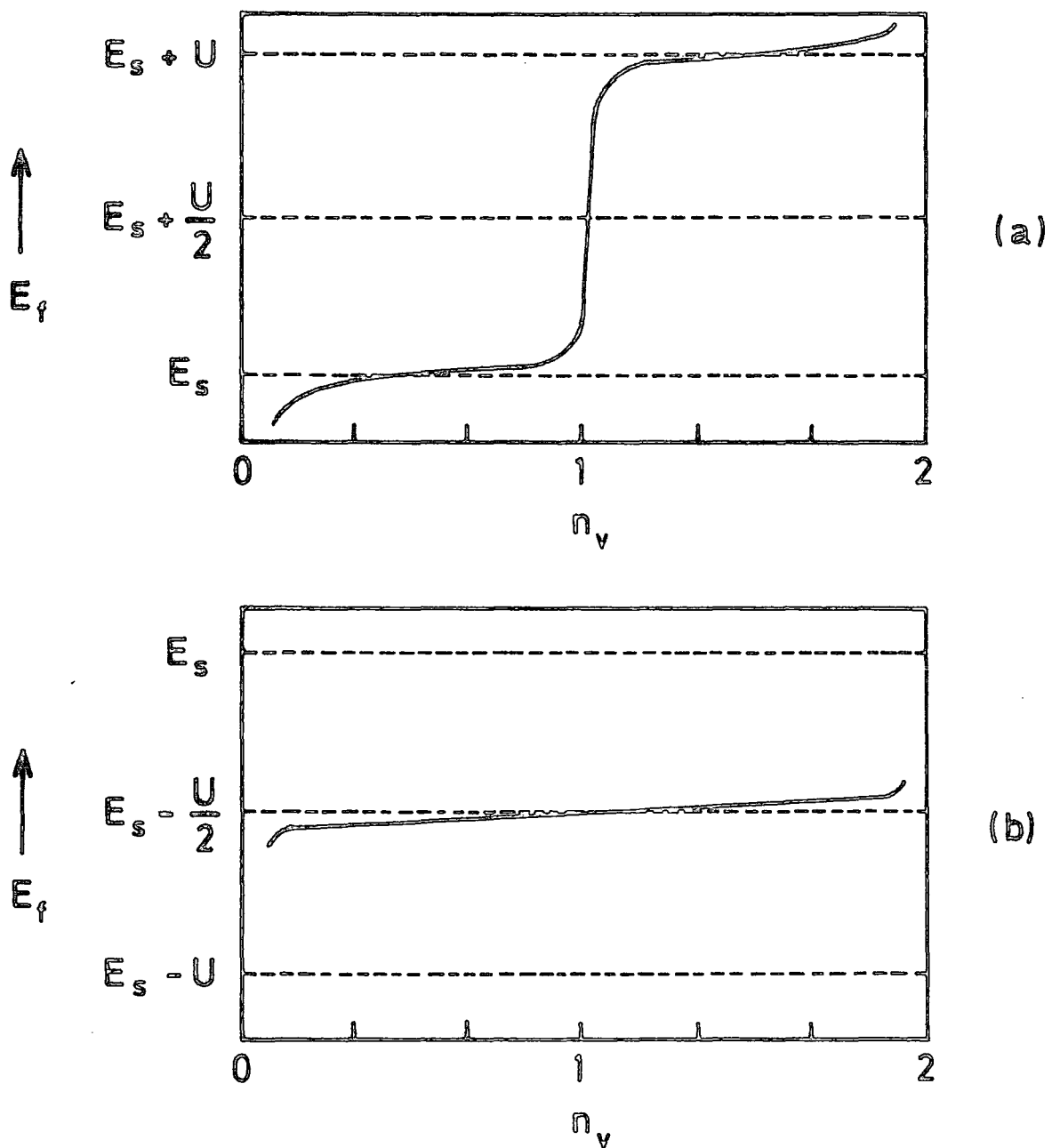doped ZnSe:In might show some of the characteristics of amorphous solids.

FIG. 6·30   FERMI   ENERGY   AS   A   FUNCTION   OF
ELECTRON   DENSITY   PER   DEFECT   AT
LOW   TEMPERATURE , $kT \ll U$.
(a) POSITIVE CORRELATION   ENERGY , U
(b) NEGATIVE CORRELATION   ENERGY ,– U

To illustrate how the two models observed here can be employed to explain the behaviour of our samples, we take as one example the well known copper compensating defect with two levels. As discussed in the previous chapter, substitutional copper may exist in ZnSe in two forms, namely as Cu_{Zn}^{x} and $Cu_{Zn}^{'}$ (i.e. as neutral and singly charged acceptors respectively), with the latter having an extra electron and which will therefore correspond to a level situated higher in the energy gap. The energy difference between the two levels will then be the positive effective correlation energy, U, with a value, after Stringfellow and Bube (1968) of 0.72 - 0.35 = 0.37 eV. On the other hand, this same example can also illustrate the case of a set of acceptor levels active in the pseudo-intrinsic conduction condition where we consider that one dominant donor level is compensated by these two copper and possibly other acceptor levels, such as doubly and singly ionized zinc vacancies (or some of the other acceptor levels that will be described in section 6.3.3) where each acceptor in turn could act as the dominant level. Hence, by using equation 6.5 for each in turn, a set of straight lines with different activation energies would be obtained when a semilogarithmic plot of n (or σ) against reciprocal of temperature was made.

6.3.2 Hall Mobility

6.3.2.1 As-grown samples

In order to obtain some idea about the operative scattering mechanism, it is necessary to know the behaviour of the mobility with tempera-ture. The average Hall mobility for all the as-grown samples at temperatures just above room temperature is of the order of 150 cm^2 V^{-1} s^{-1} and is very close to the values already reported in the literature for ZnSe:In or ZnSe:Ga crystals, by Jones and Woods (1976) and Sethi et al (1978a, 1979). This value,however,is substantially less than the best value, in the region between 500 to 600 cm^2 V^{-1} s^{-1} , observed in undoped material by Aven (1971)

Jones and Woods (1976) and Emelyanenko et al (1979).

To understand what kind of scattering or combination of scattering processes limits the mobility of the carriers in indium and gallium doped material, it is necessary to estimate the mobilities which would have resulted if only one of the possible carrier scattering mechanisms, which were described in chapter two, had been operative. The values obtained and their temperature variation is then compared with the experimental data.

(A) Lattice scattering : There are three contributions to lattice scattering, (1) deformation potential scattering, also known as acoustic mode phonon scattering (this is scattering at a potential developed as a result of local deformation in the lattice), (2) polar scattering also known as optical phonon scattering (where the electrons interact with longitudinal optical phonons) and (3) piezoelectric scattering (which is the interaction of electrons with the polarization associated with small wavevector acoustic phonons).

Acoustic mode scattering : The electron mobility limited by acoustic mode scattering can be calculated from

$$\mu_A = 3 \times 10^{-5} \rho \, C_L^2 \left[\epsilon_1^2 \, (m^*/m_e)^{5/2} \, T^{3/2} \right]^{-1} \quad cm^2 V^{-1} s^{-1}. \quad (6.10)$$

The values of the relevant parameters are :

$$\rho C_L^2 = 1.06 \times 10^{12} \text{ dynes cm}^{-2} \quad \text{(after Aven and Segall, 1963)}$$

$$\epsilon_1 = 4 \text{ eV} \quad \text{(after Aven and Segall, 1963)}$$

$$m^* = 0.17 \, m_e \quad \text{(after Marple, 1964)}.$$

However, some controversy seems to exist in the recent literature on the value of the deformation potential ϵ_1. Sethi et al (1977) obtained

a value of 5.2 eV calculated from the Hall mobility data on a ZnSe crystal heavily annealed in molten zinc, while Shmelev and Tsurkan (1979) using the same experimental data as Sethi et al, obtained a value of 15 eV. Nevertheless, if we take both extreme values, the following two equations for the acoustic phonon scattering are obtained,

$$\mu_A = 1.74 \times 10^8 \; T^{-3/2} \; cm^2 \; V^{-1} \; s^{-1} \text{ for } \epsilon_1 = 4 \text{ eV}$$

$$\mu_A = 1.24 \times 10^7 \; T^{-3/2} \; cm^2 \; V^{-1} \; s^{-1} \text{ for } \epsilon_1 = 15 \text{ eV},$$

giving values, at 300 K, of 3.4×10^4 and $2.4 \times 10^3 \; cm^2 \; V^{-1} \; s^{-1}$ respectively, each of which of course is well over the maximum experimental value obtained in this work.

Polar mode scattering :

$$\mu_{OPT} = \left[0.87 \; (m_e/m^*) \Big/ \alpha h \omega_\ell \right] (e^z - 1) \; z^{-\frac{1}{2}} \; \psi_z \; cm^2 \; V^{-1} \; s^{-1} \, . \tag{6.11}$$

One of the important parameters for the evaluation of the mobility limited by this scattering process is the polaron coupling factor α ; here again, some controversy exists about its correct value. Jones and Woods (1976) obtained a value of 0.54 while Sethi et al (1977) used 0.57 and Shmelev and Tsurkan (1979) 0.432. However, we shall use the value of 0.54 for this parameter, as well as the values employed by Jones and Woods for the other constants ; then, equation 6.11 for polar mode scattering simplifies to,

$$\mu_{OPT} = 300 \; \psi_z \; (e^z - 1) \; z^{-1/2} \; cm^2 \; V^{-1} \; s^{-1},$$

where $Z = h\omega_\ell/kT = \Theta_D/T = 364 \text{ K}/T$.

Values very close to the experimental ones are obtained with this equation, i.e. of the order of about 400 $cm^2 \; V^{-1} \; s^{-1}$ at room temperature, however,

the equation predicts a mobility decreasing with increasing temperature, which does not correspond with the behaviour of the samples investigated here.

Piezoelectric scattering :

$$\mu_{PZ} = 1.05 \, \rho \, c_L^2 \, \epsilon_s \left[c^2 \, (m^*/m_e)^{3/2} \, T^{\frac{1}{2}} \right]^{-1} \quad cm^2 \, V^{-1} \, s^{-1} \quad . \quad (6.12)$$

Taking values of 9.1 and 1.5×10^4 stat-coul cm^{-2} for ϵ_s and C respectively (see Berlincourt et al, 1963) , the formula 6.12 giving the mobility limited by this scattering mechanism reduces to,

$$\mu_{PZ} = 5.8 \times 10^6 \, T^{-\frac{1}{2}} \quad cm^2 \, V^{-1} \, s^{-1} \quad .$$

The values of μ obtained with this equation are all much too large, i.e. of the order of $10^4 \, cm^2 \, V^{-1} \, s^{-1}$, hence this process can be completely ignored.

(B) Impurity scattering : There are two contributions to this type of scattering : (1) scattering by ionized impurities (interaction of electrons with charged centres in the lattice) and (2) scattering by neutral impurities (analogous to electron scattering by a hydrogen atom). Ionized impurity scattering gives a mobility

$$\mu_I = \frac{2^{7/2} \, \epsilon_s^2 \, (kT)^{3/2}}{\pi^{3/2} \, e^3 \, m^{*\frac{1}{2}} \, N_I} \left[\ln \frac{6 \, m^* \, \epsilon_s \, (kT)^2}{e^2 \, \pi \, h^2 \, n' \, (2 - \frac{n'}{N})} \right]^{-1} . \quad (6.13)$$

If the relevant constants are substituted in this, the Brooks-Herring formula, the following equation is obtained.

$$\mu_I = 6.1 \times 10^{17} \, \frac{T^{3/2}}{N_I} \left[\ln 1.94 \times 10^{14} \, \frac{T^2}{n' \, (2 - \frac{n'}{N})} \right]^{-1} \quad .$$

In this formula, N_I represents the number of ionized imperfections per unit volume, and in the presence of both ionized donors and ionized acceptors, it must be replaced by the total number of them weighted with the appropriate charge ; n' is the total number of free carriers per unit volume and N is replaced by the absolute value of N_D-N_A. The difficulty here resides in estimating the value of N_I which in addition to added impurities may include contributions from native defects. However, the measurements of carrier concentration demonstrate that these crystals are very strongly compensated, hence, it is possible to limit the possible value of N_I to the range between 50 and 90% of the N_D + N_A which in turn will be taken as to be of the same order of the dopant concentration, assuming the number of native defects to be small. Thus, if we take as typical the results from samples from boules ╫ 407 and ╫ 405 (at room temperature), and from samples from boules ╫ 407, ╫ 405 and ╫ 349 (at 400 K) doped with about 10 ppm, 55 ppm and 800 ppm respectively, then,

at 300 K,

sample No.132 has $\eta \approx 6 \times 10^{15}$ cm^{-3}, giving

$$\mu_I = 1.6 \times 10^3 \text{ to } 2.8 \times 10^3 \text{ cm}^2 \text{ V}^{-1} \text{ s}^{-1};$$

sample No.121 has $\eta \approx 6 \times 10^{12}$ cm^{-3}, giving

$$\mu_I = 186 \text{ to } 319 \text{ cm}^2 \text{ V}^{-1} \text{ s}^{-1};$$

at 410 K,

sample No. 132 has $\eta \approx 7 \times 10^{15}$ cm^{-3}, giving

$$\mu_I = 2.4 \times 10^3 \text{ to } 4.3 \times 10^3 \text{ cm}^2 \text{ V}^{-1} \text{ s}^{-1},$$

sample No. 121 has $\eta \approx 3 \times 10^{14}$ cm^{-3}, giving

$$\mu_I = 386 \text{ to } 663 \text{ cm}^2 \text{ V}^{-1} \text{ s}^{-1} \text{ and,}$$

sample No. 142
which has $\eta \approx 3 \times 10^{10}$ cm^{-3}, giving

$$\mu_I = 14 \text{ to } 25 \text{ cm}^2 \text{ V}^{-1} \text{ s}^{-1}.$$

These results demonstrate that the mobility limited by this mechanism

depends strongly on the number of ionized impurities present in the material. The calculated mobilities are not too different from the experimental Hall values and thus this mechanism cannot be discounted. Also, this scattering mechanism does predict an increase of carrier mobility with temperature and, such an effect is observed in most of the samples so that this scattering process may well be playing a dominant role.

Neutral impurity scattering :

According to the equation proposed by Erginsoy (1950), the mobility limited by neutral defects is given by,

$$\mu_N = m^* e^3 / 20 \, N \, \varepsilon_s \, \hbar^3 \, . \qquad (6.14)$$

This equation demonstrates that this mechanism is independent of temperature. The effect of course is that the mobility is reduced if there is a significant concentration of neutral impurities.

The two impurity scattering mechanisms described here are usually of importance, in relatively pure crystalline semiconductors, at temperatures below about 150 K, where a typical $T^{3/2}$ dependence of the mobility is usually encountered. As Jones and Woods (1976) pointed out, the carrier mobility for the indium doped crystals is very low and the fact that most of them showed a mobility increasing with temperature, even at and above 300 K, suggests that their behaviour cannot be simply explained in terms of ionized impurity scattering. It is more likely that a combination of polar mode scattering with ionized and neutral impurity scattering explains the quasi-temperature independence behaviour of the Hall mobility for most of the crystals. These mechanisms would result in a carrier mobility limited by a usual combination of the form,

$$1/\mu = 1/\mu_{OPT} + 1/\mu_I + 1/\mu_N \, .$$

The temperature independence of any neutral impurity scattering will reduce the $T^{3/2}$ dependence from the ionized impurity scattering.

One reason why impurity scattering is so important may be associated with the difference between the concentration of dopant introduced, which was of the order of 10^{18} to 10^{19} atoms of indium or gallium per cm^3, and the actual free carrier concentration, many orders of magnitude less, which suggests either a high degree of compensation or the formation of neutral impurities which do not contribute to the electrical conduction, or both. This would lead to a net reduction in the mobility when more dopant was added as explained by the results quoted above when the Brooks-Herring formula was used. However, a plot of Hall mobility versus added dopant concentration at a fixed temperature, figure 6.31, shows that the absolute mobility increased with the concentration of indium or gallium in the crystals. This contradicts the explanation just given, but, according to equation 6.14, 1000 ppm of neutral impurities would be needed in ZnSe to limit μ_H to values below 300 $cm^2 V^{-1} s^{-1}$ (see Jones and Woods, 1976) . If this mechanism is to be important,therefore, a large concentration of foreign neutral impurities is required together with the possible presence of electrically inactive indium or gallium, since the group III atoms alone cannot account for that much reduction.

However, if about 500 ppm of neutral impurities were present, by combining their effects with ionized impurity and polar mode scattering, the following values for sample No.121 would be obtained,

μ (@ 250 K) $\simeq$ 90 $cm^2 V^{-1} s^{-1}$,

μ (@ 300 K) $\simeq$ 105 $cm^2 V^{-1} s^{-1}$ and,

μ (@ 400 K) $\simeq$ 140 $cm^2 V^{-1} s^{-1}$,

which seems to give reasonable agreement with the curve in figure 6.6 for this sample. Nevertheless, for most of the other samples, the discrepancy is much larger, indicating that the analysis is more complicated than has been assumed here.
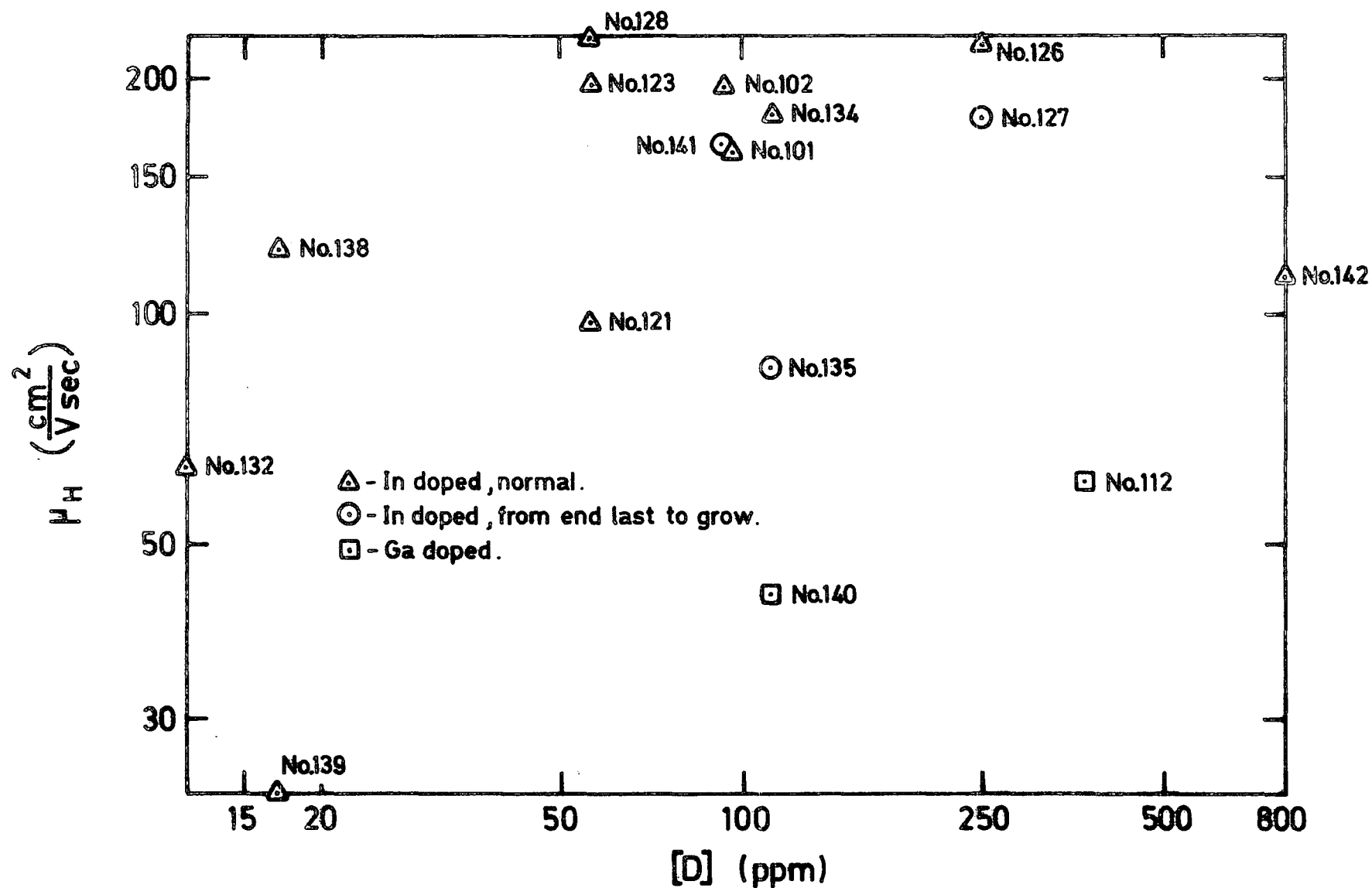
FIG. 6·31 HALL MOBILITY AT 410 K AS A FUNCTION OF THE DOPANT CONCENTRATION FOR VARIOUS ZnSe CRYSTALS CONTAINING In OR Ga.

The situation under constant illumination, figure 6.21, is not clear at all. Still, the Hall mobility does not seem to change much when the sample is illuminated with bandgap radiation, since the maximum values, which occur in the higher temperature region, are of the order of $250 \text{ cm}^2 \text{ V}^{-1} \text{ s}^{-1}$.

6.3.2.2 Annealed specimens

With the samples treated in zinc vapour, the behaviour of the Hall mobility depended strongly on the annealing temperature. The experimental results are shown in figures 6.23 and 6.25 and exhibit a gradual change in the possible limiting scattering mechanism, where we start with a combination of polar mode and impurity scattering in the heavily doped, lightly annealed sample 116 in figure 6.25, and end up with the combination of the same type of lattice scattering but with a "weaker" impurity scattering for the sample treated in zinc at the highest temperature (No.137 in figure 6.23). It is then obvious that the zinc treatment eliminates much of the impurity scattering contribution. It does this by segregating the impurities.

The scattering mechanism involved in n-type ZnSe crystals purified by the zinc extraction process has been the subject of several papers. Fukuda and Fukai (1967) and Aven (1971) suggest a combination of polar optical scattering and ionized impurity scattering with some contribution from neutral impurity and dipole scattering ; no quantitative estimates for the last two effects was given. In a short qualitative discussion it was suggested that the treatment in molten zinc diffused in some oppositely charged defects onto the nearest or next-nearest neighbour sites, where they could help scatter the carriers as dipoles. Recently, Emelyanenko et al (1979) rejected this explanation and fitted their experimental data using a different approach to the Brooks-Herring formula, combined with neutral impurity and polar mode scattering. Jones and Woods (1976) also measured the Hall mobility on undoped ZnSe heated in molten zinc and

concluded that the mobility was limited by the combination of ionized impurity and polar optical scattering down to about 50 K. They suggested that impurity band conduction occurred below this temperature, to account for the rapid decrease of the Hall mobility on cooling even further.

More recently, some further work has been done on the Hall mobility of zinc treated crystals containing group III dopants. Nedeoglo (1977) obtained a set of Hall mobility curves for gallium doped ZnSe crystals annealed in liquid zinc at 960° C and was able to fit one of his experimental curves to a combination of five mobility limiting processes, namely, (1) scattering by acoustic phonons, (2) scattering by optical phonons, (3) ionized impurity scattering, (4) dipole scattering and (5) neutral impurity scattering. He also obtained a sharp decrease in μ_H below 30 K and, by assuming different sets of impurities, associated this behaviour to a transition to conduction through the impurities which would lead to a lower mobility. Sethi et al (1978b) compared Hall mobility measurements on as-grown indium doped ZnSe and on indium doped ZnSe annealed in molten zinc and also found a change from an exponential behaviour in the as-grown material to a temperature variation more usually associated with lattice scattering, after the zinc treatment, with indications that the sample was still impure and the contribution of ionized impurity scattering was quite significant.

Finally, for completeness in discussing the mobility of zinc treated material, it is of interest to mention some work by Ray and Kröger (1979) on ZnSe:Al and ZnSe:As in equilibrium with atmospheres of known zinc vapour at temperatures between 800 K and 1000 K. After calculating the theoretical values of the mobility using several of the limiting processes and obtaining very reasonable agreement with their experimental Hall mobilities, they concluded that ionized impurity scattering plays an important part in ZnSe at dopant concentrations "as low" as 5×10^{17} cm^{-3}.

In conclusion, it seems clear that the effects of heating indium doped material in zinc are to reduce both impurity scattering processes. Hence, by increasing the temperature of the treatment in zinc vapour, the mobility will be transformed to a situation controlled by combination of ionized impurity and polar mode scattering, with some of the samples exhibiting conduction via an impurity band as determined by the exponential variation of their mobilities. Finally, the simple most important process would appear to be ionized impurity scattering which is present at even to temperatures around 700° C (Ray and Kröger, 1979 , and Emelyanenko et al, 1979) .

6.3.2.3 Impurity band conduction

Returning to as-grown crystals, the possibility that impurity band conduction occurs in ZnSe heavily doped with indium or gallium has been considered by several authors. Jones and Woods (1976) proposed this process to explain the sharp decrease in the mobility below 50 K in undoped ZnSe annealed in molten zinc. Nedeoglo (1977) suggested the same model for the same behaviour in gallium doped material annealed in molten zinc.

However, in a recent group of publications by Sethi et al (1978a, 1979) and Mathur et al (1979a, 1979b), it is claimed that impurity band conduction explains satisfactorily the anomalous behaviour of heavily indium doped ZnSe at temperatures as high as room temperature, even though it is generally accepted that this type of conduction is only dominant at low temperatures when conduction via the conduction band is very small. This usually applies when T <100 K. From a systematic study of ZnSe crystals containing different amounts of indium, they found all the typical behaviour associated with impurity band conduction. Firstly, they mentioned the important feature of the Hall mobility increasing exponentially with temperature near room temperature, and they obtained values for the mobility activation energy E_{μ} from three samples ranging from 28 to 97 meV.

In the present work, the curves of $\ln \mu_H$ versus $1/T$, plotted in figures 6.3 ; 6.7 ; 6.11 ; 6.15 and 6.19, reveal that only two of the sixteen samples showed a strong and well defined exponential behaviour, (see figure 6.3). These two were the most lightly doped crystals, i.e. No. 132 and 139 from boules ╫ 407 and ╫╫ 413 respectively, with about 12 and 17 ppm of indium, where the donor concentrations were in the region of 10^{17} cm^{-3} which is close to the limit, according to Nedeoglo (1977), for impurity band formation using Mott's criterion.

The values of E_μ for the two samples used to provide the results of figure 6.3 were 0.33 and 0.36 eV respectively, in the range 260-350 K. A few of the curves for some of the other crystals showed some exponential behaviour in different temperature ranges, these are listed in table 6.2. However, it should be emphasized that these exponential variations are very weak and more probably, as suggested earlier, can be attributed to the combined effects of lattice and ionized impurity scattering, flattened by neutral impurity scattering. Nevertheless, the fact remains that samples No.132 and 139 did behave as if the electrical conduction took place via an impurity band and this would certainly explain the relatively low values of their Hall mobilities.

The second feature pointed out by Sethi et al (1979), is the fact that the conductivity and Hall mobility curves for their samples showed two different slopes, indicative of two impurity bands. Furthermore, after some thermoelectric power measurements down to liquid nitrogen temperature, they found n-type conduction at high temperatures changing to p-type at low temperatures, confirming the suggested existence of two impurity bands. One of these, they suggested, was a donor impurity band formed by the indium substituting on zinc sites, while the other was an acceptor impurity band, hence the p-type behaviour from the thermoelectric power data, formed by complex centres of indium substituting for zinc in the

vicinity of a zinc vacancy.

To see if results reported by Sethi et al could be reproduced, some measurements of thermoelectric power were made on three as-grown samples doped with indium, one as-grown sample doped with gallium and one sample treated in zinc vapour at $850^{\circ}C$. The results are shown graphically in figure 6.32 where it can be seen that only n-type behaviour was observed over the measured range 150-410 K. Furthermore, there was no evidence of any strong reduction in the absolute value of the thermoelectric power S as the temperature was reduced, except with the zinc treated sample where | S | decreased from 68 μV/K at 410 K to just below 30 μV/K at 140 K, which was the lowest temperature that could be reached in the apparatus. | S | was still decreasing. However, three of the as-grown samples could not be measured at low temperature because their resistivities were too high, while, with the lightly doped sample, No.132 from boule # 407 ($\sim$ 12 ppm of indium) it was possible to make measurements down to 200 K but there was no sign of |S| decreasing.

Mathur et al (1979a) also measured a negative magnetoresistance in as-grown indium doped ZnSe crystals using several values of the applied magnetic field and at two different temperatures, indicative, again, of impurity band conduction. Their magnetoresistance values of $\Delta\rho/\rho_{o}$ varied from just under 0.05% to about 0.7% in magnetic fields of up to 0.7 T. Nedeoglo (1977) also reported negative magnetoresistance, but his measurements were made on highly conductive gallium doped ZnSe crystals and at temperatures well below 100 K, with absolute values of up to 2% at liquid helium temperature.

No serious magnetoresistance measurements were performed in this investigation and a fixed magnetic field only, of 0.225 T, was used throughout. However, no variation in the current was observed when the magnetic field was switched, even though a 4$\frac{1}{2}$ digit meter was used and a very stable current
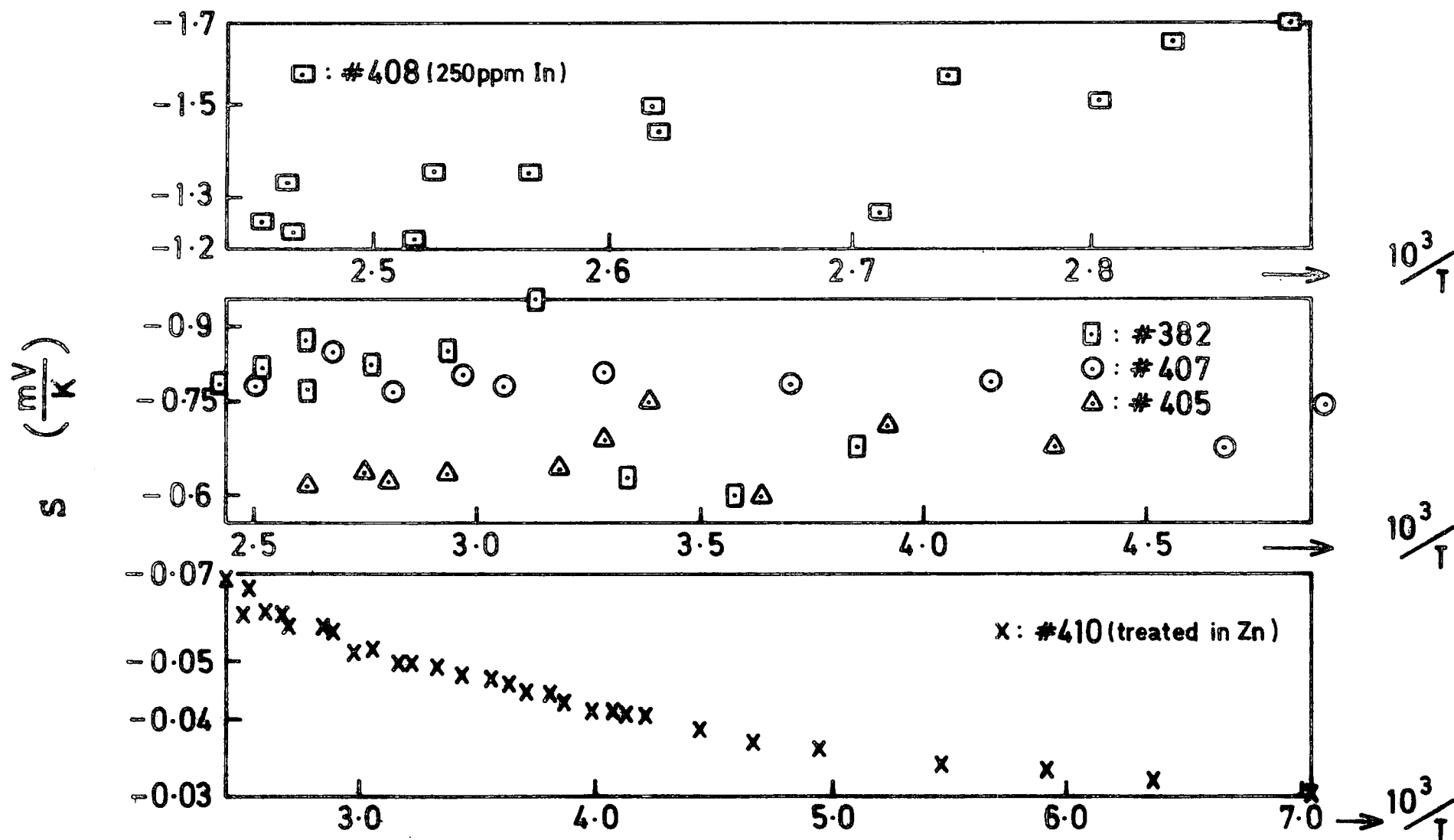
FIG. 6·32 THERMOELECTRIC POWER AS A FUNCTION OF RECIPROCAL TEMPERATURE FOR SOME ZnSe : In CRYSTALS.

supply was available (with a noise figure of around 0.01%, i.e. one part in 10^4). In other words, it should have been possible to detect variations of the order of 0.1% or better.

A final point to mention is that, even though Sethi et al and Mathur et al gave no exact values for the indium content of their samples, their conductivity data with relatively high values of σ for two of their samples with corresponding low values of the activation energies, indicate, according to our own results, that the indium content was very low. Furthermore, the technique that these workers used to introduce the indium impurity in the ZnSe was different from that employed here (see chapter four). They added 50 or 100 ppm of indium during the flow-run purification stage and assumed that all the indium remained in the ZnSe during the next stage of the process. They do not report any chemical analysis of the indium content after the crystal was grown. It is very probable that less indium than ZnSe was transported by the gas in the flow process, because indium has a very high boiling point, i.e. 2000°C, and the temperature of the furnace was 1200°C.

Having said this, it is possible to conclude that, with relatively low indium concentrations (< 50 ppm) ZnSe behaves as a heavily doped semiconductor with conduction via an impurity band occurring at temperatures as high as room temperature and above, following Mott's criterion of the overlapping of the wave functions of electrons on impurity centres. However, no evidence of the existence of two impurity bands was found in the two samples for which an exponential increase of mobility with temperature was found.

With the as-grown samples with indium or gallium contents of 50 ppm and above, another explanation has to be found and, as had already been stated, the principal mechanisms limiting the carrier mobilities in these crystals is a combination of polar mode scattering with a further combination of ionized impurity and neutral impurity scattering, these last two

processes probably being caused by the presence of large numbers of

impurities forming single donor or acceptor or even complexes or aggregates

with different degrees of ionization.

6.3.3 Carrier Concentration and Compensation Effects

6.3.3.1 Transport equations

The value of the Hall factor r in the equation $n = r(e\ R_H)^{-1}$ is

determined by the type of scattering which limits the carrier mobility.

Since two of the main scattering processes in this material are thought to

be polar scattering and neutral impurity scattering, and since for each of

these two processes, the value of r is unity, we will take r = 1 for the

combination of these scattering mechanisms with ionized impurity scattering.

By fitting the experimental values of carrier concentration n to

the equation

$$\frac{n(N_A + n)}{N_D - N_A - n} = \frac{1}{g}\ N_c\ \exp\ (-Ed/kT) \qquad (6.15)$$

where it is assumed that $n < N_A < N_D$, g = 2 if a simple donor level is considered

and, $N_c = 2\ (2\pi\ m^*\ kT/h^2)^{3/2}$ is the effective density of states in the

conduction band, it is possible to obtain values for N_D, N_A and Ed (see for

example, Blakemore, Semiconductor Statistics).

The accepted value of m* , the electron effective mass, was found

to be 0.17 m_e by Marple (1964). Measurements on electroabsorption at high

electric fields have been carried out in this department on thin undoped

ZnSe slices, and a value of (0.17 ± 0.01) m_e for m* has also been obtained,

Muhamad (1979). However, it is possible using the thermoelectric power

measurements to calculate the position of the Fermi level. Then, by knowing

the experimental value of n at the corresponding value of the absolute

temperature T, a value for m* can be obtained from the relation

$$S = - \frac{k}{e} \left[(\frac{5}{2} - s) + \ln \left\{ \frac{N_c}{n} \right\} \right] \tag{6.16}$$

where s is related to the relaxation time τ in the form $\tau = a\ E^{-s}$, and

evaluated according to the type of scattering limiting the electron mobility;

its value is usually $\frac{1}{2}$ for dominant lattice scattering or $-\frac{1}{2}$ for dominant

impurity scattering. Although neither mechanism is really dominant, a value

of $\frac{1}{2}$ will be assumed for s. With s = $\frac{1}{2}$ equation 6.16 reduces to

$$m_R = \frac{m^*}{m_e} = \frac{3.5 \times 10^{-11}}{T} \left\{ n \exp \left[- (2 + 11.6 \times S) \right] \right\}^{2/3} \tag{6.17}$$

for ZnSe, with S in mV/K and negative for n-type conduction. However, because

of the approximation to the value of s and the fact that m* depends exponentially

on S, a large error is involved ; so, only a rough estimate to the value of

m* can be given. Some of the calculated values are given in table 6.3.

If the value of $-\frac{1}{2}$ is used for s, smaller values of m* are obtained. It is

clear from the content of table 6.3 that the values of n and $|\ S\ |$ are too

small for all samples except #407 or, alternatively, that equation 6.16

for the thermoelectric power breaks down for these crystals. A few values

which have been calculated from the graphical data recorded by Sethi et al

(1979), have also been included in the table showing a large discrepancy also

with the expected value.

Recently, Lim and Brodie (1977a, 1977b, 1978) made some measurements

of the d.c. conductivity, photoconductivity, optical absorption, thermo-

electric power and a.c. conductivity of amorphous films of ZnSe and concluded

that conduction is n-type with the Fermi level near the middle of the mobility

gap ; moreover, from their d.c. conductivity in the temperature range 77-500 K,

they obtained a consistency with carriers hopping in band tail states at high

temperatures and hopping in localized states near the Fermi level at lower

T A B L E   6.3

VALUES OF THE EFFECTIVE MASS CALCULATED USING EQUATION 6.17

Crystal Boule ##	Temperature at which it was Calculated (K)	Value of m^*/m_e
382	260	0.0035
	320	0.17
	400	0.13
407	270	0.46
	330	0.40
	400	0.36
405	230	4.5×10^{-5}
	310	9.9×10^{-4}
	400	3.6×10^{-3}
408	345	0.057
	380	0.030
	410	0.016
410 ✫	140	0.012
	260	0.010
	400	0.009
323 ✦	250	19
	280	6.7×10^3
139 ✦	300	2.2×10^{-3}

✫   Annealed in zinc vapour
✦   Calculated from the results of Sethi et al (1979)

temperatures. They used this result to analyse their thermoelectric data which consisted of a small negative value with a weak temperature dependence near room temperature becoming more negative and strongly temperature dependent at higher temperatures. They concluded that these results could not be analysed by assuming only one kind of conduction mechanism. From this, they worked out a somewhat different expression for S which resulted in good agreement with their experimental values. However, this approach could not be used here since our thermoelectric power data showed a weak temperature dependence even at temperatures around 400 K.

With ambipolar conduction, the thermoelectric power associated with each carrier is weighted according to the contribution each makes to the total current (see Beyer and Stuke, 1974) , then, if there is some ambipolar behaviour (i.e. holes as well as electrons or highly compensated electron conduction because of the existence of donor-acceptor pairs), the value of $|\ S\ |$ will tend to be smaller than the effective $|\ S\ |$ for the majority carriers alone, which would explain, in part, the low $|\ S\ |$ values obtained in some of our crystals.

For the rest of the discussion, a value of 0.17 will be used for m^*/m_e. For N_D, N_A and E_d to be unambiguously determined, it is necessary to find the region where $n = N_D - N_A$, i.e. the so-called exhaustion range ; it is evident from all the experimental plots of $\ell n\ n$ vs $1/T$ that this range was not attained for any of the samples, so that the procedure is less reliable. Nevertheless, for most of the samples, well defined slopes were obtained, giving values for E_d and from them, tentative values of N_D and N_A were used until the best fit to equation 6.15 was obtained.

The results of these calculations are illustrated graphically in figures 6.33 and 6.34 where E_d and (N_D-N_A) are plotted as functions of the added dopant concentration. Figure 6.35 also shows a log-log plot of the carrier concentration at 410 K for each one of the sixteen mentioned samples against the dopant concentration.
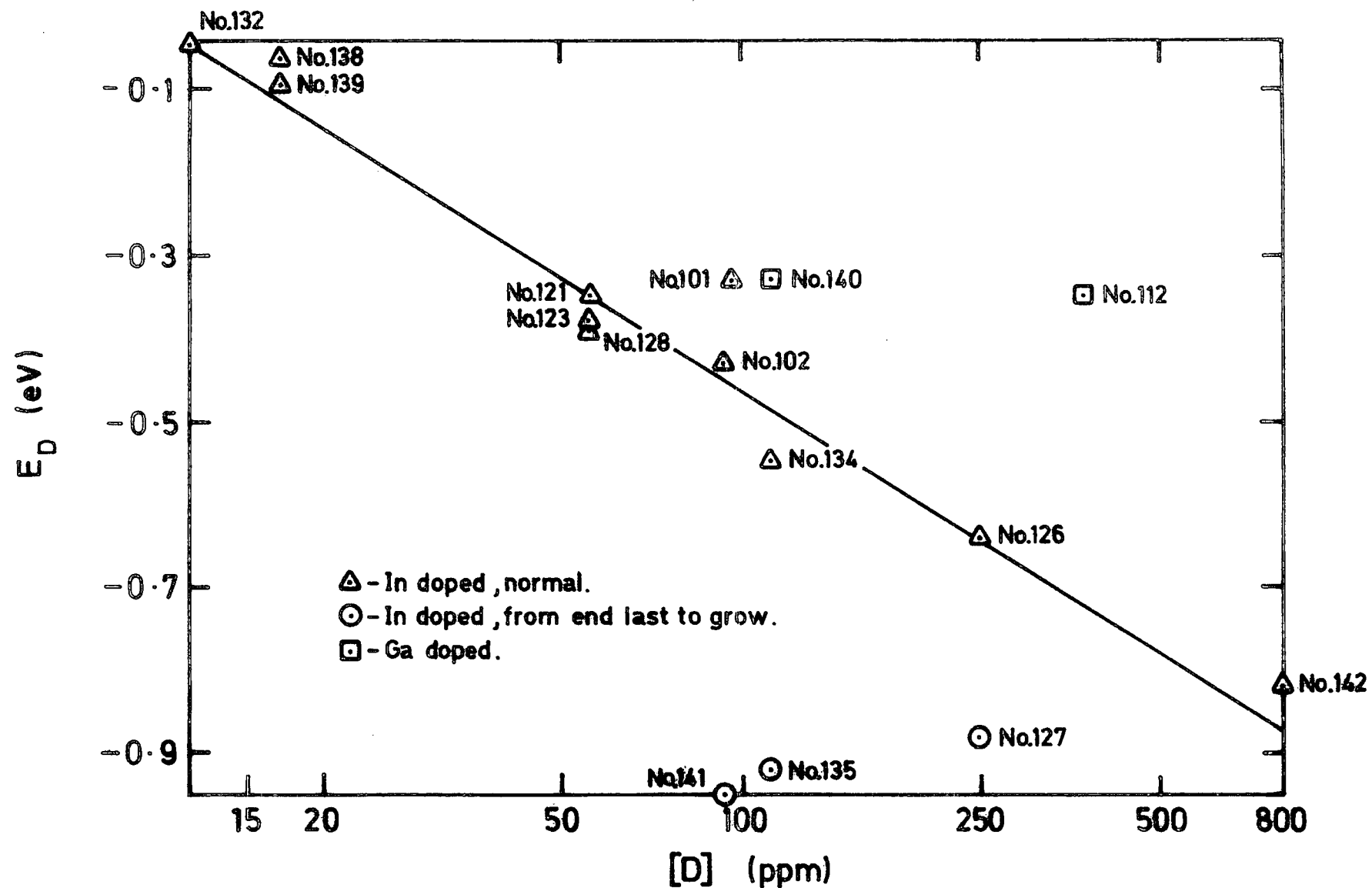
FIG. 6·33 DONOR IONIZATION ENERGY AS A FUNCTION OF THE DOPANT CONCENTRATION FOR VARIOUS ZnSe CRYSTALS CONTAINING In OR Ga.
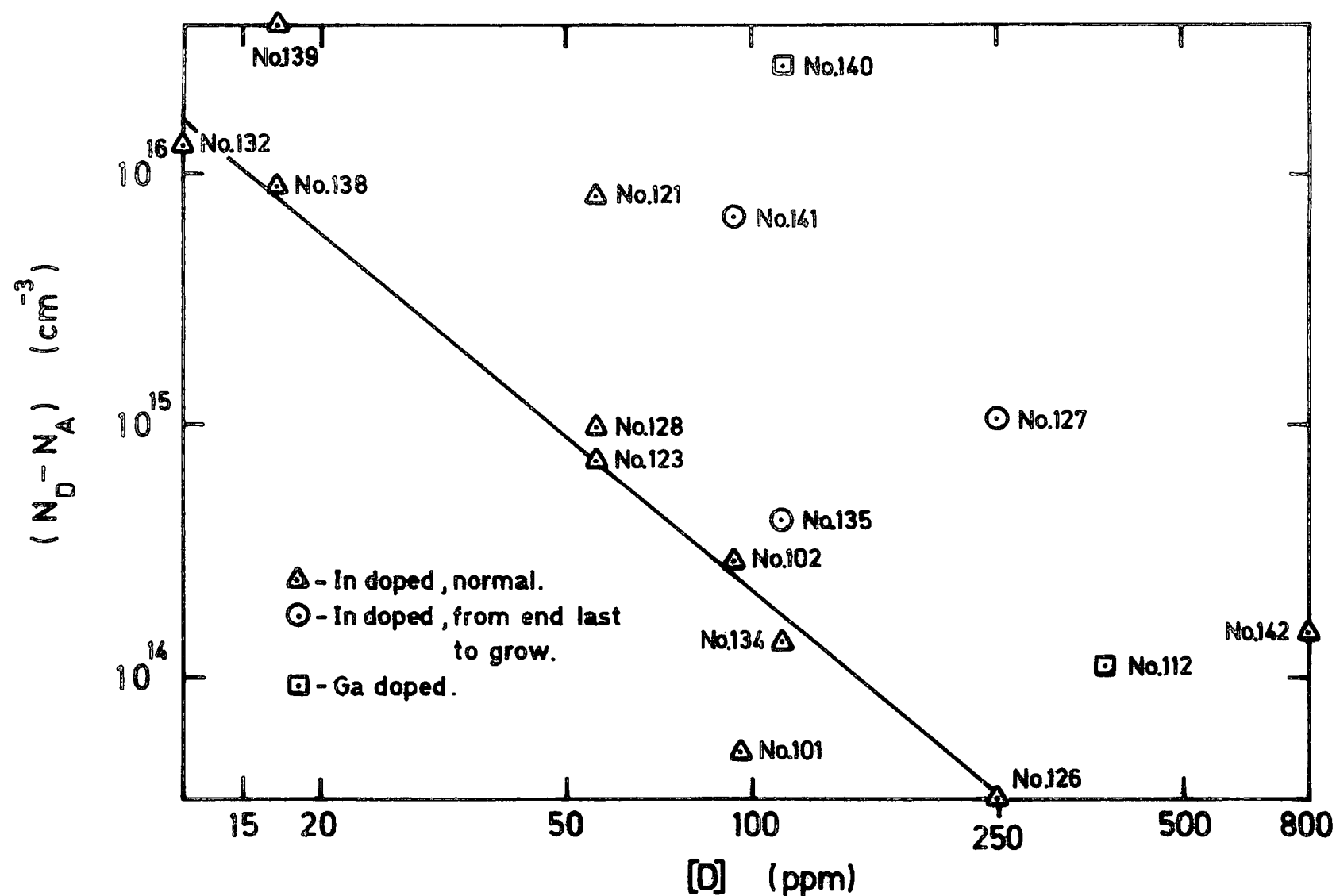
FIG. 6·34   CONCENTRATION OF UNCOMPENSATED DONORS AS A FUNCTION
OF THE DOPANT CONCENTRATION FOR VARIOUS ZnSe CRYSTALS
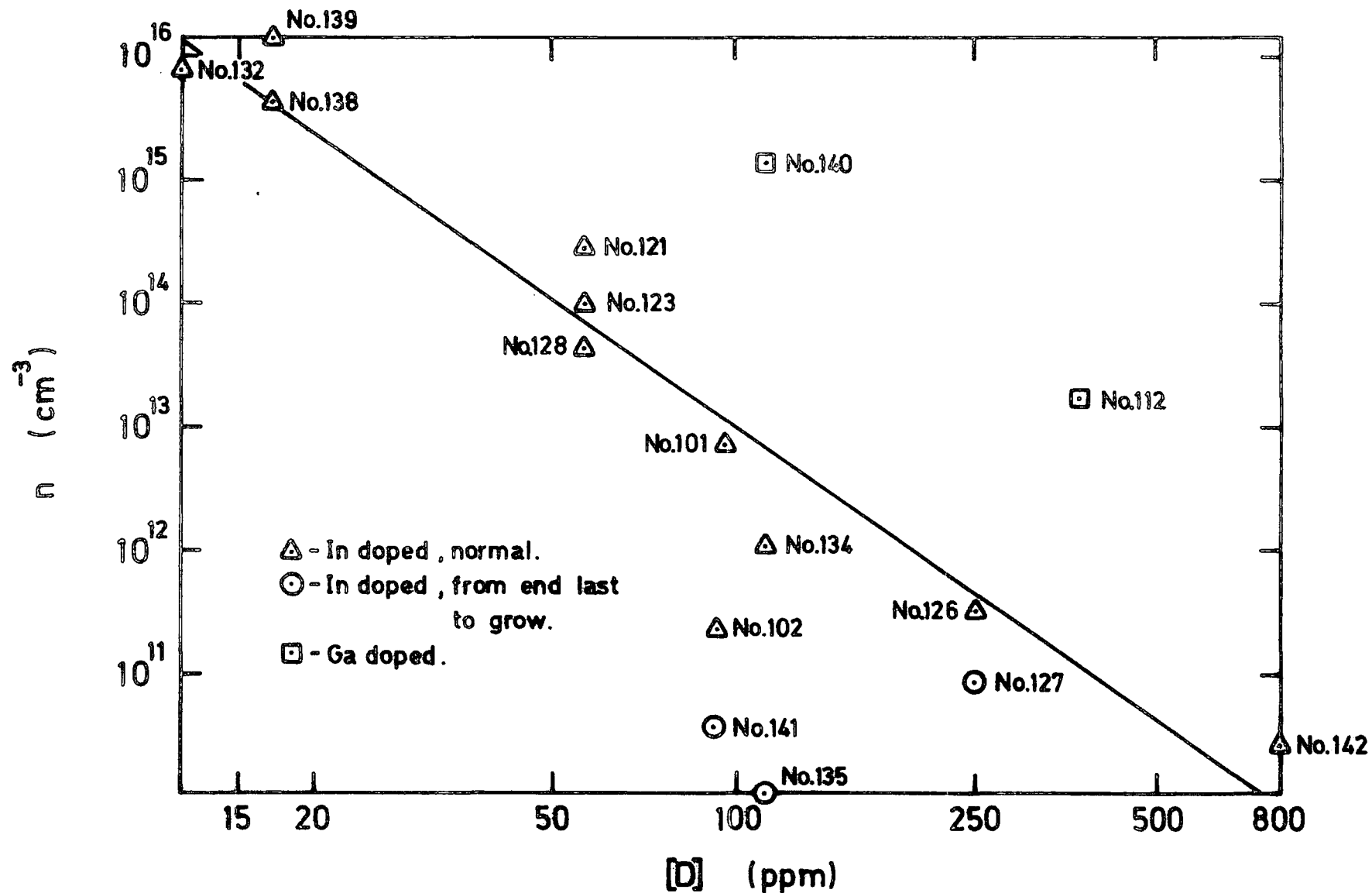CONTAINING   In OR Ga.

FIG. 6·35   VALUES OF THE FREE CARRIER CONCENTRATION AT 410 K AS A FUNCTION OF THE DOPANT CONCENTRATION FOR VARIOUS ZnSe CRYSTALS CONTAINING In OR Ga.

The conclusion that can be drawn from these three graphs is that E_d increases and (N_D-N_A) and n decrease as the concentration of indium or gallium is increased. The samples from which these results were obtained fell into three groups. Group A, containing 11 samples, represents the "normal" indium doped samples which were samples 101 ; 102 ; 121 ; 123 ; 126 ; 128 ; 132 ; 134 ; 138; 139 and 142. Group B with samples 127 ; 135 and 141, contains indium doped samples cut from the end of those boules which showed a difference in body colour between the end (reddish) and the bulk (yellow or light orange)) of the boule. Group C contains the gallium doped samples numbers 112 and 140.

Using the linear regression technique, the slopes and intercepts of each of the lines in figures 6.33 to 6.35 were calculated, leading to the results that

$$n_{410K} = (0.60 \pm 2.7) \times 10^{20} \left[I_n \right]^{-(3.38 \pm 0.76)} \tag{6.18}$$

from figure 6.35 ;

$$N_D - N_A = (2.45 \pm 0.62) \times 10^{18} \left[I_n \right]^{-(2.02 \pm 0.17)} \tag{6.19}$$

from figure 6.34 ;

and

$$E_d = -(0.196 \pm 0.029) \, \ell n \left[I_n \right] + (0.440 \pm 0.127) \tag{6.20}$$

from figure 6.33.

It is clear from these equations that there is a strong decrease in the free electron concentration along with a steep increase in the activation energy (E_d) with increasing dopant concentration. These effects are the most striking consequence of adding the group III elements indium or gallium in ZnSe.

6.3.3.2 Mechanism of compensation

As is well known, ZnSe is an n-type semiconductor and when group

IIIa elements are added, these should behave as singly charged donors by

substituting for zinc atoms on zinc sites and hence, the number of free

electrons would normally be expected to increase with increasing dopant

concentration. Although this behaviour is observed when aluminium is used

as a dopant, a totally different effect occurs with indium or gallium as

the results described in this thesis show.

This may be associated with the phenomenon of self-compensation by

native defects which is responsible for a variety of unusual relationships

between the electric conductivity and chemical doping levels of II-VI

compounds. Self-compensation appears to be the main cause preventing the

predominantly n-type materials ZnS, ZnSe, CdS or CdSe from being prepared

p-type, or the p-type ZnTe from being made n-type. Many years ago de Nobel

(1959) discussed self-compensation in CdTe by native defects. Since then,

most of the work on this topic has been carried out in CdTe.

With ZnSe, all of the acceptor impurities tried in attempting

to achieve type conversion gave very weak or inconclusive p-type conduction

in high resistivity samples, suggesting that acceptor levels in ZnSe are very

deep and highly compensated by either impurity or native donors (see

Bhargava et al, 1979 , Neumark, 1979 , Neumark et al, 1980 , and Neumark,

1980) .

A similar phenomenon also seems to occur with the indium and gallium

donor impurities and, in addition to the results discussed in this thesis,

Aven et al (1961) found that ZnSe doped with gallium was weakly n-type,

suggesting that most of the donors were compensated by zinc vacancies.

Wagner and Lorenz (1966) compared the electrical properties of gallium and

aluminium doped ZnSe crystals and concluded that heavily donor doped ZnSe:Ga

is essentially compensated because its resistivity at room temperature is

much higher than comparably doped ZnSe:Al. Jones and Woods (1976) also

reported similar behaviour of indium and gallium doped material, in comparison with ZnSe:Al.

An additional complication reported by several authors, Aven et al (1961), Fukuda and Fukai (1967), Stringfellow and Bube (1968), Aven and Devine (1973), Yu and Park (1973), Jones and Woods (1974), Adachi and Machi (1975b) and Ray and Kröger (1978a), is that copper is usually present in ZnSe, as an unavoidable impurity. The copper substitutes on a zinc site, so that copper as well as zinc vacancies, which both form deep acceptor levels, will account for some of the compensation effects.

Although most investigators have failed to prepare semiconducting p-type ZnSe, one group of workers claim to have done so. Robinson and Kun (1975), using a complicated technique, claim to have obtained highly conductive p-type layers in n-type ZnSe by in-diffusion of either indium or gallium. Their explanation for p-type conversion is that indium and gallium may be present in both monovalent and trivalent states as reported by Raüber and Schneider (1966), and that they can act as acceptors in their monovalent state. However, Ray and Kröger (1978b) suggest that this explanation cannot be correct since singly negatively charged gallium on a zinc site contains one electron more than neutrally charged gallium. It follows therefore that the energy level of the former must be above the level of the latter. However, because it is known that the neutral substitutional atom forms a hydrogenic donor level 28 meV below the conduction band, it would then imply that the level from the negatively charged substitutional atom must be even closer to the conduction band and thus unable to give rise to hole conduction.

Sethi et al (1978a, 1978b) and Sethi and Mathur (1978), as mentioned previously, performed Hall measurements on indium doped ZnSe at three different dopant concentrations and they also observed the strong reduction in the carrier concentration with increasing indium content ; they concluded that the doping of ZnSe with indium resulted in increasing compensation due to the formation of complex centres, each consisting of a zinc vacancy in the

neighbourhood of an indium on a zinc site. This complex behaves as a singly

charged acceptor and is very similar to acceptor complexes observed in

chlorine doped ZnSe by Holton et al (1965) using luminescence and spin

resonance techniques.

Finally, Ray and Kröger (1978a,b) carried out Hall measurements on

ZnSe containing different concentrations of aluminium, arsenic and gallium

at high temperatures (from 800 to 1000 K) with the crystals in equilibrium

with atmospheres of well defined zinc pressures. Their results showed that

at high zinc pressures, aluminium acts as a singly charged donor resulting

from the aluminium atom substituting on a zinc site, and its level is close

to the conduction band. At low zinc pressures, some self-compensation occurs

since two doubly charged zinc vacancies are incorporated for each singly

charged donor. On the other hand, samples with gallium were found to contain

fewer free electrons than undoped samples prepared under the same conditions ;

this stronger compensating effect could not be explained solely in terms of

doubly charged zinc vacancies. Furthermore, after cooling the crystals, they

found that in the samples with the largest gallium content there was a marked

reduction in the carrier concentration. The explanation put forward by Ray

and Kröger was that some gallium is transferred from zinc sites where it acts

as donors, to selenium sites where it acts as multiple acceptors, pairing

eventually with the positively charged gallium atoms on zinc sites (i.e. donors)

to form doubly or singly negatively charged acceptor complexes $(Ga_{Zn} \ Ga_{Se})''$

or $(Ga_{Zn} \ Ga_{Se})'$ which can act as deep electron traps. This they proposed as

a basis for a reaction equation leading to the electron concentration n

proportional to a negative power of the gallium concentration.

This result is in good agreement with the equation obtained from

the plot of $\ln n$ versus $\ln \left[I_n \right]$ in figure 6.35, i.e. equation 6.18, so that

our work offers convincing support for the suggested model put forward by

Ray and Kröger. However, the decrease of n with $\left[I_n \right]$ for our ZnSe:In

crystals is more pronounced than the one suggested by Ray and Kröger, hence, the compensation in our indium doped crystals must be even stronger, suggesting the presence of relatively large concentration of triply charged acceptor centres probably in the form of In_{Se}'''. This will be discussed further in the following chapter.

With the group B samples, mentioned at the beginning of this section, it is obvious that some deviation from stoichiometry took place in these crystals during growth, because their compensation effects are even more pronounced than those of the "normal" group A samples. From atomic absorption analysis, table 4.1, no difference in indium or copper concentrations was found between these samples cut from the ends of crystals and those from the bulk of the corresponding boule, which suggests that some other kind of crystal defect on an even larger concentration of In_{Se}''' acceptors must be present.

Similar conclusions apply to the group C gallium doped crystals. However, as reported by Jones and Woods (1976), for equal molar concentrations of dopant, the gallium doped samples are less compensated, i.e. they are more conductive than the indium doped ones. This effect can clearly be seen in figure 6.35. This difference, as reported by Yamaguchi et al (1977b) may be due to differences in the diffusion constants of gallium and indium ; the diffusion constant of gallium may be larger than that of indium, which is a reasonable supposition because the ionic radii of gallium and indium are 0.62 and 0.81 Å respectively compared with 0.74 Å for zinc (see for example Roth, 1967) .

When samples are annealed in zinc vapour, there is a strong dependence of the free carrier concentration on the temperature of the treatment. In other words, for the zinc treated material, n is dependent on the zinc vapour pressure. This effect was studied in some detail by Ray and Kröger (1978b). The overall effect of the heat treatment, as far

as the electrical properties are concerned, is to increase the value of n

with respect to the as-grown material, see figures 6.24 and 6.26.   One

explanation for this is that the large number of zinc vacancies and copper

compensators are eliminated by the indiffusion of zinc to the vacant zinc

sites and displacement of the copper to some interstitial position (Adachi

and Machi, 1975b) where it is electrically neutral. This is only part of

the explanation since the zinc vacancies and the copper centres on their

own do not account for the strong self-compensation in the as-grown

material, hence, heating these crystals in zinc must have some additional

effect.

A number of workers, including Wagner and Lorenz (1966), Jones

and Woods (1976) and Ray and Kröger (1978b) have found that heating gallium

or indium doped ZnSe in zinc produces a large number of visible, dark

precipitates ; these may be formed by the segregation of the impurities

in either elementary form or in forming an alloy with zinc or even forming

a solid solution with selenium. In any case, the precipitation reduces

the compensating effects quite markedly and returns the material to the

lightly doped situation.

The blackening of the crystals depends on the zinc treatment and

on the quantity of dopant $\left[D \right]$. With $\left[D \right]$ <50 ppm no precipitates were

found with the annealing temperature up to $950^\circ C$, but with $\left[D \right]$ equals to

50 ppm or more, the darkening of the sample and hence, the concentration

of precipitates, increased with $\left[D \right]$ at constant annealing temperature.

It also increased with annealing temperature with fixed dopant concentration.

The formation of these precipitates constitutes the major part of the

subject matter of the next chapter.

With crystals annealed at a constant temperature, the measured

carrier concentration decreased with increasing $\left[D \right]$, while with fixed

$\left[D \right]$, n increased with increasing annealing temperature. With such

samples, the donor ionization energy E_d, obtained from the slopes of the curves in figure 6.24, varied from 13 to 25 meV. This is very close to the hydrogenic donor level E_H = 28 meV for ZnSe obtained from

$$E_H = 13600 \ (m^*/m_e) \ (1/\varepsilon_s)^2$$

with ε_s = 9.1 and m^*/m_e = 0.17. In the samples annealed at the lower temperature of 600° C, figure 6.26, the carrier concentration was still rather low, indicating that strong compensation was still occurring.

6.4   SUMMARY OF THE DISCUSSION

When ZnSe is doped with a small concentration of either indium or gallium, the first effect is that shallow donors are formed when the dopant substitutes for a zinc atom on a zinc site. This donor level is probably located very near the hydrogenic level, i.e. at about 28 meV below the conduction band (see Merz et al, 1972) . If more dopant is added so that the concentration approaches the 3×10^{16} cm^{-3} region, then the formation of an impurity band is achieved and the conduction at cryogenic temperatures is mainly via this impurity band, Nedeoglo (1977) . By adding more indium or gallium, it seems likely that this impurity band will become wide enough and merge with the conduction band at a value of impurity concentration $[D] > 5 \times 10^{17}$ cm^{-3} (i.e., $\sim$ 10 to 20 ppm) and hence, the electron concentration in the conduction band will be of this order ; this extended band will form a tail of the conduction band going towards the valence band. However, if $[D]$ is increased even further, a very strong self-compensation starts to occur when, it is suggested, the dopant is transferred from zinc sites to selenium sites, Ray and Kröger (1978b) , because some "saturation" of the zinc sites takes place, thus more dopant will end up in selenium sites. Because of this, some long range disorder is bound to occur, making this semiconductor act more like an amorphous material with its Fermi level controlled by this strong group of acceptor levels. These

levels would be caused by the triply charged $In_{Se}^{'''}$ and the doubly and

singly charged complexes of $(In_{Se} \ In_{Zn})''$ and $(In_{Se} \ In_{Zn})'$, pulling the

Fermi level more and more towards the centre of the bandgap, thus reaching

a perfect balance of the "glassy semiconductor" type where the Fermi level

is pinned in this mid-region of the bandgap.

    This easily explains the strong decrease of n with increasing $\left[In\right]$ or $\left[Ga\right]$, the "linear" relation of the donor ionization energy E_d with the natural logarithm of the dopant concentration, the low values of of the Hall mobilities and the fact that these crystals obey the Meyer-Neldel rule.

CHAPTER 7

CRYSTAL DEFECTS IN ZnSe:In

7.1   INTRODUCTION

A detailed study of those problems, touched on in the last two chapters, which are concerned with crystal structure, forms the main topic of this chapter. This includes a discussion,in the next section, of the large potential barrier produced at some grain boundaries.   An attempt to find a clue to explain the gradation in colour, and hence, the anomalous electrical differences encountered in some indium doped ZnSe crystal boules grown in this department, is described in the third section. Finally, in the fourth section, an account is given of a Transmission Electron Microscope study of the precipitates formed in some of the crystals following heat treatment in zinc.

7.2   GRAIN BOUNDARY EFFECTS

When a low resistivity Hall sample, from one of the crystals studied in this work, was prepared with five or six contacts for measurement, it was frequently noticed that, although the resistance between adjacent pairs of contacts was low as expected, the resistance between the end contacts might be up to six orders of magnitude higher, making these samples completely unsuitable for Hall measurements.

This effect had already been noticed by Donnelly and Smith (1970) when preparing thin samples for Hall measurements after introducing indium under zinc atmosphere into undoped ZnSe which had previously been annealed in excess zinc at high temperatures.

7.2.1 Light Emission from the Grain Boundary

On visual examination, the first observation was that the sample started to glow, as if electroluminescence was taking place, when the

voltage applied to the end contacts exceeded 20 or 30 volts. Under an optical microscope, at medium magnification (x 125), it was noticed that the "light" appeared to come from very small spots along a grain boundary, as can be seen in figures 7.1 (a) and (b), in comparison with figure 7.1 (c) which represents the zero bias condition.

The sample in this example is No.145 from boule $\#$ 382 (i.e. ZnSe with about 110 ppm of gallium) which was annealed in zinc vapour at 700°C for three days. Figure 7.2 shows a schematic diagram of the bar and its contacts. The capital letters represent the indium contacts on the sample. The resistance between the pair E W or between any combination of pairs of A,B,C,D, or F was of the order of 50 ohms, while the resistance between E and any of A to D,F, or W and, again, any of A to D,F, was of the order of 10^{7} ohms.

Attempts were first made to measure the V-I characteristic between the end contacts A and E, but this was usually impossible because each time the voltage was increased, the current first rose to a relatively high value and then, subsequently decayed to an almost steady state taking about 30 minutes to reach equilibrium. Furthermore, when the applied potential reached 20 to 30 V, depending on the history of the sample, i.e. depending whether the voltage was applied in one step or was increased slowly, then a sudden instantaneous increase in current of up to three or four orders of magnitude occurred but, immediately afterwards, decayed slowly to a value still well above the highest measured current before the break. No reproducible results were obtained from such V-I measurements. However, when the large increase in current occurred, the sample started to emit an orange-pink light ; the intensity of which decreased with the current, so that the glow completely disappeared after a few seconds.

The grain boundary separating the two uniformly low resistivity regions of the bar is marked a-b in figure 7.2. The top end of this
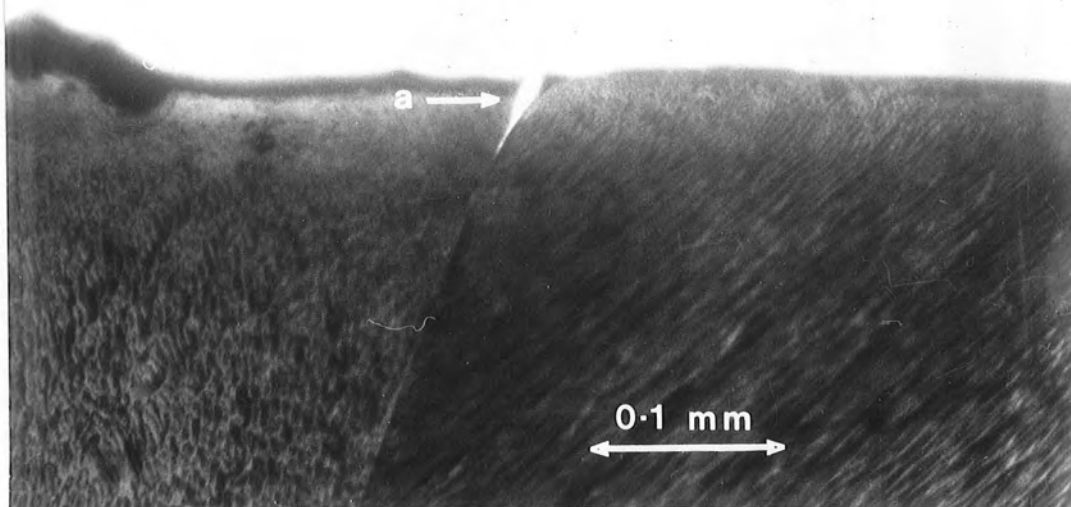
Fig. 7.1(a) Transmission Optical Micrograph of a Grain Boundary at 'a' in
ZnSe:Ga with a pulsed voltage of 25 V$_{pp}$ applied across it.
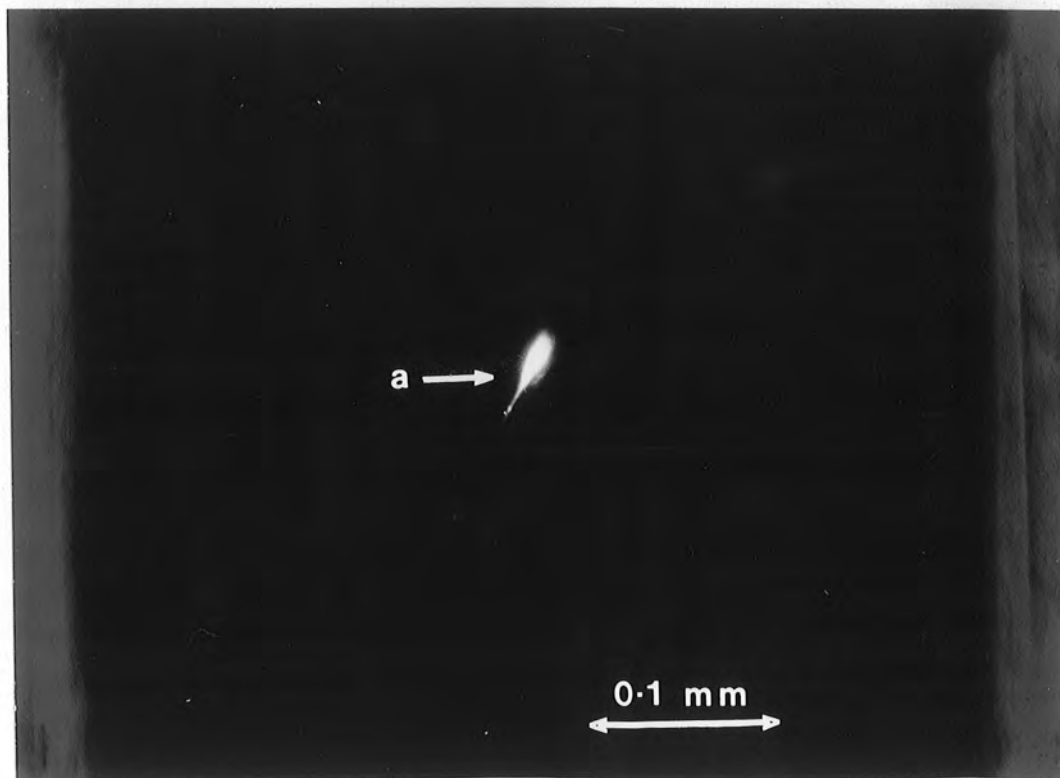
Fig. 7.1(b) Same area as in figure 7.1(a) but without external illumi-
nation.
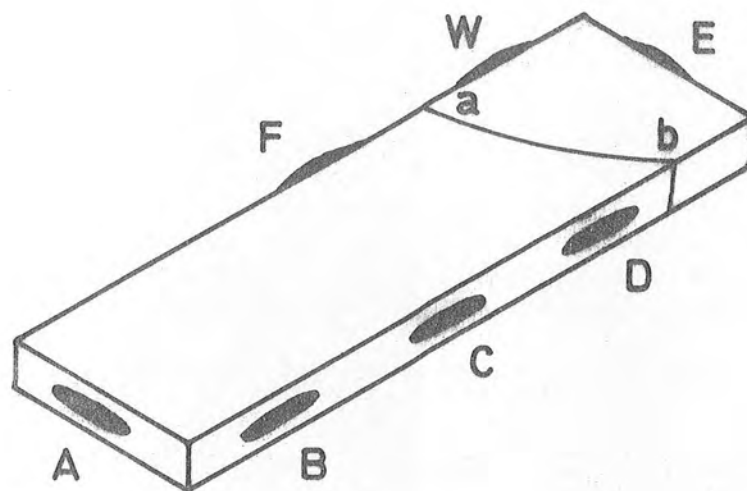
FIG. 7·2   ZnSe : Ga BAR AS USED FOR HALL
MEASUREMENTS , SHOWING A GRAIN
BOUNDARY (a→b) AND   THE   INDIUM
CONTACTS (A → F & W).

boundary is shown as 'a' in the optical transmission micrograph in figures 7.1 (a-c). In order to obtain these micrographs, a pulse generator producing a square wave was used ; the applied voltage was about 25 V peak with a pulse length of 1 ms at a frequency of 10 Hz. In this way, an almost steady light emission was obtained. The emission can be seen in figure 7.1 (a) where the crystal was illuminated for a second or two, to delineate its outline, while the voltage to excite the bright spot near 'a' was applied for a much longer time. This shows that breakdown occurred only at this part of the boundary, probably the weakest area of the voltage barrier. Only one other very weak spot of light in another part of the boundary could be observed. The major bright spot was in fact made up of a series of scintillations that moved at random over the localized area. In other samples, the bright spots looked more like a group of isolated bright dots located at different places throughout the grain boundary, appearing and disappearing apparently at random. In figure 7.1(b) the bright region is shown by itself, no external source of light was provided.

7.2.2 Scanning Electron Microscope Investigation

The next stage in the investigation was to use the Scanning Electron Microscope (SEM), described in chapter four, to study the grain boundary itself. The micrographs in figures 7.3 (a-c) illustrate some of the electron beam induced current (EBIC) effects. Figure 7.3 (a) is a secondary emission micrograph from the same region of the crystal as that from which the optical micrograph of figures 7.1 (a-c) were taken. With a positive bias of 0.2 V applied to the sample, the EBIC mode led to figure 7.3 (b), where the bright contrast follows the contour of the grain boundary. This effect is similar to the EBIC effect at p-n junctions in semiconductors. However, when the sample was biassed with the opposite polarity, the effect recorded in figure 7.3(c) was observed, i.e. the contrast was reversed ; no such behaviour occurs normally with p-n junctions.
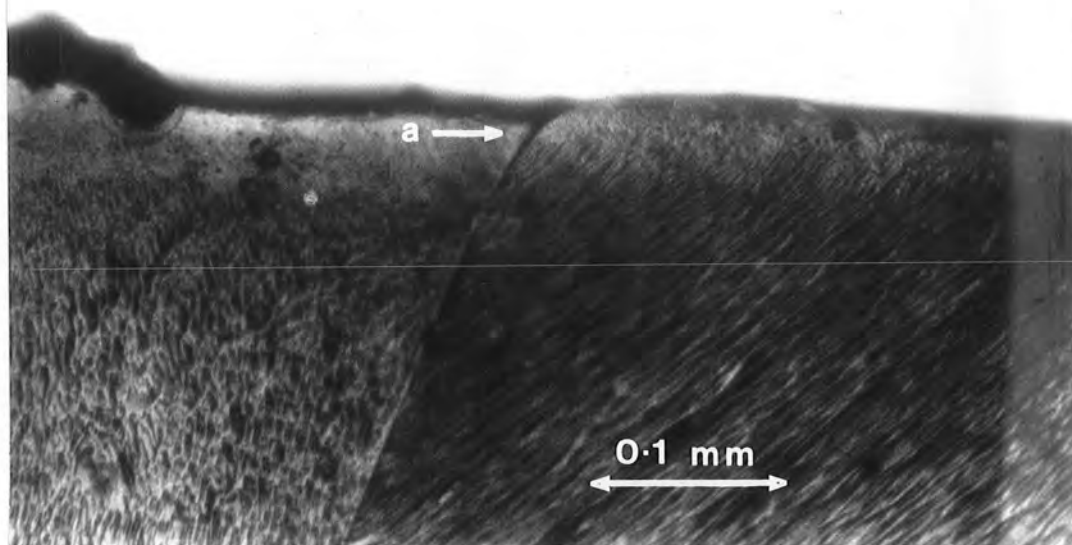
Fig. 7.1(c) Same area as in figure 7.1(a) but with zero applied
voltage.
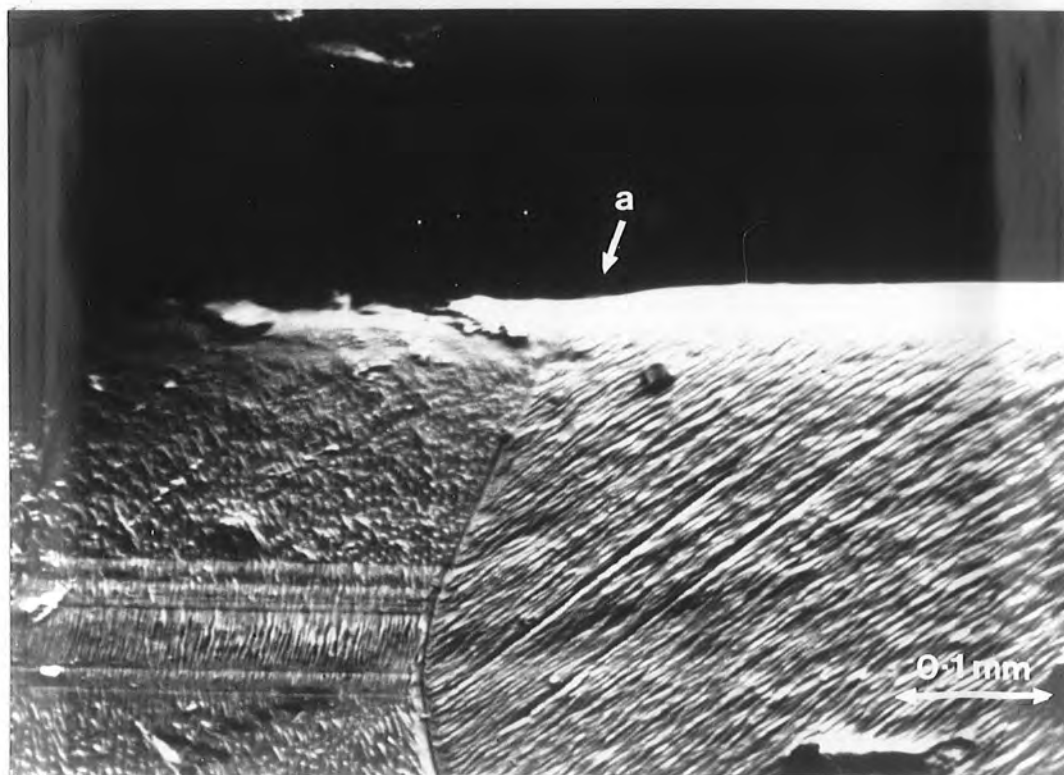
Fig. 7.3(a) Secondary Emission Micrograph of the region shown in
figure 7.1(c).
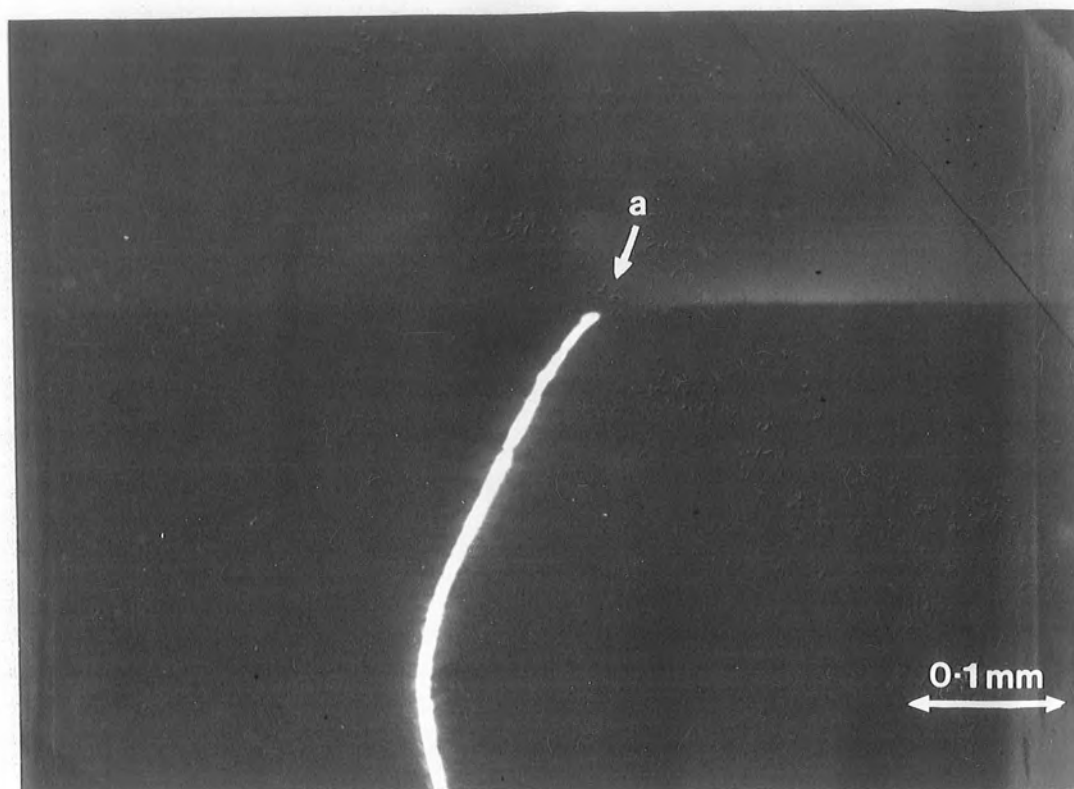
Fig. 7.3(b) EBIC Micrograph of the same area as in figure 7.3(a) with
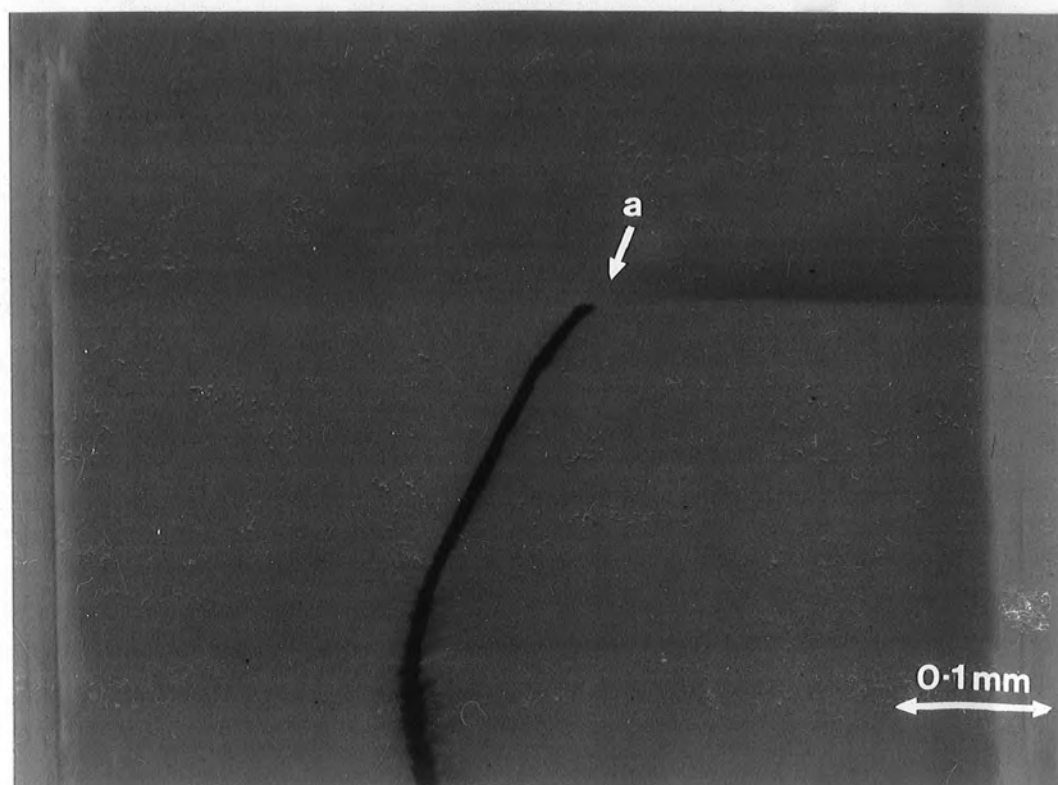0.2 V applied to the specimen.

Fig. 7.3(c) Same as figure 7.3(b) with the polarity of the applied
voltage reversed.

The micrographs in figures 7.4 (a-d) are for the same region as those of figures 7.3 (a-c), but at a higher magnification, so as to illustrate several irregularities in the EBIC signal along the top end of the grain boundary (marked as 'a' in the micrographs), where the "light" emission shown in figures 7.1 (a) and (b) was produced. Figure 7.4 (d) was obtained using zero bias, which gives rise to a white/black contrast to varying degrees along the length of the grain boundary, which might be described as an intermediate EBIC effect between positive and negative bias.

Finally, the photographs in figures 7.5 (a-c) reveal the complete grain boundary in the same conditions used to obtain figures 7.3 (a-c). It is obvious that in effect, this grain boundary lies completely across the whole bar of the specimen.

Because of this, it was decided that, when electrical measurements were to be made on low resistivity material, a whole slice, with a few appropriately placed indium contacts, should be studied first in the SEM in the EBIC mode. This was done and uniform regions of the crystal from which to cut proper bars for Hall measurements were revealed.

When this was done, a few new interesting effects were discovered. The sequence in figures 7.6 (a-c) are secondary emission micrographs of part of an as-grown slice of boule ∦ 407, i.e., ZnSe containing approximately 10 ppm of indium, and was therefore relatively highly conducting material. For micrograph 7.6 (a) no external voltage was applied to the sample. When bias was applied, a clear voltage contrast effect could be seen in the secondary emission mode which is demonstrated in figures 7.6 (b) and (c). For figure 7.6 (c), grain A was negatively biassed with respect of the rest of the slice and its brighter appearance indicates that it is negatively charged, allowing more secondary electrons to reach the detector, hence, the stronger signal. In figures 7.6 (d) and (e), the EBIC signal from the
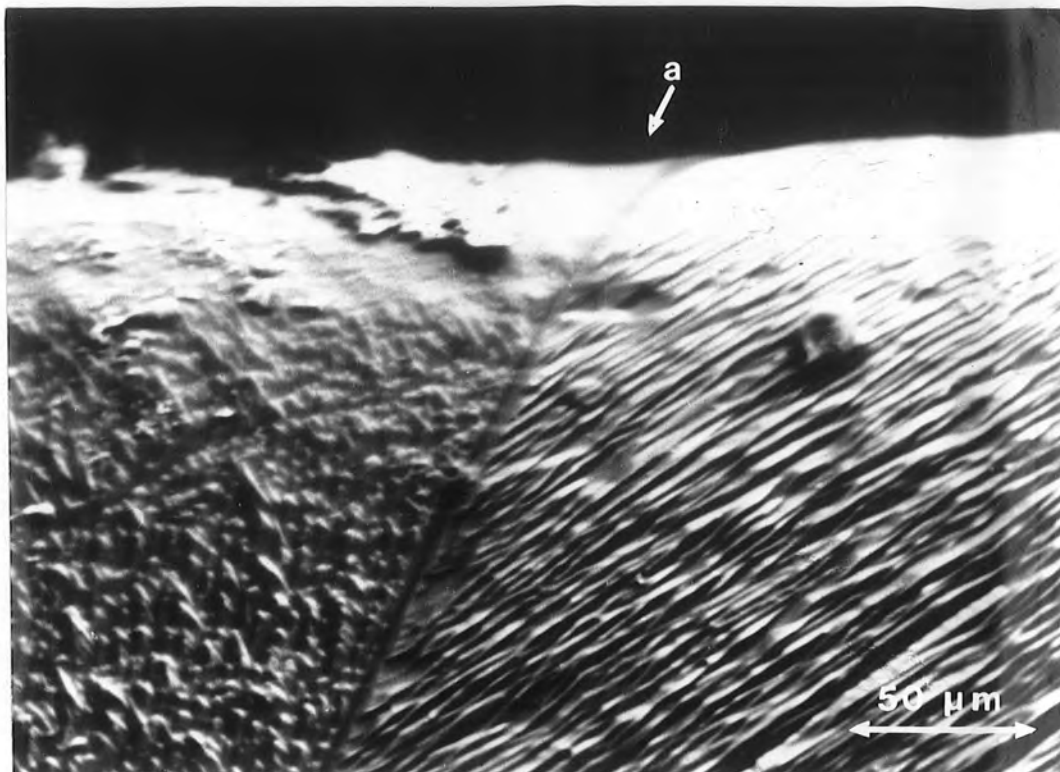
Fig. 7.4(a) Secondary Emission Micrograph of the region shown in figure 7.3(a) at larger magnification.
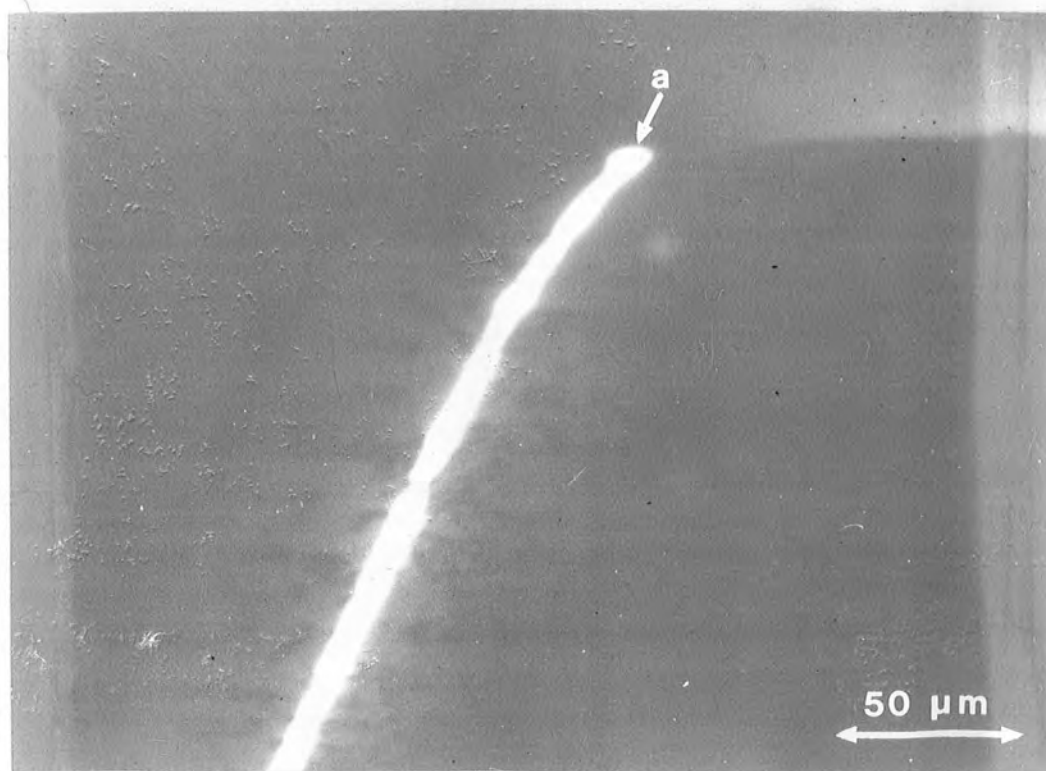

Fig. 7.4(b) EBIC Micrograph as figure 7.3(b) at larger magnification.
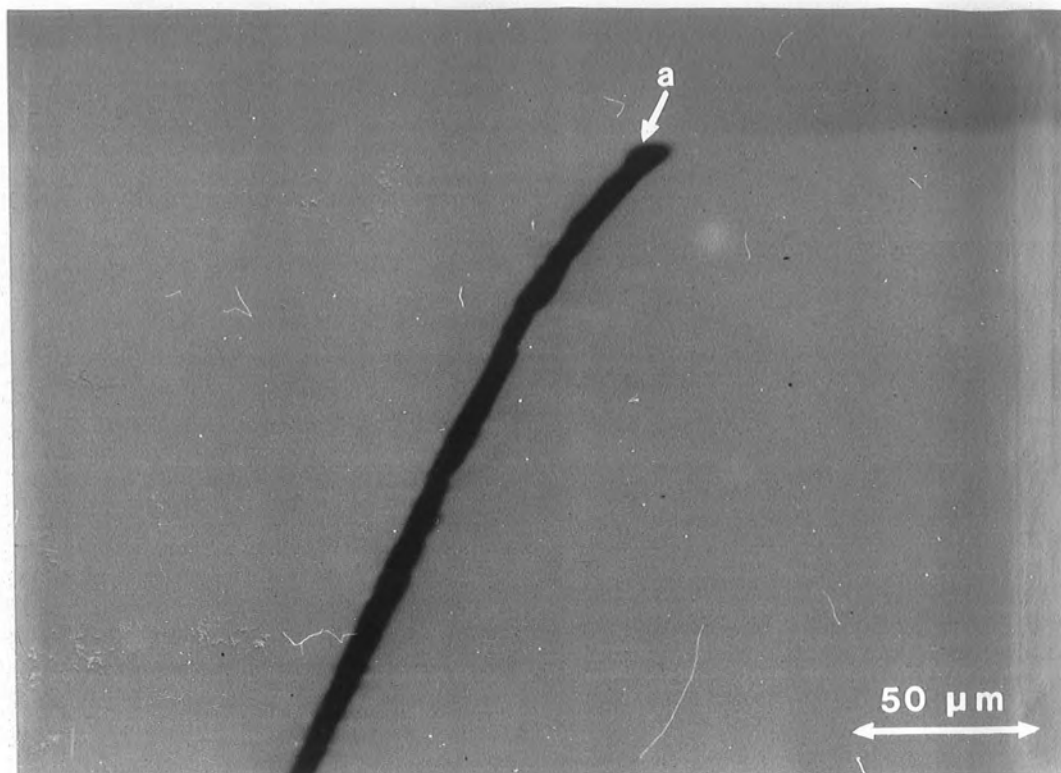
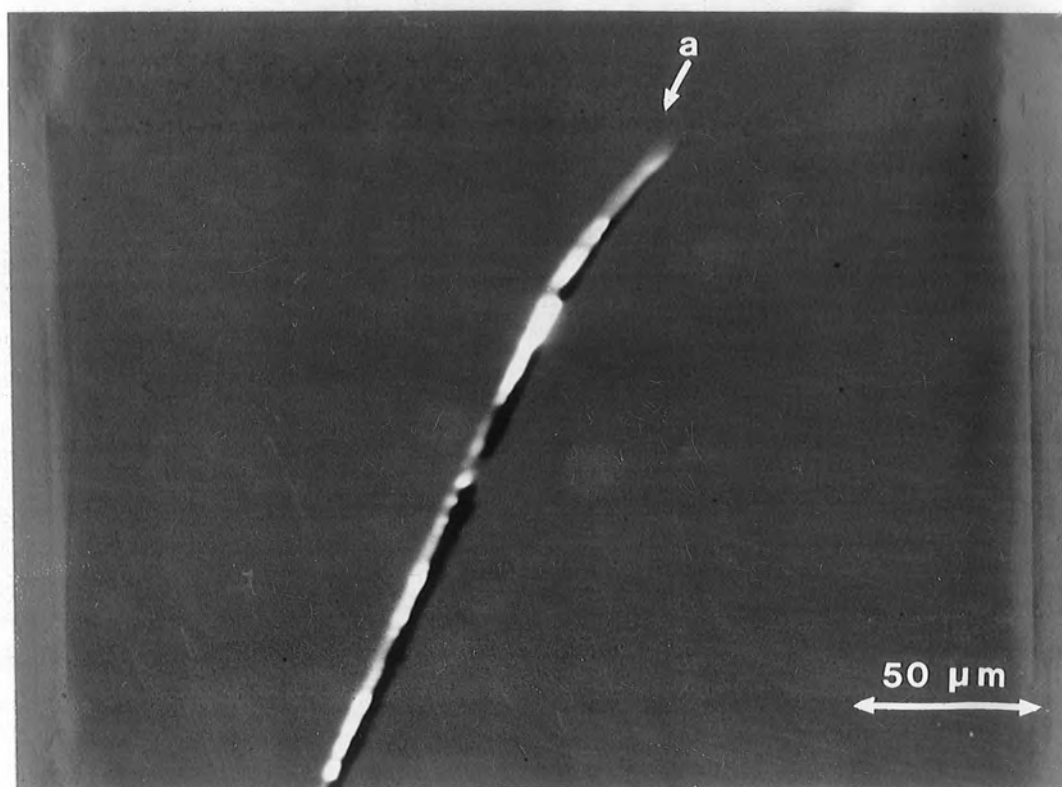Fig. 7.4(c) Same as figure 7.4(b) with the polarity of the applied
voltage reversed.

Fig. 7.4(d) EBIC Micrograph of the same Grain Boundary as in figure
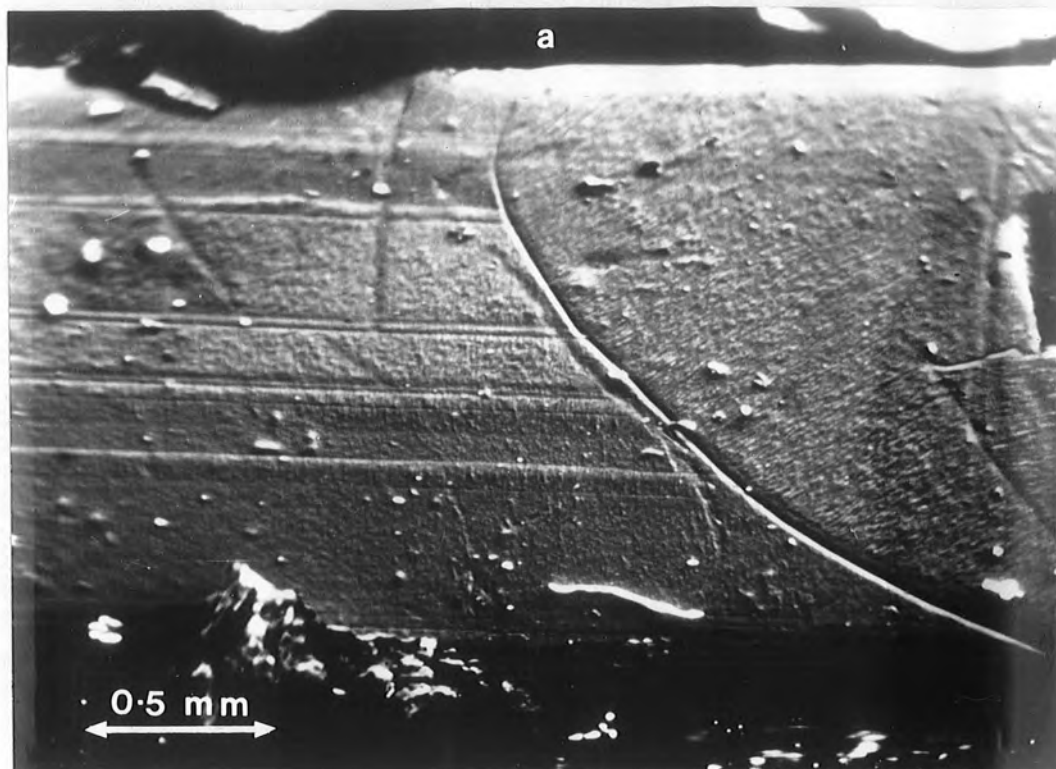7.4(a) with zero applied voltage.

Fig. 7.5(a) Secondary Emission Micrograph of the region shown in
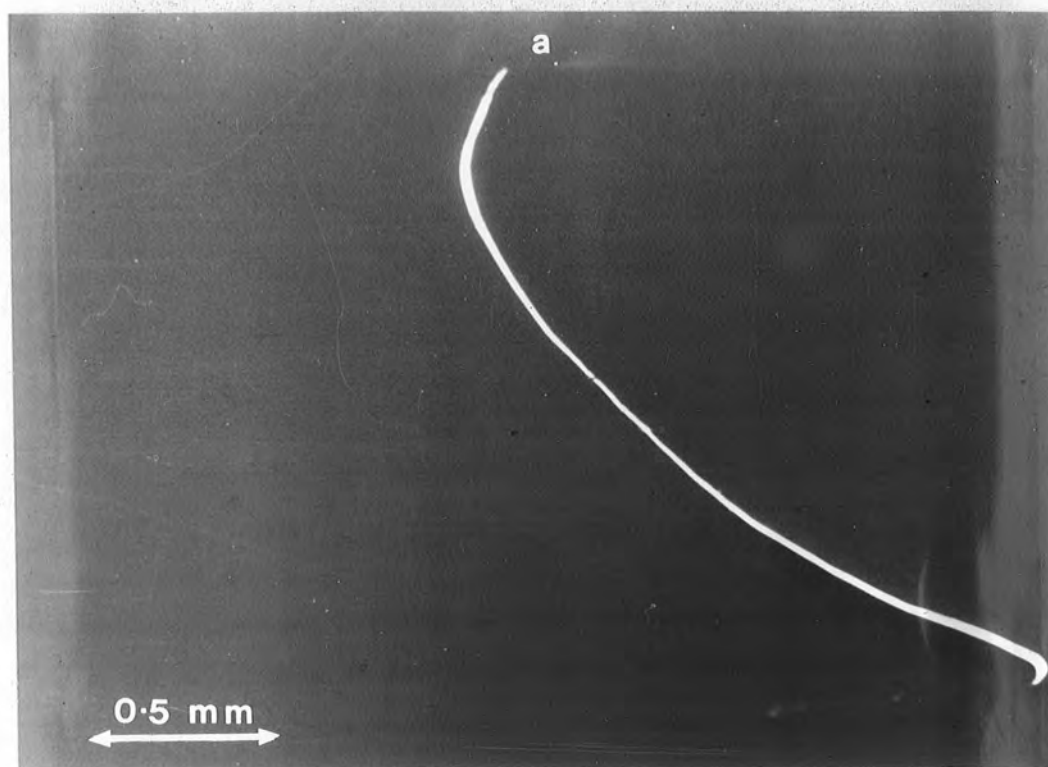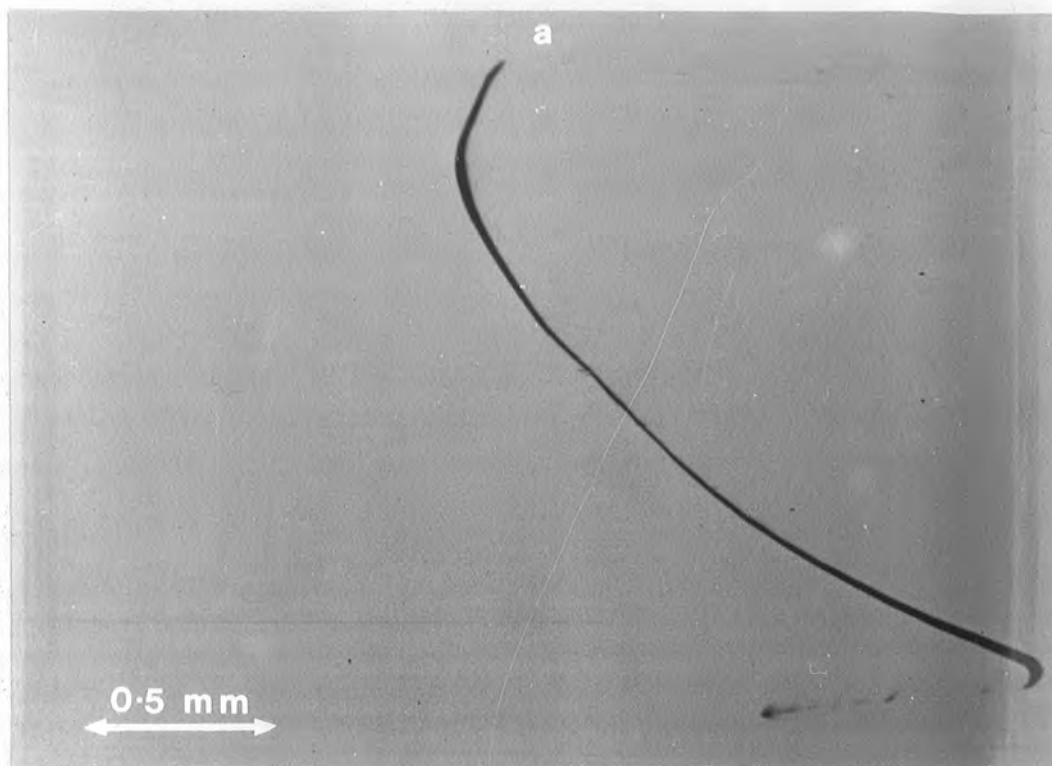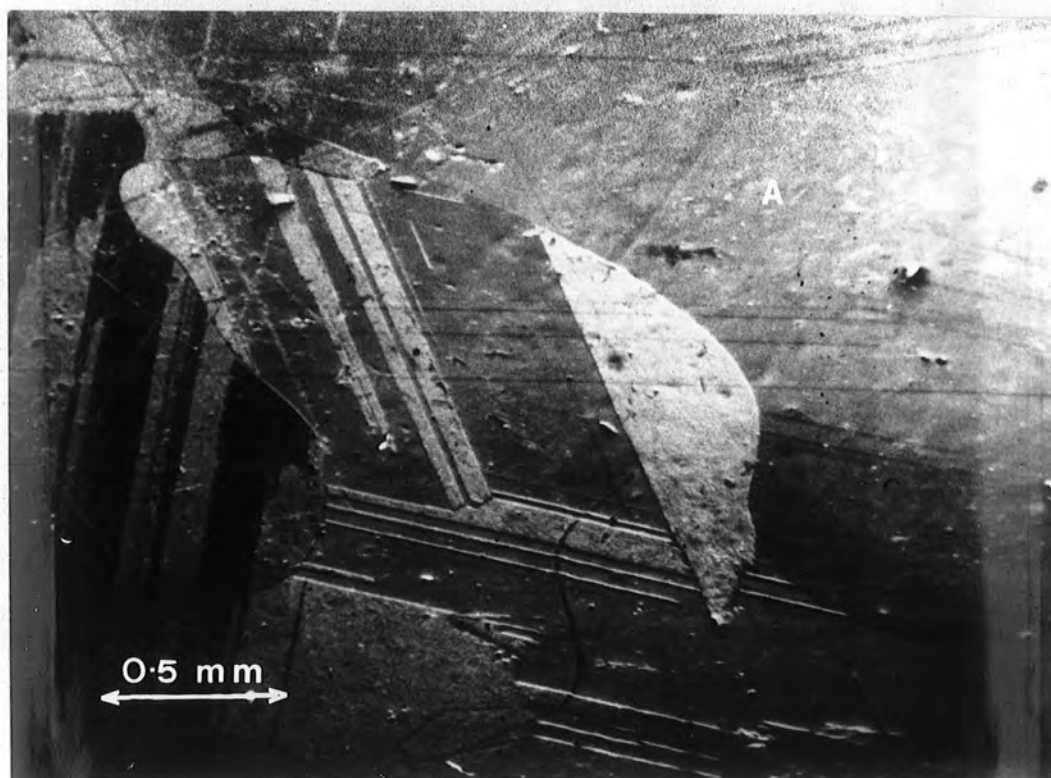figure 7.3(a) at smaller magnification.

Fig. 7.5(b) EBIC Micrograph as figure 7.3(b) at smaller magnification.

Fig. 7.5(c) Same as figure 7.5(b) with the polarity of the applied
voltage reversed.

Fig. 7.6(a) Secondary Emission Micrograph of the Surface of a ZnSe:In
Specimen with zero applied bias.
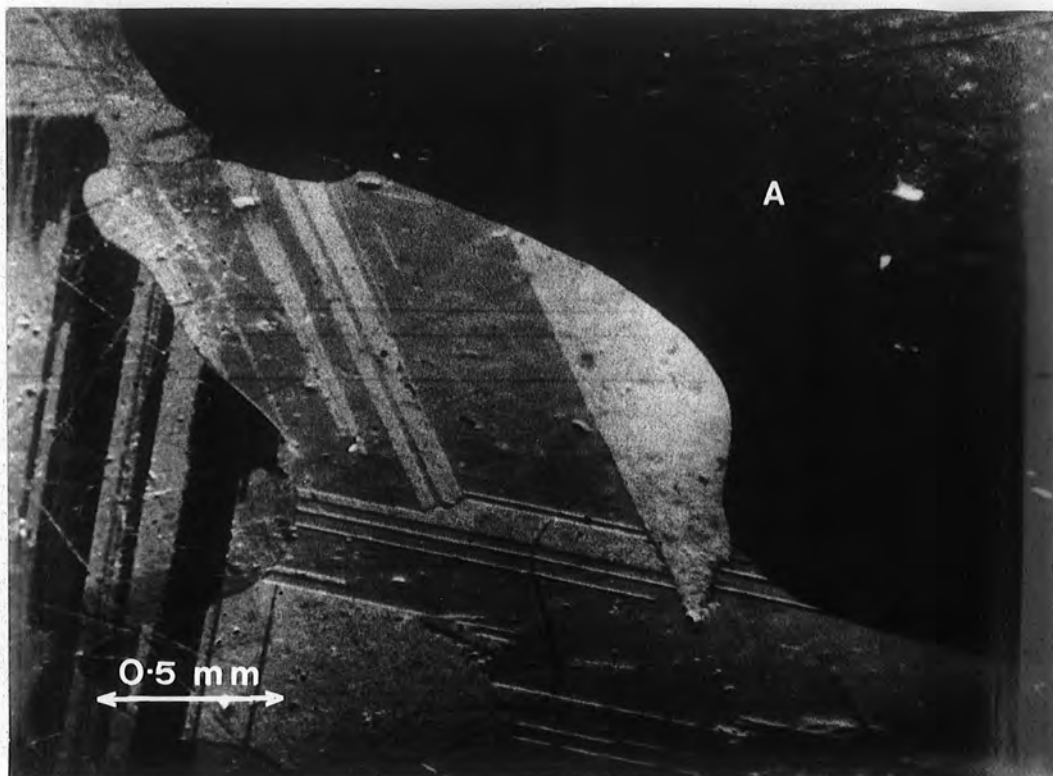
Fig. 7.6(b) Secondary Emission Micrograph of the region shown in figure
7.6(a) where +3 V is applied to grain A .
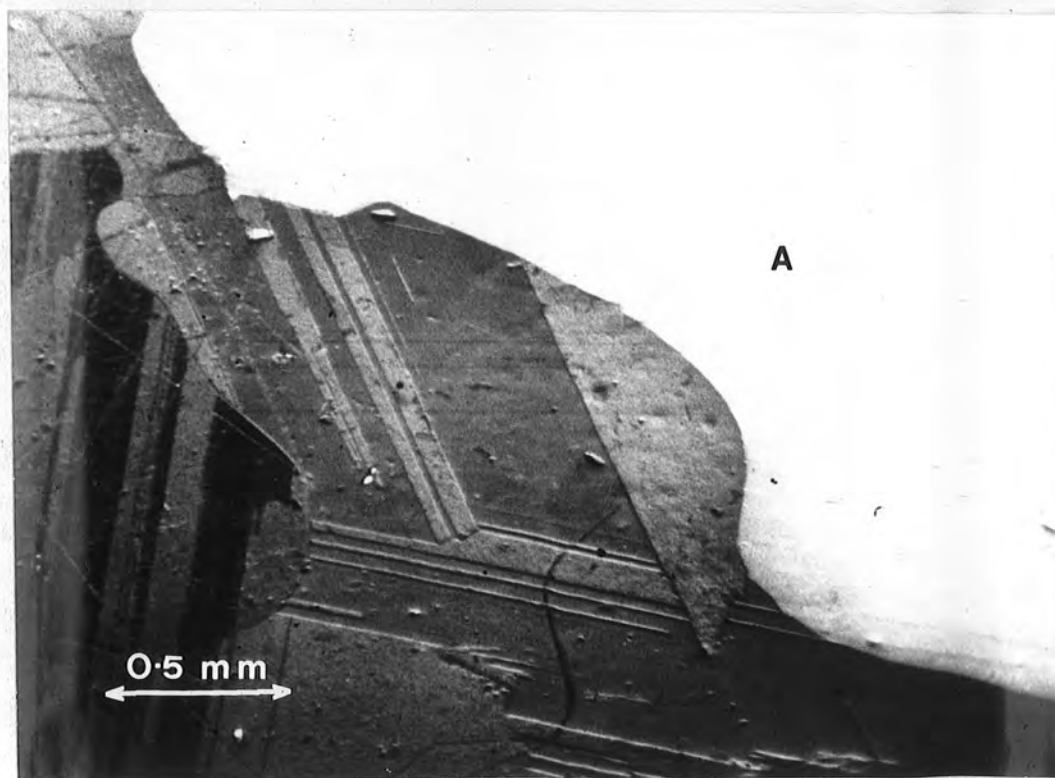
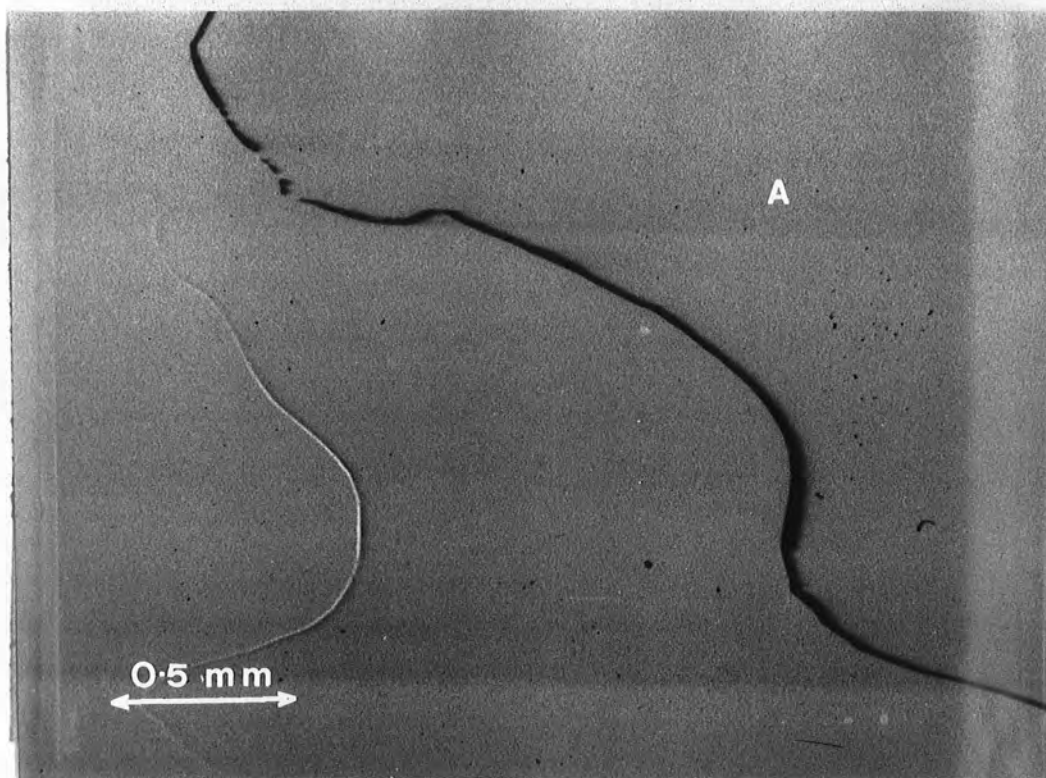Fig. 7.6(c) Secondary Emission Micrograph of the region shown in figure
7.6(a) where -3 V is applied to grain A .
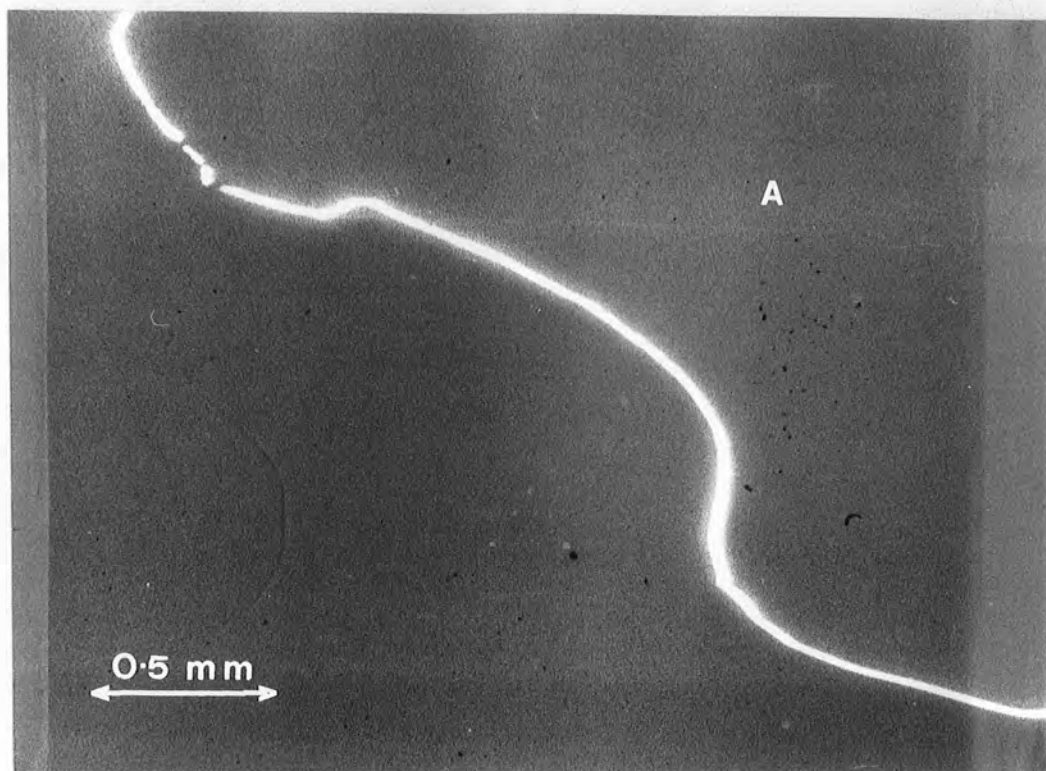
Fig. 7.6(d) EBIC Micrograph of the region shown in figure 7.6(b).

Fig. 7.6(e) Same as figure 7.6(d) with the polarity of the applied
voltage reversed.

same region is shown indicating the white and the black contrast expected
at the grain boundary. These last four micrographs clearly demonstrate
that this grain boundary did act as a voltage barrier.

Another important aspect of the contrast observed along these
grain boundaries in EBIC mode, was that the magnitude of the EBIC signal
depended on various crystallographic features. For example, twin bands
terminating at an electrically active grain, introduce local modifications
in the crystal structure at the intersection of the two grains. This
phenomenon is shown in figure 7.7 (a-c). Figure 7.7(a) which is a second-
ary emission micrograph, shows three twin bands (marked R,S and a large
one between PP and QQ), terminating at the grain boundary, while figure
7.7(b) shows the corresponding EBIC contrast. Comparison of the two
micrographs reveals that the two twin bands in the grain on the left-hand
side of figure 7.7(a) give rise to a broadening of the EBIC signal at
points R and S on the boundary, as clearly evident in figure 7.7(b). From
a closer inspection of figure 7.7(a), the presence of twin boundaries can
also be inferred along PP and QQ where the striations produced by the etching
change direction. The presence of this wide twin band on the right-hand side
of figure 7.7(a) gives rise to an EBIC signal which is broader at the top of
figure 7.7(b) than at the bottom. The effect of reversing the polarity of
the applied voltage can be seen in figure 7.7(c). Comparison of the two
EBIC images leads to the conclusion that EBIC signals that are wide for
one sign of applied voltage, are narrow for the other, and vice versa. It
can be added here that the black/white contrast produced with zero bias and
with different thicknesses along the boundary, figure 7.8, is a consequence
of the presence of twin bands.

7.2.3 Photoconductive Effect

In another series of experiments it was decided to investigate
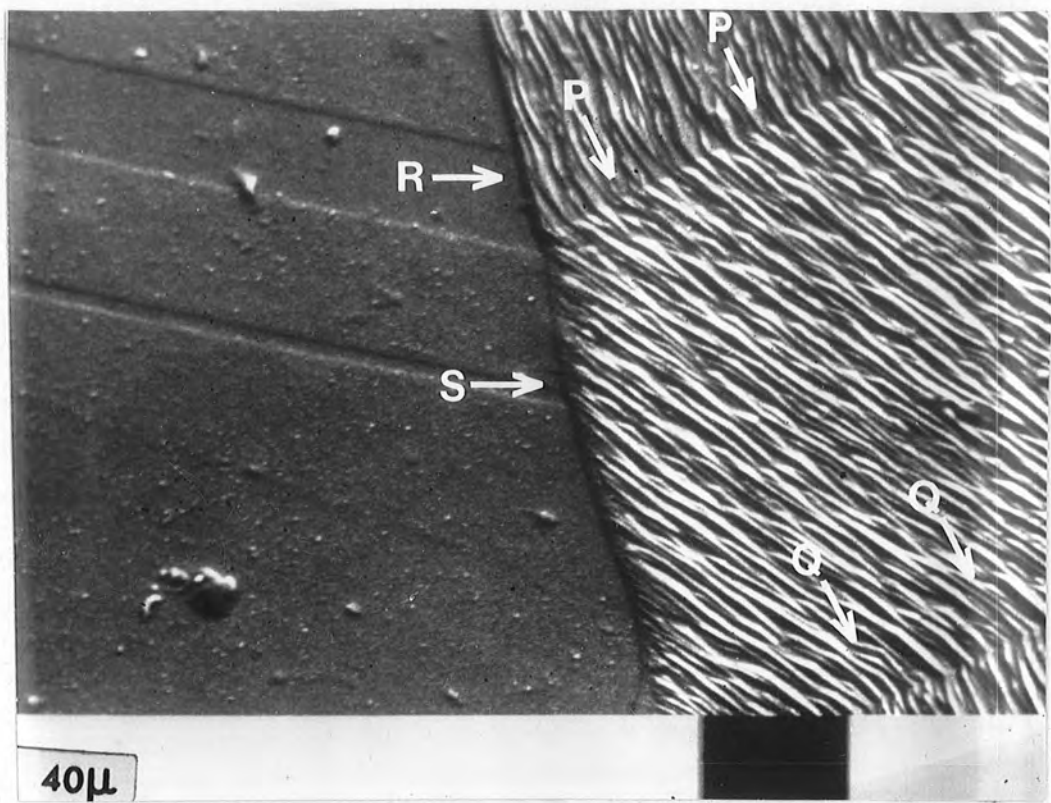what effect optical irradiation of the sample would have on the EBIC signal.

Fig. 7.7(a) Secondary Emission Micrograph showing Twin Bands R , S and PP-QQ intersecting a Grain Boundary.
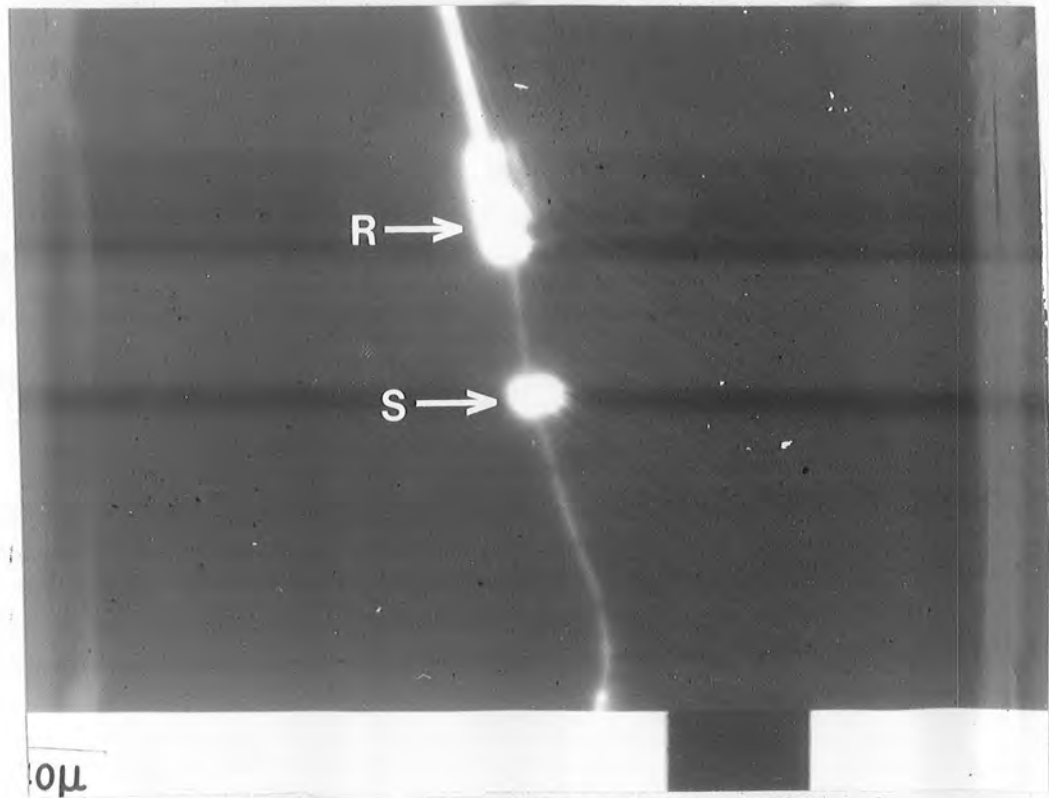

Fig. 7.7(b) EBIC Micrograph of the region shown in figure 7.7(a) showing the modification to the signal where the Twin Bands meet the Grain Boundary.
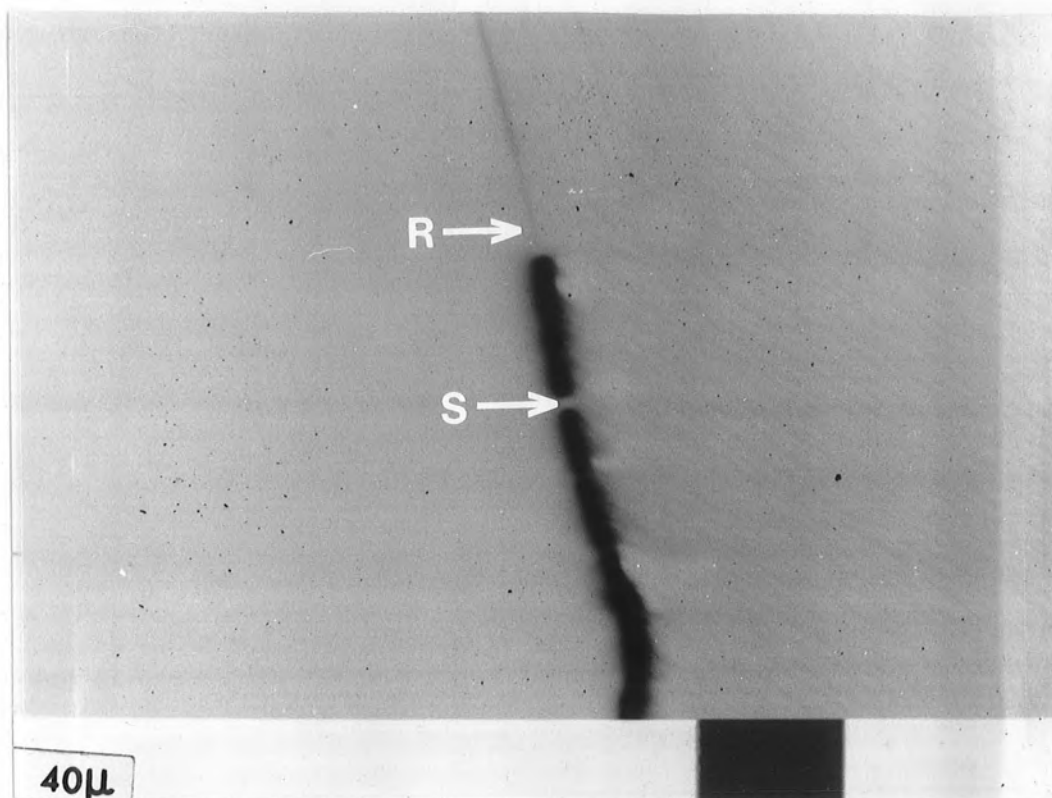
Fig. 7.7(c) Same as figure 7.7(b) with the polarity of the applied voltage reversed.
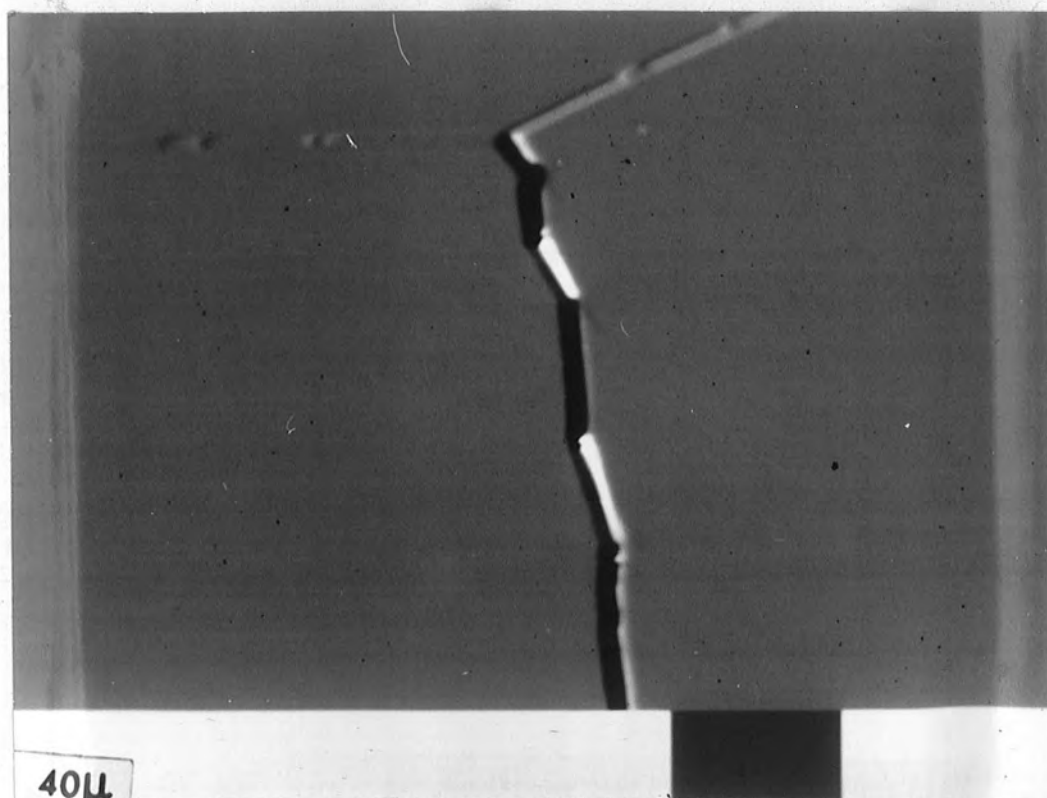

Fig. 7.8 EBIC Micrograph from another Grain Boundary in ZnSe:In with zero applied voltage.

For this purpose, a 48 watt tungsten lamp was mounted near to the sample inside the column of the SEM. The line traces in figure 7.9(a,b) were then obtained. The two traces in each photograph represent two EBIC signals of the same part of the grain boundary, but in a single line scan, which displays a graph of the magnitude of the EBIC signal as the beam scans a single line in the crystal along a direction almost perpendicular to the grain boundary. The upper trace shows the EBIC signal without illumination, while the lower trace shows the same signal with the sample illuminated, illustrating a strong reduction in the EBIC signal. This suggests that the potential barrier is reduced under illumination and hence, a larger bias current flows through the sample when the beam is remote from the grain boundary, and a relatively less pronounced increase in the electron bombard-ment induced current occurs at the boundary. Furthermore, figure 7.9(b) illustrates the same effect but for the special case with a bias of about 4 mV without light (upper trace), being reduced in the lower trace, when the lamp was on (the measured bias was then 1 mV). No change was observed when the sample was maintained in the zero bias condition. It should be noted that this photoconductive effect of the reduction of the EBIC signal was observed with either polarity of the applied bias. The effect of the illumination was to change the measured resistance between end contacts (marked A and E in figure 7.2) from about 10^7 Ω to just under 10^5 Ω.

7.2.4 Emission Spectra

Finally, with one of the slices from boule ╫ 407 from which the electroluminescence glow intensity was reasonably strong, it was possible to measure the spectral distribution of the emission, using the same experimental arrangement described for photoluminescence measurements in chapter four. The sample was pulsed, as for figures 7.1 (a,b), to obtain a steady intensity of emitted light. Spectra were recorded at room temperature and liquid nitrogen temperature. The two emission curves were
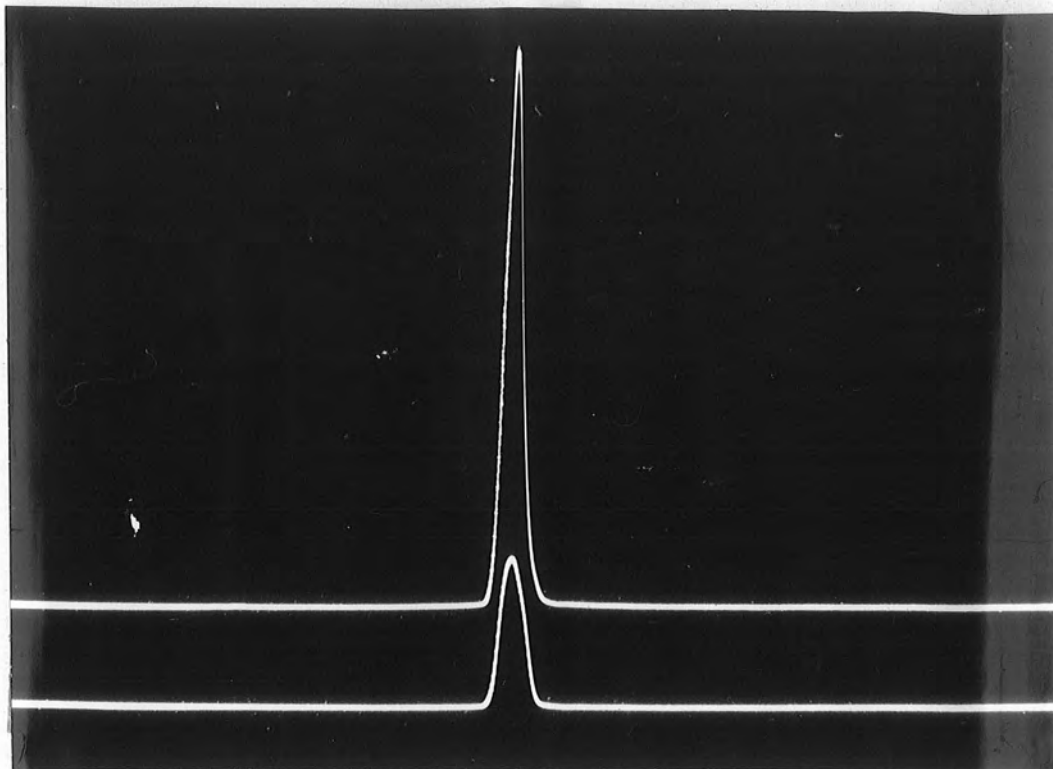
Fig. 7.9(a) EBIC line traces of the region shown in figure 7.3(a) with a positive bias. Upper trace without illumination. Lower trace under illumination.
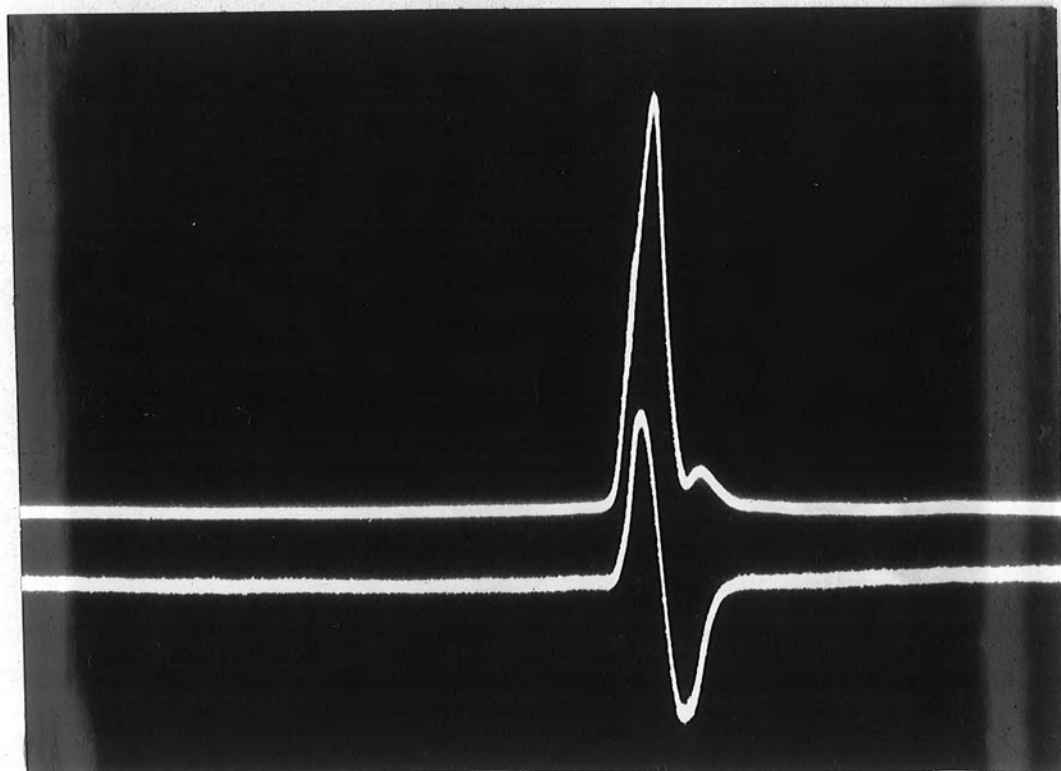

Fig. 7.9(b) Same as for figure 7.9(a) with a near zero bias.

identical to the photoluminescence spectra for a sample from the same
boule, shown as curves A in figures 5.1 and 5.2. The emission consisted
of a broad orange band centred at about 630 nm at room temperature, changing
to three bands at liquid nitrogen temperature centred at about 460 nm,
550 nm and 625 nm. Donnelly and Smith (1970) also measured similar spectra
in similar conditions ; however, their peaks were much too broad to be
resolved, probably because they used zinc treated material and not an as-
grown sample as here. The electroluminescence of their sample was very
weak so that they had to use their monochromator with its slits wide open.
Nevertheless, from their graph, it can be seen that the emission peak is
centred at about 650 nm at room temperature, while at 77 K there are two
peaks at 550 nm and 630 nm, which agrees well with our results.

7.2.5 Discussion

According to Russell et al (1980), the EBIC observations can be
explained in terms of a qualitative model which can be understood by
referring to the potential energy diagrams shown in figure 7.10. At some
grain boundaries the conduction and valence bands of the n-type ZnSe will
be bent upwards as illustrated in part (a) of this figure. The band bending
may well be a consequence of the segregation of impurities to the grain
boundaries where they can act as acceptor states. Electrons from donors
in the immediate vicinity would be captured by the acceptors, producing
a layer of negative charge at the grain boundary and leaving a region of
positive space charge in the ZnSe close to the boundary. The width of
the resultant depletion region would depend on the conductivity of the
grain and the concentration of surface acceptor states at the grain boundary.
The suggestion is therefore that each grain boundary would be accompanied
by a potential barrier similar to that in figure 7.10(a), so that each grain
boundary would have a built-in electric field associated with it. When such
grain boundaries with their associated depletion regions form a continuous
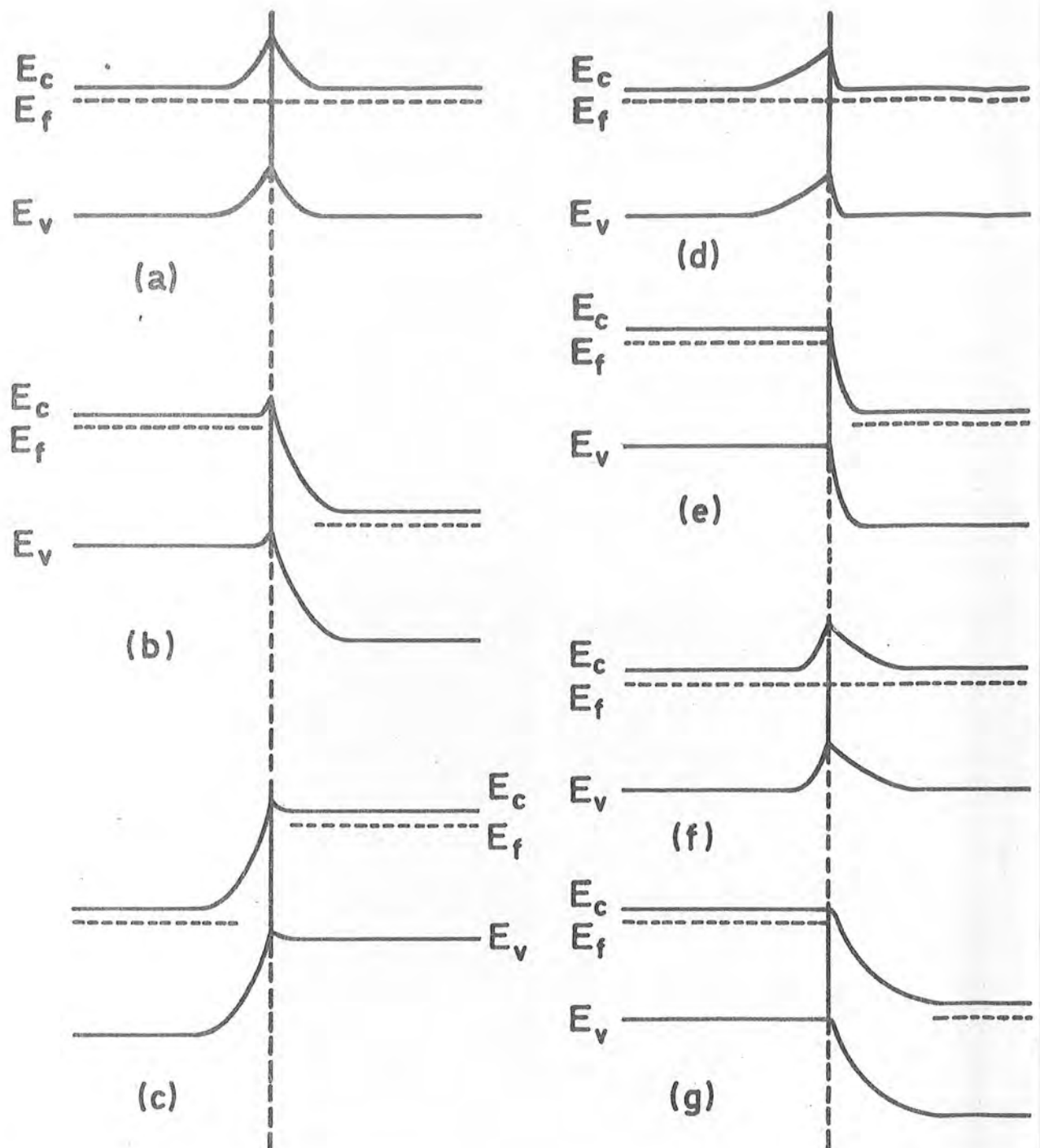barrier between contacts, they will limit the total current flow. Electron

Fig 7.10: Energy band diagrams for :

    (a) A symmetric grain boundary without bias

    (b) The boundary in (a) with negative bias on the left-hand side.

    (c) The boundary in (a) with negative bias on the right-hand side.

    (d) An asymmetric grain boundary, without bias.

    (e) The boundary in (d) with negative bias on the left-hand side.

    (f) The other configuration for an asymmetric grain boundary without bias.

    (g) The boundary in (f) with negative bias on the left-hand side.

bombardment within a depletion region will then lead to a beam induced
current so that contrast will be observed in the EBIC mode. When a grain
boundary forms a connecting path between the contacts, the accompanying
depletion regions will have a very small effect on the total current flow,
with the result that bombardment within the depletion region will have
virtually no effect on the total current flow. No EBIC contrast therefore
will be observed.

Consider next what happens when the electron beam is scanned from
left to right across a grain boundary with an associated potential barrier
such as that depicted in (a) of figure 7.10. Assume first that zero bias
is applied. When the beam reaches the left-hand depletion region, the beam-
induced electron hole pairs are separated by the internal field, and the
majority carriers (electrons) are swept towards the left-hand contact while
the minority carriers (holes) recombine via the recombination centres at
the grain boundary with electrons captured from either side of the boundary.
That such recombination centres exist is demonstrated by the cathodo-
luminescence image in figure 7.11, which is for the same region as in figure
7.8, and shows that the luminescence is suppressed at grain boundaries. If
the sample is connected so that the electron current flows to the left from
the grain boundary, it produces a dark image on the screen, then a black
line will be formed just to the left of the grain boundary. When the beam
reaches the right-hand side of the grain boundary, the current flowing in
the external circuit will reverse and electrons will flow from left to right.
A white line will then be produced in the EBIC image. This is exactly what
is observed in figure 7.8.

When a bias is applied to the sample, the potential energy barriers
become asymmetric as shown in figures 7.10 (b) and (c), which are for the
two possible polarities of the applied voltage. As the beam scans a biassed
barrier, figure 7.10(b), little separation of the induced electron-hole

pairs to the left of the barrier occurs, so that the total current is only slightly affected. On the right-hand side of the barrier, however, a high field exists so that the electron-hole pairs are readily swept apart. As a result, an intense white line appears in the EBIC image as in figure 7.3(b). With reversed polarity the potential energy diagram in figure 7.10(c) is appropriate and clearly the beam induced electron current now flows from right to left, producing a dark line in the EBIC mode, figure 7.3(c). In effect, if the barriers in (b) and (c) of figure 7.10 are regarded as two Schottky barriers back-to-back, one of the Schottky barriers is biassed in the forward direction and the other in the reverse. A beam induced current would only be expected at a reverse-biassed Schottky barrier. In this discussion of the contrast when an external voltage is applied, it has been assumed that virtually all the voltage is dropped across the grain boundary. This is indeed a reasonable assumption as the micrographs obtained in secondary emission with voltage contrast (figures 7.6(b) and (c)) show.

The more complicated EBIC effects illustrated in figures 7.7(b) and (c) can be explained if the extent of the band bending is different on either side of the grain boundary, as in (d) and (f) of figure 7.10, and varies when the crystallographic orientation of the grains changes (for example when twin bands intersect the grain boundary). The different widths of the black and white portions of the unbiassed EBIC images in figure 7.8 can also be explained with the same model, namely that a barrier such as that in (d) of figure 7.10 will have a broader stripe of contrast on the left corresponding to the wider depletion region.

With the appropriate bias applied, the barrier in figure 7.10(d) goes over to that in 7.10(e), while 7.10(f) goes to 7.10(g). In 7.10(e), the internal field is large and the depletion region is relatively narrow ; as a result the white line in the EBIC image is narrow as can be seen in the bottom half of figure 7.7(b). With the situation shown in figure 7.10(g)
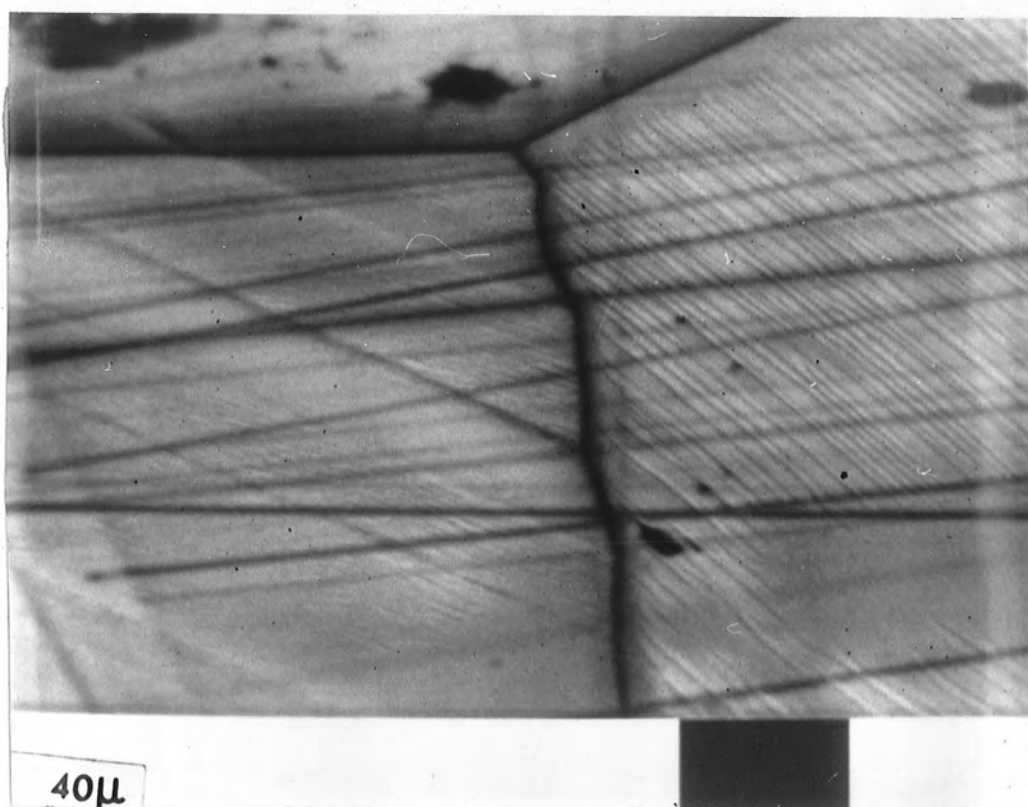
Fig. 7.11 Cathodoluminescent image of the region shown in figure 7.8 .

however, the electric field extends over a wider region, leading to the broader white region at the top of figure 7.7(b). When the bias is reversed, figure 7.10(e), for example, will be replaced with a diagram in which the space charge region now on the left of the barrier is wider than that on the right in figure 7.10(e). This means that reversal of polarity will lead to the replacement of a narrow white stripe with a broad black one ; a narrow black line will also replace a broad white one. This is clearly shown in figure 7.7(c).

Donnelly and Smith (1970) also suggested the formation of two back-to-back Schottky barriers resulting from the possible segregation of indium precipitates to the grain boundary. They carried out some X-ray analysis of the boundaries and concluded that a low angel tilt boundary (2°-4° between 111 planes) existed at the plane from which the "light" was emitted ; thus another possible explanation is that lattice misfit at the low angle boundary results in a network of edge dislocations and therefore produces dangling bonds which could act as acceptors.

The emission of light which accompanies the voltage breakdown in this material, at least for the sample from which the spectra were recorded, seems to come from the whole of the bulk of the sample, not just from the boundary, indicating a photoluminescence effect rather than an electro-luminescence one, produced by U.V. excitation resulting from the "sparks" or dots of intense white light (microplasmas) appearing in the boundary when this process is taking place.

7.3   CATHODOLUMINESCENCE MODE OF THE S.E.M.

The S.E.M. can also be used in the cathodoluminescence (CL) mode as was explained in chapter four, and this has also proved to be a valuable technique for relating defect structure to electrical behaviour as reported for instance by Magnea et al (1979), Bensahel and Dupuy (1979a,b) and Bensahel et al (1979),in annealed ZnTe. The micrograph in figure 7.11

was obtained using this mode.

It was decided to use the CL technique to examine some of the indium doped ZnSe crystals grown in the department and discussed in the last two chapters. As stated in chapter six, marked differences in electrical properties were exhibited by samples cut from different ends of the same boule, i.e. Nos. ⧣ 342, ⧣ 408 and ⧣ 410 containing approximately 100 ppm, 250 ppm and 100 ppm of indium respectively. Boule ⧣ 410 showed the largest variation in body colour and in electrical behaviour. Hence, two slices, 1 mm thick, were cut from either end of this boule and each was subsequently heated in zinc vapour at 850° C. After etching, the slices were examined under the optical microscope (OM) where a large number of dark precipitates, which are a consequence of the annealing process, were immediately evident. One specimen of each slice was then mounted side by side in the SEM and studied in the CL mode. The first effect to be noticed was that all the grain boundaries appeared as dark lines which, as will be shown in the next paragraph, indicates the presence of radiationless centres. Moreover, the precipitates observed with the optical microscope, also suppressed the luminescence. In this way, it was found that the only difference between the two pieces from either end of the boule was (figure 7.12a,b) that the sample cut from the tip (i.e. the first part of the crystal to grow) contained many more dark centres than did the sample cut from the last part of the crystal to grow, which may suggest a strong difference in stoichiometry.

Some more interesting results have been obtained by using the CL technique to study a piece of boule ⧣ 349 (nominally doped with 1000 ppm of indium) which had been heated in molten zinc at 850° C for five days. These results are shown in the four photographs of figures 7.13(a-d). Parts (a) and (c) of this figure represent SEM micrographs in the CL mode, while parts (b) and (d) of the same figure are the corresponding optical trans-
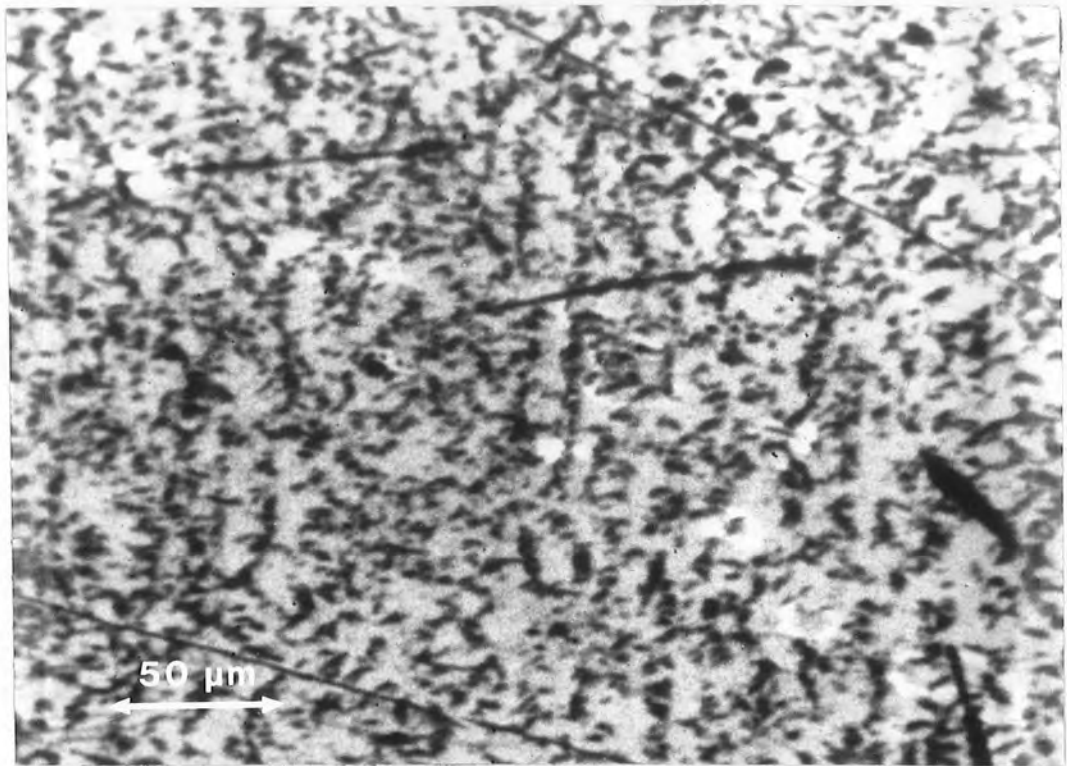
Fig. 7.12(a) Cathodoluminescent image of a zinc vapour annealed ZnSe:In Sample which was cut from the end of the Crystal that grew first.
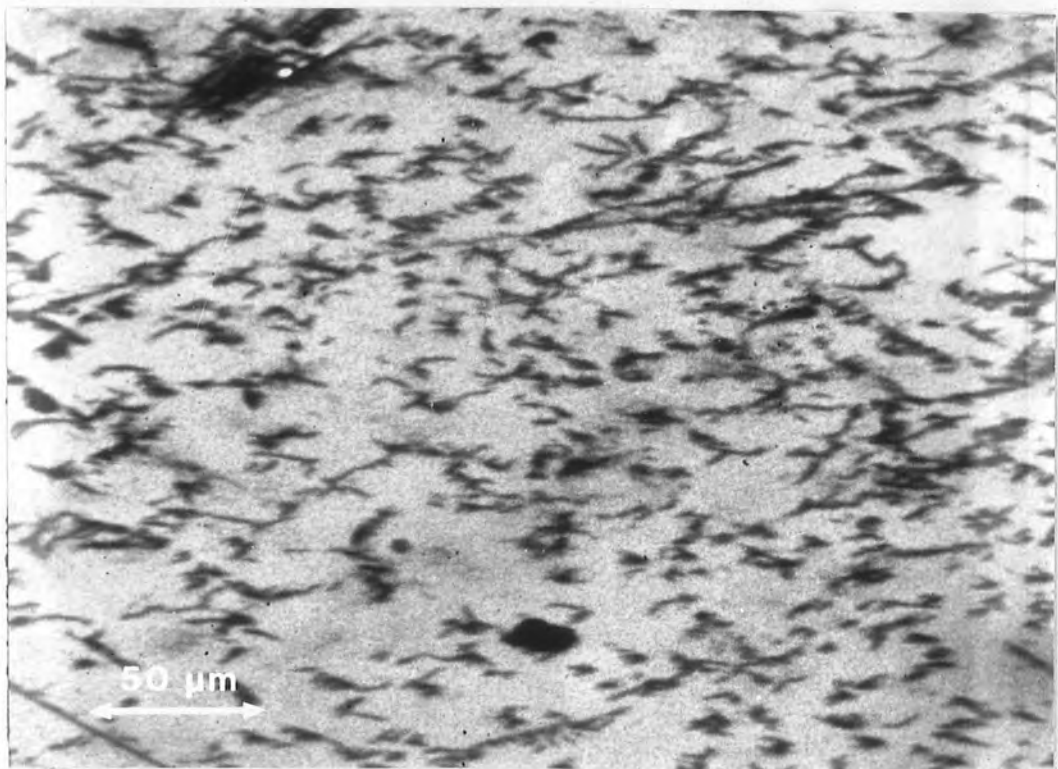

Fig. 7.12(b) Cathodoluminescent image from a zinc vapour annealed piece of the same ZnSe:In Crystal Boule as in figure 7.12(a) but cut from the end that grew last.

Fig. 7.13(a) Cathodoluminescent image of a ZnSe:In Sample annealed
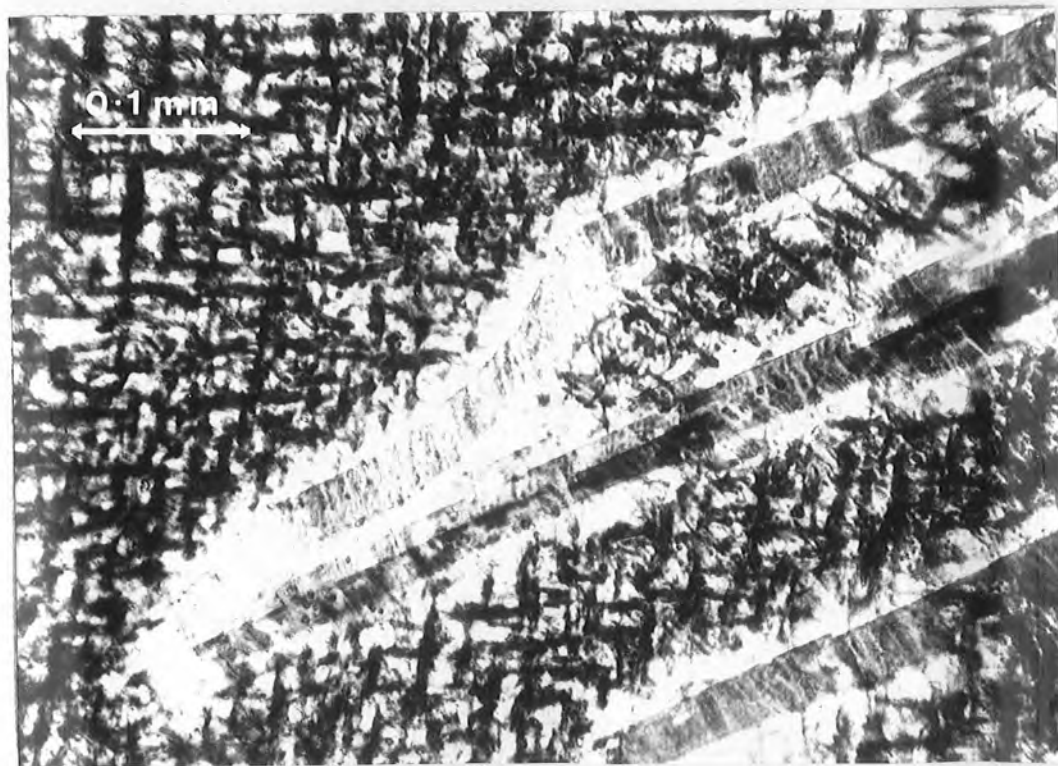in molten zinc.

Fig. 7.13(b) Optical Transmission Micrograph of the same region shown
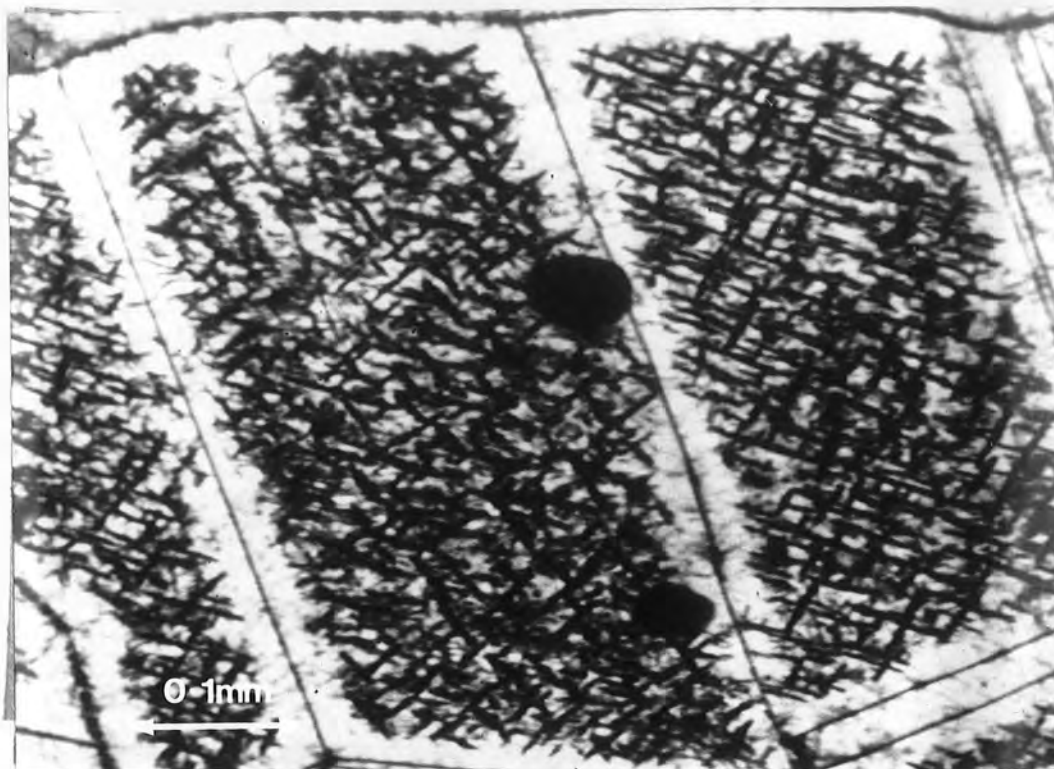in figure 7.13(a).

Fig. 7.13(c) Cathodoluminescent image of a different region from the same Sample as in figure 7.13(a).

Fig. 7.13(d) Optical Transmission Micrograph of a region adjacent to that shown in figure 7.13(c).

mission micrographs. The micrographs in figures 7.13 (a) and (c) show the CL response of the specimen surface and the dark regions indicate the presence of radiationless recombination centres. From the micrographs in parts (b) and (d) of the same figure 7.13, some decorated grain boundaries and/or stacking faults are seen as broad dark lines, while the precipitates appear as badly formed short segments forming a cross. If these optical transmission micrographs are compared with the micrographs in figures 7.13 (a) and (c), it is then clear that the precipitates, as well as the grain boundaries and stacking faults contain mainly radiationless centres. The effect of such a large number of dark regions is to reduce the total integrated luminescence intensity from the sample. This explains the observation reported in chapter five that the as-grown crystals had a stronger emission intensity than those treated in zinc vapour.

Another interesting result is that in the vicinity of the grain boundaries, a relatively large region denuded of precipitates appears. This seems to indicate that the precipitates formed in the proximity of the grain boundary migrate preferentially to the boundary to decorate it. The broadening of all the dark features in figure 7.13 (b) compared to figure 7.13 (a) is due to the fact that the CL mode looks at the surface only, while in the optical microscope, at medium magnification, a larger depth inside the crystal is imaged showing that the dark surface features in figure 7.13(a) do go slightly deeper, at an angle with respect to the direction of view in the OM.

7.4   PRECIPITATES

When ZnSe crystals containing a dopant concentration of at least 50 ppm of indium or gallium were annealed in zinc vapour, at temperatures of 600° C or more, some darkening of the samples resulted. This darkening, as reported by Wagner and Lorenz (1966), Jones and Woods (1976) and Ray and Kröger (1978b), is caused by the presence of dark precipitates. If the extent of the precipitation is assumed to be proportional to the darkness

of the crystal, then the number of precipitates grows with the dopant concentration $\begin{bmatrix} In \end{bmatrix}$ or $\begin{bmatrix} Ga \end{bmatrix}$ at a fixed annealing temperature. It also increases with the annealing temperature for fixed $\begin{bmatrix} In \end{bmatrix}$ or $\begin{bmatrix} Ga \end{bmatrix}$. The precipitates are undoubtedly caused by the presence of indium or gallium in the material, since undoped or aluminium doped crystals of ZnSe, heavily annealed in zinc shows no precipitation at all.

7.4.1 Study Under the Optical Microscope

Figure 7.14 is an optical transmission micrograph of a slice from boule $\#$ 408 (about 250 ppm of indium) heat treated in zinc at 850° C showing short segments of precipitates crossing each other at different planes giving the appearance of badly formed rosettes. Figures 7.15(a), (b) illustrate further short segments of precipitates together with decorated stacking faults. The micrographs suggest that these particular precipitates lie in crystallographic planes. A closer look at the groups marked A and B in the photograph of figure 7.14 shows what may be two perpendicular planes (e.g.(100) planes) of precipitates which are parallel to the direction of view and therefore are sharply defined, while there are also some more diffuse planes (possibly (111)) intersecting the former at 45°; the (111) planes do not contrast as well as the (100) because the precipitates appear in a larger area of the field of view. This leads to the conclusion that some precipitate nucleation began at the intersection of the (100) type planes, and segregation followed the crystallographic symmetry of the particular grain as can be seen in the two micrographs of figures 7.15(a) and (b).

Finally, figure 7.16 illustrates a piece of boule $\#$ 349 similar to the one shown in figure 7.13 but chemically thinned for later use in the T.E.M. The edge of the specimen can be seen towards the bottom right-hand side of the picture where it is already thin enough to show interference fringes when viewed in reflection in the OM. The specimen becomes uniformly thicker towards the left of the figure. Some decorated stacking faults which
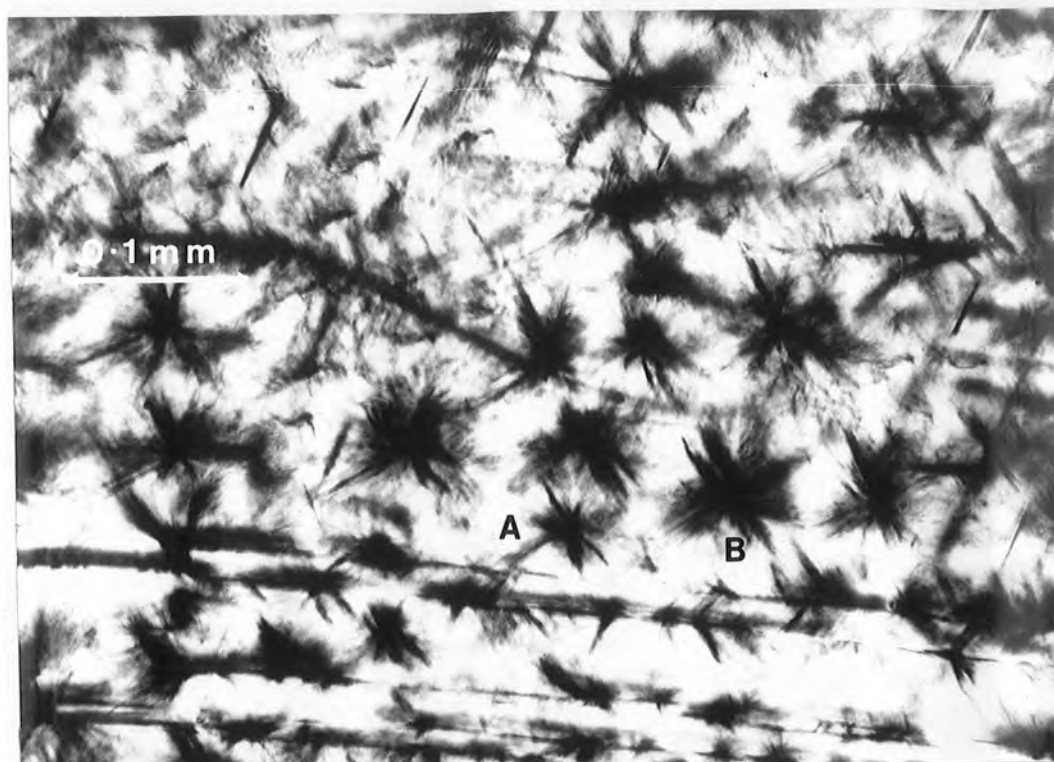
Fig. 7.14   Optical Transmission Micrograph of a ZnSe:In Sample annealed
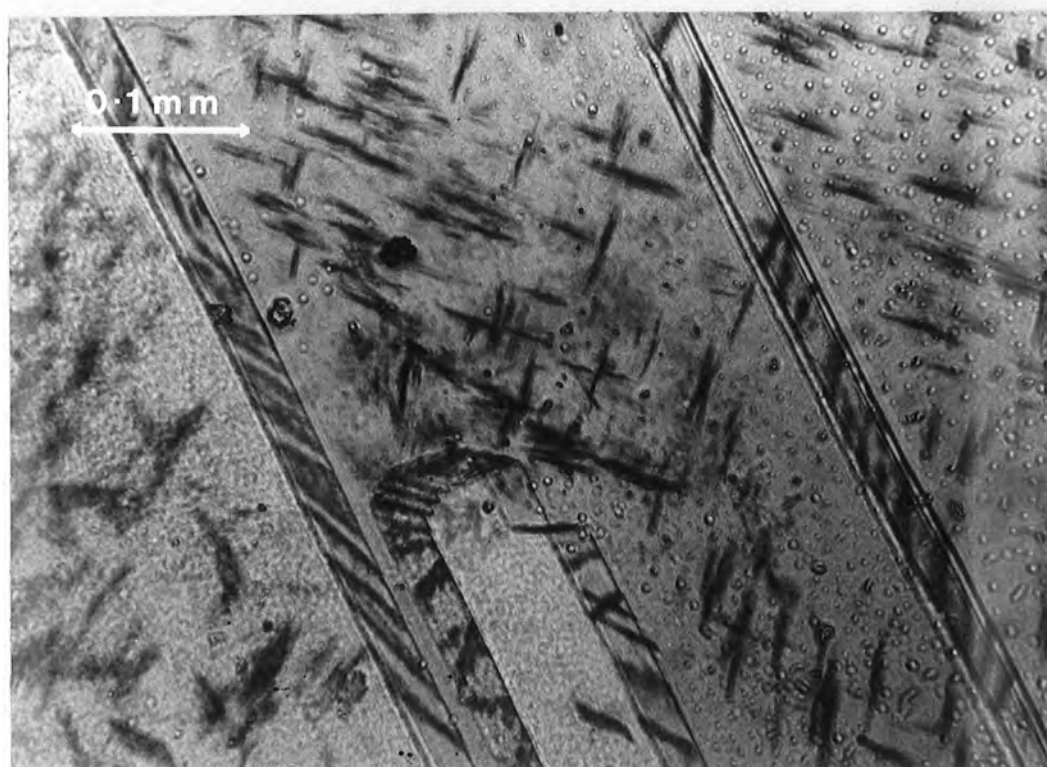   in zinc vapour.

Fig. 7.15(a) Optical Transmission Micrograph of a ZnSe:In Sample
             annealed in zinc vapour.

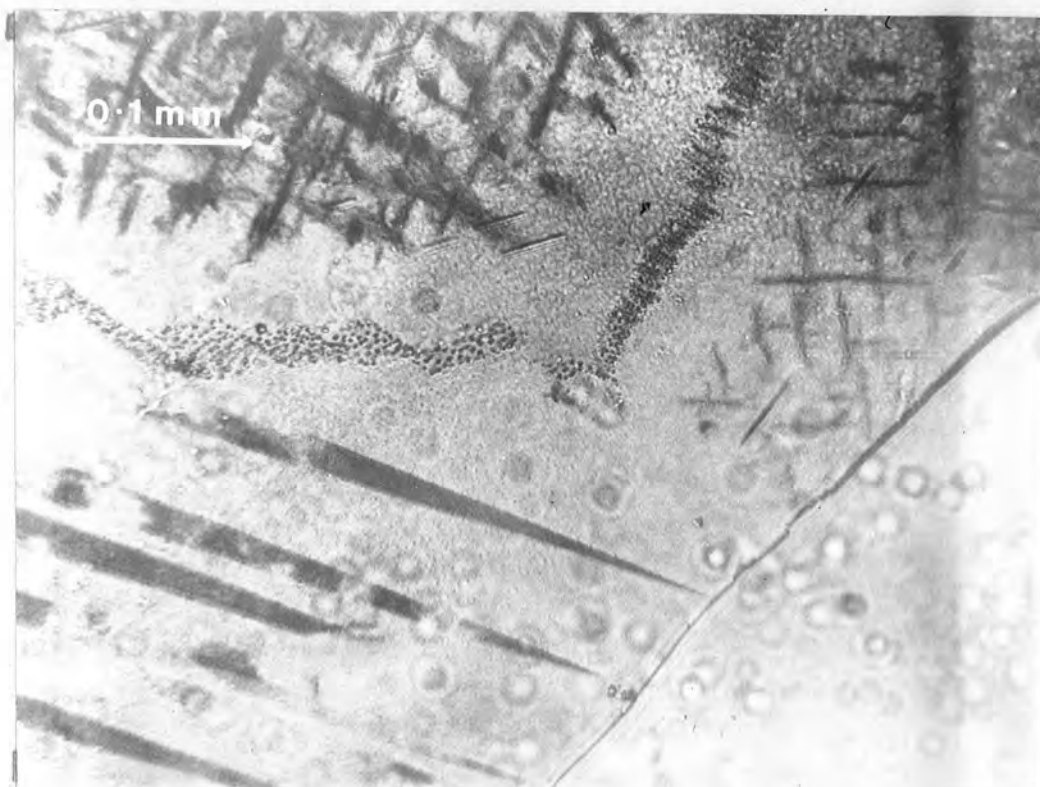Fig. 7.15(b) Same as figure 7.15(a) for a different region.

Fig. 7.16 Optical Transmission Micrograph of a ZnSe:In Sample annealed
in molten zinc.

are almost parallel to the direction of view can be seen in the lower part of the specimen ; they seem to disappear towards the thin edge. A grain boundary, clustered with either precipitates or voids, runs from the mid left-hand side and disappears from the picture near the centre at the top. On either side of the top part of this grain boundary, another group of precipitates forming short cross-shaped segments can be seen ; they also tend to disappear where the specimen is thin. A denuded region is clearly seen at either side of the grain boundary.

7.4.2 Transmission Electron Microscope (TEM) Studies

Both as-grown and heat treated slices were prepared for study in the TEM, by chemically polishing them in HPC which consists of one part of a freshly made saturated solution of chromium trioxide in phosphoric acid, and two parts of concentrated hydrochloric acid, (Hemmatt and Weinstein, 1967). The progress of the polishing was followed by observing the surfaces of the slices under normal illumination in the OM at various stages of the process. Regions of the specimen were judged to be thin enough for TEM investigation when they gave rise to interference fringes when viewed in the OM.

All of the as-grown crystals doped with indium which were examined in the TEM exhibited a defect structure which was indistinguishable from that of undoped as-grown ZnSe, Cutter et al (1976). The same was also true of the samples from boules $\#$ 407 and $\#$ 413 (with about 10 and 20 ppm of indium respectively) which had been heated at 850°C in liquid zinc for five days. To illustrate the various features observed in these samples, micrographs taken from a representative selection exhibiting a defect structure similar to that of as-grown and undoped ZnSe are shown in figure 7.17 (a-c). Figure 7.17 (a) shows a region of an undoped crystal heavily heat treated in zinc. The thickness fringes or extension contours lie parallel to the thin edge of the sample and, in the absence of defects that give rise to contrast in the TEM, they are not interrupted across the entire field of view. In contrast, the extinction

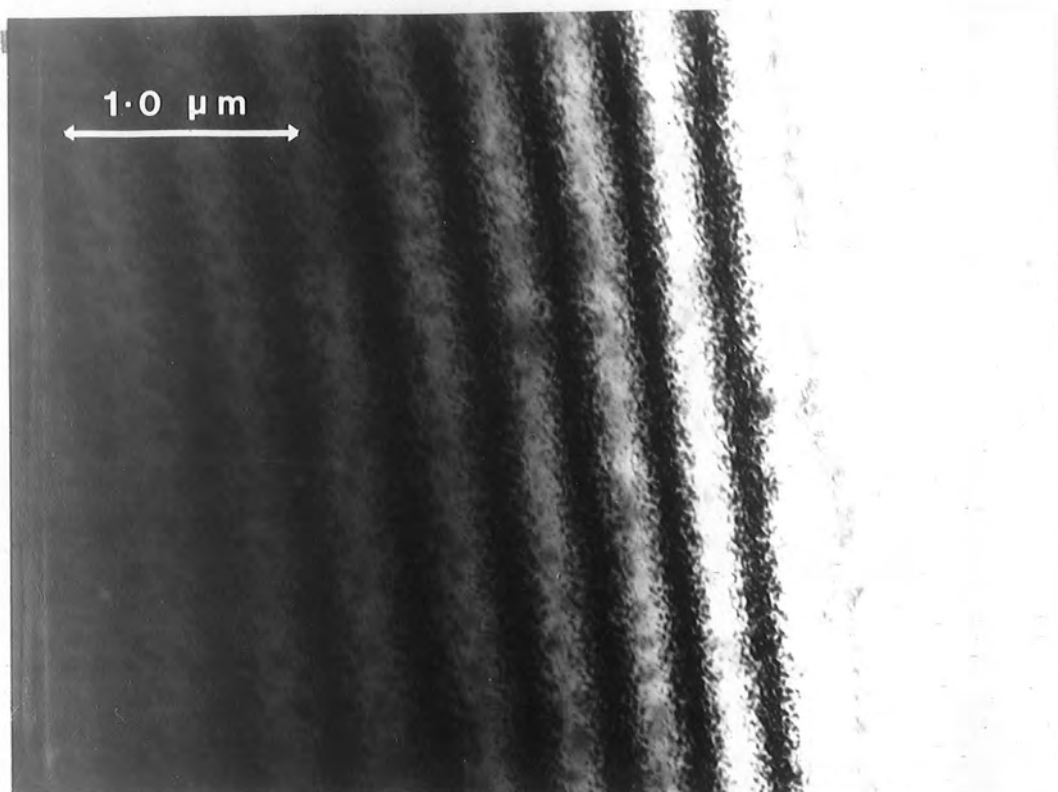Fig. 7.17(a) Transmission Electron Micrograph of Undoped ZnSe annealed
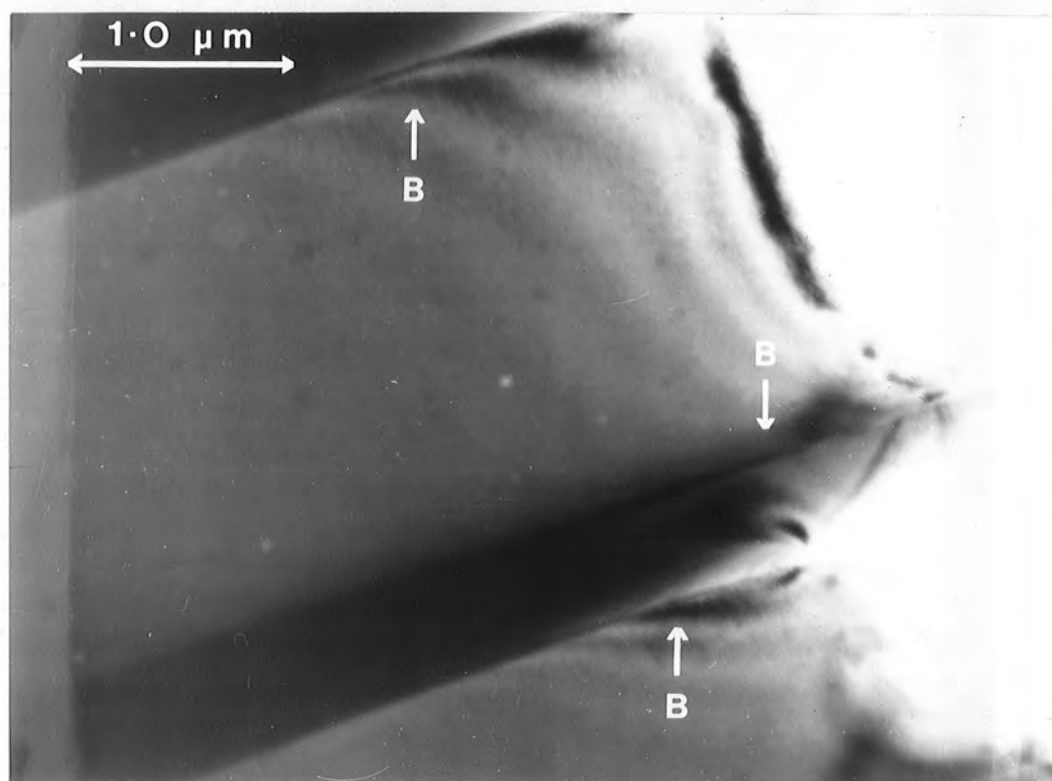in molten zinc at 850°C .

Fig. 7.17(b) Transmission Electron Micrograph of ZnSe:In (~10 ppm)
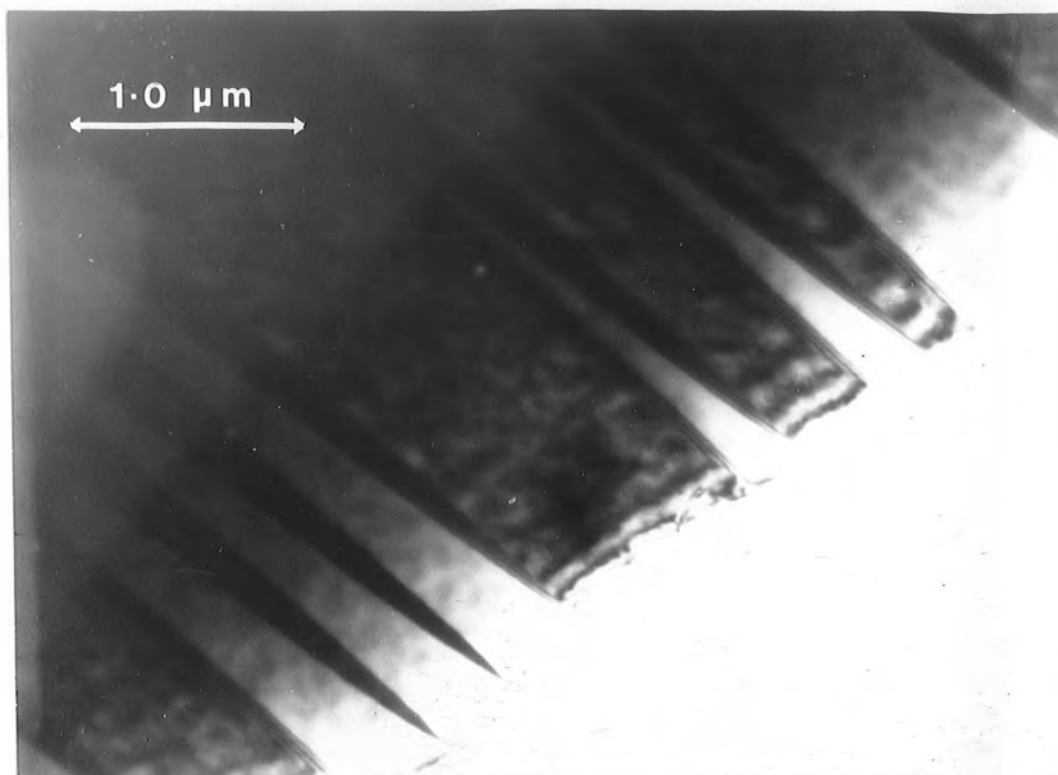annealed in molten zinc at 850°C .

Fig. 7.17(c) Transmission Electron Micrograph of ZnSe:In (~250 ppm) annealed in zinc vapour at 600°C .
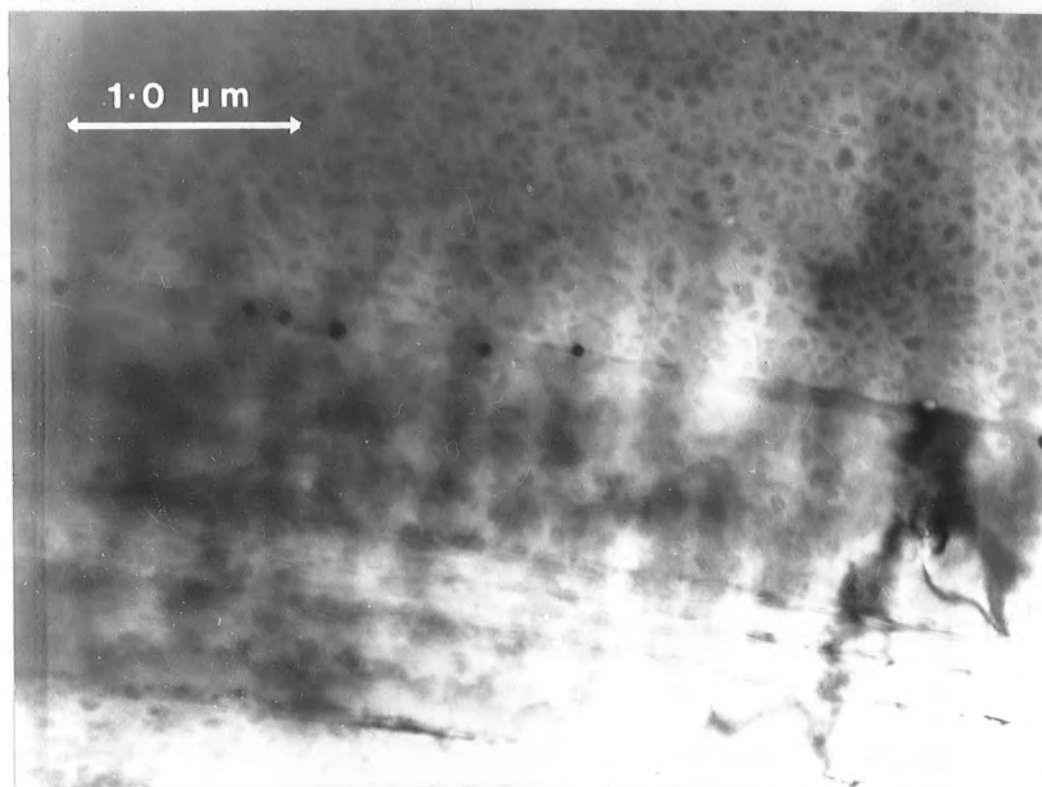

Fig. 7.18 The same as in figure 7.17(c) from another region showing small Precipitates along a Twin Boundary.

contours in figure 7.17 (b), which was taken from a sample from boule $\#$ 407, and which had been heated in zinc at 850° C, deviate abruptly at the points B which indicate the position of twin boundaries. In fact, twin bands were the defects most frequently encountered in this material. The frequency of the twinning varied enormously from sample to sample and even within the same sample. For instance, there are no twins at all in the undoped sample of figure 7.17(a) while regions like that in 7.17 (c) (representing a piece from boule $\#$ 408 heat treated in zinc vapour at 600° C) have several twin bands in an area of comparable size. Dislocations and stacking faults were not observed, and most of the specimens prepared from the slice cut from boule $\#$ 408 and heated in vapour at 600° C only exhibited twins. Small precipitates were observed to decorate some of the twin boundaries as shown in figure 7.18. The fine scale features, some 500 $\overset{o}{A}$ in size, in the top half of this micrograph are due to surface contamination arising during specimen preparation. The precipitates were only observed in a few boundaries in specimens which had received this particular heat treatment, but they usually occurred in groups on the isolated boundaries that they did decorate as shown in figure 7.18.

When samples containing 50 ppm or more of indium were heat treated at 850° C in liquid zinc for five days, then the precipitation process became much more pronounced. In particular, the precipitates were found to decorate all the twin boundaries as well as the intrinsic stacking faults and dis- locations, which were formed as a consequence of the heat treatment given to these crystals. Some micrographs showing stacking faults and dislocations in a specimen from boule $\#$ 405 are shown in figure 7.19 (a-d). The precipi- tates appear as small dark dots superimposed on the stacking fault fringes in figure 7.19 (a). The row of smaller features away from the stacking fault at A may also be precipitates. More definite evidence of small precipitates in the absence of stacking faults in this material is provided in figure 7.19(b). This micrograph illustrates a feature of the precipitation process which is
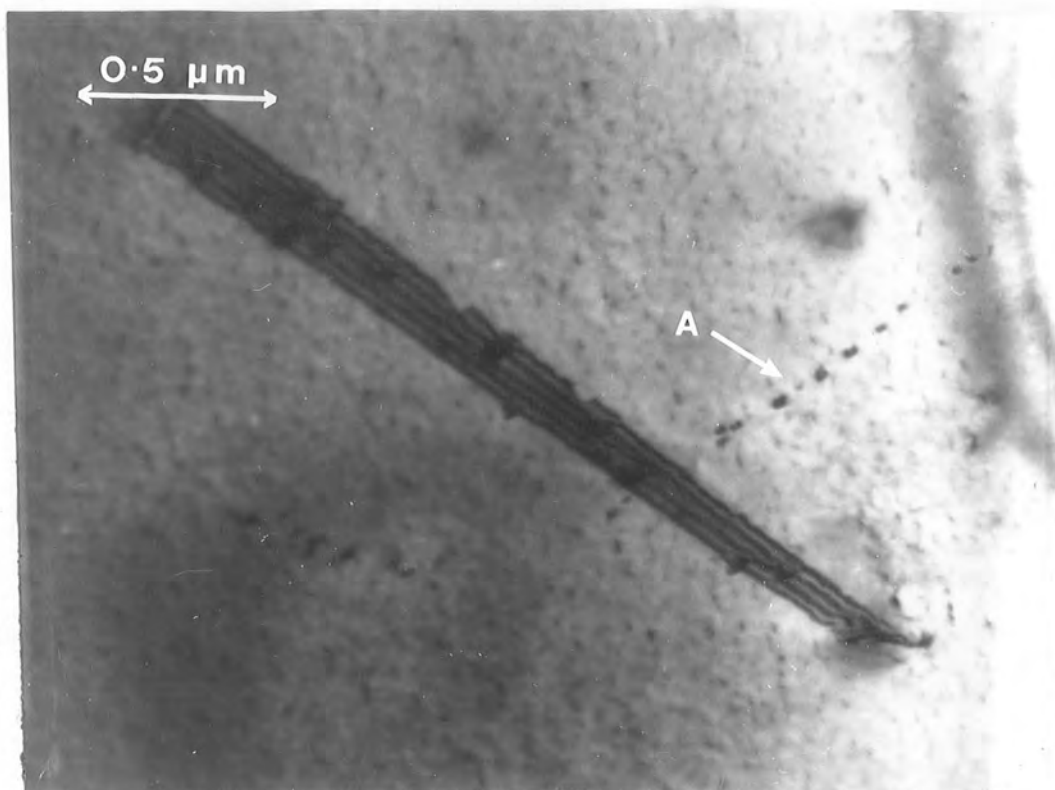
Fig. 7.19(a) Transmission Electron Micrograph of ZnSe:In (~55 ppm) annealed in molten zinc at 850°C showing Stacking Fault Fringes with Precipitates.

Fig. 7.19(b) Transmission Electron Micrograph of a different Specimen from the same Crystal as in figure 7.19(a).
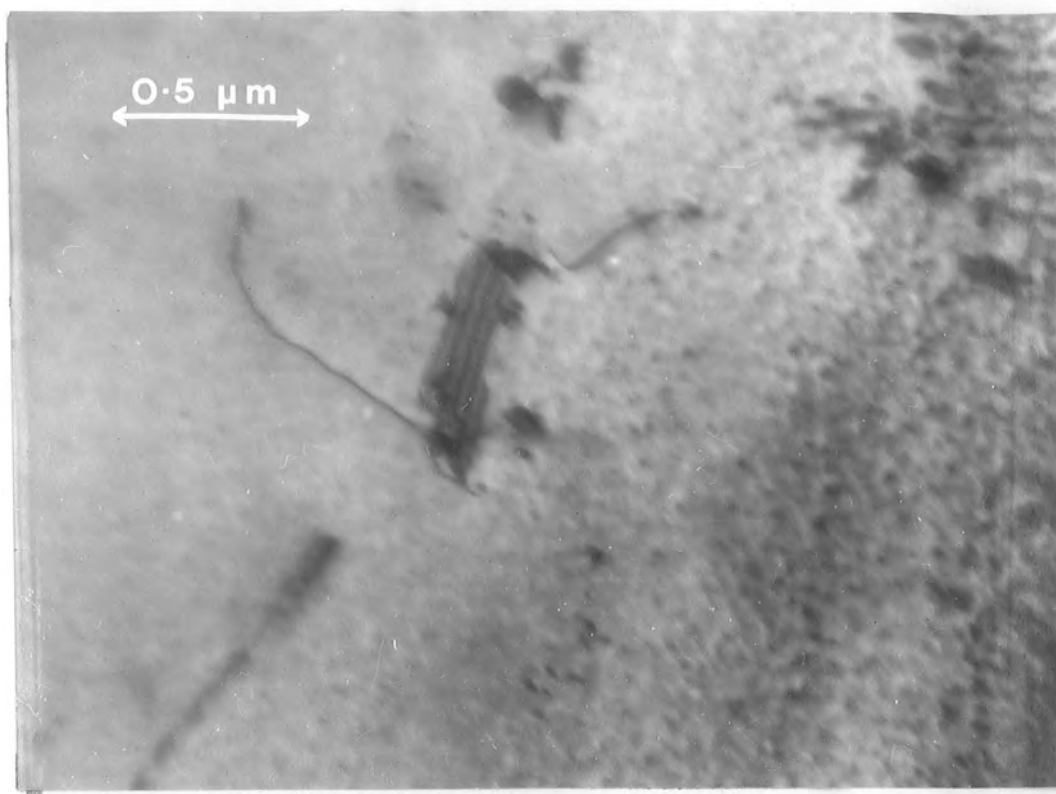
Fig. 7.19(c) Transmission Electron Micrograph of a third Specimen from
the same Crystal as in figure 7.19(a).
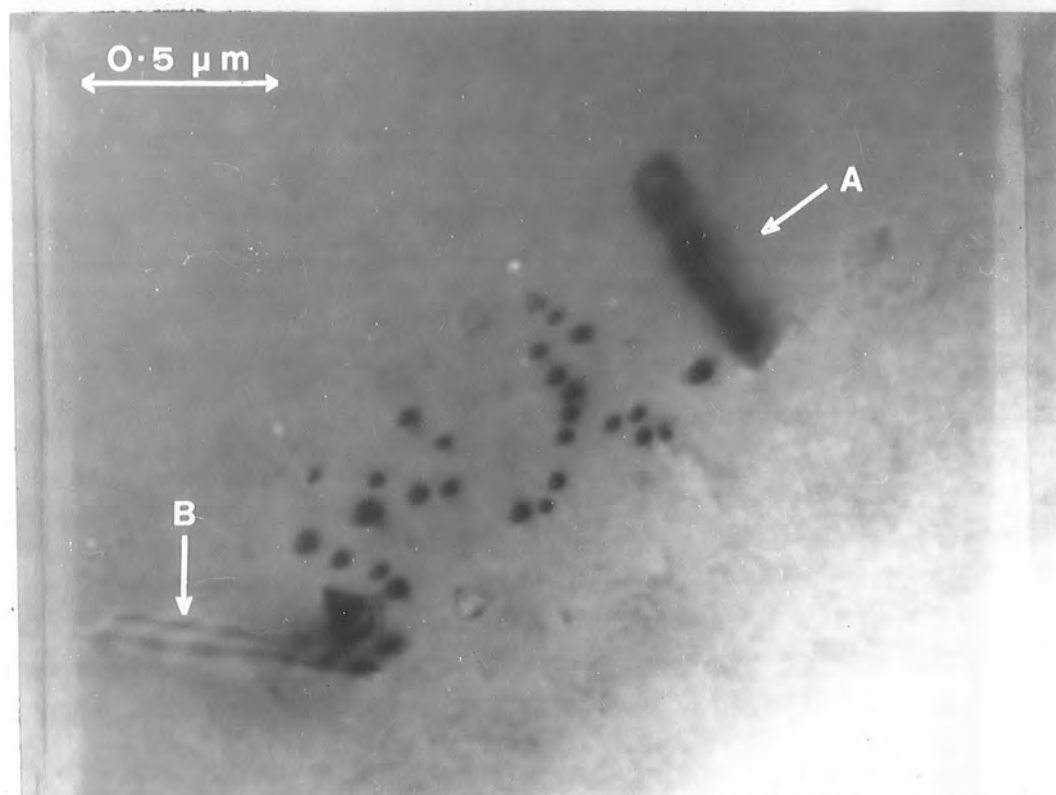
Fig. 7.19(d) Transmission Electron Micrograph of a fourth Specimen from
the same Crystal as in figure 7.19(a).

that the precipitates decorating stacking faults were invariably larger
than those not associated with other defects. Decorated defects such as
dislocations were also encountered but, as shown in figure 7.19(c), they
were usually present in association with stacking faults. A general feature
in all the samples with a low concentration ($\sim$ 50 ppm) of indium, is that
the precipitates even when as large as those shown in figure 7.19(d) did not
exhibit any well defined shape. The precipitates in this micrograph are
in particularly good contrast because the diffraction conditions are such
that the fringes of the stacking fault that they decorate between the
partial dislocations at A and B are in the invisible condition.

At higher indium concentrations as in boule ⧲ 408 with 250 ppm
of indium, the heat treatment at 850° C produced a correspondingly larger
number of precipitates on the stacking faults as shown in figure 7.20 (a).
Rather surprisingly the dislocation in this micrograph does not appear to
be decorated but at this concentration some of the precipitates, like that
at A, began to exhibit regular shapes. In this particular orientation, the
precipitates show a four-fold symmetry. In fact most of the precipitates
observed in samples from boule ⧲ 408 showed a well developed shape. Those
decorating the stacking fault in figure 7.20(b) are mainly spherical while
the others on the twin boundary in figure 7.20(c) are triangular.

As expected, the largest precipitates were found in the heat treated
samples from boule ⧲ 349 which contained the highest indium concentration of
1000 ppm. The precipitates decorating the stacking fault in figure 7.21(a)
are either spherical or show four-fold symmetry. Others lying along the
twin boundary in figure 7.21(b) represent the largest ones observed in this
study being about 0.2 µm in diameter. It was in this material that random
precipitation in the absence of other defects was most evident as illustrated
in figure 7.21(c). The large dark feature on the left-hand side of this
micrograph did not appear to interact with the dislocation network and is

Fig. 7.20(a) Transmission Electron Micrograph of ZnSe:In (~250 ppm) heated in molten zinc at 850°C showing Stacking Fault Fringes with Precipitates.

Fig. 7.20(b) The same as in figure 7.20(a) from another region showing Spherical Precipitates.
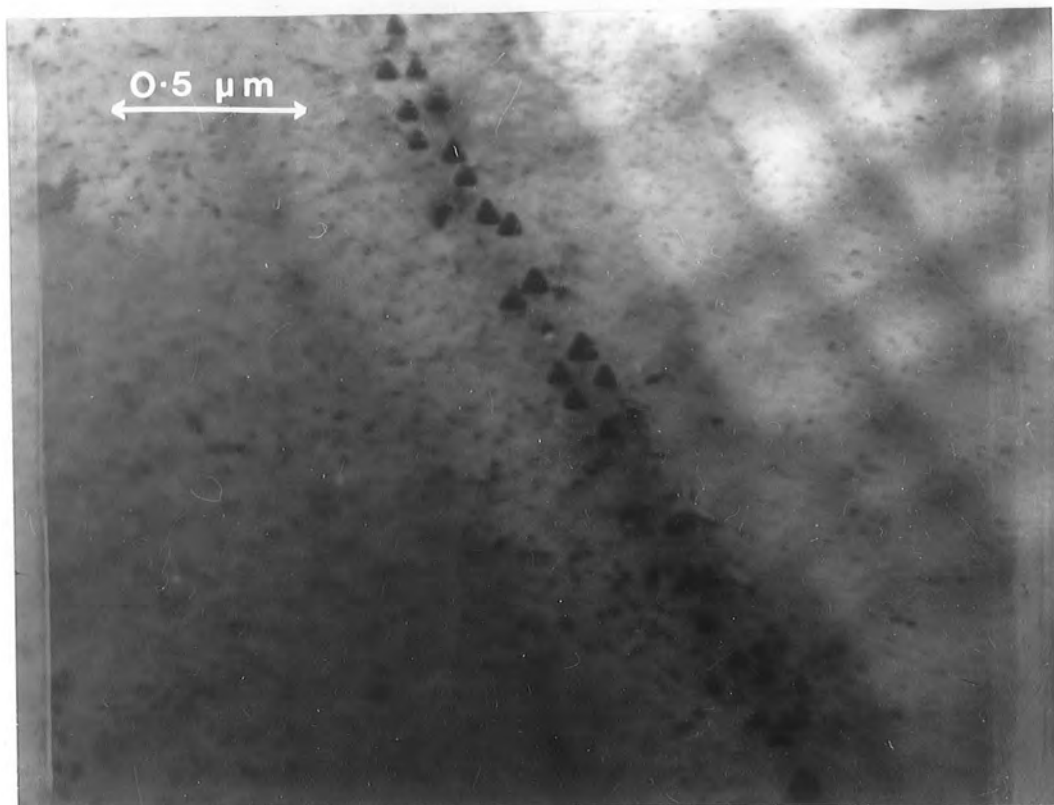
Fig. 7.20(c) The same as in figure 7.20(a) from another region showing "Triangular" Precipitates.
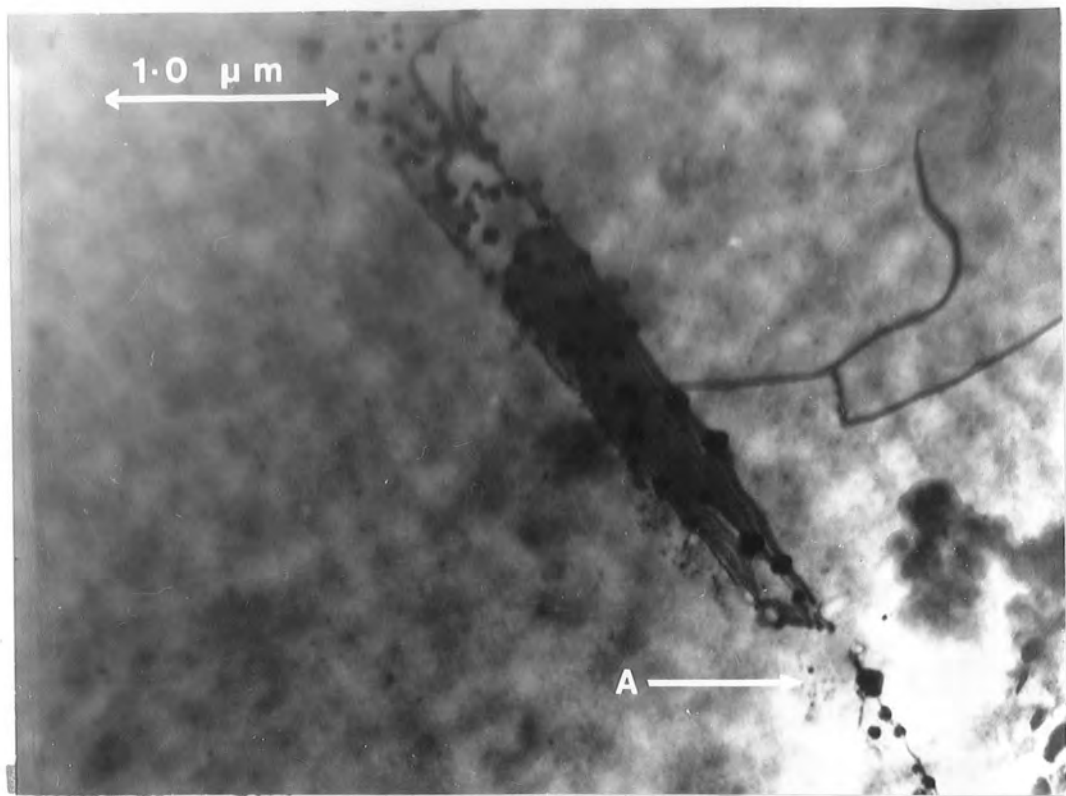

Fig. 7.21(a) Transmission Electron Micrograph of ZnSe:In (~800 ppm) heated in molten zinc at 850°C showing Precipitates Decorating a Stacking Fault.
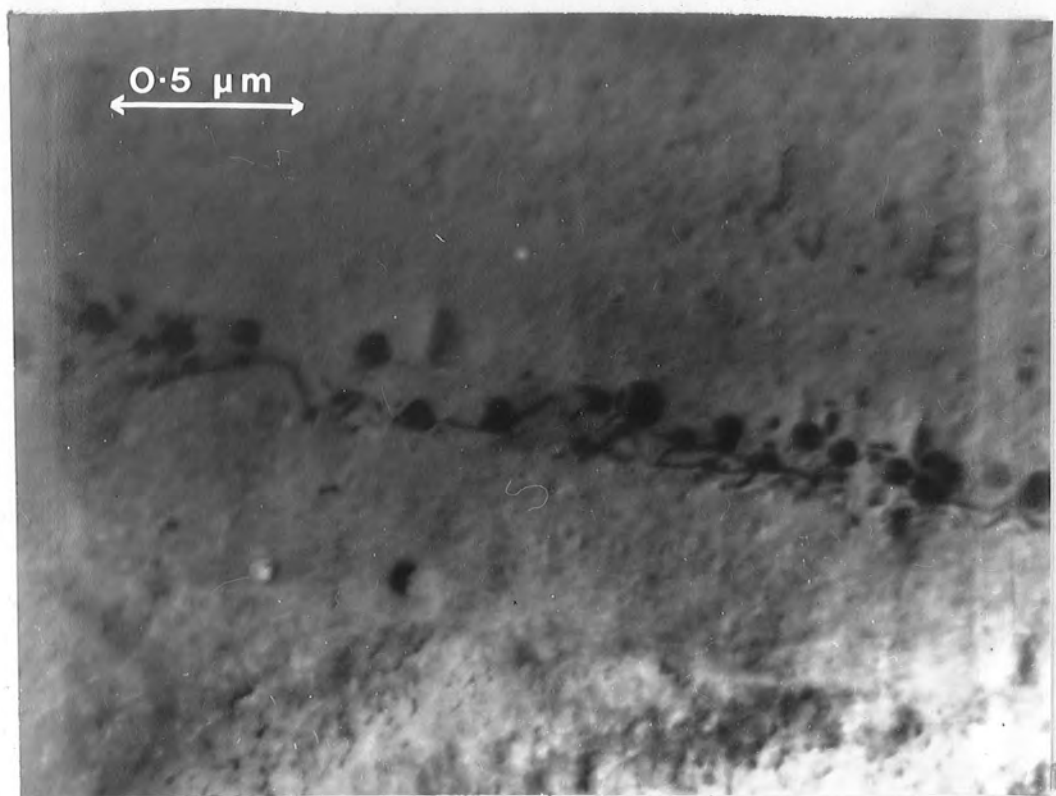
Fig. 7.21(b) The same as in figure 7.21(a) from another region showing
large Precipitates along a Twin Boundary.

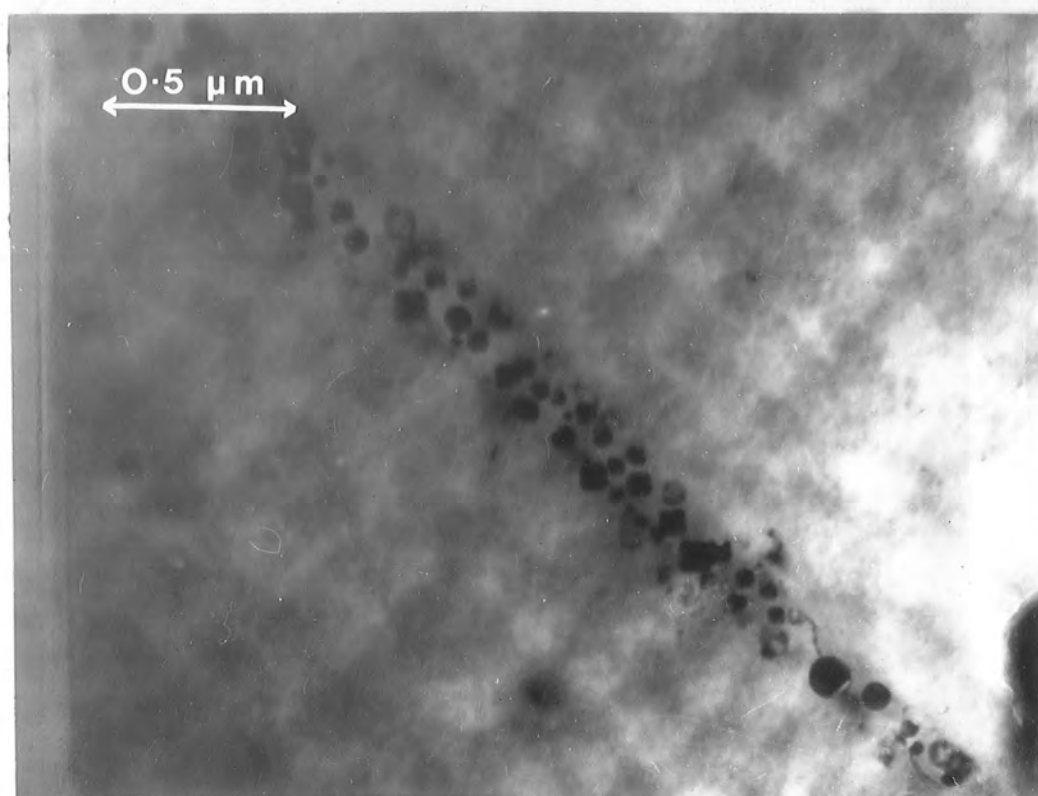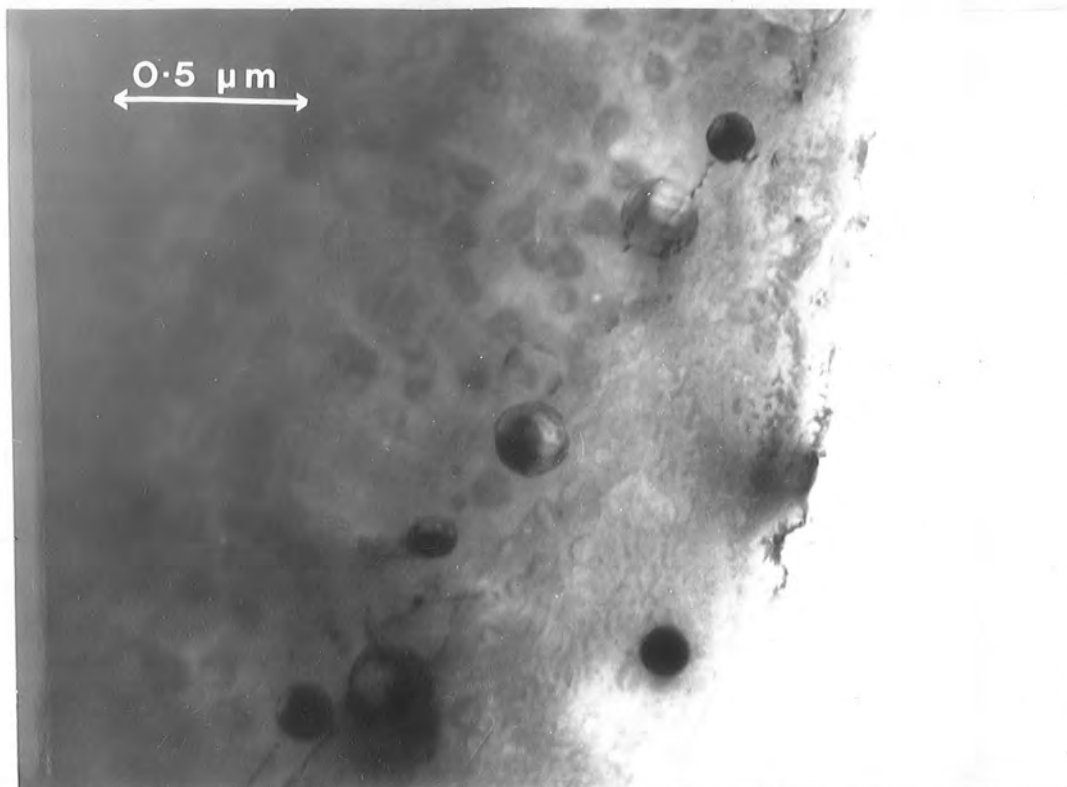Fig. 7.21(c) The same as in figure 7.21(a) from another region showing
Precipitates and Decorated Dislocations.

considered to be an artefact arising from specimen preparation. The variation in the extent of the precipitation from different regions of the same material is typified by the micrographs in figures 7.21 (a-c). This variation made a meaningful examination of the precipitates density at any of the levels of doping impracticable. Even the increase in number and size of the precipitates was not sufficient to give rise to additional spots in the diffraction pattern to enable a chemical identification to be made.

7.4.3 Discussion

The black precipitates have also been studied under the optical microscope by Jones and Woods (1976) and Ray and Kröger (1978b). Several shapes have been described, but no firm conclusion about the mechanism of their formation has been given. However, Ray and Kröger, working on gallium doped ZnSe heated in zinc vapour, have suggested that, because of their apparent colour, the precipitates may either be a solid solution of gallium with selenium giving the black compound Ga_2Se, or a (Ga,Zn) metallic alloy.

From our TEM study of the precipitates, three conclusions can be drawn :

(i) the size and number of the precipitates increases with the indium concentration as well as with the annealing temperature,

(ii) there appear to be two definite types of precipitate, one with a crystallographic morphology and the other having a spherical form,

(iii) the precipitates are found preferentially in association with crystallographic defects.

The first conclusion is unexceptional. From the second it could perhaps be argued that the triangular precipitates, because of their crystallographic symmetry, might be In_2Se in epitaxial register with the host lattice, while the spherical ones might be a metallic alloy of (In,Zn).

When ZnSe crystals are grown from the vapour phase with some indium in the charge ($\geqslant$ 50 ppm) and with a partial pressure of P_{min} established

in the zinc reservoir, there is a small zinc overpressure at the growing

interface and selenium vacancies will dominate over zinc vacancies in the

growing boule. Furthermore, the indium, which is transported with the

sublimed ZnSe, will arrive at the surface of the growing crystal in an

atomic state, and since its atomic radius ($\sim$ 1 $\overset{o}{A}$) is much larger than the

ionic radius (0.74 $\overset{o}{A}$) of zinc but smaller than the ionic radius (1.98 $\overset{o}{A}$)

of selenium, some indium ions may prefer to lie in the newly formed selenium

vacancies because there are more of these available and it will be easier

geometrically for them to be accommodated there.

If this were to happen, the as-grown indium doped material would

be heavily compensated by many indium ions substituting on selenium sites -

In_{Se} - where they would act as triply charged acceptors.

When such an indium doped ZnSe crystal is subsequently heat

treated in zinc vapour at a temperature of 600° C and above, the concentra-

tion of selenium vacancies will be increased and that of zinc vacancies will

be decreased. Indium atoms substituting on zinc sites will then be ejected

to interstitial positions. The In_{Se} atoms will be able to migrate through

the lattice via the newly formed selenium vacancies, as will the indium

atoms displaced by the excess zinc. They will eventually come to rest at

some crystal defect, such as a stacking fault where the nucleation of indium

clusters will then occur. The clusters of indium atoms may come to rest

in the vicinity of a group of zinc atoms (aggregated selenium vacancies)

and spherically shaped precipitates of an (In,Zn) metallic alloy may then

form. Another possibility is that the indium clusters will stop in the

neighbourhood of a group of selenium atoms and form an epitaxial compound

such as In_2Se.

The formation of neutral precipitates such as the In-Zn alloy and

the In_2Se compound will reduce the concentration of the triply charged acceptors

as well as that of the singly charged donors (In_{Zn}^{o}) and, along with the

reduction of the zinc vacancies which act as compensating acceptors in ZnSe, the net effect will be reduction of the strong self-compensation. However, as the electrical measurements have shown some compensation still remains, particularly in heavily doped crystals, indicating that some of the triply ionized acceptors are still present. Such material will have properties similar to those described by Ray and Kröger (1978b).

This last suggestion is supported by the fact that the experimental relation (see chapter six) between the carrier concentration n and the indium concentration $\begin{bmatrix} In \end{bmatrix}$ in as-grown ZnSe:In crystals is of the form :

$$n \quad \propto \quad \begin{bmatrix} In \end{bmatrix}^{-\gamma} \quad \text{with} \quad \gamma \sim 3. \tag{7.1}$$

Ray and Kröger obtained a similar relation :

$$n \quad \propto \quad \begin{bmatrix} Ga \end{bmatrix}^{-\gamma} \quad \text{with} \quad \gamma = \frac{1}{4} \tag{7.2}$$

for ZnSe:Ga crystals after heat treatment in zinc vapour, thus a strong reduction in self-compensation takes place from the situation where γ has a value of about 3 in equation 7.1 to a situation where γ is just 0.25 (equation 7.2). A feature to note when discussing gallium doped ZnSe is that gallium may not substitute on to selenium sites to the same extent as indium does. The atomic radius of gallium, of about 0.8 $\overset{\text{o}}{\text{A}}$, is nearer in value to that of zinc than indium is, indicating, in agreement with experiment, that as-grown gallium doped material is less heavily compensated. This has also been inferred by Yamaguchi et al (1977b). This fact probably accounts, in part, for the difference in the values of γ for indium and gallium doped crystals (equations 7.1 and 7.2).

It should be added, for completeness, that a slice from boule ⧫ 405 (containing 55 ppm of indium) was also annealed in selenium vapour at 480$^{\text{o}}$ C for three days (this temperature was chosen in order to obtain

a selenium vapour pressure slightly larger than the vapour pressure used when annealing in zinc vapour at 600°C). Even though no systematic measurements of the resulting electrical or optical properties were carried out, it was quite clear that there was definitely no precipitation. The photo-luminescence emission of the sample did not change although the electrical resistivity increased slightly (by about one order of magnitude). This last result was expected since several workers have shown (see for example Stringfellow and Bube, 1968) that heat treatment in selenium vapour increases the concentration of zinc vacancies and hence the donor compensation. The fact that no dark precipitates were formed is explained by the large number of zinc vacancy sites made available to the indium.

Hitherto, the discussion suggests that atomic size is the key to the behaviour of the group IIIa elements in ZnSe. This would also explain why self-compensation in ZnSe doped with aluminium is almost non-existent (see for example Jones and Woods, 1976, and Ray and Kröger, 1978a). The atomic radius of aluminium is smaller than that of both indium and gallium and for this reason, aluminium will naturally sit on a zinc site indicated by their similar electronegativity. Furthermore, no precipitation occurs when ZnSe:Al is heavily annealed in zinc, which again is explained by the differences in the atomic radii of indium and gallium, since it seems energetically more favourable for the excess zinc atoms simply to fill zinc vacancies rather than to displace aluminium atoms.

As a final point, the differences in the electrical resistivities between samples from different ends of a crystal boule of ZnSe:In which has been discussed in several parts of this thesis, may now be explained in the following way :

It was concluded from the SEM study in the CL mode that the specimen from the tip of the boule had many more precipitates than did the sample cut from the last end to grow (figures 7.12 a,b) which was also the one with

the higher resistivity. Atomic absorption analysis also showed that the indium content at both ends was practically the same. This suggests that the abnormal sample (i.e. the one cut from the last end of the crystal to grow) contained more indium on selenium sites and less indium on zinc sites than that of the normal sample (i.e. the one cut from the first end to grow), leading to a larger compensation and a smaller concentration of precipitates.

The conclusion is therefore that when indium is incorporated in ZnSe in relatively large quantities, it goes substitutionally on to selenium as well as on to zinc sites, hence, creating large compensation effects. Subsequently, when the as-grown material is annealed in the presence of zinc, some indium atoms will be ejected from their zinc sites, starting the nuclea- tion, preferentially at crystallographic defects, with other indium atoms from selenium sites which migrate via the newly created selenium vacancies. The rejected indium with either zinc or selenium, will then form neutral precipitates of (In,Zn) or In_2Se, thereby, reducing the compensating effect.

CHAPTER 8

CONCLUSIONS

8.1   SUMMARY

The main purpose of the research reported in this thesis was to investigate the anomalous properties of ZnSe doped with either indium or gallium.

For this, crystals of ZnSe containing different concentrations of indium and gallium were grown using the vapour phase technique. The method used to incorporate the dopant allowed concentrations from 5 to 1000 ppm to be achieved. These concentrations were confirmed, to within 10-20%, by atomic absorption spectroscopy.

Measurements of the Hall coefficient showed that the donor compensation increased very rapidly with increasing concentration of the group IIIa element. A wide range of conductivities was obtained at room temperature. The highest values (of about $10^{-2} \ \Omega^{-1} \ cm^{-1}$) were found with those crystals with the lowest dopant content ($\sim$ 5-20 ppm) while the lowest values (of about $10^{-6} \ \Omega^{-1} \ cm^{-1}$) were found with dopant contents of the order of 100 ppm. By extending the measurements to higher temperatures (up to 420 K) it was possible to observe that the conductivity was still decreasing with increasing dopant concentration. In fact, from the free electron concentration data at 410 K, a relation of the form

$$n \quad \propto \quad \left[\text{In} \right]^{-3.4}$$

was obtained. This result shows that fewer free electrons are available when more donors might be expected to be present. The same Hall effect data also allowed an empirical relationship between the activation energy

E_d and the indium concentration to be derived in the form

$$E_d = -A \, \ell n \, \left[In \right] + B \qquad (A > 0)$$

where the zero energy level is situated at the bottom of the conduction band. This shows that the Fermi level is pulled towards the centre of the bandgap as the dopant concentration is increased. A similar conclusion was reached from our study of the Meyer-Neldel rule applied to the measured electrical conductivity.

The reduction in the free electron concentration is attributed to several self-compensating effects. It has already been established by several authors that n-type ZnSe can contain unavoidable acceptor levels such as zinc vacancies and copper impurities, which can assume three charge states, i.e. neutral (Cu_{Zn}^{x}), singly charged (Cu_{Zn}' and V_{Zn}') or doubly charged (V_{Zn}''). However, it has been suggested that the presence of these donor compensating centres is insufficient to account for the strong compensation encountered in the indium or gallium doped crystals. Hence, as inferred by Ray and Kröger (1978b) a possible explanation might be that some of the indium atoms replace selenium atoms in the lattice and then acceptor complexes such as $(In_{Zn} - In_{Se})'$ and $(In_{Zn} - In_{Se})''$ could be formed. Moreover, because the compensation in our crystals was even more pronounced than that observed by Ray and Kröger, in ZnSe:Ga, the possible presence of triply charged acceptors of the form In_{Se}''' is proposed. In this case the self-compensation in ZnSe:In crystals would be due to the presence of all the types of acceptors described above. The concentration of each individual acceptor will depend on the growth conditions, stoichiometry and post-growth heat treatment but, above all, it will depend on the indium concentration itself.

We also observed that the compensating effect was slightly less pronounced when gallium was used as the dopant. It was then concluded that

the solubility of gallium and indium in ZnSe are different and, as suggested
by Yamaguchi et al (1977b), the solubility may be dependent on the atomic
radii of the different constituents, hence, more gallium atoms might be
expected to sit in zinc sites than indium atoms do.

Apart from the acceptor centres, there is obviously a net excess
of donor centres since all the crystals, as shown by the thermoelectric
power measurements, were n-type. The dominant donor level was then
provided by substitutional indium In_{Zn} but, selenium vacancies and interstitial
copper atoms might have played significant roles. The presence of all the
various donor and acceptor levels within the bandgap might well have led to
the formation of band tails at either side of the gap (i.e. tailing of the
conduction as well as tailing of the valence band). This would account for
the samples obeying the Meyer-Neldel rule following the model proposed by
Roberts (1971) of pseudo-intrinsic conduction extended to disordered semi-
conductors. We, therefore, conclude that ZnSe crystals grown by the vapour
phase technique cannot be converted to p-type by doping with either indium
or gallium alone.

When dealing with low resistivity material, which included lightly
doped crystals or those heavily treated in zinc vapour, it was found that
some grain boundaries had large potential barriers associated with them.
This may have been caused by the segregation of some impurity to the boundary,
creating crystallographic disorder and asymmetric band bending on either side
of the grain boundary. Thus the potential barrier could be regarded as two
Schottky barriers back-to-back (see Russell et al, 1980).

It was also observed that dark precipitates were produced in
heavily doped ZnSe:In and ZnSe:Ga after annealing in zinc. Following
examination in the transmission electron microscope, it was found that the
precipitates formed in different shapes, namely, spherical or with a four-
fold symmetry or triangulars, and furthermore, the precipitates tended to

decorate stacking faults and grain boundaries. Some of the largest precipitates measured up to 0.2 μm in diameter. Under the optical microscope, these precipitates appeared to form clusters of dark compounds oriented on low index planes within the crystal grain, suggesting perhaps the epitaxial growth of In_2Se. When examined in the scanning electron microscope in the CL mode, it was apparent that the groups of precipitates acted as radiationless centres. This would explain the fact that after heating in zinc, the overall photoluminescence intensity was considerably reduced.

The luminescence measurements confirmed the presence of deep centres already reported by many authors as associated with zinc vacancies or copper impurity, but no evidence of any luminescence associated with either indium or gallium was obtained. Analysis of the TSC and TSL curves revealed a trap giving rise to a peak at about 115 K with an ionization energy of 0.13 eV. Other features of the TSC and TSL curves giving peaks between 150 and 250 K were found in all the samples, suggesting the presence of a quasi-continuous set of deep trap centres. This would also account for some tailing of the bands towards the middle of the bandgap, indicative of heavily doped and compensated semiconductor behaviour. However, no correlation was found between the existence of these traps and the presence of the group IIIa impurity in the crystals.

8.2   FUTURE WORK

One of the challenging aspects remaining from the investigation reported in this thesis is the location of the acceptor levels associated with indium, present in the heavily doped ZnSe crystals. These are the triply ionized $In_{Se}^{'''}$ and the doubly and singly ionized complexes of $In_{Se}-In_{Zn}$. The comparative study of lightly doped (< 50 ppm) and heavily doped ($\geq$ 50 ppm) samples could be extended to other experimental techniques,

in order to achieve a better understanding of these levels. In this extended study, several techniques of transient spectroscopy could be used. Transient photoconductivity combined with steady state photoconductivity, photocapacitance and deep level transient spectroscopy (DLTS) could provide useful information. They could be applied on Schottky diodes fabricated from suitable semiconducting samples which had received a series of controlled heat treatments in either zinc or selenium.

Another aspect worthwhile extending, is the study of the formation of the impurity band and the hopping conduction regimes in lightly doped crystals, down to liquid helium temperatures. If measurements of the transport properties were to be carried out in this temperature range, these should reveal a more definite indication of the different conduction regions.

As far as the precipitates are concerned, these might be analysed by the energy dispersive X-ray technique. The successful application of this method would depend on the production of sufficiently large precipitates. These could be produced by doping ZnSe heavily with indium and heat treating it subsequently in molten zinc at high temperatures for long periods. A comparative study on the formation of precipitates associated with the other three group IIIa metallic elements, should produce some clues about the solubility of these elements in ZnSe, and its relation to the ionic sizes of the elements.

REFERENCES

Adachi S and Machi Y (1975a) Japan. J. Appl. Phys. <u>14</u> 1599

Adachi S and Machi Y (1975b) Japan J. Appl. Phys. <u>14</u> 2087

Adler D and Yoffa E J (1976) Phys. Rev. Lett. <u>36</u> 1197

Anderson P W (1975) Phys. Rev. Lett. <u>34</u> 953

Aranovich J , Fahrenbruch A L and Bube R H (1978) J. Appl. Phys.
    <u>49</u> 2584

Austin I G and Mott N F (1969) Advanc. Phys. <u>18</u> 41

Aven M (1962) J. Electrochem. Soc. <u>11</u> 46

Aven M (1971) J. Appl. Phys. <u>42</u> 1204

Aven M and Devine J Z (1973) J. Lumin. <u>7</u> 195

Aven M and Halsted R E (1965) Phys. Rev. A <u>137</u> 228

Aven M and Segall B (1963) Phys. Rev. <u>130</u> 81

Aven M and Woodbury H H (1962) Appl. Phys. Lett. <u>1</u> 53

Aven M , Marple D T F and Segall B (1961) J. Appl. Phys. Suppl.
    <u>32</u> 2261

Banda D and Roberts G G (1980) Private communication

Bensahel D and Dupuy M (1979a) Phys. Stat. Sol. (a) <u>55</u> 203

Bensahel D and Dupuy M (1979b) Phys. Stat. Sol. (a) <u>56</u> 99

Bensahel D , Dupuy M and Pfister J C (1979) Phys. Stat. Sol. (a)
    <u>55</u> 211

Berlincourt D , Jaffe H and Shiozawa L R (1963) Phys. Rev. <u>129</u> 1009

Bergstresser T K and Cohen M L (1967) Phys. Rev. <u>164</u> 1069

Beyer M and Stuke J (1974) 'Amorphous and Liquid Semiconductors'
    Taylor and Francis Ed. p.251

Bhargava R N , Herko S P and Fitzpatrick B J (1979) Bull. Am. Phys.
    Soc. <u>24</u> 402

Birchak I , Serdyuk V and Chemeresyuk G (1976) Phys. Stat. Sol. (a)
    <u>33</u> K145

Böer K W , Oberländer S and Voigt J (1958) Ann. Phys. Lpz. <u>2</u> 130

Boiko I I , Rashba E I and Trofimenko A P (1960) Sov. Phys. S. S.

 <u>2</u> 99

Bouley J C , Blanconnier P , Herman A , Ged Ph , Henoc P and Noblanc J P

 (1975) J. Appl. Phys. <u>46</u> 3549

Brooks H (1955) 'Advances in Electronics and Electron Physics' Vol. 7

 Marton Ed. (Academic Press) pp 85-182

Bube R H (1955) J. Chem. Phys. <u>23</u> 18

Bube R H (1964) J. Appl. Phys. <u>35</u> 3067

Bube R H (1974) 'Electronic Properties of Crystalline Solids - An

 Introduction to Fundamentals' (Academic Press) Ch. 7 & 8

Bube R H (1978) 'Photoconductivity of Solids' (Krieger Publishing

 Co., Inc.)

Bube R H and Lind E L (1958) Phys. Rev. <u>110</u> 1040

Burr K F and Woods J (1971) J. Cryst. Growth <u>9</u> 183

Busch G (1950) Z. Angew. Math. Phys. <u>1</u> 81

Chen R (1969) J. Appl. Phys. <u>40</u> 570

Chen R (1970) Chem. Phys. L. <u>6</u> 125

Chen R (1971) Chem. Phys. L. <u>11</u> 371

Chen R and Fleming R J (1973) J. Appl. Phys. <u>44</u> 1393

Chen R and Winer S (1970) J. Appl. Phys. <u>41</u> 5227

Clark L and Woods J (1968) J. Cryst. Growth <u>3</u> 127

Cohen M L and Bergstresser T K (1966) Phys. Rev. <u>141</u> 789

Conwell E M and Weisskopf V F (1950) Phys. Rev. <u>77</u> 388

Cutter J R and Woods J (1975) J. Phys. D <u>8</u> 314

Cutter J R , Russell G J and Woods J (1976) J. Cryst. Growth <u>32</u> 179

Davis E A and Mott N F (1970) Phil. Mag. <u>22</u> 903

De Nobel D (1959) Philips Res. Rep. <u>14</u> 361

Dean P J and Bishop S G (1980) J. Lumin. <u>21</u> 193

Dean P J and Merz J L (1969) Phys. Rev. 178 1310

Donnelly J P and Smith F T J (1970) Sol.-State Electron. 13 516

Dunstan D J , Nicholls J E , Cavenett B C , Davies J J and Reddy K V

(1977) Sol. State Commun. 24 677

Dussel G A and Bube R H (1967) Phys. Rev. 155 764

Elliot R J and Gibson A F (1974) 'An Introduction to Solid State

Physics and its Applications' (MacMillan Press) Ch. 8

Emelyanenko O V , Ivanova G N , Lagunova T S , Nedeoglo D D , Shmelev G M

and Simashkevich A V (1979) Phys. Stat. Sol. (b) 96 823

Erginsoy C (1950) Phys. Rev. 79 1013

Etienne D and Bougnot G (1975) Mat. Res. Bull. 10 1365

Fitzpatrick B J , Bhargava R N , Herko S P and Harnack P M (1979)

J. Electrochem. Soc. 126 341

Franks J and Keating P N (1961) J. Phys. Chem. Solids 22 25

Fujita S , Mimoto H and Noguchi T (1979) J. Appl. Phys. 50 1079

Fukuda Y and Fukai M (1967) J. Phys. Soc. Japan 23 902

Garlick G F J and Gibson A F (1948) Proc. Phys. Soc. 60 574

Gavrikova I G , Migal V P and Rvachev A L (1975) Phys. Stat. Sol. (a)

30 K95

Gezci S and Woods J (1975) J. Lumin. 10 267

Gobrecht H and Hoffmann D (1966) J. Phys. Chem. Solids 27 509

Grimmeis H G , Ovren C and Mach R (1979) J. Appl. Phys. 50 6328

Grimmeis H G , Ovren C , Ludwig W and Mach R (1977) J. Appl. Phys.

48 5122

Grossweiner L I (1953) J. Appl. Phys. 24 1306

Gutmann F and Lyons L E (1967) 'Organic Semiconductors' (J. Wiley

and Sons Inc.) p.428

Haering R R and Adams E N (1960) Phys. Rev. 117 451

Halperin A and Braner A (1960) Phys. Rev. 117 408

Haanstra J H and Dieleman J (1965) J. Electrochem. Soc. 14 2

Harrison W A (1956) Phys. Rev. 101 903

Heaton J L , Hammond E H and Goldner R B (1972) Appl. Phys. Lett.
20 333

Hemmatt N and Weinstein M (1967) J. Electrochem. Soc. 114 851

Hite G , Marple D T F , Aven M and Segall B (1967) Phys. Rev.
156 850

Holton W C , De Wit M and Estle T L (1965) Internat. Symp. Lumin.
Munich

Hoogenstraaten W (1958) Philips Res. Rept. 13 515

Howarth D and Sondheimer E H (1953) Proc. Roy. Soc. A 219 53

Hubbard J (1963) Proc. Roy. Soc. London A 276 238

Iida S (1968) J. Phys. Soc. Japan 25 177

Iida S (1969) J. Phys. Soc. Japan 26 1140

Ioffe A F and Regel A R (1960) Progress in Semiconductors (Heywood)
4 237

Jones G and Woods J (1973) J. Phys. D 6 1640

Jones G and Woods J (1974) J. Lumin. 9 389

Jones G and Woods J (1976) J. Phys. D 9 799

Kivits P and Hagebeuk H J L (1977) J. Lumin. 15 1

Kivits P , Reulen J , Hendricx J , van Empel F and van Kleef J (1978)
J. Lumin. 16 145

Klasens H A (1953) J. Electrochem. Soc. 100 72

Lambe J and Klick C C (1955) Phys. Rev. 98 909

Lawther C and Woods J (1977) Phys. Stat. Sol. (a) 44 693

Lawther C and Woods J (1978) Phys. Stat. Sol. (a) 50 491

Lim P K and Brodie D E (1977a) Can. J. Phys. 55 1512

Lim P K and Brodie D E (1977b) Can. J. Phys. 55 1641

Lim P K and Brodie D E (1978) Sol. State Commun. 26 59

Luschik Ch B   (1955)   Dok. Akad. Nauk S. S. S. R.   <u>101</u>   641

Maeta S   and   Saguchi K   (1980a)   Jpn. J. Appl. Phys.   <u>19</u>   519

Maeta S   and   Saguchi K   (1980b)   Jpn. J. Appl. Phys.   <u>19</u>   597

Magnea N ,   Bensahel D   and   Pfister J C   (1979)   Sol. State Commun.

   <u>29</u>   35

Marple D T F   (1964)   J. Appl. Phys.   <u>35</u>   1879

Mathur P C ,   Sethi B R   and   Sharma O P   (1979a)   J. Appl. Phys.   <u>50</u>   4463

Mathur P C ,   Sethi B R ,   Talwar P L ,   Sharma O P   and   Sharma R P   (1979b)

   Phys. Lett.   <u>73A</u>   234

Merz J L ,   Kukimoto H ,   Nassau K   and   Shiever J W   (1972)   Phys. Rev. B

   <u>6</u>   545

Merz J L ,   Nassau K   and   Shiever J W   (1973)   Phys. Rev. B   <u>8</u>   1444

Meyer W   and   Neldel H   (1937)   Z. Tech. Phys.   <u>18</u>   588

Mitchell R   (1977)   PhD Thesis   University of Durham

Mooser E   and   Pearson W B   (1960)   Progress in Semiconductors (Heywood)

   <u>5</u>   105

Mott N F   (1968)   Rev. Mod. Phys.   <u>40</u>   677

Mott N F   and   Davis E A   (1979)   'Electronic Processes in Non-Crystalline

   Materials' (Clarendon Press)

Mott N F ,   Davis E A   and   Street R A   (1975)   Phil. Mag.   <u>32</u>   961

Muhamad M R B   (1979)   Private communication

Nag B R   (1972)   'Theory of Electrical Transport in Semiconductors'

   (Pergamon Press)   Ch. 3 & 4

Nedeoglo D D   (1977)   Phys. Stat. Sol. (b)   <u>80</u>   369

Neumark G F   (1979)   Bull. Am. Phys. Soc.   <u>24</u>   402

Neumark G F   (1980)   To be published

Neumark G F ,   Fitzpatrick B J ,   Harnack P M ,   Herko S P ,   Kosai K   and

   Bhargava R N   (1980)   J. Electrochem. Soc.   <u>127</u>   983

Nicholas K H   and   Woods J   (1964)   Brit. J. Appl. Phys.   <u>15</u>   783

Nitsche R , Bolsterli H U and Lichtensteiger M (1961) J. Phys. Chem. Solids 21 199

Özsan M E and Woods J (1974) Appl. Phys. Lett. 25 489

Özsan M E and Woods J (1977a) Sol.-State Electron. 20 343

Özsan M E and Woods J (1977b) J. Phys. D 10 1335

Papadopoulo A C , Jean-Louis A M and Charil J (1978) J. Cryst. Growth 44 587

Park Y S , Hemenger P M and Chung C H (1971) Appl. Phys. Lett. 18 45

Piper W W and Polich S J (1961) J. Appl. Phys. 32 1278

Prener J S and Weil D J (1959) J. Electrochem. Soc. 106 409

Prener J S and Williams F E (1956a) J. Electrochem. Soc. 103 342

Prener J S and Williams F E (1956b) J. Chem. Phys. 25 361

Raüber A and Schneider J (1966) Phys. Stat. Sol. 18 125

Ray A K and Kröger F A (1978a) J. Electrochem. Soc. 125 1348

Ray A K and Kröger F A (1978b) J. Electrochem. Soc. 125 1355

Ray A K and Kröger F A (1979) J. Appl. Phys. 50 4208

Reinberg A R , Holton W C , De Wit M and Watts R K (1971) Phys. Rev. B 3 410

Reynolds D C and Czyzack S J (1950) Phys. Rev. 79 543

Roberts G G (1971) J. Phys. C 4 3167

Roberts G G and Schmidlin F W (1969) Phys. Rev. 180 785

Roberts G G , Apsley N and Munn R W (1980) Phys. Rep. 60 59

Robinson R J and Kun Z K (1975) Appl. Phys. Lett. 27 74

Rose A (1951) 'Concepts in Photoconductivity and Allied Problems' (J. Wiley and Sons Inc.)

Rosenberg B , Bhowmik B B , Harder H C and Postow E (1968) J. Chem. Phys. 49 4108

Roth W L (1967) in 'Physics and Chemistry of II-VI Compounds' Aven and Prener Ed. (North Holland Pub. Co.) p.137

Russell G J and Woods J (1979) J. Cryst. Growth 46 323

Russell G J , Robertson M J , Vincent B and Woods J (1980) J. Mater.
Sci. 15 939

Sagar A , Lehmann W and Faust J (1968) J. Appl. Phys. 39 5336

Sandomirskii V B and Zhdan A G (1970) Sol.-State Electron. 13 69

Satoh S and Igaki K (1980) Jpn. J. Appl. Phys. 19 485

Schneider J , Raüber A , Dischler N , Estle T L and Holton W C (1965)
J. Chem. Phys. 42 1839

Schockley W and Bardeen J (1950) Phys. Rev. 80 72

Schön M (1942) Z Physik 119 463

Sclar N (1956) Phys. Rev. 104 1559

Sethi B R and Mathur P C (1978) Phys. Stat. Sol. (a) 46 717

Sethi B R , Mathur P C and Woods J (1978a) J. Appl. Phys. 49 3618

Sethi B R , Mathur P C and Woods J (1979) J. Appl. Phys. 50 352

Sethi B R , Talwar P L , Sharma O P and Mathur P C (1977) Phys. Stat.
Sol. (a) 42 791

Sethi B R , Talwar P L , Sharma O P and Mathur P C (1978b) Phys.
Stat. Sol. (a) 47 699

Shing Y H and Walsh D (1980) J. Appl. Phys. 51 1842

Shionoya S , Era K and Washizawa Y (1966) J. Phys. Soc. Japan 21
1624

Shirakawa Y and Kukimoto H (1980) J. Appl. Phys. 51 2014

Shmelev G M and Tsurkan G I (1979) Sov. Phys. Semicond. 13 198

Smith R A (1978) 'Semiconductors' (Cambridge University Press)
Ch. 5 , 6 & 8

Street R A and Mott N F (1975) Phys. Rev. Lett. 35 1293

Stringfellow G B and Bube R H (1968) Phys. Rev. 171 903

Swaminathan V and Greene L C (1976) Phys. Rev. B 14 5351

Terada K (1976) J. Phys. Soc. Japan 40 4

Tews H , Venghaus H and Dean P J (1979) Phys. Rev. B <u>19</u> 5178

Toyozawa Y (1962) J. Phys. Soc. Japan <u>17</u> 986

Tsujimoto Y , Onodera Y and Fukai M (1966) Jpn. J. Appl. Phys. <u>5</u> 636

Unger K (1962) Phys. Stat. Sol. <u>2</u> 1279

Wagner P and Lorenz M R (1966) J. Phys. Chem. Solids <u>27</u> 1749

Waite P (1979) Private communication

Wakim F G (1970) J. Appl. Phys. <u>41</u> 835

Watkins G D (1974) Phys. Rev. Lett. <u>33</u> 223

Weichman F L and Kužel R (1970) Can. J. Phys. <u>48</u> 63

Woodbury H H and Aven M (1974) Phys. Rev. B <u>9</u> 5195

Yamaguchi M , Yamamoto A and Kondo M (1977a) J. Appl. Phys. <u>48</u> 196

Yamaguchi M , Yamamoto A and Kondo M (1977b) J. Appl. Phys. <u>48</u> 5237

Yu P W and Park Y S (1973) Appl. Phys. Lett. <u>22</u> 345